frontiers | Research Topics

Reviews in pathology of infectious diseases

Edited by
Francisco Javier Salguero, Jaime Gómez-Laguna and Francisco José Pallarés

Published in
Frontiers in Veterinary Science

ISSN 1664-8714
ISBN 978-2-8325-5072-4
DOI 10.3389/978-2-8325-5072-4

About Frontiers

Frontiers is more than just an open access publisher of scholarly articles: it is a pioneering approach to the world of academia, radically improving the way scholarly research is managed. The grand vision of Frontiers is a world where all people have an equal opportunity to seek, share and generate knowledge. Frontiers provides immediate and permanent online open access to all its publications, but this alone is not enough to realize our grand goals.

Frontiers journal series

The Frontiers journal series is a multi-tier and interdisciplinary set of open-access, online journals, promising a paradigm shift from the current review, selection and dissemination processes in academic publishing. All Frontiers journals are driven by researchers for researchers; therefore, they constitute a service to the scholarly community. At the same time, the *Frontiers journal series* operates on a revolutionary invention, the tiered publishing system, initially addressing specific communities of scholars, and gradually climbing up to broader public understanding, thus serving the interests of the lay society, too.

Dedication to quality

Each Frontiers article is a landmark of the highest quality, thanks to genuinely collaborative interactions between authors and review editors, who include some of the world's best academicians. Research must be certified by peers before entering a stream of knowledge that may eventually reach the public - and shape society; therefore, Frontiers only applies the most rigorous and unbiased reviews. Frontiers revolutionizes research publishing by freely delivering the most outstanding research, evaluated with no bias from both the academic and social point of view. By applying the most advanced information technologies, Frontiers is catapulting scholarly publishing into a new generation.

What are Frontiers Research Topics?

Frontiers Research Topics are very popular trademarks of the *Frontiers journals series*: they are collections of at least ten articles, all centered on a particular subject. With their unique mix of varied contributions from Original Research to Review Articles, Frontiers Research Topics unify the most influential researchers, the latest key findings and historical advances in a hot research area.

Find out more on how to host your own Frontiers Research Topic or contribute to one as an author by contacting the Frontiers editorial office: frontiersin.org/about/contact

Reviews in pathology of infectious diseases

Topic editors

Francisco Javier Salguero — UK Health Security Agency (UKHSA), United Kingdom

Jaime Gómez-Laguna — University of Cordoba, Spain

Francisco José Pallarés — University of Cordoba, Spain

Citation

Salguero, F. J., Gómez-Laguna, J., Pallarés, F. J., eds. (2024). *Reviews in pathology of infectious diseases*. Lausanne: Frontiers Media SA.

doi: 10.3389/978-2-8325-5072-4

Table of contents

frontiers | Frontiers in Veterinary Science

TYPE Editorial
PUBLISHED 14 June 2024
DOI 10.3389/fvets.2024.1435676

OPEN ACCESS

EDITED AND REVIEWED BY
Gabriele Rossi,
Murdoch University, Australia

*CORRESPONDENCE
Francisco J. Salguero
✉ javier.salguero@ukhsa.gov.uk

RECEIVED 20 May 2024
ACCEPTED 30 May 2024
PUBLISHED 14 June 2024

CITATION
Gomez-Laguna J, Pallares FJ and Salguero FJ (2024) Editorial: Reviews in pathology of infectious diseases.
Front. Vet. Sci. 11:1435676.
doi: 10.3389/fvets.2024.1435676

Editorial: Reviews in pathology of infectious diseases

Jaime Gomez-Laguna[1], Francisco J. Pallares[1] and Francisco J. Salguero[2,3]*

[1]Department of Anatomy, Comparative Pathology, and Toxicology, Pathology and Immunology Group (UCO-PIG), UIC Zoonosis y Enfermedades Emergentes ENZOEM, University of Córdoba, International Excellence Agrifood Campus 'CeiA3', Córdoba, Spain, [2]Department of Pathology, UK Health Security Agency (UKHSA), Porton Down, Salisbury, United Kingdom, [3]School of Biosciences and Medicine, University of Surrey, Guildford, United Kingdom

KEYWORDS

pathology, infectiuos diseases, review, emerging disease, animal model

Editorial on the Research Topic
Reviews in pathology of infectious diseases

The importance of infectious diseases in animals, especially zoonotic diseases, has increased dramatically in recent years with the COVID-19 pandemic, the emergence and/or re-emergence of vector-borne diseases, avian influenza, Mpox infection and many others, together with the persistence of endemic diseases such as PRRS in pigs or tuberculosis in multiple hosts (1–3). This Research Topic focuses on the pathology of infectious diseases that affect animals and humans, emphasizing the value of animal disease models to combat them.

Hunter et al. reviewed the pathological aspects of pulmonary tuberculosis in animal models, including rodents, guinea pigs, non-human primates, rabbits, ruminants, and zebrafish. They produced a comprehensive description of the lesions induced by *Mycobacterium tuberculosis* complex (MTBC) in the lungs of infected animals and the use of these models in research. Moreover, they described the pulmonary lesions observed in human tuberculosis, as a comparative exercise with a "One Health" approach.

Larenas-Muñoz et al. described the characterization of the pathological lesions present in the guinea pig model of *Mycobacterium tuberculosis* infection, using a combination of classic histopathology, immunohistochemistry and digital image analysis. The detailed description of the evolution of granulomatous lesions in this important pre-clinical model of tuberculosis, will be very valuable in evaluating antimicrobial therapies and vaccines that may eventually progress to clinical phases.

Layton et al. described the impact of stress and anesthesia on animal models of infectious disease analyzing the most recent scientific evidence on these two variables and reviewing the strategies and technologies used to monitor animal models during infectious diseases.

Ruedas-Torres et al. reviewed the host-pathogen interactions during Porcine Reproductive and Respiratory Syndrome (PRRS) infection in pigs. They described the main lesions observed in the pulmonary aspect of this disease: interstitial pneumonia, suppurative bronchopneumonia and proliferative and necrotising pneumonia, emphasizing the differences observed between strains of different virulences.

Sorensen et al. described the effects of water temperature on Piscine orthoreovirus genotype 3 (PRV-3) infection in rainbow trout (*Oncorhynchus mykiss*), showing that low water temperatures allow for higher PRV-3 replication, which is associated with more severe heart pathology and increased expression of important antiviral genes.

Rodrigues da Silva et al. reviewed the porcine circovirus 3 infection in pigs, an increasing problem for the pork industry worldwide, describing the epidemiology, clinical manifestations, pathological co-infections and diagnostics.

Dorfelt et al. presented a comprehensive retrospective study of tetanus in dogs, a severe neurological disease that can also affect humans, caused by *Clostridium tetani*, and associated with high mortality.

Naseem et al. described the pathology and pathogenesis of the cutaneous lesions observed in beef cattle associated with buffalo fly (*Haematobia irritans exigua*) infestation, including the secondary infections that may be associated with this parasitic disease.

Flores-Velazquez et al. reviewed the pathogenesis, and host-parasite interactions in fasciolosis, another parasitic disease caused by infestation with *Fasciola hepatica*, also focusing on the current work being carried out to develop a vaccine against this disease, which suffers from an increasing problem of anthelmintic resistance.

Author contributions

JG-L: Writing – original draft, Writing – review & editing. FP: Writing – original draft, Writing – review & editing. FS: Writing – original draft, Writing – review & editing.

Funding

The authors declare that no financial support was received for the research, authorship, and/or publication of this article.

Conflict of interest

The authors declare that the research was conducted in the absence of any commercial or financial relationships that could be construed as a potential conflict of interest.

The author(s) declared that they were an editorial board member of Frontiers, at the time of submission. This had no impact on the peer review process and the final decision.

Publisher's note

References

1. Muñoz-Fontela C, Dowling WE, Funnell SGP, Gsell PS, Riveros-Balta AX, Albrecht RA, et al. Animal models for COVID-19. *Nature.* (2020) 586:509–15.

2. Stilpeanu RI, Stercu AM, Stancu AL, Tanca A, Bucur O. Monkeypox: a global health emergency. *Front Microbiol.* (2023) 14:1094794. doi: 10.3389/fmicb.2023.1094794

3. Plaza PI, Gamarra-Toledo V, Euguí JR, Lambertucci SA. Recent changes in patterns of mammal infection with highly pathogenic avian influenza A(H5N1) virus worldwide. *Emerg Infect Dis.* (2024) 30:444–52. doi: 10.3201/eid3003.231098

frontiers | Frontiers in Veterinary Science

TYPE Original Research
PUBLISHED 18 January 2023
DOI 10.3389/fvets.2022.971813

OPEN ACCESS

EDITED BY
Marie Christine Cadiergues,
Ecole Nationale Vétérinaire de Toulouse (ENVT), France

REVIEWED BY
Didier Pin,
VetAgro Sup, France
Vinícius Longo Ribeiro Vilela,
Instituto Federal de Educação, Ciência e Tecnologia da Paraíba, Brazil

*CORRESPONDENCE
Peter James
p.james1@uq.edu.au

SPECIALTY SECTION
This article was submitted to Veterinary Experimental and Diagnostic Pathology, a section of the journal Frontiers in Veterinary Science

RECEIVED 17 June 2022
ACCEPTED 29 December 2022
PUBLISHED 18 January 2023

CITATION
Naseem MN, Allavena R, Raza A, Constantinoiu C, McGowan M, Turni C, Kamran M, Tabor AE and James P (2023) Pathology and pathogenesis of cutaneous lesions in beef cattle associated with buffalo fly infestation. *Front. Vet. Sci.* 9:971813. doi: 10.3389/fvets.2022.971813

Pathology and pathogenesis of cutaneous lesions in beef cattle associated with buffalo fly infestation

Muhammad Noman Naseem[1], Rachel Allavena[2], Ali Raza[1], Constantin Constantinoiu[3], Michael McGowan[2], Conny Turni[1], Muhammad Kamran[1], Ala E. Tabor[1,4] and Peter James[1]*

[1]The University of Queensland, Queensland Alliance for Agriculture and Food Innovation, Centre for Animal Science, St. Lucia, QLD, Australia, [2]School of Veterinary Science, The University of Queensland, Gatton, QLD, Australia, [3]College of Public Health, Medical and Veterinary Sciences, James Cook University, Townsville, QLD, Australia, [4]School of Chemistry and Molecular Biosciences, The University of Queensland, St. Lucia, QLD, Australia

Haematobia irritans exigua, commonly known as buffalo fly, is the major hematophagous ectoparasite of north Australian cattle herds. Lesions associated with buffalo fly infestation are generally alopecic, hyperkeratotic, or scab encrusted wounds with variable hemorrhagic ulceration. Buffalo flies can transmit a filarial nematode, *Stephanofilaria* sp., which has been implicated in the pathogenesis of buffalo fly lesions, but *Stephanofilaria* infection has not been detected in all lesions suggesting that other causal factors may be involved. This study characterized the pathology of buffalo fly lesions to identify the role of *Stephanofilaria* in lesion development, as well as to identify other potential agents. Lesion biopsies were collected from north and south Queensland and tested for the presence of *Stephanofilaria* by qPCR. Each lesion was scored grossly (0–4) for hemorrhage, ulceration, exudation, and alopecia. Lesions were also scored microscopically (0–4) for epidermal and dermal damage and inflammatory characters. *Stephanofilaria* infection was detected in 31% of lesion biopsies. Grossly, *Stephanofilaria*-infected lesions had significantly larger lesion area and higher scores for alopecia and hyperkeratosis than lesions where no nematodes were found ($P < 0.05$). Histologically, epidermal, dermal, and adnexal damage was significantly higher in *Stephanofilaria* infected lesions than lesions without nematodes. Eosinophils, macrophages, and lymphocytes were significantly more abundant in *Stephanofilaria* positive lesions as compared to negative lesions. This study also noted bacterial infection with colonies of coccoid bacteria, observed in skin sections from 19 lesions. Grossly, lesions with bacterial infection had significantly higher ulceration scores compared to *Stephanofilaria* positive lesions, and histologically epidermal disruption was significantly greater in bacteria-infected lesions. We found no evidence of bacteria or *Stephanofilaria* infection in 49% of the lesions assessed and tissue damage patterns and eosinophilic inflammation suggested hypersensitivity to buffalo fly feeding as a possible cause of these lesions. These findings suggest that although the presence of *Stephanofilaria* infection may increase the severity of lesion pathology, it is not essential for lesion development. These outcomes also suggest a potential role of bacteria and hypersensitivity in pathogenesis of some lesion. A better understanding of buffalo fly lesion etiology will contribute to the optimal treatment and control programmes.

KEYWORDS

haematobia, *Stephanofilaria*, buffalo fly, skin lesions, histopathology

1. Introduction

Flies from the genus *Haematobia* are obligate hematophagous ectoparasites that feed mainly on cattle and buffalo (1). Two major and closely related species of this genus are the buffalo fly (*Hematobia irritans exigua*) (BF) prevalent in the tropical and subtropical parts of Asia, Australia and other parts of Oceania, and the horn fly (*Haematobia irritans irritans*) (HF) widespread throughout Europe, Africa and the Americas (1). Buffalo flies (BFs) are considered a major pest affecting animal production and welfare, particularly in northern Australian herds (2). Infestation with BFs is frequently accompanied by the development of skin lesions associated with BF feeding that occur mainly near the medial canthus of the eye, along the lateral and ventral neck and on the abdomen. These lesions can range from raised dry, alopecic, hyperkeratotic or scab encrusted to severe haemorrhagic ulcerated areas (3, 4) and occur in up to 95% of northern Australian herds (5). When surveyed, northern dairy farmers noted BF as a problem on 91% of farms and animal welfare aspects due to BF infestation were noted as the most serious BF-related issue (6). Often the key concern of cattle producers are the lesions associated with BF feeding because of their visual appearance (most particularly the open and suppurating wounds) and the associated irritation to the animal (3). Buffalo fly lesions can also penetrate the dermis, affecting hide quality, cattle saleability, and can increase animal susceptibility to secondary infections (7).

In Australia, BFs transmit an unnamed species of filarial nematode, *Stephanofilaria* sp., which has been associated with the pathogenesis of BF lesions (5, 7, 8). This nematode is closely related to, or potentially the same species as *Stephanofilaria stilesi* vectored by horn flies (HFs)in the northern hemisphere and South America (3, 9). However, *Stephanofilaria* nematodes and their microfilariae were detected in only 40% of the lesions examined histologically in a study by Johnson et al. (5) and Naseem et al. (10) found that only 11% of 120 BF lesions assessed were positive for *Stephanofilaria* infection by qPCR. In addition, nematode distribution was limited to northern and central Queensland, and qPCR testing found no *Stephanofilaria* in either lesions or BF from southern Queensland although BF-associated lesions are prevalent in these areas (10).

Although lesion development is associated with BF feeding, there is a poor correlation between BF numbers and lesion development (7, 11) suggesting that there are additional contributing factors. In addition, although HFs have been reported to vector *Stephanofilaria stilesi* causing granular abdominal dermatitis, udder and teat lesions in cattle in North and South America (9, 12–14), the nematode was not found in all cases (14, 15). Thus these lesions were suggested to be potentially due to hypersensitivity induced by HF feeding (16) and infection with *Staphylococcus* spp. bacteria vectored by HFs (17). These observations taken together suggest that *Stephanofilaria* infection may not be essential for the pathogenesis of BF lesions, and that other causal factors may be involved.

In this study, we utilized a recently developed *Stephanofilaria* specific qPCR (18) to identify the presence of nematodes in lesions, and characterized and compared the gross and microscopic pathology of BF-associated lesions with various pathogens present to clarify the key factors involved in the pathogenesis of these lesions.

2. Material and methods

2.1. Skin lesion sample collection and *Stephanofilaria* testing

Lesion samples ($n = 86$) were collected from skins of recently slaughtered cattle at a commercial abattoir in north Queensland ($n = 62$) as well as from biopsies from live cattle ($n = 24$). All abattoir samples were from lesions near the medial canthus of the eyes whereas biopsies from live cattle were from two herds kept in southern Queensland (Pinjarra Hills -27.50^{O}S, 152.91^{O}E and Forest Hill -27.60^{O}S, $152.39\ ^{O}$E) and were collected from the neck ($n = 17$), shoulder ($n = 2$), belly ($n = 3$) and from near the eye ($n = 2$). All biopsies were taken from the center of the lesion using 8 mm sterile skin punches (Paramount Surgimed Ltd., New Delhi, India) together with a control skin biopsy from unaffected skin 3–4 cm away from each lesion. A sub sample was taken from each of the 86 samples collected and confirmed as positive or negative for *Stephanofilaria* by TaqMan^{TM} qPCR assay (18). All samples were preserved in 10% neutral buffered formalin until histological processing. These studies were conducted under The University of Queensland Animal Ethics approval no. 2021/AE000054.

2.2. Gross examination and scoring

The initial gross appearance of each lesion was scored at the time of sample collection according to a *de novo* scoring scheme shown in Table 1. Each lesion was scored (0–4) grossly for the presence of ulceration, exudation, hemorrhage, alopecia, scab formation and hyperkeratosis. All lesions were also photographed alongside a measurement scale before collection of the biopsies and the area of each sampled lesion was measured from photographs using an online tool SketchAndCalc (https://www.sketchandcalc.com/).

2.3. Histological processing

Skin biopsies were dehydrated and cleared using an automated Tissue Processor (Shandon Excelsior ES, Thermofisher Scientific, Waltham, MA, USA). The biopsies were then embedded in paraffin using a tissue embedding machine (Leica EG1160, Leica Biosystem, Wetzlar, Germany). A 4 µm thick section was taken from each biopsy using a manual microtome (Leica RM2235, Leica Biosystem, Wetzlar, Germany) and stained with hematoxylin and eosin. Staining was performed on an auto-stainer (Leica ST5020, Leica Biosystems, Wetzlar, Germany) according to the manufacturer's instructions. Each section was scanned (Leica Aperio CS2, Leica Biosystems, Wetzlar, Germany) and examined on a computer screen.

2.4. Histological examination and scoring

All 86 samples were reviewed for the presence of *Stephanofilaria* adult nematodes or microfilariae, and bacteria. For quantitation of the tissue damage, all epidermal and dermal changes were scored by the scoring systems given in Table 2. Epidermal changes including epidermal disruption, crust over epidermis, hyperkeratosis,

10.3389/fvets.2022.971813

TABLE 1 Grading scales for scoring gross changes in buffalo fly lesions.

Parameter	Observation	Score
Hemorrhage	Absent	0
	<10% of lesion area	1
	11–40% of lesion area	2
	41–80% of lesion area	3
	>80% of lesion area	4
Ulceration	Absent	0
	<10% of lesion area	1
	11–40% of lesion area	2
	41–80% of lesion area	3
	>80% of lesion area	4
Exudation	Absent	0
	Sero-haemorrhagic	1
	Fibrous	2
	Fibro-purulent	3
	Purulent	4
Scab	Absent	0
	<10% of lesion area	1
	11–40% of lesion area	2
	41–80% of lesion area	3
	>80% of lesion area	4
Hyperkeratosis	Absent	0
	Periphery (poorly circumscribed outline)	1
	Periphery (well define outline)	2
	Thick on the periphery and protruding to center	3
	Cover more than 80% of the lesion	4
Alopecia	Absent	0
	<10% of lesion area	1
	11–40% of lesion area	2
	41–80% of lesion area	3
	>80% of lesion area	4

The total gross lesion score was calculated as the sum of each parameter score.

acanthosis and spongiosis were scored individually for each sample and a total epidermal damage score for each sample was calculated by summing the individual score of all parameters. Similarly dermal damage was scored for adnexal destruction, endothelial activity, vascular changes and collagenolysis, and the total dermal damage was determined for each section by summing the individual scores of all assessed dermal parameters. Differential inflammatory cell scores and total inflammatory response in each lesion were scored according to the scoring scheme shown in Table 3. The scoring schemes for histological changes in this study were created with reference to observations of the biopsies from unaffected skin areas processed in this study. All parameters for histological changes were scored in ten different fields selected randomly from three fields each from the left and right side, and four from the center of each biopsy. A final score was calculated as an average of the ten individual field scores.

2.5. Statistical analysis

All the gross and histological scores were compared between different groups using the Mann–Whitney *U*-test (19) and the lesion areas were compared by two tailed *t*-tests in GraphPad Prism version 9.1.0 (GraphPad Software, La Jolla, CA; by www.graphpad.com). The level of statistical significance was $P < 0.05$.

3. Results

3.1. Detection of potential causal factors

Of 62 lesion samples collected from north Queensland, 27 were positive for *Stephanofilaria* infection by TaqMan^{TM} qPCR while the adult nematodes or its microfilariae or both were detected in the histological sections of only 14 samples. Of these 14 histologically positive samples, adult nematodes and microfilariae were observed in seven and four respectively, while both were observed in three samples (Figure 1). The number of adult *Stephanofilaria* nematodes ranged from 1 to 11 in individual sections, and microfilariae ranged from 5 to 15. No false PCR positive samples were recorded and none of the 24 lesions tested from south Queensland was positive for *Stephanofilaria* infection by either qPCR or histological examination.

Multiple clusters of ~1.5 μm purple-stained cocci were observed within the superficial serocellular crust of 19 lesion samples (Figure 2). This included 11 samples from south Queensland and eight from north Queensland. Of these bacteria-positive samples, only two were also positive for *Stephanofilaria* by qPCR.

3.2. Gross pathology of BF lesions

The BF lesions examined ranged from dry, hyperkeratotic hairless areas to severe open suppurative wounds with hemorrhagic or scab encrusted surface (Figure 3). Body lesions including lesions sampled from the neck, dewlap and belly, had areas ranging from 5.14 to 40 cm^2, while the lesions sampled near the eyes of cattle had lesion areas ranging from 3.04 to 54.44 cm^2. There were no obvious differences in the gross pathology of lesions sampled from different anatomical locations.

When the lesion areas and scores for total gross damage, alopecia, ulceration and hyperkeratosis from north Queensland were compared between BF lesions which tested positive ($n = 25$) and negative ($n = 29$) for *Stephanofilaria* infection with PCR, *Stephanofilaria* positive lesions had significantly larger lesion areas (ranging from 7.02 to 54.44 cm^2) as compared to negative lesions (3.04 to 15.07 cm^2) (Figure 4A). This comparison excluded two lesions that were positive for both *Stephanofilaria* and bacterial infection to avoid any confounding effects due to bacterial infection. Total gross damage, alopecia and hyperkeratosis were significantly higher in *Stephanofilaria* positive lesions (Figures 4B–D). Notably, all of the animals in the *Stephanofilaria* positive group had a score of 4 for alopecia (>80% of the lesion area affected), whereas the occurrence of alopecia was more variable (score 2–4) in the *Stephanofilaria* negative group. There was only one animal with ulceration score >0 in the *Stephanofilaria* positive group and this animal had severe (score 4) ulceration whereas in the *Stephanofilaria*

10.3389/fvets.2022.971813

TABLE 2 Grading scales for scoring histological changes in buffalo fly lesions.

Parameter	Magnification/field area	Observation	Score
Epidermal changes			
Epidermal disruption	100X/1.9 × 1.030 mm	Absent	0
		<10% of lesion area cover	1
		11–40% of lesion area cover	2
		41–80% of lesion area cover	3
		>80% of lesion area cover	4
Spongiosis	200X/950 × 515 μm	Absent	0
		Focal (1-10)/field	1
		Multifocal (>10)/ field	2
		Locally extensive	3
		Diffused throughout the biopsy	4
Acanthosis	100X/1.9 × 1.030 mm	Normal epidermis (40-60 μm thick or 4-5 cell layers)	0
		Twice the thickness of the normal epidermis	1
		Three times the thickness of the normal epidermis	2
		Four times the thickness of the normal epidermis	3
		More than 5 times the thickness of the normal epidermis	4
Crust over epidermis	100X/1.9 × 1.030 mm	Absent	0
		Serous	1
		Serocellular crust (fine thin band)	2
		Serocellular crust (thick band)	3
		Haemorrhagic crust	4
Hyperkeratosis	100X/1.9 × 1.030 mm	Normal stratum corneum (4–8 μm thick)	0
		Twice the thickness of the normal st. corneum	1
		Three times thickness to the normal st. corneum	2
		Four times thickness to of the normal st. corneum	3
		More than 5 times the thickness of the normal st. corneum	4
Dermal changes			
Adnexal destruction	100X/1.9 × 1.030 mm	Normal (HF[a], 5-6; SG[b], 1-2; Sb-G[c], 4-5)	0
		(HF, 3-4; SG, 1-2; Sb-G, 2-3)/field	1
		(HF, 2-3; SG, 1; Sb-G, 1-2)/field	2
		(HF, 1-2; SG, 1; Sb-G, 1)/ field	3
		No adnexal structure observed	4
Number of vessels	200X/950 × 515 μm	Not observed	0
		1–2/ fields	1
		3–4/ fields	2
		Greater than 4/in at least 5 fields	3
		Present throughout section	4
Hemorrhage	200X/950 × 515 μm	Absent	0
		1–3 haemorrhagic foci	1
		Over 4 haemorrhagic foci	2
		Multifocal (≥10) hemorrhage	3
		Diffuse hemorrhages	4

(Continued)

TABLE 2 (Continued)

Parameter	Magnification/field area	Observation	Score
Collagenolysis	100X/1.9 × 1.030 mm	Absent	0
		<10% of the specimen	1
		11–40% of the specimen	2
		41–80% of the specimen	3
		> 80% of the specimen	4

[a]Hair follicle, [b]Sweat gland, [c]Sebaceous gland. The total epidermal and dermal damage score was calculated as the sum of each parameter score for epidermis and dermis damage respectively.

TABLE 3 Grading scales for scoring inflammatory cells in buffalo fly lesions.

Cell type/ Response	Score				
	0	1	2	3	4
Neutrophils	1–2/hpf*	3–7/hpf	8–15/hpf	>15/hpf	Heavy Infiltrate
Lymphocytes					
Plasma cells					
Eosinophils					
Macrophages					

*phf = High powered (400X) field. A total inflamatory score was calculated as the sum of each inflammatory cell type score.

negative group, more animals had a score of 1–3 for ulceration, but none had a score 4 (Figure 4E).

In the comparison between BF lesions with bacterial infection (n = 17) and without bacterial infection (n = 42), a non-significant difference was noted in lesion areas between lesions positive (ranged 4.77–27 cm^2) and negative (3.04 to 40 cm^2) for bacterial infection (Figure 4F). The scores for total gross damage, alopecia and ulceration were not significantly different between these two groups (Figures 4G, H, J). Lesions with no bacterial growth had significantly higher hyperkeratosis as compared to bacteria-infected lesions (Figure 4I).

When the gross pathology scores for BF lesions positive for *Stephanofilaria* but not bacteria (n = 25) were compared with lesions observed with bacterial infection but not *Stephanofilaria* (n = 17), *Stephanofilaria*-infected lesions had significantly larger lesion areas (7.02 to 54.44 cm^2) as compared to bacterial infected lesions (4.77 to 27 cm^2) (Figure 4K). The scores for total gross damage, alopecia and hyperkeratosis were also significantly higher in *Stephanofilaria*-infected lesions (Figures 4L–N), whereas bacteria-infected lesions had significantly higher ulceration scores (Figure 4O). For this comparison, there was only one animal in the *Stephanofilaria* group with ulceration (score 3) whereas in the bacteria affected lesions ulceration was more common with most animals affected (only one animal with score 0) and scores ranging from 0 to 4.

3.3. Microscopic pathology of BF lesions

The most consistent differences in the epidermis between lesion-affected and unaffected skin included the degree of hyperkeratosis, acanthosis, spongiosis, epidermal disruption and formation of a serocellular crust of varying thickness. There were also varying degrees of cellular infiltration in lesion-affected areas with cell composition including necrotic epidermal cells, neutrophils, and eosinophils (Figure 1A). Epidermal disruption was most commonly observed in sections biopsied from body lesions from south Queensland. Changes observed in the dermis included varying degrees of adnexal destruction, endothelial reactivity, vascular changes and infiltration of inflammatory cells. Acute lesions had moderate to severe superficial dermal collagenolysis whereas varying degrees of fibrosis were observed in chronic wounds indicating the commencement of scarring. Cellular infiltrate was predominately eosinophils along with macrophages, neutrophils and lymphocytes.

Adult *Stephanofilaria* nematodes were observed up to 0.5–2.5 mm deep in the dermis, mostly within cysts formed at the base of the damaged hair follicles (Figure 1B). In two lesion sections, adult nematodes were observed close to the epidermis with necrotic tracts in the dermal layer suggesting nematode migration through the dermis. Microfilariae were mostly observed close to the epidermis in the dermal papillae and rete pegs and enclosed in a round to oval-shaped vitelline membrane that also contained numerous small spherical eosinophilic bodies (Figures 1C, D). Similar membrane-enclosed microfilariae were also observed in the uteri of gravid female nematodes. Eosinophils were dispersed throughout the superficial dermal layer with markedly abundant numbers near *Stephanofilaria* adults and microfilariae.

To characterize the microscopic pathology of BF lesions with different causal factors, histopathological scores were compared among lesions grouped according to potential causal factors.When histopathological scores for north Queensland lesions qPCR positive for *Stephanofilaria* were compared with lesions without *Stephanofilaria* infection, total epidermal damage in *Stephanofilaria* positive lesions was significantly higher than in the negative lesions (Figure 5A). Epidermal disruption was not significantly different between these two groups (Figure 5B). Total dermal damage and particularly adnexal damage was significantly higher in *Stephanofilaria* positive lesions (Figures 5C, D). Similarly, *Stephanofilaria*-infected lesions had significantly higher inflammation compared to non-infected lesions (Figure 5E). Although infiltration of eosinophils, neutrophils, macrophages, lymphocytes and plasma cells was evident in both lesion groups, the scores for eosinophils, macrophages and lymphocytes were significantly higher in lesions with *Stephanofilaria* (Figures 5F–J).

When the histological scores for BF lesions with and without bacterial infection were compared, total epidermal damage, epidermal disruption, total dermal damage, and adnexal destruction in BF lesions with bacteria were significantly higher compared to non-infected lesions (Figures 6A–D). However, total inflammation scores and the differential leukocytic counts were not significantly different, except for macrophages, which

10.3389/fvets.2022.971813

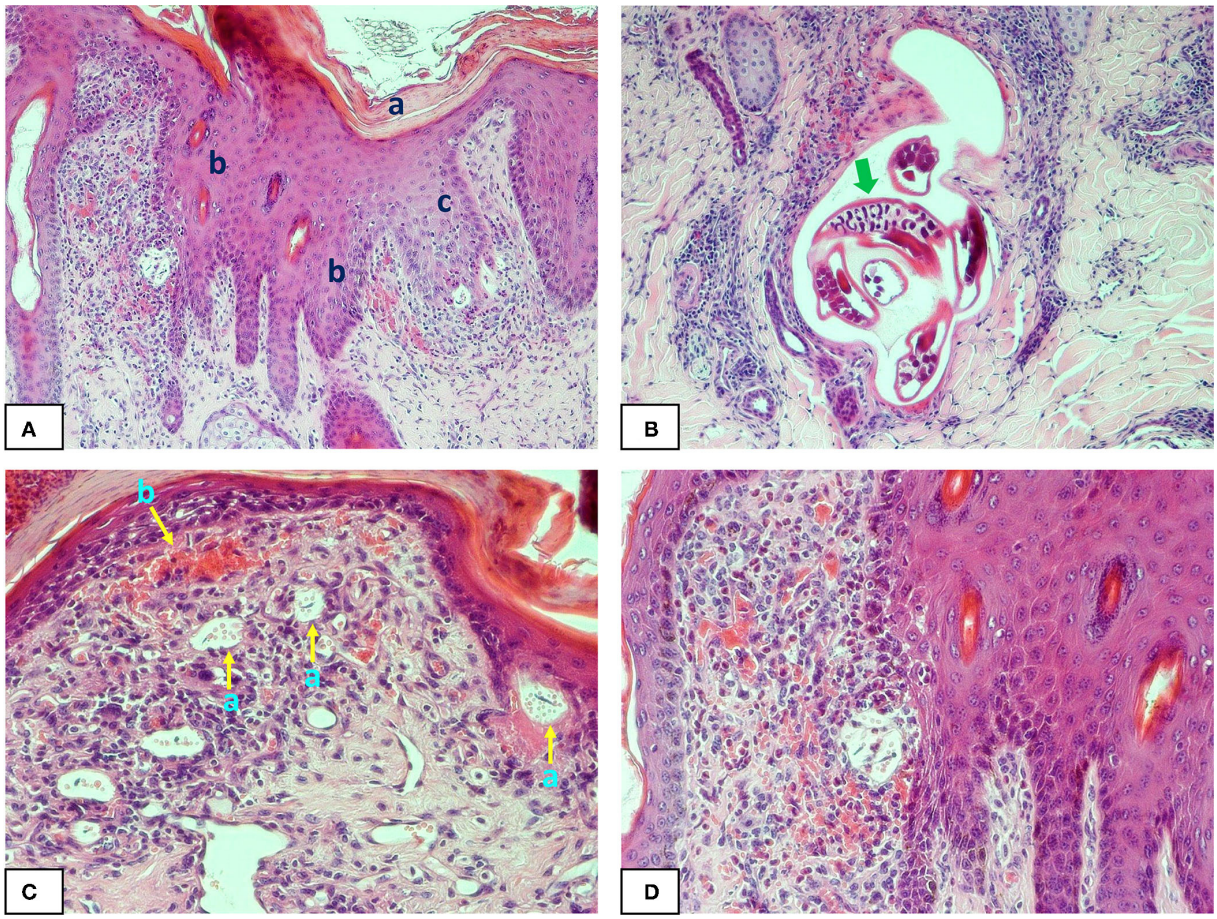

FIGURE 1
Photomicrographs of buffalo fly lesion histology: **(A)** shows hyperkeratosis (a) acanthosis (b) and spongiosis (c) in the epidermal layer of a *Stephanofilaria* infected lesion (100X); **(B)** shows adult *Stephanofilaria* in a cyst-like structure surrounded by inflammatory cells. The arrow shows the microfilariae within the gravid uterus of an adult female nematode (200X); **(C)** Shows microfilariae close to the epidermis and enclosed in a round to oval-shaped vitelline membrane that also contains numerous small spherical eosinophilic bodies (a) and hyperaemia (b) with extensive inflammation in the superficial dermis (200X); **(D)** shows acanthosis, severe hyperaemia and eosinophilic inflammation in *Stephanofilaria*-infected lesion (200X).

were significantly higher in lesions where bacteria were present (Figures 6E–J). Notably, there was no difference in eosinophil count between lesions with and without bacteria, in contrast to the difference observed between *Stephanofilaria* positive and negative lesions.

When the histopathological scores of *Stephanofilaria* positive BF lesions were compared with bacteria-infected lesions, although epidermal disruption was significantly higher in lesions with bacteria (Figure 7B), total epidermal damage was not significantly different (Figure 7A). Out of 17 bacteria-positive lesions, only two had zero scores for epidermal disruption. The score for total dermal damage was not significantly different between bacteria and *Stephanofilaria* positive lesions (Figure 7C). Adnexal damage was significantly higher in *Stephanofilaria*-infected lesions than in bacteria-infected lesions (Figure 7D) and *Stephanofilaria*-infected lesions had a significantly higher inflammation score (Figure 7E). Infiltration of eosinophils, neutrophils, macrophages, lymphocytes, and plasma cells was evident in both lesion groups but the scores for eosinophils, lymphocytes and plasma cells were significantly higher in *Stephanofilaria*-infected lesions (Figures 7F–J).

4. Discussion

Our study has highlighted the complex interplay amongst BFs, *Stephanofiliaria* and bacteria in BF lesion development. Johnson et al. (4) were the first to report the association between BF lesions and *Stephanofilaria* infection, which at that time was considered to be the main etiological agent of these lesions. However, Johnson et al. (5) only detected *Stephanofilaria* in 40% of the lesions they examined, an observation which the authors (5) attributed to the low sensitivity of histology and saline extraction techniques they used, the only detection methods available at that time. It is notable however that in controlled studies Johnson (3) was able to induce lesions similar in appearance to field BF lesions by exposing cattle held in fly proof cages to high numbers of BF not known to be infected with *Stephanofilaria* sp.

The recent development of a more sensitive qPCR for detecting the presence of *Stephanofilaria* in lesions and BFs (18) provided further evidence that *Stephanofilaria* is not present in all BF lesions and indeed appears to be completely absent from BF populations in some regions where BF lesions are prevalent (10). The availability of this test provided the opportunity to further examine the importance

10.3389/fvets.2022.971813

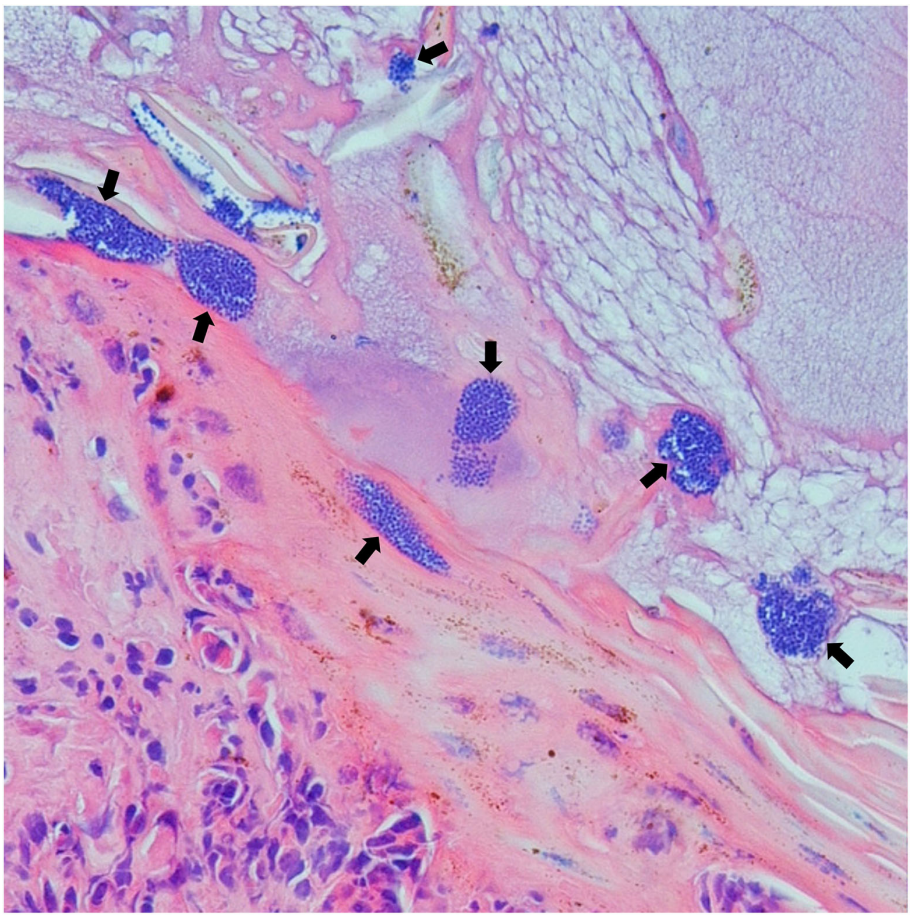

FIGURE 2
Photomicrograph (400X) of buffalo fly lesions shows multiple clusters of coccoid shaped bacteria (arrow) within the superficial crust.

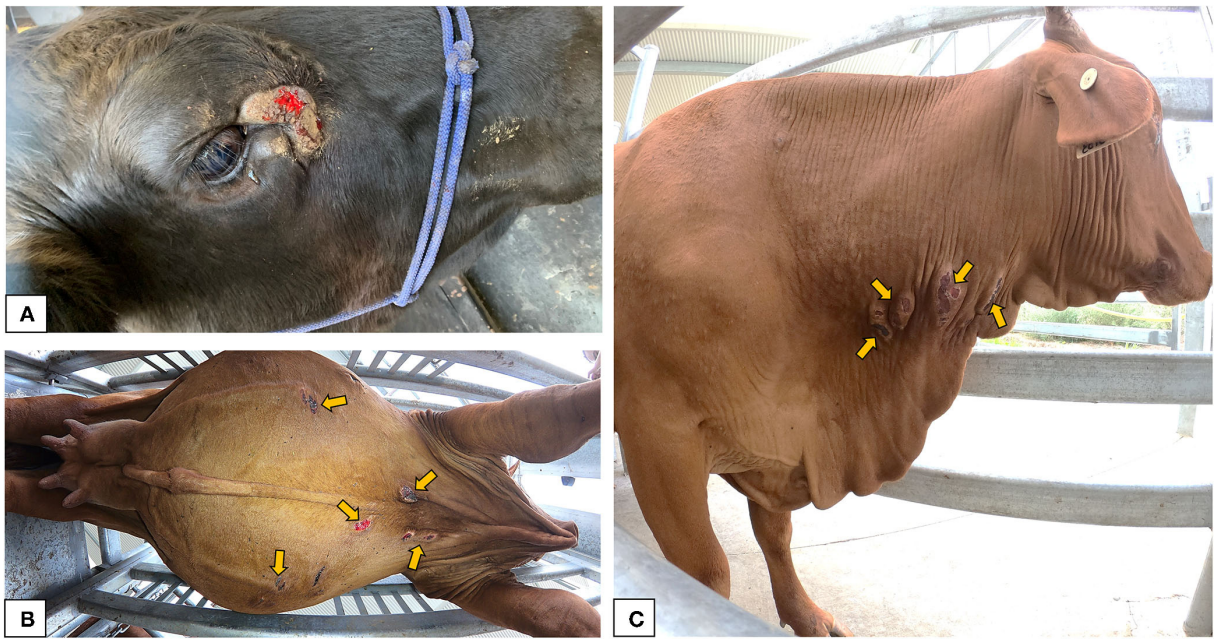

FIGURE 3
Gross appearance of the buffalo fly lesions: **(A)** lesion adjacent to the medial canthus of the eye in a Brangus steer indicating raised, circumscribed, hairless, ulcerative area partially covered with scab forming from the periphery; **(B)** multiple ulcerative to scab encrusted lesions near the ventral midline of a Droughtmaster cow; **(C)** multiple raised scabbed lesions on the neck of a Droughtmaster cow.

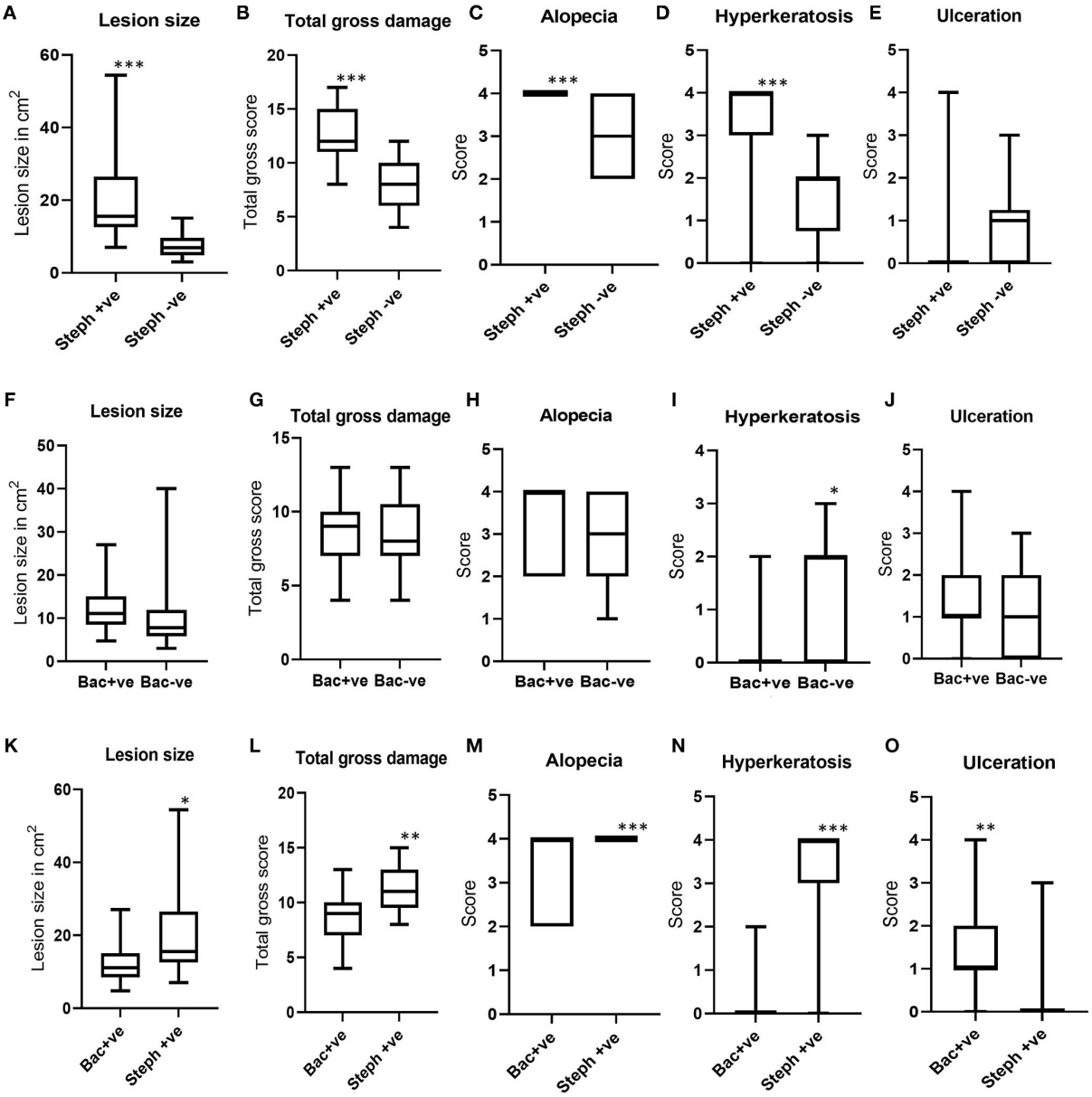

FIGURE 4
Boxplots showing the distribution of lesion areas and pathology scores for total gross damage, alopecia, ulceration, and hyperkeratosis. **(A–E)** Show gross pathology comparisons between *Stephanofilaria* positive (Steph +ve) and negative (Steph -ve) lesions; **(F–J)** Show gross pathology comparisons between bacteria positive (Bac +ve) and negative (Bac-ve) lesions; **(K–O)** Show gross pathology comparisons between Steph +ve and Bac +ve lesions (*$P < 0.05$, **$P < 0.01$, ***$P < 0.001$).

of potential causal factors in the development of BF lesions. Our study extended on previous work, comprehensively describing and differentiating the gross and microscopic pathological features of BF lesions involving potential comorbid etiological factors including *Stephanofilaria* sp., bacteria, and host immune response.

When the size of the BF lesions which had *Stephanofilaria* was compared to bacterial infected lesions or lesions negative for both *Stephanofilaria* and bacteria, the area of the lesions with *Stephanofilaria* was significantly greater than for either of the other two groups, extending up to 54 cm^2 area in some instances. However, even in the absence of both *Stephanofilaria* and bacteria, BF lesions could attain a lesion size up to 40 cm^2 and it is hypothesized that this could be a function of individual animal hypersensitivity to BF antigens as has been previously suggested for HF-associated lesions in some instances (16, 20). In addition, the presence of BF lesions causes mild to severe pruritus (7) manifesting as frequent scratching and rubbing of the lesions which could also act to increase the lesion area and the severity of the tissue damage.

Hyperkeratosis and alopecia were more obvious gross features in *Stephanofilaria* infected lesions than in lesions without nematodes and there was no difference between bacteria-infected and non-infected lesions for these gross changes. These observations are consistent with previous reports for *Stephanofilaria*-infected lesions (21, 22) and consistent with our casual observations that hyperkeratotic hairless lesions are commonly present in cattle in northern Queensland where *Stephanofilaria* is prevalent, but not

10.3389/fvets.2022.971813

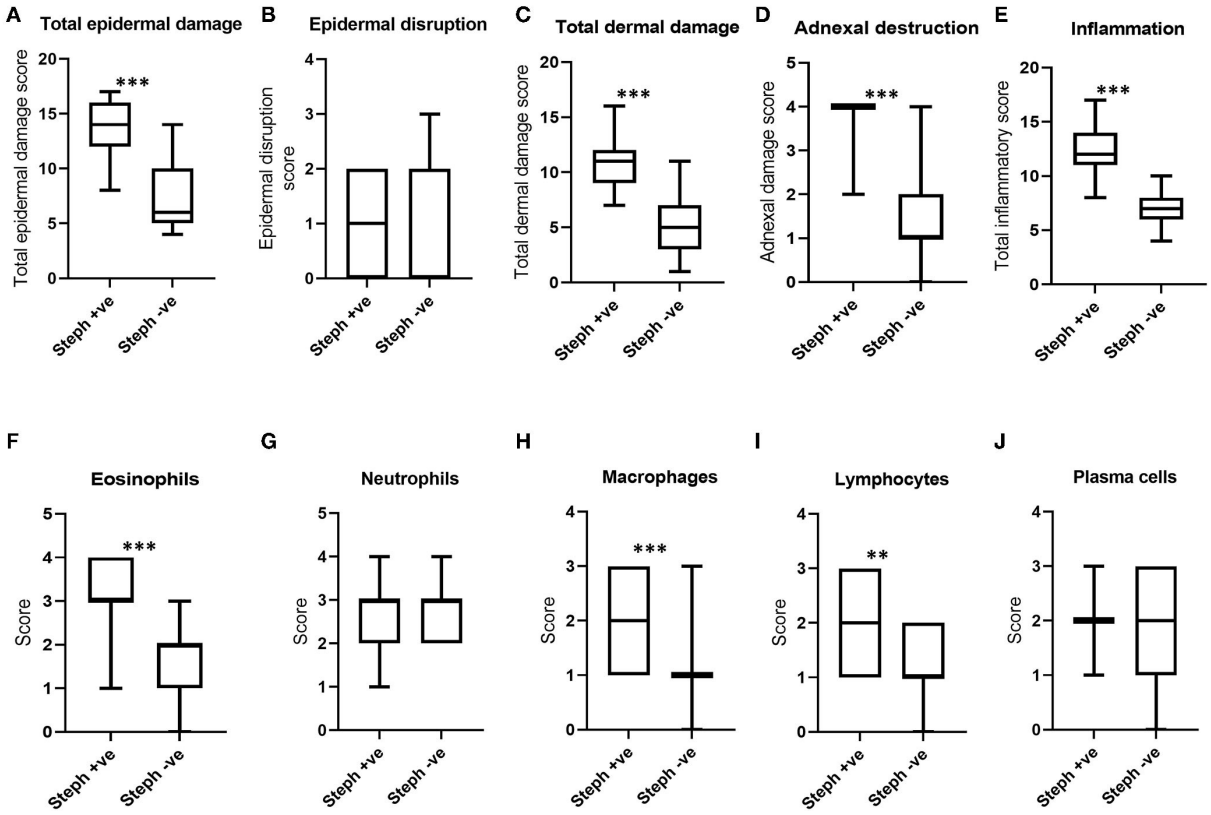

FIGURE 5
Boxplots **(A–D)** show the distribution of scores for total epidermal damage, epidermal disruption, total dermal damage and adnexal destruction scores for *Stephanofilaria* positive (Steph +ve) and negative (Steph -ve) lesions. The boxplots **(E–J)** show the total inflammation and individual inflammatory cell scores of these two groups ($^{**}P < 0.01$, $^{***}P < 0.001$).

commonly seen in southern Queensland where no *Stephanofilaria* was found (10). The occurrence of ulceration in bacteria-infected lesions is consistent with observations of Devriese and Derycke (23) and Hazarika et al. (24), who isolated *Staphylococcus hyicus* from ulcerative cattle skin lesions. Although the difference in ulceration scores between bacteria positive and negative lesions was not significant in our study, ulceration was significantly higher in lesions with bacteria than in lesions with *Stephanofilaria.*

Epidermal disruption was the most noticeable epidermal change associated with the bacterial infection in our study, but was not evident in *Stephanofilaria*-infected lesions. Johnson (3) also observed breached epidermis associated with bacterial growth in some lesions, but in common with the current study rarely observed this change in the *Stephanofilaria*-infected lesions. Naseem et al. (25) isolated *Staphylococcus hyicus* and *S. agnetis* from BF lesions and both these bacterial species were found to have exfoliative toxin type A and C genes. These toxins are epidermolytic serine proteases that can digest skin desmoglein, destroying keratinocyte adhesion and can cause epidermal damage (26). Similar toxins have been identified in *S. hyicus* isolates associated with exudative epidermitis in pigs ("greasy pig disease") (27). However, clinical expression of exfoliative toxins has not yet been confirmed and it is possible that these toxins are not actively involved in lesion development as we observed some uncircumscribed ulcerated lesions. Based on the isolation of *Staphylococcus* spp. from ulcerative BF lesions by Naseem et al. (25), it appears that the cocci-shaped bacterial colonies observed in this study are likely to be *S. hyicus* or *S. agnetis*, although *S. aureus* was also reported from similar lesions in dairy cattle associated with HF (17).

The varying degrees of hyperkeratosis and serocellular crust formation observed in all *Stephanofilaria* positive lesions are consistent with the epidermal changes described with typical *Stephanofilaria* spp. associated lesions (3, 21, 22). However, there was also a significant difference between bacteria negative and positive lesions in the hyperkeratotic score. Mild to moderate epidermal changes including spongiosis, hyperkeratosis, acanthosis, epidermal disruption and formation of serocelluar crust, were also noted in sections examined from BF lesions negative for *Stephanofilaria* and bacteria. Similar epidermal changes have also been reported by Mosca et al. (20) who attributed these lesions to an allergic response to HF feeding. The failure to detect either *Stephanofilaria* or bacteria in these lesions and the resemblance of these epidermal changes to those seen in the HF-associated lesions suggests that these changes could be immunopathological effects resulting from an immune response to BF feeding.

Both *Stephanofilaria*-infected and bacteria-infected lesions had more severe dermal damage and adnexal destruction than lesions without infection. Johnson (3) suggests that in *Stephanofilaria* infected lesions, this could be due to a severe localized host immune reaction, comprising histiocytes, lymphocytes and eosinophils, elicited by the adult nematodes present at the base of the hair follicle. A similar response was seen in our study where eosinophils were seen clustered around *Stephanofilaria* adult nematodes and microfilariae.

10.3389/fvets.2022.971813

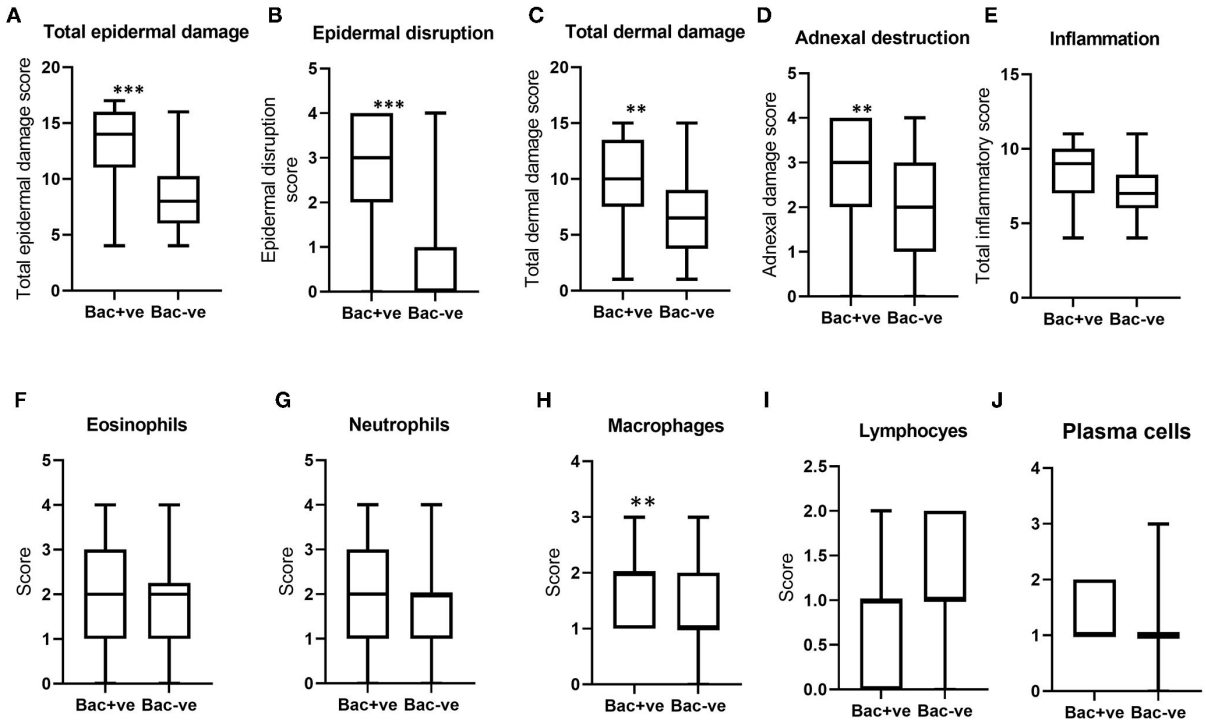

FIGURE 6
Boxplots **(A–D)** indicate the distribution of scores for total epidermal damage, epidermal disruption, total dermal damage and adnexal destruction for bacterial positive (Bac+ve) and negative (Bac-ve) lesions. Boxplots **(E–J)** show total inflammation and individual inflammatory cell scores of these two groups (**$P < 0.01$, ***$P < 0.001$).

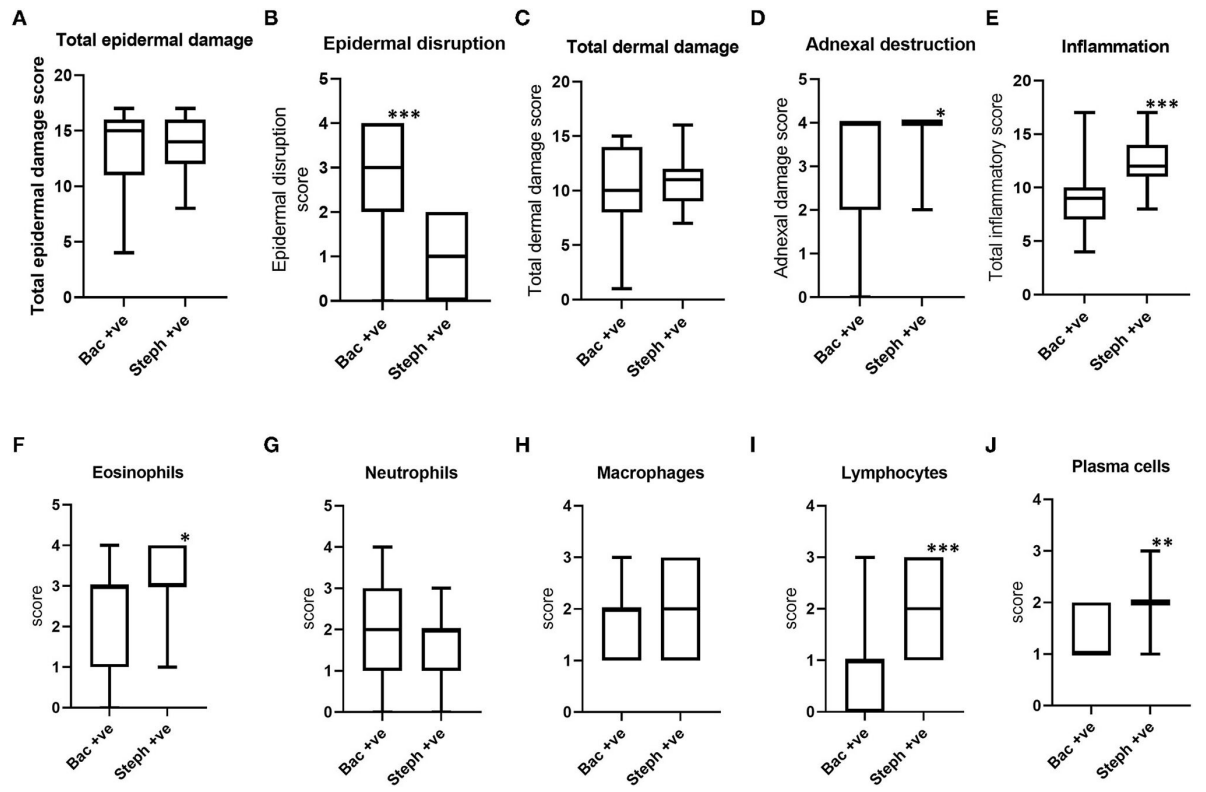

FIGURE 7
Boxplots **(A–D)** indicating the distribution of scores for total epidermal damage, epidermal disruption, total dermal damage and adnexal destruction scores for bacterial positive lesions (Bac+ve) and *Stephanofilaria* positive lesions (Steph +ve). Boxplots **(E–J)** show total inflammation and individual inflammatory cell scores of these two groups (*$P < 0.05$, **$P < 0.01$, ***$P < 0.001$).

This could subsequently result in the destruction of the hair follicles. Our study also observed complete loss or early signs of adnexal destruction in the BF lesions without *Stephanofilaria* infection. Thus adnexal destruction could result from an allergic response triggered by BF feeding in addition to the response to *Stephanofilaria*. Further evidence for this is provided by Mosca et al. (20) and Guglielmone et al. (28) who reported severe dermal oedema, folliculitis and furunculosis in HF-associated skin lesions without the presence of *Stephanofilaria*. There was also a significant difference in dermal damage and adnexal destruction scores between bacteria-infected and noninfected lesions, which suggest that bacterial infection could also play a role.

Although eosinophil infiltration in the superficial dermal layer was observed in all the BF lesions examined in this study, *Stephanofilaria* infection produced significantly higher eosinophilic infiltration, especially around the adult nematode and microfilariae. Eosinophilic dermatitis has also been reported by Whittier et al. (22) and Watrelot-Virieux and Pin (21) in *Stephanofilaria*-infected lesions. In contrast to our finding of significantly higher numbers of eosinophils, macrophages, and lymphocytes in *Stephanofilaria* positive lesions, Johnson (3) indicated eosinophils and neutrophils as the major inflammatory cells in lesions without *Stephanofilaria* whereas he observed histiocytes and lymphocytes were the predominant inflammatory cells in *Stephanofilaria*-infected lesions. The difference between our observations and those of Johnson (3) could be explained by difference in lesion stage when biopsied, as Patnaik (29) also observed lymphocytes and histiocytes dominated inflammatory response around dead worms in chronic infections of *Stephanofilaria assamensis*. The eosinophil-dominant inflammatory reaction in the BF lesions, without nematode or bacterial infection, may also indicate that hypersensitivity responses to BF feeding play a major role in lesion pathology, as a similar inflammatory pattern was reported for *Stephanofilaria* sp.-negative HF associated lesions (20, 28).

Overall our findings suggest that both *Stephanofilaria* and bacteria can play a role in BF lesion development. However, it appears that neither of these factors is essential for lesion development as we did not find either in 49% of the samples studied. This suggests that either there is a further unidentified factor involved, or that BF feeding can initiate lesion development without the involvement of other factors. *Stephanofilaria* infection caused more severe damage to the dermal layer, and could be a key factor in the formation of dry crusted type lesions often described in association with *Stephanofilaria* infection, whereas bacteria-infected lesions had more severe epidermal damage, which may drive the development of more open ulcerative lesions. Hypersensitivity to BF feeding is hypothesized to be an important contributing factor, particularly in the case of highly allergic individuals, as tissue damage and eosinophilic inflammation were important histological features in the absence of *Stephanofilaria* or bacteria. In addition, pruritis and rubbing of lesion areas, likely mediated by IgE based responses, may exacerbate the severity of lesions and resultant hemorrhage. Another possible explanation for the causality of lesions with unidentified co-factors could be the physical damage to skin caused by abrading mouthparts of BFs during feeding. As BFs have been shown to vector both *Stephanofilaria* (3, 8) nematodes and *Staphylococcus* spp. bacteria (25) they could also contribute to the development and severity of lesions by this means. Furthermore, lesions are often seen to persist well after the BF season has ended, suggesting that infection with *Stephanofilaria* or bacteria or any unknown factor may increase the longevity of lesions.

Treatment of cutaneous lesions associated with BF or HF, most commonly targeting *Stephanofilaria* nematodes, have given variable results (3, 14). Notably, the best effect has generally been seen with macrocyclic lactones that affect both the nematodes and flies (3, 14, 30), reported from the areas where both flies and *Stephanofilaria* are prevalent. Our results suggest that approaches that directly target BF, in addition to *Stephanofilaria*, could give more consistent treatment results and including a bacteriaocide, may also help to limit the severity of lesions.

Data availability statement

The original contributions presented in the study are included in the article/supplementary material, further inquiries can be directed to the corresponding author.

Ethics statement

The animal study was reviewed and approved by the University of Queensland Animal Ethics approval no. 2021/AE000054.

Author contributions

MN, RA, and PJ contributed to conceptualization and design of study. MN, RA, AR, CC, MM, and MK contributed to methodology. MN and RA contributed to investigations and data visualization. MN and PJ contributed to statistical analysis. PJ, RA, AR, CT, MM, CC, and AT supervised this study. PJ and AT contributed to project administration and acquisition of funding. MN contributed to writing original draft, review, and editing. RA, CC, PJ, AR, AT, CT, and MM contributed to review and editing. All authors contributed to the article have approved the submitted version.

Funding

This study was funded as part of the Meat and Livestock Australia (MLA) Donor company-funded project (Grant No. P.PSH.798).

Acknowledgments

The authors thank the Meat and Livestock Australia (MLA) Donor Company, Grant P.PSH.0798, for funding this research. We thank the JBS Townville staff for access to cattle hides for sample collection. We are also grateful to the University of Queensland Pinjarra Hills Research Precinct staff (Ms. Alison Moore and Mr. Tom Connelly) for their help in sample collection.

Conflict of interest

The authors declare that the research was conducted in the absence of any commercial or financial relationships that could be construed as a potential conflict of interest.

Publisher's note

References

1. James P, Madhav M, Brown G. Buffalo flies (*Haematobia exigua*) expanding their range in Australia. In: Hendrichs J, Pereira R, Vreysen MJB, editor. *Area-wide Integrated Pest Management: Development and Field Application*. FL: CRC Press (2020). p. 463–82. doi: 10.1201/9781003169239-24

2. Jonsson NN, Mayer DG. Estimation of the effects of buffalo fly (*Haematobia irritans exigua*) on the milk production of dairy cattle based on a meta-analysis of literature data. *Med Vet Entomol.* (1999) 13:372–6. doi: 10.1046/j.1365-2915.1999.00179.x

3. Johnson SJ. *Studies of stephanofilariasis in Queensland*. [PhD thesis]. Douglas, QLD: James Cook University (1989).

4. Johnson SJ, Parker RJ, Norton JH, Jaques PA, Grimshaw AA. *Stephanofilariasis* in cattle. *Aust Vet J.* (1981) 57:411–3. doi: 10.1111/j.1751-0813.1981.tb00544.x

5. Johnson SJ, Arthur RJ, Shepherd RK. The distribution and prevalence of *stephanofilariasis* in cattle in Queensland. *Aust Vet J.* (1986) 63:121–4. doi: 10.1111/j.1751-0813.1986.tb07679.x

6. Jonsson NN, Matschoss AL. Attitudes and practices of Queensland dairy farmers to the control of the cattle tick, *Boophilus microplus*. *Aust Vet J.* (1998) 76:746–51. doi: 10.1111/j.1751-0813.1998.tb12306.x

7. Sutherst RW, Bourne AS, Maywald GF, Seifert GW. Prevalence, severity, and heritability of *Stephanofilaria* lesions on cattle in central and southern Queensland, Australia. *Aust J Agric Res.* (2006) 57:743–50. doi: 10.1071/AR05265

8. Shaw SA, Sutherland IA. The prevalence of *Stephanofilaria* in buffalo fly, *Haematobia irritans exigua*, in central Queensland. *Aust J Entomol.* (2006) 45:198–201. doi: 10.1111/j.1440-6055.2006.00545.x

9. Hibler CP. Development of *Stephanofilaria stilesi* in the horn fly. J Parasitol. (1966) 52:890–898. doi: 10.2307/3276527

10. Naseem MN, Raza A, Fordyce G, McGowan M, Constantinoiu C, Turni C, et al. Detection and distribution of *Stephanofilaria* sp. in buffalo flies and buffalo fly skin lesions in cattle in Queensland, Australia. *Vet Parasitol.* (2022) 305:109715. doi: 10.1016/j.vetpar.2022.109715

11. Holroyd RG, Hirst DJ, Merrifield AW, Toleman MA. The effect of spraying for buffalo fly (*Haematobia irritans exigua*) on infestations, growth rate and lesion development on *Bos indicus* x *B.* taurus cattle in the dry tropics of north Queensland. *Aust J Agric Res.* (1984) 35:595–608. doi: 10.1071/AR9840595

12. Foil LD. Tabanids as vectors of disease agents. *Parasitol.* (1989) 5:88–96. doi: 10.1016/0169-4758(89)90009-4

13. Newsholme SJ, Verster AJ, Jacobs JC. Bovine skin lesions of possible filarial origin associated with heavy horn fly infestations (*Haematobia meridiana*). *Onderstepoort J Vet Res.* (1983) 50:73–5.

14. Silva L, Elias RR. de-Moura I, Fioravanti MCS, Borges M, de-Oliveira L, et al. Epidemiological aspects and treatment of parasitic lesions similar to *stephanofilariasis* disease in nursing cows. *Semin Cienc Agrar.* (2010) 31:689–98. doi: 10.5433/1679-0359.2010v31n3p689

15. Miyakawa VI, Reis ACF, Lisbôa JAN. Epidemiological and clinical features of *stephanofilariasis* in dairy cows and diagnostic methods. *Pesqui Vet Bras.* (2009) 29:887–93. doi: 10.1590/S0100-736X2009001100004

16. Edwards JF, Wikse SE, Field RW, Hoelscher CC. Herd DB. Bovine teat atresia associated with horn fly (*Haematobia irritans irritans* (L))-induced dermatitis. *Vet Pathol.* (2000) 37:360–4. doi: 10.1354/vp.37-4-360

17. Owens WE, Oliver SP, Gillespie BE, Ray CH, Nickerson SC. Role of horn flies (*Haematobia irritans*) in *Staphylococcus aureus*-induced mastitis in dairy heifers. *Am J Vet Res. (*1998) 59:1122–4.

18. Naseem MN, Raza A, Allavena R, McGowan M, Morgan JAT, Constantinoiu C, et al. Development and validation of novel PCR assays for the diagnosis of bovine *stephanofilariasis* and detection of *Stephanofilaria* sp. nematodes in vector flies. *Pathogens.* (2021) 10:1211. doi: 10.3390/pathogens10091211

19. Meyerholz DK, Tintle NL, Beck AP. Common pitfalls in analysis of tissue scores. *Vet Pathol.* (2019) 56:39–42. doi: 10.1177/0300985818794250

20. Mosca M, Vabret M, Randleff-Rasmussen P, Pin D. Skin lesions in Aubrac cows strongly associated with fly bites (*Haematobia irritans*). *Vet Dermatol.* (2018) 29:254–e94. doi: 10.1111/vde.12530

21. Watrelot-Virieux D, Pin D. Chronic eosinophilic dermatitis in the scrotal area associated with *stephanofilariasis* infestation of charolais bull in France. *J Vet Med B Infect Dis Vet Public Health.* (2006) 53:150–2. doi: 10.1111/j.1439-0450.2006.00923.x

22. Whittier CA, Murray S, Holder K, McGraw S, Fleischer R, Cortes-Rodriguez N, et al. Cutaneous filariasis in free-ranging Rothschild's Giraffes (*Giraffa camelopardalis rothschildi*) in Uganda. *J Wildl Dis.* (2020) 56:234–8. doi: 10.7589/2018-09-212

23. Devriese LA, Derycke J. *Staphylococcus hyicus* in cattle. *Res Vet Sci.* (1979) 26:356–8. doi: 10.1016/S0034-5288(18)32893-5

24. Hazarika RA, Mahanta PN. Dutta, GN, Devriese LA. Cutaneous infection associated with *Staphylococcus hyicus* in cattle. *Res Vet Sci.* (1991) 50:374–5. doi: 10.1016/0034-5288(91)90146-F

25. Naseem MN, Turni C, Gilbert R, Raza A, Allavena R, McGowan M, Constantinoiu C, Ong CT, Tabor AE, James P. The role of *Staphylococcus agnetis* and *Staphylococcus hyicus* in the pathogenesis of buffalo fly skin lesions in cattle. *Microbiol Spectr.* (2022) 10:e00873-22. doi: 10.1101/2022.03.11.483979

26. Fudaba Y, Nishifuji K, Andresen LO, Yamaguchi T, Komatsuzawa H, Amagai M, et al. *Staphylococcus hyicus* exfoliative toxins selectively digest porcine desmoglein 1. *Microb Pathog.* (2005) 39:171–6. doi: 10.1016/j.micpath.2005.08.003

27. Wegener HC, Andresen LO, Bille-Hansen V. *Staphylococcus hyicus* virulence in relation to exudative epidermitis in pigs. *Can J Vet Res.* (1993) 57:119–25.

28. Guglielmone AA, Gimeno E, Idiart J, Fisher WF, Volpogni MM, Quaino O, et al. Skin lesions and cattle hide damage from *Haematobia irritans* infestations. *Med Vet Entomol.* (1999) 13:324–9. doi: 10.1046/j.1365-2915.1999.00167.x

29. Patnaik MM. Histopathology of lesions in *stephanofilariasis* and onchocerciasis in buffalo and cattle. *Ind J Anim Sci.* (1982) 52:159–66.

30. Miyakawa VI, Reis ACF, Lisbôa JAN. Comparison among therapeutic protocols for *stephanofilariasis* in dairy cows. *Semin Cienc Agrar.* (2012) 33:343–50. doi: 10.5433/1679-0359.2012v33n1p343

frontiers | Frontiers in Veterinary Science

TYPE Review
PUBLISHED 02 February 2023
DOI 10.3389/fvets.2023.1086003

OPEN ACCESS

EDITED BY
Francisco José Pallarés,
University of Cordoba, Spain

REVIEWED BY
Ismael Hernández Avalos,
Faculty of Higher Studies Cuautitlán, National Autonomous University of Mexico, Mexico
Alejandro Casas Alvarado,
Autonomous Metropolitan University, Mexico

*CORRESPONDENCE
Rachel Layton
✉ Rachel.Layton@csiro.au

SPECIALTY SECTION
This article was submitted to Veterinary Infectious Diseases, a section of the journal Frontiers in Veterinary Science

RECEIVED 31 October 2022
ACCEPTED 09 January 2023
PUBLISHED 02 February 2023

CITATION
Layton R, Layton D, Beggs D, Fisher A, Mansell P and Stanger KJ (2023) The impact of stress and anesthesia on animal models of infectious disease. *Front. Vet. Sci.* 10:1086003. doi: 10.3389/fvets.2023.1086003

The impact of stress and anesthesia on animal models of infectious disease

Rachel Layton[1]*, Daniel Layton[1], David Beggs[2], Andrew Fisher[2], Peter Mansell[2] and Kelly J. Stanger[1]

[1]Australian Centre for Disease Preparedness, CSIRO, Geelong, VIC, Australia, [2]Faculty of Veterinary and Agricultural Sciences, Melbourne Veterinary School, University of Melbourne, Melbourne, VIC, Australia

Stress and general anesthesia have an impact on the functional response of the organism due to the detrimental effects on cardiovascular, immunological, and metabolic function, which could limit the organism's response to an infectious event. Animal studies have formed an essential step in understanding and mitigating infectious diseases, as the complexities of physiology and immunity cannot yet be replicated *in vivo*. Using animals in research continues to come under increasing societal scrutiny, and it is therefore crucial that the welfare of animals used in disease research is optimized to meet both societal expectations and improve scientific outcomes. Everyday management and procedures in animal studies are known to cause stress, which can not only cause poorer welfare outcomes, but also introduces variables in disease studies. Whilst general anesthesia is necessary at times to reduce stress and enhance animal welfare in disease research, evidence of physiological and immunological disruption caused by general anesthesia is increasing. To better understand and quantify the effects of stress and anesthesia on disease study and welfare outcomes, utilizing the most appropriate animal monitoring strategies is imperative. This article aims to analyze recent scientific evidence about the impact of stress and anesthesia as uncontrolled variables, as well as reviewing monitoring strategies and technologies in animal models during infectious diseases.

KEYWORDS

infectious disease research, laboratory animal welfare, impacts of anesthesia, impacts of stress, animal monitoring, animal models of disease, animal immunity, surgical stress

Introduction

The complex interplay of the immune system and physiology of infection can't be replicated *in vitro* and is very limited in *ex vivo* studies (1), meaning animal models are still essential to the study of infectious disease (2). Animal models are used to study infectious diseases in both human and veterinary medicine, but the results of these studies are vulnerable to a series of variables such as handling, cage environment, and technical procedures, which can generate varying degrees of stress (3). The physiological and immunological consequences of stress, in addition to other factors such as the induction of general anesthesia, have the potential to alter scientific outcomes resulting in less applicable science (4). Additional consequences of these uncontrolled variables in infectious disease research are poorer animal welfare outcomes (5). There is increasing societal scrutiny and expectations on how animal research is conducted by the general public, with increasing expectations that research involving animals is both well-justified and conducted in a manner that not only minimizes animal suffering but results in an overall positive welfare experience (6). Continually improving the applicability of science from the laboratory to real-world application is therefore crucial, in addition to enhancing animal welfare by adapting and further developing best-practice methods of laboratory animal care and management (5). Both objectives can be achieved *via* the identification and reduction of study variables.

Of the many variables that can impact upon studies of infectious disease, the effects of stress on immunity and disease susceptibility are well-documented (7, 8). Stress is a complex and multi-faceted process (chronic vs. acute, beneficial vs. adverse effects) and consequently, there are inherent difficulties in identifying what causes stress in different species under diverse study conditions (9). Stress experienced by animals in disease research can be caused by the disease itself and accompanying inflammatory responses (10, 11), as well as regular animal handling and repeated procedures and interventions (3–5, 12). The factors that cause stress also promote the organism's response as a homeostasis-related compensatory mechanism or returning to homeostasis, by modifying the physiological parameters and generating compensatory metabolic, hormonal or neurological responses that can alter study results (13–16). The impacts of stress can be detrimental to both animal welfare and scientific outcomes in animal models (17), but stress is certainly not the only significant cause of study variables in infectious disease research.

The administration of sedatives and anesthetics is a common requirement in animal studies for sample collection (18). Yet despite its accepted and regular use in animal studies of infectious disease, general anesthesia has multi-modal effects on immune system functioning (19). Although general anesthetics are known to interfere with the immune system causing immunosuppression, repeated and regular anesthetic events commonly occur throughout animal studies. Whilst the use of anesthesia plays a crucial role in the effective management of animal welfare and meeting scientific objectives, potential immunomodulatory effects of anesthetic induction should not be ignored. In addition, the induction of anesthesia often introduces its own negative impacts on animal welfare such as cognitive dysfunction (20). This dysfunction can present as a decrease in learning, memory capacity or inability to concentrate, only if the appearance of central inflammation and neuronal apoptosis is induced, where synaptic loss could promote neuroinflammation (21).

Accurately quantifying the impacts of stress and anesthesia as variables in animal models of infectious disease relies on the methods of assessment being used. In addition to the more traditional clinical and subjective assessment methods, recent developments in non-invasive monitoring technology are beginning to be adapted and utilized for the collection of physiological data in animal studies of disease. This includes the measure of heart rate and heart rate variability in rodent stroke models (22), the use of collar monitors for the identification of subclinical mastitis in dairy cattle (23), and the detection of respiratory disease in pigs using infrared and conventional imaging (24). This multi-faceted monitoring approach leads to an improved understanding of disease, enhanced animal welfare *via* monitoring and humane endpoint refinement, and the potential to more effectively identify and mitigate the detrimental effects of stress and anesthesia on infectious disease study outcomes (25).

This review aims to describe how stress and anesthesia act as uncontrolled variables that impact upon scientific and animal welfare outcomes in animal studies of infectious disease. It discusses how the effects of stress and anesthesia can be understood and addressed during the planning and conduct of *in vivo* infectious disease studies, and presents novel recommendations for future research to better understand and mitigate the physiological and immunological impacts of stress, pain, and anesthesia. Current and emerging monitoring strategies and technologies to assess animal health and disease most effectively are described. In addition, this review presents recommendations for the future refinement and enhanced uptake of optimized monitoring strategies in experimental animal models of infectious disease.

Methodology

Literature was searched *via* PubMed, Google Scholar, and Scopus *via* keyword searches for all topics reviewed. For the analysis of animal monitoring methods between 2012/2013 to 2020/2021 a search of title, abstract, and key words on web of science was conducted using the following search categories: Veterinary Sciences, Infectious Diseases, Agriculture multidisciplinary, and Zoology. Animal monitoring methods were categorized and search terms used as described in Table 1.

The impact of stress on infectious disease study outcomes

In the context of laboratory animals stress can be defined as a negative emotional experience accompanied by predictable biochemical, physiological, cognitive, and behavioral changes that are directed either toward altering the stressful event or accommodating to its effects (26). This definition is in line with the founding principles of humane animal research developed by Russel and Burch (27), which defines distress in laboratory animals as a central nervous state of a certain rank on a scale, in the direction of the mass autonomic response which if protracted, would lead to the physiologic stress syndrome (27). Animals maintained in laboratory conditions are often far removed from their evolved or natural environment, and this can predispose these animals to experiencing greater levels of stress (4). In addition, keeping animals in controlled environments away from stress factors may predispose animals to experience a greater degree of stress, resulting in neurobiological, hormonal, and metabolic compensatory responses that result in the development of chronic stress (16, 28).

The effects of chronic stress on immunity and disease susceptibility in humans and animals is well-established in the literature, as demonstrated in a study by Cohen et al. (29). The authors experimentally exposed healthy human volunteers to rhinoviruses with varied histories of experience with chronic stressors. Their results showed those individuals with recent long-term exposure to a threatening stressful experience demonstrated glucocorticoid receptor resistance and were at higher risk of succumbing to a viral infection. In addition, glucocorticoid receptor resistance predicted the production of higher levels of pro-inflammatory cytokines and disease among infected subjects. This is a clear demonstration of not only the effects of chronic stress on increasing the risk of disease susceptibility, but also the mechanisms that lead to reduced disease resistance. Zhou et al. (30) have also demonstrated compromised immunity due to chronic stress in animal cancer models. The authors applied chronic mild stress to mice with cancerous tumors undergoing immunotherapy and found that tumor regression occurred in mice undergoing immunotherapy, but this regression was attenuated in mice undergoing mild chronic stress (30). These results have implications for infectious disease

TABLE 1 Categories of animal monitoring and search terms used per category.

	Machine learning and algorithms	Subjective assessment and operator scoring	Clinical parameter assessment	Sensors and wearable devices	Video monitoring
Search terms used within category	- Machine learning animal disease - Machine learning animal disease - Algorithm animal disease	- Subjective assessment animal disease - Clinical scoring animal disease - Grimace score animal disease - Operator assessment animal disease	- Heart rate animal disease - Rectal temperature animal disease - Blood pressure animal disease - Respiration animal disease	- Sensors animal disease - Wearable animal disease	- Video monitoring animal disease - Infrared monitoring animal disease - Motion detection monitoring animal disease

research, where compromised immunity can result in altered disease outcomes.

Such altered disease outcomes were demonstrated by Gervasi et al. (31). The authors experimentally altered levels of the stress hormone corticosteroid *via* a hormone implant in two groups of zebra finches (10 finches implanted with low corticosterone devices and 10 finches implanted with high corticosterone devices), with a third control group of 10 finches not receiving any corticosteroid implants. Blood was collected from all finches prior to exposure to West Nile virus, with the average corticosterone level of control birds being ∼15 ng/ml, low dose corticosterone group birds ∼50 ng/ml, and high dose corticosterone group birds ∼100 ng/ml (31). They found that although all birds became infected, only birds with elevated corticosteroid had viral loads at or above the infectious threshold. Further, no mortality was observed in control birds, whilst mortality rates of 40 and 70% were observed in low corticosterone and high corticosterone implanted finches, respectively. This suggests that immunosuppression caused by elevated glucocorticoid stress hormones leads to a higher susceptibility to disease. In a similar study in mice, Zhou et al. (32) inoculated cancer cells into mammary fat pads of control, stress, and stress + chewing groups where mice were provided wooden blocks to chew on whilst undergoing psychosocial stress. They found that psychosocial stress enhanced tumor growth, but chewing behavior markedly inhibited this growth by ameliorating the effects of stress, and in turn modulating stress hormones and their receptors (32). This highlights the importance of identifying and reducing chronic stressors in animal studies in order to prevent the development of physiological compensatory mechanisms that lead to chronic stress responses, such as impaired immune and altered metabolic, neurobiological, and cardiovascular functions (16, 28). As laboratory animal stress can result from many common animal husbandry, environmental, and procedural factors, there is considerable potential for everyday stressors to impact upon scientific outcomes in infectious disease studies (33).

Manual handling and blood collection are two such stressors that are known to cause stress-induced immunomodulation in laboratory animals. Balcombe et al. analyzed data from 80 published *in vivo* studies and determined changes in physiologic parameters correlated with stress (including elevated serum corticosterone, glucose, blood pressure, and heart rate) were associated with both manual handling and blood collection (34). Similar stress responses in mice resulting from noise pollution were also observed in a study by Jafari et al. (35). The authors compared glucocorticoid responses in 32 mice exposed to daily traffic noise (16 mice exposed daily during the light cycle, 16 mice exposed daily during the dark cycle) and equal numbers of control mice not exposed to noise. They found that mice exposed to traffic noise had significantly higher glucocorticoid levels than mice not exposed to traffic noise during both light and dark cycles, regardless of sex (35). Noise sources and levels in animal laboratories are numerous and varied, and can commonly include music, human voices, incidental noise from animal husbandry, and vocalization from other animals in the room (including distress vocalization). The demonstration of elevated glucocorticoid responses in mice exposed to traffic noise indicates the ease in which noise can act as a chronic stressor that has the potential to influence study outcomes and compromise animal welfare. This highlights the importance of identifying and mitigating chronic animal stressors in the laboratory, and indicates that the early recognition of stress factors could help to prevent, control, and diminish the effect of these elements as study variables. A study by Marcon et al. (36) investigated the effects of environmental enrichment of zebrafish responses to chronic stress. The authors submitted two groups of zebra fish, housed with or without environmental enrichment, to unpredictable chronic stress. They found that environmental enrichment attenuated the effects of chronic stress, with zebrafish provided with environmental enrichment displaying significantly less anxiety-like behaviors and reduced cortisol and reactive oxygen species compared to controls with no environmental enrichment (36). In all of these studies, the mechanism of activation of stress responses was found to be directly *via* the hypothalamic-pituitary-adrenal (HPA) axis in the form of enhanced production of glucocorticoids, or *via* neural network changes over time in response to enhanced activation of sympathetic nervous activity and chronic exposure to glucocorticoids, rendering glucocorticoid responses more sensitive to stress as described in Figure 1 (16, 28, 37–39).

The HPA activation and stress responses observed in studies of laboratory animal stressors demonstrate poorer welfare outcomes for laboratory animals experiencing chronic stress. A study by Jin et al. (40) takes this a step further, by directly demonstrating the effects of heat stress on immunity and disease susceptibility in mice. The authors infected mice with H5N1 highly pathogenic avian influenza that were previously held in either thermoneutral conditions or placed under chronic heat stress. They found that mice subjected to chronic heat stress exhibited significantly reduced local immune responses in the respiratory tract, in addition to reduced dendritic cell maturation and reduced mRNA levels of IL-6 and interferon (40). Mortality rate and viral load in lungs was also significantly higher in mice that had experienced chronic heat stress, indicating chronic heat stress caused reduced immunity and increased viral susceptibility. When viewed as a whole, the literature demonstrates substantial and varying impacts of stress on HPA axis activity and immune responses in laboratory animals. When interpreting the

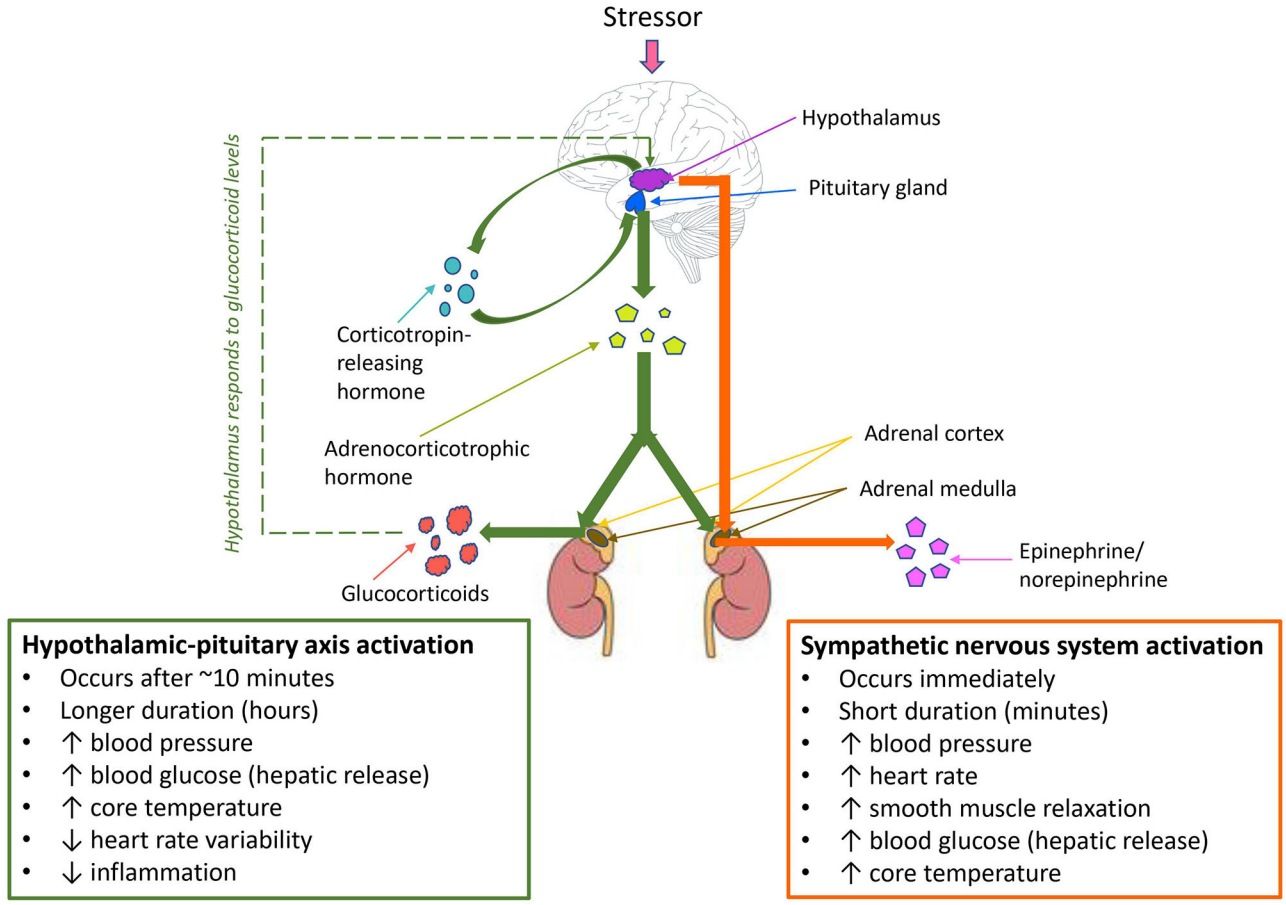

FIGURE 1
Hypothalamic-pituitary axis (HPA) activation, sympathetic nervous system activation, and compensatory mechanisms in response to stress. Sympathetic nervous system activation occurs as the primary response to stress, followed by HPA axis activation where the stressor is prolonged or chronic. A negative feedback loop leads to compensatory mechanisms *via* the HPA axis in response to threats to homeostasis.

effects of stress in the context of animal studies of infectious disease, it is important to consider whether the stressor is likely to be defined as acute or chronic as described in Figure 2 (29, 30, 34, 35, 40, 41). In infectious disease research, both immunosuppressive (commonly resulting from chronic stress) and temporary immunoenhancing /inflammatory (commonly resulting from acute stress) effects are equally important to identify, but understanding the effect is critical for both mitigation of the stressor and interpretation of potential impacts on study results (42). Whilst decreasing laboratory animal stress is crucial for reducing study variables, stress alone is not the only variable that influences outcomes in studies of infectious disease. The administration of preanesthetic drugs and those used for the maintenance of general anesthesia generate a physiological adaptation response that consists of metabolic, neuroendocrine, hemodynamic, immunological, and behavioral changes through the neurosecretion of chemical mediators, which also have the potential to influence the results of infectious disease research (16).

Physiological impacts of general anesthesia in infectious disease studies

Using anesthesia in animal studies of disease can be crucial for the management of animal welfare, operator safety, and the achievement of scientific objectives. This is particularly true for performing invasive procedures, or when conscious restraint or sample collections cause unacceptable stress (43). Whilst the benefits of anesthesia are significant, the use of sedatives, analgesics and anesthetics must be balanced with their own potential risks to animal welfare and altered study outcomes from anesthesia effects (4). Different authors mention that anesthetics can have a depressant effect on the immune, cardiovascular, and metabolic response in healthy animals (44–46). These effects are in addition to behavioral and cognitive deficits, neuroinflammation, and mitochondrial dysfunction (47–52). Figure 3 describes the commonly observed effects of anesthesia (44–46, 48–55).

General anesthesia causes a multitude of physiological effects, which are apparent even in healthy animals. Reductions in arterial pressure of ~30% in healthy dogs have been reported after induction with propofol (5 mg/Kg over 30 s followed by a continuous infusion of 25 mg/Kg/h) (56), as well as medetomidine (0.01 mg/Kg), butorphanol (0.2 mg/Kg) and acepromazine (0.02 mg/Kg) (57). Mrazova et al. (57) further demonstrated an increased respiratory rate and decreased heart rate after fentanyl administration (0.01 mg/Kg), and decreased heart rate and respiratory rate after medetomidine administration in healthy dogs. In sick animals, the effects and potentially detrimental consequences of anesthesia can be exacerbated. A cohort study conducted by Brodbelt et al. (58)

10.3389/fvets.2023.1086003

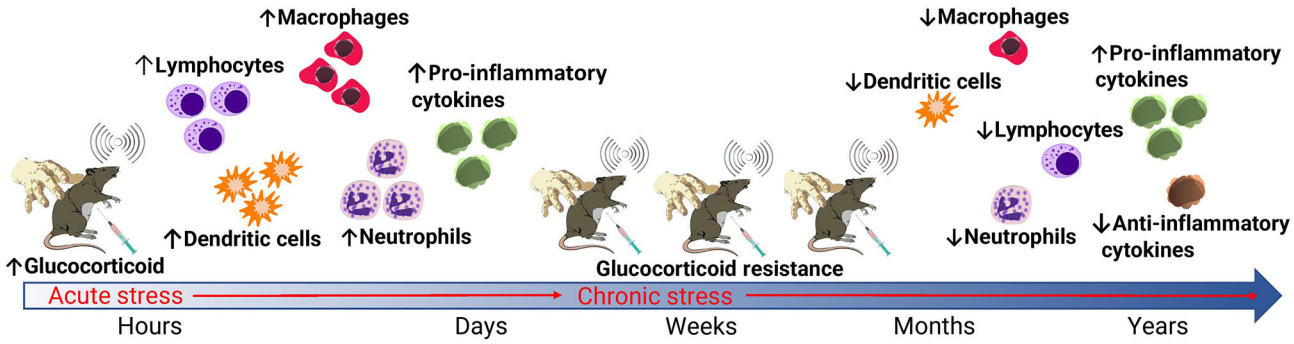

FIGURE 2
Effects of acute and chronic stress on glucocorticoid and immune responses in laboratory animals. Common routine stressors of laboratory animals include manual handling, blood collection, and noise. When these stressors are acute, enhanced glucocorticoid production *via* stimulation of the sympathetic nervous system and HPA axis result in an enhanced immune response. When stressors are chronic, the development of glucocorticoid resistance leads to immunosuppression. This primarily occurs *via* a decreased and altered leukocyte production in addition to a reduced production of anti-inflammatory cytokines *via* a negative feedback loop.

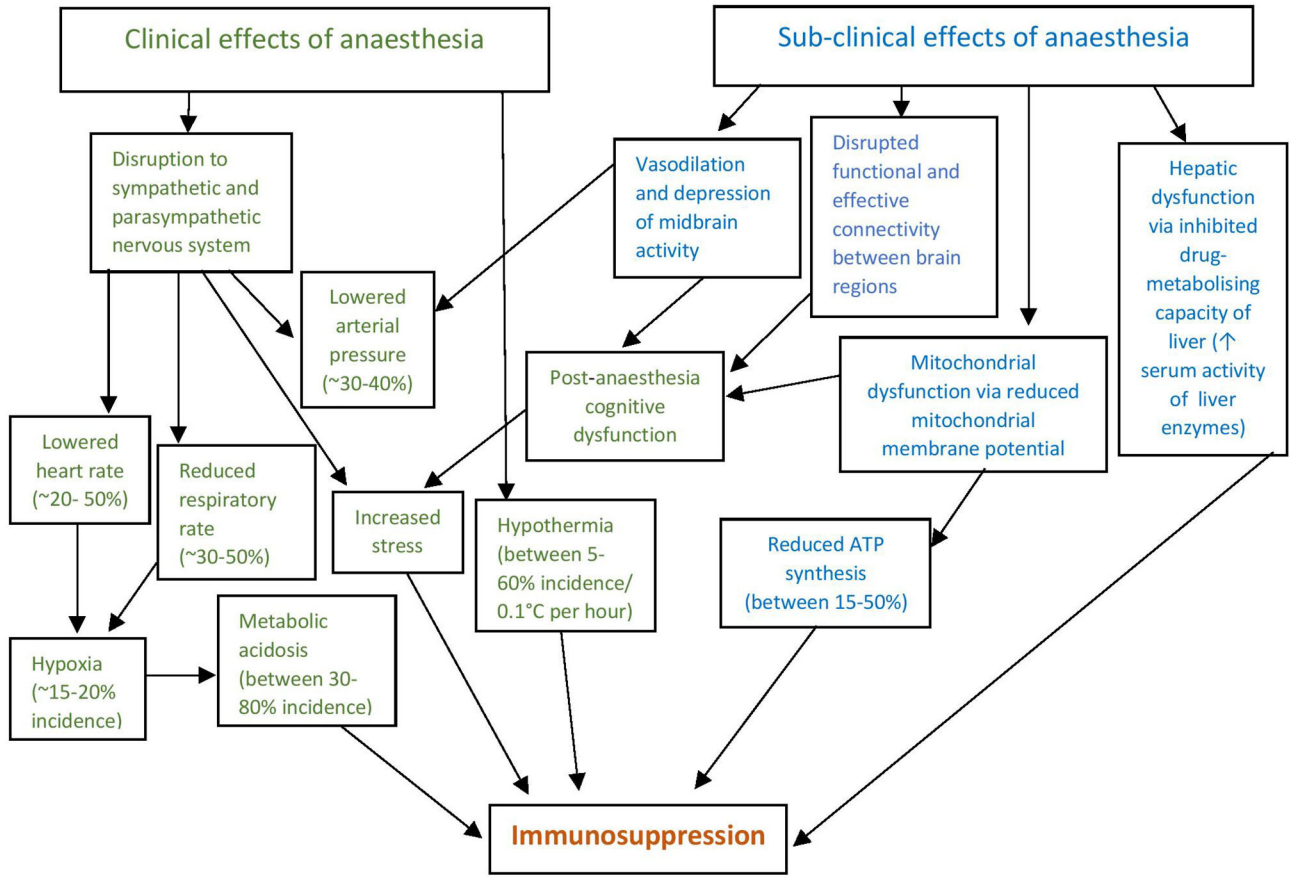

FIGURE 3
Clinical and subclinical effects of anesthesia lead directly and indirectly to immunosuppression. Clinical effects are those that can be detected by monitoring and assessment, whilst sub-clinical effects are not readily detected. In both instances anesthetic effects either directly result in immunosuppression or result in further physiological effects that in turn result in immunomodulation, most commonly immunosuppression *via* a reduced inflammatory response. The incidence and significance of effects vary depending on the anesthetic agents used, time spent under anesthesia, species being anesthetized and degree of supportive care provided.

surveyed 117 veterinary practices in the United Kingdom, analyzing data obtained from 98,036 dogs, 79,178 cats and 8,209 rabbits that had been anesthetized and sedated using various anesthetic and sedation regimes. The authors found that in healthy animals with no pre-existing disease, the risk of death from anesthesia or sedation was 0.05% for dogs, 0.11% for cats, 0.73% for rabbits, and 3.8% for guinea pigs (58). However, these risks increased dramatically for sick animals-−1.33% (two–three-fold increase)

for dogs, 1.40% (12–13-fold increase) for cats, and 7.37% (10-fold increase) for rabbits. This dramatic increase in mortality risk in sick compared to healthy animals illustrates the significantly enhanced impacts of anesthesia on compromised animals. Given that disease research models typically result in illness, the impact of anesthesia on animal welfare and resultant study outcomes in disease research is of concern. More specifically, the effects of a standard ketamine/xylazine mouse anesthetic regime were investigated by Schuetze et al. (59). By anesthetizing both young (2.14 ± 0.23 months) and aged (26.31 ± 2.15 months) mice with a standard dose, the authors found that 0 of the 26 young mice died under anesthesia, compared to 4 out of 26 aged mice (15.4% mortality) (59). In addition to the physiological variables that could be introduced to surviving mice in a disease study, the loss of such a large number of mice in a study can reduce statistical power, risking the ability to achieve study objectives (60). Studies into the mortality of commonly used research species that are not commonly anesthetized in veterinary practice, such as pigs, are needed to more accurately quantify the mortality rate of anesthesia in these species. This will allow for further understanding of anesthetic risk levels, which is important for study design and improved research animal management practices (61).

An important consequence of general anesthesia is a reduced ability to thermoregulate and maintain core body temperature within a thermoneutral zone. Contributing factors to this reduced thermoregulatory ability under general anesthesia include vasodilation leading to greater heat loss to the surrounding environment, changes to central brain structure activity, cooling effects of disinfectant application, and heat loss resulting from surgical penetration of the body cavity (62). These factors can be mitigated by the use of management techniques peri- and post-anesthesia such as effective warming and supportive care. However, where this is not optimized, the physiological and physical effects of anesthesia can be exacerbated (63). The ability to provide optimal supportive care to reduce the impacts of anesthesia in research animals is highly variable, and dependent on many factors. The core temperature of smaller animals (such as rodents) is relatively easy to maintain through portable heat mats and lamps and is largely deemed necessary and considered standard practice (64). Even short-term interruptions to thermoregulation from anesthetic induction can easily lead to serious complications or death in smaller species, due in part to the large surface-area-to-volume ratio of small mammals (65). For larger research animals (such as pigs and cattle) the management of anesthesia-associated issues is often more difficult, due to the increased complexity of providing effective warming and other means of supportive care to larger animals in the infectious disease research setting. Rodriguez-Diaz et al. (66) analyzed the incidence of perioperative inadvertent hypothermia in dogs and cats. The authors demonstrated that despite the standard use of warming equipment and supportive care protocols in veterinary practice, a high incidence of perioperative anesthesia-associated hypothermia was identified (66). Given that warming and supportive care for larger animals undergoing anesthesia in infectious disease studies is often less optimized compared to the clinical veterinary setting, it is reasonable to expect the incidence and severity of hypothermia to be even more pronounced than that identified by Rodriguez-Diaz et al. (66). Hypothermia has significant and wide-ranging effects on the immune response, with lowered core temperature driving anti-inflammatory/resolution-type effector functions (67). In animal infectious disease studies, using anesthesia and the associated varying degrees of hypothermia that can result (often at repeated timepoints) is therefore likely to impact upon the immune response to the diseases being studied, but further direct research is required to quantify these potential effects. Adverse neurological effects have been described during an induced hypothermic circulatory arrest for cardiac surgery (68), but this degree of hypothermia (reduction in core temp to 18 degrees) is not seen as a consequence of standard anesthesia (69).

Besides immunomodulation, anesthesia-associated hypothermia results in an increased risk of coagulopathies, most likely to occur *via* two mechanisms- reduced platelet function, and the functional impairment of several enzymes of the coagulation cascade and subsequent reduction in clot formation (70). This has significance for infectious disease studies in general, but even more specifically for the study of diseases that cause coagulopathies. Petrilli et al. (71) demonstrated a mechanism by which coagulopathic infectious disease morbidity outcomes are influenced by disruptions to the coagulation cascade. The authors retrospectively studied patients with COVID-19 and identified that elevated d-dimer levels were strongly associated with critical illness (71). D-dimer is a product of fibrin degradation and is only present in plasma as a result of activation of the coagulation cascade, as occurs after degradation of blood clots (72). The findings of Petrilli et al. (71) therefore demonstrate that increased coagulopathy and clot formation leads to increased morbidity in COVID-19 patients. Building on this observation, Wang et al. (73) studied retrospective cases of COVID-19 patients and found that elevated d-dimer is a significant component of disseminated intravascular coagulation, which develops due to abnormalities with the coagulation cascade and is a leading cause of in-hospital deaths in COVID-19 patients. These findings suggest that anesthesia-associated hypothermia could result in altered study outcomes in SARS-CoV-2 animal studies, by pre-disposing and increasing the susceptibility of research animals to coagulopathies and clot formation which in turn increases mortality risk (74). Additionally, hypothermia induces multiple cardiopulmonary effects including reductions in heart rate, respiratory rate, and systolic blood pressure (75). As COVID-19 can elicit severe acute respiratory syndrome and cardiac and lung injury, changes to cardiopulmonary function as a result of hypothermia may also increase disease susceptibility or lead to alterations in disease course and presentation (76). These effects may also be true for other infectious diseases that can result in coagulopathy such as Ebola, Dengue, and Chikungunya virus, but further investigation is required to determine this.

Whilst there is a distinct lack of research demonstrating how general anesthetic induction specifically affects infectious disease study outcomes, a recent study by Nash (77) reported on the administration of a low pathogenic strain of influenza to mice anesthetized with ketamine/xylazine and to a control group not administered anesthetic. They found that mice not administered anesthetic displayed very mild or no signs of disease, whilst anesthetized mice succumbed to disease (77). This study directly demonstrates the effects of general anesthesia on disease outcomes and shows the need for more direct studies in varied animal models of infectious disease. The impact of anesthesia on disease outcomes in mice was also demonstrated in an earlier study by Penna et al. (78). Mice were anesthetized with either ketamine

or halothane and inoculated with a non-lethal Influenza A virus. They found that mice anesthetized with ketamine had higher viral titres 12 h post-inoculation, and a more rapid lung infiltration of neutrophils and monocytes suggesting differences in the recruitment of immunological effector cells (78). This study shows that different types of anesthesia can result in different immune responses, and therefore cause different disease outcomes. As there are multiple anesthetic combinations used in animal models of disease research, the variables and immunomodulation that can be introduced by different anesthetics are therefore many and varied.

Impacts of anesthesia-induced immunomodulation on infectious disease outcomes

The wide range of anesthetic combinations utilized in animal models of disease makes identifying the effect of every drug combination, on every species and animal strain, an impossible task. Instead, identifying the known immune-altering consequences of drug classes commonly used in infectious disease research demonstrates the wide-ranging impacts of routinely utilized anesthetics.

Alpha-2 adrenergic agonists

Commonly used alpha-2 adrenergic agonists include medetomidine, dexmedetomidine, and xylazine, acting on alpha-2 receptors in the central nervous system and peripheral tissues (79). The physiological impacts of these drugs, particularly on the cardiovascular and pulmonary systems, are well-described in laboratory and small animal medicine and most notably include hypotension/hypertension, bradycardia, and decreased cardiac output (80).

Literature on the immune effects of alpha-2 agonists in this field is less abundant yet studies from human patients demonstrate immunomodulation caused by alpha-2 adrenergic agonists (81–83). Wang et al. (84) analyzed 4,842 human surgical patients, approximately half of which were administered dexmedetomidine for anesthesia. They found that patients administered dexmedetomidine had significantly decreased interleukin (IL)-6 and tumor necrosis factor-α (TNFα) in the blood, and increased IL-10 (84). Compared to the control group the authors also found a significant increase in natural killer cells, B cells, $CD4^+$ T cells and a significant decrease in CD8 T cells. Additionally, they observed an increase in the ratios of CD4:CD8 T cells. Overall, the administration of dexmedetomidine in the peri-operative period reduced hyper-inflammatory effects of surgery on the immune system, resulting in improved immune functioning. Interestingly, chickens administered clonidine, another alpha adrenergic agonist, at various doses demonstrated that higher clonidine doses resulted in increased circulating B cells and IgG levels (85). As IgG is critical to host protection during infection and virus neutralization (86), the increased levels caused by clonidine may also have an immunoenhancing effect. However, further studies are required to determine the binding mechanisms of the circulating IgG observed to determine this. Studies in sepsis (87) and myocardial injury (88) demonstrate anti-inflammatory effects of dexmedetomidine primarily as a result of reduced cytokine activity. Anti-inflammatory effects of dexmedetomidine in human infectious disease was also demonstrated by Hamilton et al. (89). The authors conducted a retrospective analysis of 214 adult human patients with severe COVID-19 requiring invasive mechanical ventilation and sedation. They found that risk of mortality was 58.2% lower in patients that were administered dexmedetomidine for sedation within 3.4 days of intubation compared to patients that were not (89). In addition to the reduction in pro-inflammatory cytokine production, dexmedetomidine has also been shown to reduce inflammation by suppressing catecholamine release (90, 91) and reducing immune cell activity and recruitment at sites undergoing inflammatory signaling (92, 93). Further studies in animal models are required to ascertain the anti-inflammatory effects of alpha-2 adrenergic agonists on various infectious disease models. Romifidine is an alpha-2 agonist used primarily in horses, and of which physiological effects have been studied and documented in the literature (94). There is an absence of studies on the effects of romifidine on the immune system, therefore the potential effects on infectious disease study outcomes are currently not known.

Alpha-2 agonists are also known to cause neuroendocrine changes, including blocking insulin release from beta cells and elevating blood glucose levels (95). These effects were demonstrated in a study by Connell et al. (96), who monitored blood glucose levels of diabetic and non-diabetic rats anesthetized with xylazine, medetomidine or pentobarbital. The authors found that both medetomidine and xylazine, but not pentobarbital, elicited marked hyperglycemia in non-diabetic rats. A study by Zhu et al. (97) demonstrates how hyperglycemia may impact upon infectious disease study outcomes. The authors conducted a retrospective, multi-centered study of 7,337 human cases of COVID-19, among which 752 had type 2 diabetes (97). They found that well-controlled blood glucose was associated with markedly lower mortality compared to individuals with poorly controlled blood glucose and hyperglycemia. For studies of infectious disease, this suggests that hyperglycemia induced by the use of alpha-2 agonists could alter disease course and severity and impact upon study outcomes. Alpha-2 agonist effects on beta cells also include the suppression of growth hormone and testosterone (98) and changes to serum prolactin, which acts as both a hormone and a cytokine and has been demonstrated to play an important role in autoimmunity (99). The effects of prolactin on infectious disease study outcomes are not known, and further studies are needed to determine both the effects of prolactin on infectious disease susceptibility and the neuroendocrine impacts of alpha-2 agonists in infectious disease studies.

Overall, the literature is increasingly demonstrating that alpha-2 adrenergic agonists have an overall anti-inflammatory effect on immune responses in relation to infectious disease outcomes. It is important to note that the bulk of research published on the immune altering effects of this drug class is based on single use administration. The immunomodulatory effects of repeated or chronic use, as is common in infectious disease animal studies, is not known and warrants further research.

NMDA receptor antagonists

N-methyl-D-aspartate (NMDA) receptor antagonists act by blocking NMDA receptors in the brain, which interact with the neurotransmitter glutamate (100). Ketamine is a commonly used NMDA receptor antagonist that is known to have a range of effects on

the immune system. Takahashi et al. (101) conducted laparotomies on mice anesthetized with either sevoflurane or ketamine, followed by intraperitoneal administration of *Escherichia coli* to induce septicemia. The authors found that mice administered ketamine had suppressed TNF-α and reduced phagocytosis. Immunosuppressive effects of ketamine were also found in a study by Gao et al. (102), who isolated peripheral blood mononuclear cells from human blood samples and incubated the cells in either the presence or absence of ketamine. They found that ketamine inhibited Th2 cell differentiation, which are a key cell responsible for the regulation of humoral immune responses (102). Braun et al. (103) demonstrated further effects of ketamine *in vitro* by exposing human immune cells to various doses of ketamine. The authors found that ketamine induced apoptosis in lymphocytes *via* the mitochondrial pathway at lower doses, and *via* necrosis at higher concentrations (103). Additionally, a study by Zeng et al. (104) investigated the effects of ketamine both *in vitro* and *in vivo*, and found that ketamine inhibited the maturation of dendritic cells. The mechanism of this dendritic cell inhibition by ketamine was further explored by Laudanski et al. (105), who obtained monocytes from 36 human subjects and stimulated differentiation into immature dendritic cells in the absence or presence of ketamine at (100, 10 or 1 μg/ml for 5 days). The authors found that at 10 μg/ml or higher, ketamine diminished the differentiation of monocytes into immature dendritic cells *in vitro* (105). As a key role of dendritic cells is the presentation of antigen during infection, the results from both Zeng et al. (104) and Laudanski et al. (105) demonstrate ketamine to have immunosuppressive effects.

As ketamine is administered for non-anesthetic purposes such as chronic pain management, immunosuppressive and anti-inflammatory effects of ketamine have also been demonstrated over repeated use (106) including a reduction in pro-inflammatory cytokines IL-6, IL-1, IL-8 and TNF-α (107). Li et al. (108) further explored the effects of ketamine on hippocampal inflammatory cytokines in both acute and chronic administration mouse models. They found that in mice administered ketamine acutely or chronically, IL-1β and IL-6 levels were both elevated in the hippocampus (108). Additionally, levels of TNF-α were elevated in the single dose model, but significantly decreased in mice administered multiple dose or long-term ketamine. This finding of elevated inflammatory cytokines differs from the bulk of literature that demonstrates immunosuppressive effects of ketamine. This may be due to this study measuring hippocampal cytokine levels as opposed to serum levels, as changes in hippocampal cytokines have been shown to not be reflective of serum cytokine profiles (109). Whilst the measurement of hippocampal cytokines is appropriate to the objectives of this study, in the context of infectious disease serum cytokine levels provide a more relevant and accurate measure of cytokine activity due to differences in cytokine perfusion through the blood-brain barrier (110). The downregulation of systemic inflammatory cytokines by ketamine is also supported by the known mechanisms of ketamine-induced immunosuppression, which includes the downregulation of inflammatory cytokine-producing macrophages and associated protein activation factors (111). Ketamine affects a variety of key immune functions, with the literature demonstrating these effects of be overwhelmingly immunosuppressive even as the result of a single dose.

Inhalational anesthetics

Inhalational anesthetics provide the benefit of rapid induction and recovery, the ability to swiftly adjust anesthetic depth as required, and their suitability for use in a wide range of companion, laboratory and livestock animal species (112). Rapid recovery from inhalational anesthesia has the potential benefits of reduced physiological impacts (for example, a reduced incidence and severity of hypothermia) (53). However, immunosuppressive effects of commonly used inhalational agents still occur. Isoflurane, and sevoflurane have all been shown to decrease cytokines, neutrophil cell numbers and adhesion, macrophages and phagocytosis, and natural killer cell cytotoxicity (113). All of these immune effects result in isoflurane and sevoflurane being immunosuppressive. Desflurane is another volatile anesthetic that has also been studied for its effects on immune responses, as demonstrated by Kalimeris et al. (114). The authors compared bronchiolar lavage fluid from 27 pigs anesthetized with either desflurane, sevoflurane or propofol (nine pigs per group), or not anesthetized (an additional four pigs). They found that pigs anesthetized with sevoflurane and desflurane had decreased alveolar macrophages and increased lymphocyte counts compared to controls and pigs anesthetized with propofol (114). The results of these authors reaffirm the immunosuppressive effects of inhalational anesthetics on possibly local cellular immunity, which coincided with a study carried out by Woo et al. (115). The authors assessed immune responses in patients undergoing anesthesia with desflurane. They found that patients had higher levels of neutrophils after desflurane anesthesia, providing an immune protective response (115). In contrast to the literature on isoflurane, desflurane and sevoflurane, Arruda et al. (116) collected blood from patients before and after surgery with halothane anesthesia, and found significant increases in proinflammatory cytokines IL-6 and IL-8. The significantly higher degree of inflammation that halothane induces compared to other inhalational anesthetics has resulted in the largely discontinued use of halothane, as it is this increased production of pro-inflammatory cytokines that can lead to halothane-induced liver injury (117). Studies on desflurane indicate a combination of immunosuppressive and immunoenhancing effects, whilst the literature on isoflurane and sevoflurane demonstrates overwhelmingly immunosuppressive effects. The literature demonstrates that halothane has a substantial inflammatory effect on the immune response, leading to hyper-inflammation which can ultimately result in organ damage and a compromised immune response.

General anesthesia and viral proliferation

Besides these immunomodulatory effects of specific drug classes, the administration of general anesthetics can directly affect viral proliferation. A key mechanism of how this occurs is *via* changes to the balanced redox state, which shifts toward oxidant conditions during viral infection (118). Alternatively, a shift away from oxidant conditions, due to higher levels of antioxidants as part of the balanced redox stat, have variable effects on viral growth and can result in viral inhibition or facilitation (119). Erbas et al. (120) studied the effect of general anesthetic agents on the oxidant/antioxidant redox balance in human patients after surgery. They found that both sevoflurane and propofol significantly increased antioxidant levels, whilst desflurane significantly increased oxidant levels (120). Therefore, the antioxidant and immunomodulatory effects of desflurane, sevoflurane, and propofol are likely to affect health

and disease outcomes and may affect scientific outputs in animal disease studies.

Opioids

Opioids act on mu and kappa receptors in differing ways; as agonists (e.g., morphine, fentanyl), agonist-antagonists (e.g., butorphanol), antagonists (e.g., naloxone), or partial agonists (e.g., buprenorphine) (121). The main opioid receptors are expressed by T lymphocytes and macrophages (122), making these immune cells susceptible to modulation by opioids *via* binding to mu receptors present on these cells (123). Morphine is the most used analgesic in humans and is known to have a wide range of immunosuppressive effects (124) but a more commonly used opioid in infectious disease animal studies is buprenorphine. In a study by Filipczak-Bryniarska et al. (125), mice were administered either buprenorphine, morphine or oxycontin and immune responses compared to baseline. The authors found that mice administered buprenorphine had an enhanced humoral immune response *via* B cell activation, compared to a reduced B cell response in mice administered morphine and no B cell response in mice administered oxycontin (125). Allen and Kendall (126) also investigated the immunosuppressive effects of buprenorphine, by inoculating mice with ovalbumin followed by either saline or slow-release buprenorphine. They found that antibody responses between control and treatment groups did not differ, though IL-10 was significantly higher in mice administered slow-release buprenorphine compared to the control group (126). This indicates that whilst buprenorphine did cause some degree of immune suppression *via* an increase in IL-10 (an anti-inflammatory cytokine), the effects on overall immune function was negligible.

Butorphanol is another commonly used opioid in laboratory animal medicine and is known to have dose-dependent anti-inflammatory and immunosuppressive effects (127). One mechanism of the anti-inflammatory action of butorphanol was demonstrated in a study by Luan et al. (128). The authors induced lung tissue injury in mice *via* sepsis resulting from intraperitoneal lipopolysaccharide injection, then administered butorphanol to one group of mice whilst the other group remained untreated. They found that mice administered butorphanol had lower numbers of pro-inflammatory and higher numbers of anti-inflammatory macrophages compared to untreated mice (128). A reduction in pro-inflammatory macrophages result in a reduction in IL-1β, IL-6, and IL-12, whilst an increase in anti-inflammatory macrophages causes an increase in cytokines including IL-10 (129). These cytokines, both pro-inflammatory and anti-inflammatory, play an important role in the immune response to pathogens, particularly for the development in humoral immunity (130). Modulation of cytokines by butorphanol may therefore affect study outcomes in animal models of infectious disease.

The literature shows that opioids, including commonly used veterinary opioids buprenorphine and butorphanol, can cause immunosuppression *via* a reduced production and proliferation of macrophages and T lymphocytes, with a subsequent modulation of cytokines. When combined with the changes to innate immunity *via* macrophage phagocytosis, both buprenorphine and butorphanol can alter the immune response to pathogens in infectious disease studies, potentially altering study outcomes by enhancing disease susceptibility.

Whilst the literature demonstrates that the majority of opioids have overwhelmingly immunosuppressive effects a notable exception is tramadol, an opioid utilized for analgesia. The immunomodulatory effects of tramadol have previously been shown to cause immunoenhancement *via* significantly enhanced NK cell activity and IL-2 production when administered acutely, but with ongoing chronic administration these immune effects disappeared (131). In other studies, the use of tramadol has been shown to preserve, but not stimulate, immune function when compared to other opioids such as morphine (132). This includes *in vitro* studies showing that morphine decreased monocyte phagocytosis but tramadol did not (133); morphine, methadone, and oxycodone inhibited IL-6 production but tramadol did not (134); that NK cell count decreases were less pronounced in gastric patients administered tramadol compared to morphine (135); and that tramadol administration reduced localized oedema and hyperalgesia without affecting immune mechanisms (136). Whilst the majority of literature demonstrates preservation of immune responses by tramadol, particularly with multiple or chronic administration, some studies have also shown immunosuppressive effects. Bastami et al. (137) investigated the *in vitro* effects of various opioids on TNF-α and IL-8 release. They found that tramadol had the greatest inhibitory effects on IL-8 and TNF-α release compared to morphine, ketobemidone and fentanyl (137). In the context of infectious disease research, tramadol demonstrates potential as an analgesic for moderate pain that results in less immunomodulation than other opioids. Further research is required to determine the effects of tramadol on disease presentation and course in animal models of infectious disease.

Local anesthetics

Local anesthesia is a useful tool for both the reduction or elimination of pain in minor procedures and as an addition to multi-modal anesthesia in more invasive surgical procedures (138). Local anesthetics work by blocking voltage-gated sodium channels, which suppresses action potentials in excitable tissues and in turn blocks the transmission of pain impulses (139). The effects of amide local anesthetics (including lidocaine and bupivacaine) on immune responses have been demonstrated in studies of human cancer patients. By reducing the pain response post-surgery and reducing the need for opioids, local anesthetics have been shown to reduce the incidence of tumor recurrence (140). In addition, Piegeler et al. (141) demonstrated direct effects of amide local anesthetics on cancer metastases. The authors incubated lung cancer cells with TNF-α in the presence or absence of amide local anesthetics (lidocaine and ropivacaine). They found that both ropivacaine and lidocaine inhibited tumor cell migration and had an anti-inflammatory effect (141). In the context of infectious disease research, an anti-inflammatory response may impact upon study outcomes, with both ropivacaine and lidocaine being shown to reduce TNF-α-induced upregulation of CD11b/CD18 surface expression on polymorphonuclear leukocytes (PMNs) (142). Another study by Kolle et al. (143) compared the effects of lidocaine and bupivacaine *in vitro* on PMNs, and also found a reduction in granulocyte defense mechanisms for both local anesthetics. These findings are likely to be more relevant for some infectious disease models than others; for example, where local anesthesia is applied to sites of viral inoculation, resulting in reduced PMN activity at the sites of viral replication. In most studies, the locally suppressive effects of local anesthetics on PMNs are unlikely to be of concern given

the broad and systemic nature of many infectious disease animal models. Overall, local anesthetics are known for their ability to inhibit excessive inflammatory responses, particularly at the regional level, without causing excessive impairment to host immunity (144).

An additional consideration for the use of local anesthetics in animal models of infectious disease is the potential for an overall reduction in study variables introduced by pain or stress. Given that the use of local anesthesia is so effective at reducing both pain and stress responses (145, 146), the potential direct confounding effects are likely less than the indirect confounding effects of pain and stress if local anesthesia is warranted but not used. Further research comparing different anesthetic and animal management regimes (e.g., general vs. local anesthetic) is warranted in animal models of disease to determine the impacts of local anesthesia on infectious disease study outcomes.

Non-steroidal anti-inflammatory drugs

The use of non-steroidal anti-inflammatory drugs (NSAIDs) for the management of pain and inflammation in animals has the benefit of reduced immunomodulatory effects compared to corticosteroids, and act by competitively inhibiting the formation of the inflammatory mediator prostaglandin (147). This limiting of prostaglandin formation occurs *via* NSAID inhibition of cyclo-oxygenase enzymes, of which there are three forms; COX-1, a constitutive member of most tissues including gastrointestinal mucosa, platelets, endothelium, kidneys and uterus; COX-2, which is also constitutive but highly restricted under basal conditions but is upregulated significantly during inflammation; and COX-3, which is mainly expressed in the heart and cerebral cortex (148). Meloxicam is a commonly used NSAID in veterinary medicine and research that inhibits COX-2 (149), and has been demonstrated to effect the immune system by enhancing splenocyte IL-2 release and inhibiting the production of TNF-α, IL-10, and IL-4 in mice (150). In contrast, meloxicam has also been shown to increase TNF-α production in guinea pigs, due to the negative feedback control exerted by prostaglandins on TNF-α formation (151). Prostaglandins play a crucial role in immune responses by supporting activation of dendritic cells whilst suppressing their ability to attract naïve, effector and memory T-cells, modulating chemokine production, and inhibiting the attraction of proinflammatory cells while enhancing local accumulation of regulatory T-cells (152). As meloxicam suppresses prostaglandin release (153), this is likely to have at least some degree of immunosuppression during the infectious disease process. However, a study by Kolstad et al. (154) investigated the impacts of meloxicam, administered at the time of immunization, on antibody titres of mice. They found that use of meloxicam to manage immunization side effects did not affect antibody titres (154).

No effects on antibody titres post-immunization were also demonstrated in rabbits administered carprofen, another commonly used NSAID selective for COX-2 inhibition (155). Carprofen has also been shown to reduce TNF-α activity in rats in a subcutaneous pouch inflammatory model (156) and reduce inflammatory cell infiltrates and serum levels of IL-6 in a mouse model of venous thrombosis (157). These results demonstrate that carprofen and meloxicam have similar anti-inflammatory and immune suppressive effects (158), though whether these anti-inflammatory actions result in significant impacts on disease outcomes in wider studies of infectious disease is not known. Robenacoxib, is a NSAID that is highly selective for COX-2, resulting in its high concentration in and targeting of inflamed tissues (159). Robenacoxib at therapeutic levels has been demonstrated to significantly reduce both lameness scores and synovial fluid levels of C-reactive proteins (CRP), a marker of inflammation, in dogs with osteoarthritis, but not significantly affect CRP serum levels (160). This highly selective nature suggests that robenocoxib may introduce less variables as a NSAID for the management of localized pain and inflammation (e.g., post-surgery) followed by infection in some systemic animals models of infectious disease. However, as NSAIDs with higher selectivity for COX-2 have been shown to have higher risk of cardiovascular complications, their use in infectious disease models that induce cardiovascular compromise may increase the risk of these events occurring (161). Whilst non-selective COX-1 and COX-2 inhibiting NSAIDs (such as piroxicam) have a greater risk of gastrointestinal complications such as pain and bleeding due to their inhibition of COX-1 as well as COX-2 enzymes, transdermal delivery has been shown to significantly reduce these side effects (162). These may provide additional options in infectious disease models where cardiovascular impacts of highly selective COX-2 inhibiting NSAIDS may be of concern. Further research investigating and comparing effects of various NSAIDs in infectious disease studies is required to determine this.

The literature demonstrates that whilst the use of NSAIDs does cause immunomodulation, namely immunosuppression, the impacts on study outcomes in infectious disease studies are likely to be varied and at times negligible depending on the study objectives. The timing and use of NSAIDs should therefore be utilized where deemed necessary for the management of animal welfare and the control of potentially more confounding variables such as unresolved pain and excessive inflammation (158).

Pain and uncontrolled inflammation in infectious disease studies

Whilst the use of anesthetic and analgesia can cause immunomodulation, literature showing the significant immunosuppressive impacts of both pain and excessive inflammation (often from tissue trauma or surgery) is extensive (163–165). It is therefore crucial in animal research that in an attempt to reduce variables by avoiding the use of anesthesia and analgesia, that potentially more significant variables in the form of uncontrolled pain and inflammation are not introduced (166). Pain in the absence of tissue injury can suppress NK cell activity and mitogen induced cell proliferation (167, 168) and reduced antibody production (169). Surgical trauma, which commonly combines various degrees of tissue trauma and pain, has been well-demonstrated to cause a variety of immunomodulatory issues including the development of systemic inflammatory immune responses, compensatory anti-inflammatory immune responses, and overall immunosuppression resulting in enhanced disease susceptibility (170). It is therefore crucial that pain and excessive inflammation, for example post-surgery, are well-controlled in studies of infectious disease for the protection of animal welfare and reducing study variables. Despite the known immunomodulatory effects, choosing and administering adequate anesthesia and analgesia for the species and procedure should be a paramount consideration. To minimize negative animal welfare impacts and potential effects on study outcomes, care should be taken to select the least invasive procedures and regimes for achieving study objectives, and utilizing multi-model anesthesia and analgesia

to reduce reliance on potentially more impactful drug classes such as opioids (171).

Regardless of the mechanism of effect of anesthetics and analgesics on immune functioning, or indeed whether the effect is immunosuppressive or immunoenhancing, their use can impact scientific outcomes in animal models of infectious disease (65). Where anesthesia and analgesia use are deemed essential for achieving scientific objectives, minimizing potentially more impactful variables such as pain and excessive inflammation, protecting animal welfare, and keeping regimes consistent wherever possible is important. Where different anesthetic or analgesic regimes are utilized, an understanding of their potential effects on disease progression and outcomes is crucial for identifying and understanding study impacts. One way of potentially identifying the effects of study variables, such as stress and different anesthesia regimes, is *via* the selection and use of appropriate and sensitive animal monitoring strategies (172, 173).

Methods of animal disease and welfare assessment

To assess health, disease state and welfare in infectious disease animal research, a wide range of assessment methods are utilized (174). To better observe and understand the potential effects of stress and anesthesia, the methods of assessment and data collection used need to measure parameters with adequate sensitivity (175). In disease studies, a standardized approach to the assessment of health, disease and welfare state can be difficult to implement due to the large variation in the mechanisms of action and immune responses induced by the diseases being studied (176). Figure 4 describes methods of animal assessment commonly utilized in animal models of disease separated into five broad categories of assessment techniques, and demonstrates the change in focus of these methods of assessment over the past 7–9 years.

The increased prevalence in published literature of all methods of animal assessment in recent years is likely due to the heightened focus on animal welfare, leading to improved refinement of monitoring practices and increased reporting. Between 2012/2013 and 2020/2021, a search utilizing the same search parameters as used for Figure 4 shows a 48% increase in the term "welfare," highlighting the increasing focus on animal welfare in research over the past 10 years. The specific broad categories of animal monitoring as represented in Figure 4 are explored in more detail below.

Subjective assessment and operator scoring

Subjective operator assessment of animals, for example using grimace scores and visual activity assessment, is widely utilized in animal studies of disease. The incidence of clinical assessment and operator scoring reported in the literature has increased by 96% between 2012/2013 to 2020/2021 (Figure 4). Of the five assessment categories discussed in this review, this category of assessment has seen the second lowest increase in recent years. Given the heightened focus on reporting of factors affecting research animal welfare, this increase is likely due to improved reporting in the literature, in addition to the increased use of this assessment method over time.

In recent years, the development of grimace scores has attempted to develop a more standardized approach to the assessment of pain in a range of laboratory species. These scoring systems were initially developed for laboratory mice but have since been expanded to a range of research animal species (177). Using the grimace score as a measure of pain and welfare in mice has resulted in an overall improvement and enhanced sensitivity for the assessment and detection of pain in a range of studies (178). More recently, Reijgwart et al. (179) compared facial musculature of ferrets pre- and post-surgery, to investigate and develop a ferret grimace score system. They found differences in facial musculature presentations and concluded that a ferret grimace score system could be useful in a multifactorial pain assessment (179). Similarly, a feline grimace score system has recently been developed by Evangelista et al. (180). They assessed cats post-operatively, and determined that the facial scoring system assessing ear position, orbital tightening, muzzle tension, whisker change, and head position was a valid and reliable tool for acute pain assessment in cats (180). Navarro et al. (181) developed a facial recognition scale for sows as a measure of pain, with observers reviewing photographs to score tension above eyes, snout angle, neck tension, temporal tension and ear angle. They determined that the scale was a useful tool for recognizing and assessing pain in farrowing sows, which indicates scope for employing such a facial pain assessment tool to further investigate its usefulness in infectious disease research in pigs (181). Benato et al. (182) expanded upon facial-based grimace scores by developing the Bristol rabbit pain score, encompassing demeanor, posture, locomotion, ears, eyes and grooming. A subsequent study by the authors where veterinary professionals used the scoring system to assess rabbits in acute pain determined it to be a suitable tool for quantifying pain in rabbits in a useful, valid and reliable way (183). One limitation of facial grimace scoring in infectious disease research is that clinical signs of disease that affect the face (eg, facial swelling in influenza) can make facial assessments less reliable (184). A pain recognition system such as the Bristol rabbit pain score may act as a more reliable pain measure in infectious disease research as it assesses more than just facial effects of pain, and should be investigated for use in infectious disease animal studies. There is scope to develop more holistic measures of pain and welfare assessment for laboratory animals in disease research that are more fit-for-purpose, with the potential to encompass facial, whole body and behavioral elements (185).

Behavioral scoring systems such as play and interaction scores are also commonly utilized in animal disease studies, which rely upon a visual assessment of activity level and behavior as judged by the assessor (186). These behavioral scoring systems are a useful tool in the identification and grading of disease impact, particularly for inquisitive and active species where changes in activity and behavior are readily apparent to the assessor. However, these scoring systems have limitations because they do not quantify the state of disease progression alone (187). They therefore must be utilized alongside the presence or absence of specific signs of disease for the particular disease model (188). This multi-faceted approach is an effective means of assessment of animals in disease studies, yet it is still prone to error and variability due to the inherent reliance on the subjective assessments of individuals. An understanding of the physiological mechanisms of the clinical signs exhibited can result in a more robust interpretation of health state, however the ultimate interpretation will depend on the assessor (188). The variability between research institutions will

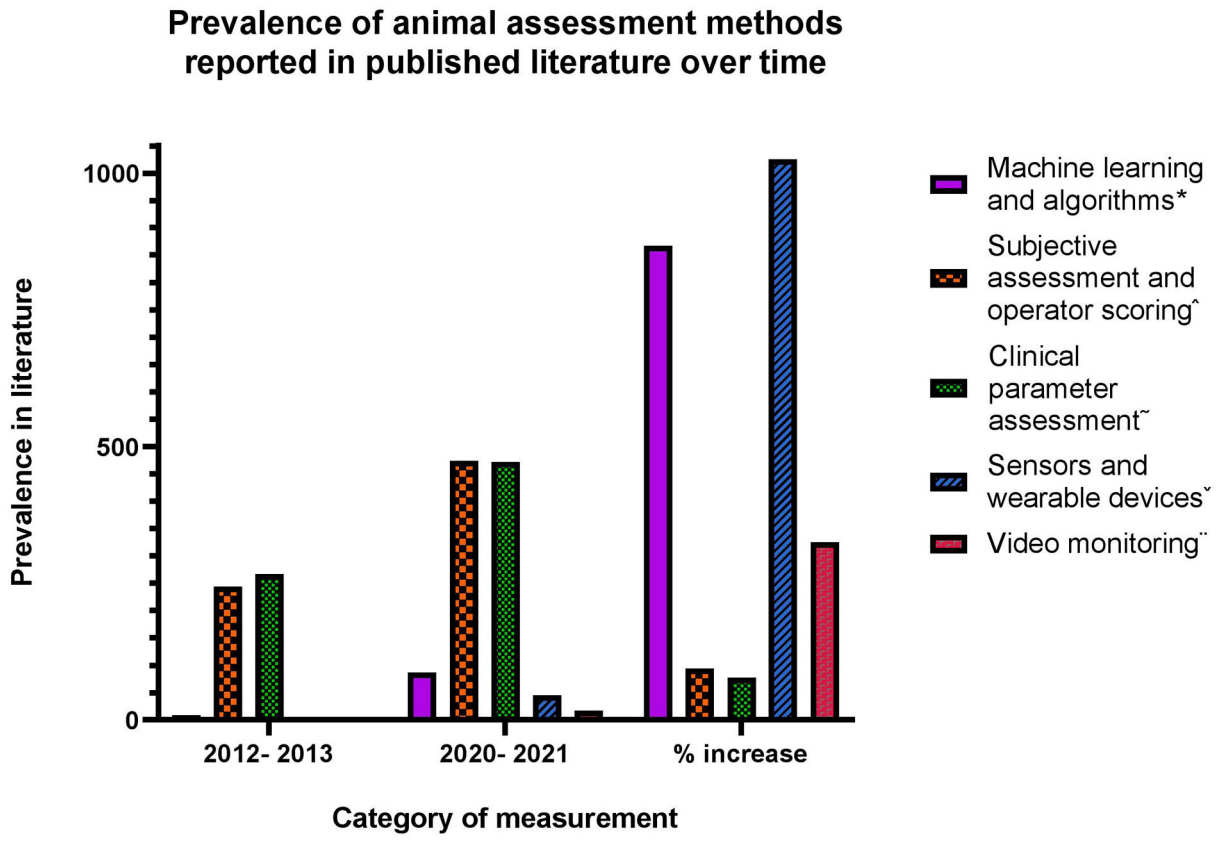

FIGURE 4
Data collected from Web of Science. Search refined by categories of Veterinary Sciences, Infectious Diseases, Agriculture multidisciplinary, Zoology. Search conducted of title, abstract, and key words using these terms per category: *Machine learning animal disease, algorithm animal disease. ^Subjective assessment animal disease, clinical scoring animal disease, grimace score animal disease, clinical assessment animal disease. ~Heart rate animal disease, rectal temperature animal disease, blood pressure animal disease, respiration. ˅Sensors animal disease, wearable animal disease. ¨Video monitoring animal disease, infrared monitoring animal disease, motion detection monitoring animal disease.

also vary as often the finer details of animal scoring systems and assessments are not published in the literature (189). This decreases the reproducibility of results in animal disease research. To enhance both scientific and welfare outcomes additional animal assessment methods should be implemented in infectious disease studies and details published, to complement existing subjective assessment methods.

Measurement of clinical parameters

Continual monitoring of clinical parameters such as body temperature and heart rate can be a useful means of data collection and health assessment in research animals (190). The prevalence of clinical parameter assessment in the literature has increased by 77% between 2012/2013 and 2020/2021 (Figure 4), which of the five categories of assessment discussed in this review is the lowest category to increase over the past 5 years. Due to enhanced reporting on welfare related aspects of animal studies, this increase could be reasonably attributed to an increase in the reporting of assessment methods, in addition to increased use to some degree. Whilst measurement of clinical parameters proves a useful monitoring strategy, it commonly requires the surgical implantation of telemetry devices where regular undisturbed data is required (191). The alternative is manual handling and disturbed measurements, which commonly leads to handling stress and artificially impacts clinical readouts (4).

Whilst the ability to collect this data *via* surgically implanted devices is invaluable in many disease studies, the effects of tissue trauma and surgery on the immune response has been well-categorized in the literature, with the strong consensus being that tissue damage from both trauma and surgery result in immunomodulation (38, 164, 192). Tissue damage caused by surgery results in the emission of large amounts of damage-associated molecular patterns, which induce a systemic cytokine and chemokine-mediated hyperinflammatory response (193). These responses typically result in immunoenhancement when these effects are acute, and immunosuppression when effects become chronic. However, hyperinflammation as a result of surgery can also result in acute tissue damage, resulting in increased disease susceptibility both acutely and chronically (170). This was demonstrated by Jia et al. (194) by conducting a meta-analysis of 25 articles, to investigate correlations between cytokine production capacity and the development of inflammatory complications post-surgery. The authors determined that elevated cytokine production capacity correlated with inflammatory complications post-surgery (194). This is consistent with previous theories that hyper-inflammation post-surgery triggers an anti-inflammatory compensatory immune response, causing immunosuppression and an increased risk of

secondary complications (170). Whilst the degree of this response typically correlates with the degree of tissue damage, even minor surgery for telemetry implantation could be expected to result in a degree of hyperinflammation which, in addition to the welfare impacts of a surgical procedure, may affect disease study results (170).

The effects of a surgical procedure should therefore not be underestimated in animal disease studies and must be carefully weighed against the benefits of implanted telemetry devices. Using devices that capture multiple clinical parameters, as opposed to single measures like temperature alone, would assist in the risk/benefit assessment of surgically implanted devices, and result in better justification for the surgical procedures required for their use. Where surgical procedures are deemed important for achieving study outcomes, careful consideration of the time between surgery and disease induction should occur to minimize impacts on study objectives (195).

Sensors and wearable devices

Of the five categories of animal assessment and monitoring discussed in this review, the use of sensors and wearable devices has seen the most significant increase in published literature in recent years. From 2012/2013 to 2020/2021 the reported use of sensors and wearable devices has increased 1,025% (Figure 4), with the significance of the increase over time being as a result of limited reporting of this method in the literature using these search parameters in 2012–2013. This substantial increase strongly indicates a true increase in using these methods, more so than an increase in the reporting of assessment methods. Using sensors for physiological data collection in research has shown promise for the collection of some, but not all, metrics. González-Sánchez et al. (196) developed and trialed a circuit sensor system for the collection of heart activity and breathing pattern data using contactless sensors in mice, to avoid the need for restraint and sedation. Whilst they were able to collect breathing pattern data in a contactless manner, the system required a relatively complex set-up (196). This would likely prove to be an obstacle for many infectious disease studies, due to the restrictive nature of entry to rooms for troubleshooting complex technology (176). Equipment in disease studies must also be disposable or effectively decontaminated at the end of a study, and therefore complex equipment is often not well-suited or cost effective (176). In addition, González-Sánchez et al. (196) determined that heart activity could not be reliably monitored *via* the contactless system, and therefore required mice to stand on sensors to reliably collect data. Whilst still an effective means of data gathering that avoids the need for surgery, these results suggest that circuit sensor systems would not provide a practical and continual means of clinical parameter measurement in animal studies of infectious disease, and reliable data collection for multiple clinical parameters would still depend on anesthesia or handling.

In recent years, the uptake in wearable devices in the veterinary profession and amongst pet owners has increased (197). These devices typically involve sensor units attached to collars or bands for ease of use and a non-invasive means of monitoring clinical parameters. Heart rate variability (HRV) is being increasingly utilized for the measure of physiological and welfare state, and acts as a measure of cardiac autonomic modulation (198). The measurement of HRV can be conducted in various ways, including *via* the use of Holter-type monitors or electrocardiogram (199) using electrodes attached to the skin. Wearable monitors increasingly allow for these technologies to be used in a way that reduces the requirement for complex technological setups. These devices typically involve sensor units attached to collars or bands for ease of use. They can provide a non-invasive means of monitoring clinical parameters, including heart rate variability, and can be useful measures of pain (200) acute systemic inflammation (201) and stress (202). Despite the ease of use and apparent low welfare impacts, using wearable devices in animal disease research is not common practice. As with other technology-based data collection in disease research, complexity of set-up and use in the research setting, in addition to devices requiring disposal at the end of a study if they cannot be decontaminated, may be barriers to the uptake of wearable devices in animal disease research. In addition, the scarcity of published literature on the use of wearable devices in research animals may be a contributing factor to lack of validation of their effectiveness in off-label use for species commonly used in disease research.

A preliminary observational study by Paci et al. (203) demonstrated altered behaviors in a cat wearing a collar monitoring device compared to a control (no collar). Significant increases in grooming, scratching, biting, and head shaking were all observed with wearing of the collar, indicating discomfort. The authors propose that the focus on designing wearable data collection devices is on the user (human), more so than from the perspective of the animal wearing the device. For uptake of wearable devices in animal research, there is a need to ensure devices are indeed "non-invasive" from the experience of the animal. This ensures that wearability of devices is optimized, leading to real welfare benefits and optimized scientific outcomes by avoiding the introduction of altered behaviors that may influence study results. If these elements can be addressed, there is great promise in the ability to capture multi-parameter physiological data for the improvement of data collection, monitoring of animals, and refinement of humane endpoints in animal studies of infectious disease.

An area of research that has demonstrated successful development and uptake of wearable devices for physiological data collection is dairy cattle research. The successful implementation of wearable collars and devices in the research arena has led to uptake by dairy farmers for health management and production optimisation in dairy herds (204). For many other species used in research, the development of species-specific devices is likely not feasible due to a lack of market demand for such technology. The use and validation of devices already developed for production and companion animals may therefore be a cost-effective way to increase the uptake of wearable monitoring technologies in animal disease studies.

Video monitoring

Video monitoring has seen an increased prevalence in published literature of 325% between 2012/2013 and 2020/2021 (Figure 4). Whilst this is likely in part attributable to an increase in reporting of assessment methods, it also likely demonstrates a genuine increase in using video monitoring assessment. The desire to remove surgery (as required for implanted telemetry devices) as an experimental variable and improve upon welfare outcomes has more recently led to the advancement of less invasive vital sign and activity monitoring in research animals, *via* video-based assessments. As a result, the use and refinement of video monitoring in animal studies has increased

significantly over the past decade, and is considered a useful tool for the non- or minimally invasive collection of behavioral data and clinical parameters in disease research (205).

Video monitoring systems are used in research to gather a wide range of metrics including respiratory rate, temperature *via* infra-red, heart rate, movement, and activity. These metrics can be a useful indicator of not only disease and inflammatory state, but also as a measure of pain and stress responses occurring *via* the autonomic nervous system (206). Infra-red thermography technology is being increasingly used in laboratory animal science to detect pain *via* skin surface vasoconstriction and vasodilation, in order to detect the effectiveness of analgesia and identify where pain may be causing confounding effects within studies (207). Optimized use of infra-red technology is dependent on a tailored approach to the species and study objectives. For example, pain and stress detection has been shown to be the most sensitive using ocular surfaces; aversive stimuli are more greatly detected *via* lowered tail and ear temperatures; and small mammal thermogenesis capacity can be most usefully measured *via* an interscapular window (208). The accuracy of infra-red detection can be affected by external factors such as wind speed, temperature, and humidity, requiring additional system processes to ensure consistency and accuracy of readings (209). Yet due to the commonly more controlled containment conditions of infectious disease research, the requirement for the control of these external variables is likely to be less. The presence, thickness and color of fur is another factor that can cause variability and lead to reduced reliability of readings (210). However, Loughin and Marino (211) determined that whilst the mean temperature of infra-red readings was lower in unshaved vs. shaved dogs, the thermal pattern was equally consistent. For infectious disease studies, where disease is commonly measured by comparing repeated measures throughout the disease course to healthy baseline data, the presence of fur would be unlikely to preclude the collection of valuable data (212). This was demonstrated by Schaefer et al. (213), who infected unshaved calves with type 2 bovine viral diarrhea virus and compared infra-red readings with unshaved, uninfected control calves. They found that infected calves displayed higher infra-red temperature readings prior to the onset of clinical disease or serum acute phase proteins, suggesting infra-red thermography successfully predicted clinical disease onset on calves (213).

Video systems vary significantly in cost and technological complexity, with simpler video setups commonly being restricted to temperature, movement, and activity monitoring. For the collection of these clinical parameters and metrics, video systems are an effective non-invasive method of collecting data on undisturbed animals. Yet the collection of additional parameters such as heart and respiratory rate generally requires a more technologically complex set-up and the requirement for animals to be still during measurement periods, leading to most studies using video monitoring for collection of heart and respiratory rate being conducted in anesthetized animals (214). In infectious disease studies, using video monitoring is uncommon, likely because of the need to anesthetize animals to gain a broad data set of clinical parameters. This presents additional safety risks to operators resulting from increased handling of infected animals, and an increased risk of sharps injury from parenteral anesthetic administration (215). Increasing the number of anesthetic inductions and/or time under anesthesia to measure clinical parameters *via* video systems also has potential detrimental effects on animal welfare and study outcomes, as already discussed in this review. Although anesthesia is not required or conducive for the collection of activity measurement, the measurement of activity in infectious disease studies is not common practice. This may be due to the technical aspects of activity monitoring *via* video capture, which commonly requires restrictive enclosure set-ups and for the body of the animal to represent much of the image (214). To overcome these issues, Oh et al. (216) temporarily placed individual ferrets infected with H1N1 and undergoing various antiviral treatments into a filming box daily. They found that video-tracking was more sensitive than manual behavior scoring in detecting activity changes, and that the video-tracking demonstrated that oseltamivir treatment alleviated the effect of influenza infection on activity in ferrets (216). These results demonstrate the value in incorporating the measurement of activity as a less subjective measure than operator assessments alone.

Overall, using video monitoring for the assessment of clinical parameters and activity metrics in animal research has progressed significantly in the past decade, yet the use of these technologies has not been adapted well to infectious disease research. Further studies into adapting technology to infectious disease research that is non-invasive and continuous, in addition to investigating the use of simpler technology that incorporates a range of measurements for real-time assessment, is required for the increased uptake of video monitoring in animal disease studies.

Machine learning and algorithms

There are a multitude of benefits to scientific outcomes and animal welfare by performing basic assessments of individual physical and physiological parameters in disease studies. However, the collection and assessment of individual metrics can be unreliable in capturing the complete disease and welfare state of an animal, and reliable predictions can be difficult to make (174). Therefore, a gold-standard approach to improving the assessment and prediction of disease outcomes is the incorporation of these metrics into machine learning algorithms (25). By feeding data of multiple physiological and behavioral metrics of a species into a machine learning program, algorithms can be developed that not only result in a more accurate assessment of overall health and disease state, but also allow for the prediction of short- and long-term outcomes of morbidity and mortality (217). By using algorithms in this way, animals can be identified as being at high risk of severe disease or death (218). Machine learning has also be utilized for pain and welfare assessment in animals, as has been done *via* the use of convolutional neural networks or facial action coding systems to detect pain in cats (219).

The development and use of machine learning algorithms in recent years, as described in Figure 4, has increased 867%. However, the small number of animal studies utilizing machine learning algorithms compared with other means of monitoring and assessment means that whilst a substantial percentage increase has occurred, this increase is inflated. The continued low relative use of this method of assessment demonstrates the significant potential for machine learning algorithms to be further adopted to improve animal welfare and scientific outcomes in disease research. An example of the benefits of machine learning algorithms is seen in a study by Mei et al. (220), who used published data from mouse models of stroke. They found large inter- and intra-model variance in humane endpoint determination and application due to varying animal models, lack of standardized experimental protocols, and heterogeneity of performance metrics (220). The

authors then used previously published data on weight, temperature, and sickness scores from mouse models of sepsis and stroke and applied machine learning models to assess the usefulness of this method for parameter selection and endpoint definition across models. They found that the machine learning algorithms identified animals with a high risk of early death in both mouse models of stroke (male: 93.2% at 72 h post-treatment; female: 93.0% at 48 h post-treatment) and sepsis (96.2% at 24 h post-treatment), thus demonstrating generalizability of endpoint determination across models. Such research demonstrates the significant potential for machine learning algorithms in disease research, and strongly suggests the great potential of utilizing machine learning more broadly in animal models of infectious disease.

Hughes et al. (221) utilized machine learning and video footage to develop an algorithm for a model of Parkinson's disease in zebra fish. By improving the detection of early onset Parkinson's disease, they were able to improve data collection for the development of therapeutics (221). In addition, Ellmann et al. (222) developed a machine learning algorithm for the early detection of metastases in an experimental rat model, by utilizing various imaging data, tomography analysis and calculation of tumor-take rate. They found that the algorithm significantly outperformed the detection ability of each individual parameter, and that in addition the algorithm could be extrapolated for use with different organs or areas of multimodal and multiparametric imaging research (222). These studies further demonstrate both the feasibility and the potential for machine learning algorithms to be utilized more widely in animal disease research. In addition to this potential use of machine learning in future animal studies, there is also substantial opportunity for machine learning to be applied to existing data from previously conducted animal studies, which can then be refined as technology and the understanding of disease models advances.

Using behavioral and movement data collected *via* wearable sensors and video monitoring has also enabled the successful development of machine learning algorithms. Carslake et al. (223) equipped dairy calves with collar-mounted sensors and monitored their behavior with video cameras. They used sensor data and video observations to develop an algorithm to predict locomotor play behavior, which identified locomotor play (99.73% accuracy), self-grooming (98.18% accuracy), ruminating (94.47% accuracy), non-nutritive suckling (94.96% accuracy), nutritive suckling (96.44% accuracy), active lying (90.38% accuracy) and non-active lying (90.38% accuracy) (223). In animal disease research, the development of similar behavioral and movement algorithms would likely lead to an increased accuracy of detection of developing disease, by removing the subjectivity of operator assessments, combining several metrics, and allowing behavior and movement changes to be accurately detected over prolonged periods of time where animals are not disturbed by human presence.

The development and use of algorithms require specialist knowledge, in addition to the time investment of identifying and collecting the data required. However, the benefits of a significantly more accurate assessment of disease and improved predictions of humane endpoints holds great potential to improve both scientific outcomes and animal welfare. It is likely that the initial time investment to develop algorithms would lead to time savings in future studies utilizing the model by reducing the reliance on subjective operator assessments, and allowing for a more accurate and effective use of resources for animal monitoring. In addition, the potential for algorithms to be adapted between models would lead to further ease of development and application to a wider range of animal models in infectious disease research (224).

Future directions

A holistic approach to study design and animal management practices in studies of infectious disease is crucial to reduce the physiological and immune impacts of stress, pain and anesthesia. Studies should firstly be designed to minimize the number of potentially stressful interventions required to achieve study objectives (such as sample collection events). To reduce the impacts of necessary interventions on animal welfare and scientific outcomes, further research is required to establish methods that reduce stress and reliance on anesthesia, whilst not introducing additional or unmanaged pain. This can undoubtedly be challenging in the field of infectious disease research due to the requirement for strict safety and biocontainment protocols. Yet small time investments in animal management techniques in studies during the animal habituation phase can reduce stress and the degree of chemical and physical restraint, as demonstrated in the use of training and restraint slings in research mini-pigs (225). The development of species-specific positive reinforcement training protocols, combined with multi-modal anesthesia regimes (such as local anesthetic with additional sedation to effect if required), tailored to the high biocontainment environment, should be explored as alternatives to forced manual handling and general anesthesia for repeated sample collections (226). Assessing and quantifying the impacts of new animal management regimes on animal welfare, scientific outcomes and staff safety, compared to methods that rely more heavily on manual and chemical restraint, is required to encourage the development and uptake of improved methods of conducting infectious disease research. The use and validation of a broader range of monitoring strategies and technologies, in particular minimally invasive wearable devices and video monitoring systems for the capture of physiological data, will aid in the comparative assessment of new methods (227). Additionally, data captured from the use of monitoring technologies will aid in an improved understanding of the diseases under investigation, and allow for a greater focus on machine learning and algorithm development (228). This has the potential to enhance our understanding of infectious disease processes, and improve animal welfare by refining animal monitoring strategies and refining humane endpoints in high-impact disease models.

Conclusion

Stress and general anesthesia can result in reduced animal welfare and altered physiology and immunity. Both stress and general anesthesia have been found to cause immunomodulation, most commonly immunosuppression, which results in the introduction of variables in animal studies of infectious disease. Using general anesthesia in infectious disease research is integral where procedures or management practices cause undue or unmanaged pain or distress, but further research into improved management regimes for research animals is important to determine where anesthesia induction can be minimized without compromising animal welfare, increasing stress or causing pain and excessive inflammation to be

poorly managed. Using monitoring technologies such as non-invasive wearable monitors, and the development of machine learning algorithms to better predict and manage disease and welfare, are required for a more multi-faceted monitoring approach in animal studies of infectious disease. This will lead to both a reduced reliance on subjective assessment measures and enhance our understanding of the effects of stress and anesthesia in disease studies. Further studies directly investigating the impacts of anesthesia and stress in infectious disease studies are required to improve research animal welfare and ensure greater science translatability from the laboratory to real world outcomes. This can be achieved by designing animal studies that use the least invasive techniques required to achieve study objectives; utilizing multi-modal anesthesia and analgesia to ensure pain, stress, and excessive inflammation are well-managed; and developing improved methods of animal management that result in less stress and a reduced reliance on anesthesia.

Author contributions

RL wrote the manuscript with support from DL, DB, AF, PM, and KS. DB, AF, PM, and KS provide supervision. All authors contributed to the article and approved the submitted version.

Funding

Funding support was provided through an Australian Government Research Training Program Scholarship.

Conflict of interest

The authors declare that the research was conducted in the absence of any commercial or financial relationships that could be construed as a potential conflict of interest.

Publisher's note

All claims expressed in this article are solely those of the authors and do not necessarily represent those of their affiliated organizations, or those of the publisher, the editors and the reviewers. Any product that may be evaluated in this article, or claim that may be made by its manufacturer, is not guaranteed or endorsed by the publisher.

References

1. Zusinaite E, Ianevski A, Niukkanen D, Poranen MM, Bjørås M, Afset JE, et al. A systems approach to study immuno- and neuro-modulatory properties of antiviral agents. *Viruses*. (2018) 10:423. doi: 10.3390/v10080423

2. Swearengen JR. Choosing the right animal model for infectious disease research. *Animal Model Exp Med.* (2018) 1:100–8. doi: 10.1002/ame2.12020

3. Gouveia K, Hurst JL. Improving the practicality of using non-aversive handling methods to reduce background stress and anxiety in laboratory mice. *Sci Rep*. (2019) 9:20305. doi: 10.1038/s41598-019-56860-7

4. Bailey J. Does the stress of laboratory life and experimentation on animals adversely affect research data? A critical review. *Altern Lab Anim.* (2018) 46:291–305. doi: 10.1177/026119291804600501

5. Bailoo JD, Murphy E, Boada-Saña M, Varholick JA, Hintze S, Baussière C, et al. Effects of cage enrichment on behavior, welfare and outcome variability in female mice. *Front Behav Neurosci.* (2018) 12:232. doi: 10.3389/fnbeh.2018.00232

6. Petetta F, Ciccocioppo R. Public perception of laboratory animal testing: historical, philosophical, and ethical view. *Addict Biol.* (2021) 26:e12991. doi: 10.1111/adb.12991

7. Antoni MH, Dhabhar FS. The impact of psychosocial stress and stress management on immune responses in patients with cancer. *Cancer.* (2019) 125:1417–31. doi: 10.1002/cncr.31943

8. O'Connor DB, Thayer JF, Vedhara K. Stress and health: a review of psychobiological processes. *Annu Rev Psychol.* (2021) 72:663–88. doi: 10.1146/annurev-psych-062520-122331

9. Hennessy MB, Willen RM, Schiml PA. Psychological stress, its reduction, and long-term consequences: what studies with laboratory animals might teach us about life in the dog shelter. *Animals*. (2020) 10:2061. doi: 10.3390/ani10112061

10. Williams DP, Koenig J, Carnevali L, Sgoifo A, Jarczok MN, Sternberg EM, et al. Heart rate variability and inflammation: a meta-analysis of human studies. *Brain Behav Immun.* (2019) 80:219–26. doi: 10.1016/j.bbi.2019.03.009

11. Wiley NC, Dinan TG, Ross RP, Stanton C, Clarke G, Cryan JF. The microbiota-gut-brain axis as a key regulator of neural function and the stress response: implications for human and animal health. *J Anim Sci.* (2017) 95:3225–46. doi: 10.2527/jas2016.1256

12. Patchev VK, Patchev AV. Experimental models of stress. *Dialogues Clin Neurosci.* (2006) 8:417–32. doi: 10.31887/DCNS.2006.8.4/vpatchev

13. Van Dievel M, Janssens L, Stoks R. Short- and long-term behavioural, physiological and stoichiometric responses to predation risk indicate chronic stress and compensatory mechanisms. *Oecologia.* (2016) 181:347–57. doi: 10.1007/s00442-015-3440-1

14. Calefi AS, Quinteiro-Filho WM, Ferreira AJP, Palermo-Neto J. Neuroimmunomodulation and heat stress in poultry. *Worlds Poultry Sci J.* (2017) 73:493–504. doi: 10.1017/S0043933917000472

15. Pietrelli A, Di Nardo M, Masucci A, Brusco A, Basso N, Matkovic L. Lifelong aerobic exercise reduces the stress response in rats. *Neuroscience.* (2018) 376:94–107. doi: 10.1016/j.neuroscience.2018.02.019

16. Hernández-Avalos I, Flores-Gasca E, Mota-Rojas D, Casas-Alvarado A, Miranda-Cortés AE, Domínguez-Oliva A. Neurobiology of anesthetic-surgical stress and induced behavioral changes in dogs and cats: a review. *Vet World.* (2021) 14:393–404. doi: 10.14202/vetworld.2021.393-404

17. Dhabhar FS. Effects of stress on immune function: the good, the bad, and the beautiful. *Immunol Res.* (2014) 58:193–210. doi: 10.1007/s12026-014-8517-0

18. Lewis CE, Pickering B. Livestock and risk group 4 pathogens: researching zoonotic threats to public health and agriculture in maximum containment. *ILAR J.* (2022) 61:86–102. doi: 10.1093/ilar/ilab029

19. Ackerman RS, Luddy KA, Icard BE, Piñeiro Fernández J, Gatenby RA, Muncey AR. The effects of anesthetics and perioperative medications on immune function: a narrative review. *Anesth Analg.* (2021) 133:676–89. doi: 10.1213/ANE.0000000000005607

20. Tian Y, Guo S, Wu X, Ma L, Zhao X. Minocycline alleviates sevoflurane-induced cognitive impairment in aged rats. *Cell Mol Neurobiol.* (2015) 35:585–94. doi: 10.1007/s10571-014-0154-6

21. Tan XX, Qiu LL, Sun J. Research progress on the role of inflammatory mechanisms in the development of postoperative cognitive dysfunction. *Biomed Res Int.* (2021) 2021:3883204. doi: 10.1155/2021/3883204

22. Gonçalves VC, Pinheiro D, de la Rosa T, de Almeida AG, Scorza FA, Scorza CA. Propolis as a potential disease-modifying strategy in parkinson's disease: cardioprotective and neuroprotective effects in the 6-ohda rat model. *Nutrients*. (2020) 12:1551. doi: 10.3390/nu12061551

23. Antanaitis R, Juozaitiene V, Malašauskiene D, Televičius M, Urbutis M, Rutkaukas A, et al. Identification of changes in rumination behavior registered with an online sensor system in cows with subclinical mastitis. *Vet Sci*. (2022) 9:454. doi: 10.3390/vetsci9090454

24. Jorquera-Chavez M, Fuentes S, Dunshea FR, Warner RD, Poblete T, Morrison RS, et al. Remotely sensed imagery for early detection of respiratory disease in pigs: a pilot study. *Animals*. (2020) 10:451. doi: 10.3390/ani10030451

25. Jirkof P, Rudeck J, Lewejohann L. Assessing affective state in laboratory rodents to promote animal welfare-what is the progress in applied refinement research? *Animals*. (2019) 9:1026. doi: 10.3390/ani9121026

26. Baum A. Stress, intrusive imagery, and chronic distress. *Health Psychol.* (1990) 9:653–75. doi: 10.1037/0278-6133.9.6.653

27. Russell WMS, Burch RL. *The Principles of Humane Experimental Technique*. London: Methuen (1959).

28. Mota-Rojas D, Miranda-Cortés A, Casas-Alvarado A, Mora-Medina P, Boscato-Funes L, Hernández-Ávalos I. Neurobiology and modulation of stress-induced hyperthermia and fever in animal. *Abanico Vet*. (2021) 11:21. doi: 10.21929/abavet2021.11

29. Cohen S, Janicki-Deverts D, Doyle WJ, Miller GE, Frank E, Rabin BS, et al. Chronic stress, glucocorticoid receptor resistance, inflammation, and disease risk. *Proc Natl Acad Sci U S A*. (2012) 109:5995–9. doi: 10.1073/pnas.1118355109

30. Zhou Q, Qian Z, Ding W, Jiang G, Sun C, Xu K. Chronic psychological stress attenuates the efficacy of anti-Pd-L1 immunotherapy for bladder cancer in immunocompetent mice. *Cancer Invest*. (2021) 39:571–81. doi: 10.1080/07357907.2021.1943746

31. Gervasi SS, Burgan SC, Hofmeister E, Unnasch TR, Martin LB. Stress hormones predict a host superspreader phenotype in the west nile virus system. *Proc Biol Sci*. (2017) 284:20171090. doi: 10.1098/rspb.2017.1090

32. Zhou Q, Katano M, Zhang JH, Liu X, Wang KY, Iinuma M, et al. Chewing behavior attenuates the tumor progression-enhancing effects of psychological stress in a breast cancer model mouse. *Brain Sci*. (2021) 11:479. doi: 10.3390/brainsci11040479

33. Henderson LJ, Dani B, Serrano EMN, Smulders TV, Roughan JV. Benefits of tunnel handling persist after repeated restraint, injection and anaesthesia. *Sci Rep*. (2020) 10:14562. doi: 10.1038/s41598-020-71476-y

34. Balcombe JP, Barnard ND, Sandusky C. Laboratory routines cause animal stress. *Contemp Top Lab Anim Sci*. (2004) 43:42–51.

35. Jafari Z, Kolb BE, Mohajerani MH. Chronic traffic noise stress accelerates brain impairment and cognitive decline in mice. *Exp Neurol*. (2018) 308:1–12. doi: 10.1016/j.expneurol.2018.06.011

36. Marcon M, Mocelin R, Benvenutti R, Costa T, Herrmann AP, de Oliveira DL, et al. Environmental enrichment modulates the response to chronic stress in zebrafish. *J Exp Biol*. (2018) 221(Pt 4):jeb176735. doi: 10.1242/jeb.176735

37. Hernández-Avalos I, Mota-Rojas D, Mendoza-Flores JE, Casas-Alvarado A, Flores-Padilla K, Miranda-Cortes AE, et al. Nociceptive pain and anxiety in equines: physiological and behavioral alterations. *Vet World*. (2021) 14:2984–95. doi: 10.14202/vetworld.2021.2984-2995

38. Desborough JP. The stress response to trauma and surgery. *Br J Anaesth*. (2000) 85:109–17. doi: 10.1093/bja/85.1.109

39. Kumar A, Rinwa P, Kaur G, Machawal L. Stress: neurobiology, consequences and management. *J Pharm Bioallied Sci*. (2013) 5:91–7. doi: 10.4103/0975-7406.111818

40. Jin Y, Hu Y, Han D, Wang M. Chronic heat stress weakened the innate immunity and increased the virulence of highly pathogenic avian influenza virus H5n1 in mice. *J Biomed Biotechnol*. (2011) 2011:367846. doi: 10.1155/2011/367846

41. Nicolaides NC, Kyratzi E, Lamprokostopoulou A, Chrousos GP, Charmandari E. Stress, the stress system and the role of glucocorticoids. *Neuroimmunomodulation*. (2015) 22:6–19. doi: 10.1159/000362736

42. Rohleder N. Stress and inflammation - the need to address the gap in the transition between acute and chronic stress effects. *Psychoneuroendocrinology*. (2019) 105:164–71. doi: 10.1016/j.psyneuen.2019.02.021

43. Clutton RE. An anglocentric history of anaesthetics and analgesics in the refinement of animal experiments. *Animals*. (2020) 10:1933. doi: 10.3390/ani10101933

44. Kim R. Effects of surgery and anesthetic choice on immunosuppression and cancer recurrence. *J Transl Med*. (2018) 16:8. doi: 10.1186/s12967-018-1389-7

45. Redondo JI, Rubio M, Soler G, Serra I, Soler C, Gómez-Villamandos RJ. Normal values and incidence of cardiorespiratory complications in dogs during general anaesthesia. a review of 1281 cases. *J Vet Med A Physiol Pathol Clin Med*. (2007) 54:470–7. doi: 10.1111/j.1439-0442.2007.00987.x

46. Pottie RG, Dart CM, Perkins NR, Hodgson DR. Effect of hypothermia on recovery from general anaesthesia in the dog. *Aust Vet J*. (2007) 85:158–62. doi: 10.1111/j.1751-0813.2007.00128.x

47. Vutskits L, Xie Z. Lasting impact of general anaesthesia on the brain: mechanisms and relevance. *Nat Rev Neurosci*. (2016) 17:705–17. doi: 10.1038/nrn.2016.128

48. Bonhomme V, Staquet C, Montupil J, Defresne A, Kirsch M, Martial C, et al. General anesthesia: a probe to explore consciousness. *Front Syst Neurosci*. (2019) 13:36. doi: 10.3389/fnsys.2019.00036

49. Numan T, Slooter AJC, van der Kooi AW, Hoekman AML, Suyker WJL, Stam CJ, et al. Functional connectivity and network analysis during hypoactive delirium and recovery from anesthesia. *Clin Neurophysiol*. (2017) 128:914–24. doi: 10.1016/j.clinph.2017.02.022

50. Kishikawa JI, Inoue Y, Fujikawa M, Nishimura K, Nakanishi A, Tanabe T, et al. General anesthetics cause mitochondrial dysfunction and reduction of intracellular ATP levels. *PLoS ONE*. (2018) 13:e0190213. doi: 10.1371/journal.pone.0190213

51. Haas RH. Mitochondrial dysfunction in aging and diseases of aging. *Biology*. (2019) 8:48. doi: 10.3390/biology8020048

52. Yang Y, Liu Y, Zhu J, Song S, Huang Y, Zhang W, et al. Neuroinflammation-mediated mitochondrial dysregulation involved in postoperative cognitive dysfunction. *Free Radic Biol Med*. (2022) 178:134–46. doi: 10.1016/j.freeradbiomed.2021.12.004

53. Tremoleda JL, Kerton A, Gsell W. Anaesthesia and physiological monitoring during *in vivo* imaging of laboratory rodents: considerations on experimental outcomes and animal welfare. *EJNMMI Res*. (2012) 2:44. doi: 10.1186/2191-219X-2-44

54. Topal A, Gül N, Ilçöl Y, Görgül OS. Hepatic effects of halothane, isoflurane or sevoflurane anaesthesia in dogs. *J Vet Med A Physiol Pathol Clin Med*. (2003) 50:530–3. doi: 10.1111/j.1439-0442.2004.00589.x

55. Lalonde S, Truchetti G, Otis C, Beauchamp G, Troncy E. Management of veterinary anaesthesia and analgesia in small animals: a survey of english-speaking practitioners in Canada. *PLoS ONE*. (2021) 16:e0257448. doi: 10.1371/journal.pone.0257448

56. Cattai A, Rabozzi R, Ferasin H, Isola M, Franci P. Haemodynamic changes during propofol induction in dogs: new findings and approach of monitoring. *BMC Vet Res*. (2018) 14:282. doi: 10.1186/s12917-018-1608-8

57. Mrazova M, Rauser P, Burova J, Georgiou M, Fichtel T. Influence of medetomidine, acepromazine, fentanyl and butorphanol on intraocular pressure and pupil size in healthy dogs. *Vet Med*. (2018) 63:413–9. doi: 10.17221/51/2018-VETMED

58. Brodbelt DC, Blissitt KJ, Hammond RA, Neath PJ, Young LE, Pfeiffer DU, et al. The risk of death: the confidential enquiry into perioperative small animal fatalities. *Vet Anaesth Analg*. (2008) 35:365–73. doi: 10.1111/j.1467-2995.2008.00397.x

59. Schuetze S, Manig A, Ribes S, Nau R. Aged mice show an increased mortality after anesthesia with a standard dose of ketamine/xylazine. *Lab Anim Res*. (2019) 35:8. doi: 10.1186/s42826-019-0008-y

60. Percie du Sert N, Ahluwalia A, Alam S, Avey MT, Baker M, Browne WJ, et al. Reporting animal research: explanation and elaboration for the arrive guidelines 2.0. *PLoS Biol*. (2020) 18:e3000411. doi: 10.1371/journal.pbio.3000411

61. Begley CG, Ioannidis JP. Reproducibility in science: improving the standard for basic and preclinical research. *Circ Res*. (2015) 116:116–26. doi: 10.1161/CIRCRESAHA.114.303819

62. Sessler DI. Perioperative thermoregulation and heat balance. *Ann N Y Acad Sci*. (1997) 813:757–77. doi: 10.1111/j.1749-6632.1997.tb51779.x

63. Rauch S, Miller C, Bräuer A, Wallner B, Bock M, Paal P. Perioperative hypothermia-a narrative review. *Int J Environ Res Public Health*. (2021) 18:8749. doi: 10.3390/ijerph18168749

64. Longley L. Anaesthesia and analgesia in rabbits and rodents. *In Pract*. (2008) 30:92–7. doi: 10.1136/inpract.30.2.92

65. Cicero L, Fazzotta S, Palumbo VD, Cassata G, Lo Monte AI. Anesthesia protocols in laboratory animals used for scientific purposes. *Acta Biomed*. (2018) 89:337–42. doi: 10.23750/abm.v89i3.5824

66. Rodriguez-Diaz JM, Hayes GM, Boesch J, Martin-Flores M, Sumner JP, Hayashi K, et al. Decreased incidence of perioperative inadvertent hypothermia and faster anesthesia recovery with increased environmental temperature: a nonrandomized controlled study. *Vet Surg*. (2020) 49:256–64. doi: 10.1111/vsu.13328

67. Appenheimer MM, Evans SS. Temperature and adaptive immunity. *Handb Clin Neurol*. (2018) 156:397–415. doi: 10.1016/B978-0-444-63912-7.00024-2

68. Centofanti P, Barbero C, D'Agata F, Caglio MM, Caroppo P, Cicerale A, et al. Neurologic and cognitive outcomes after aortic arch operation with hypothermic circulatory arrest. *Surgery*. (2016) 160:796–804. doi: 10.1016/j.surg.2016.02.008

69. Groene P, Zeuzem C, Baasner S, Hofmann-Kiefer K. The influence of body mass index on temperature management during general anaesthesia-a prospective observational study. *J Eval Clin Pract*. (2019) 25:340–5. doi: 10.1111/jep.13064

70. Ruetzler K, Kurz A. Consequences of perioperative hypothermia. *Handb Clin Neurol*. (2018) 157:687–97. doi: 10.1016/B978-0-444-64074-1.00041-0

71. Petrilli CM, Jones SA, Yang J, Rajagopalan H, O'Donnell L, Chernyak Y, et al. Factors associated with hospital admission and critical illness among 5279 people with coronavirus disease 2019 in New York City: Prospective Cohort Study. *BMJ*. (2020) 369:m1966. doi: 10.1136/bmj.m1966

72. Khan F, Tritschler T, Kahn SR, Rodger MA. Venous thromboembolism. *Lancet*. (2021) 398:64–77. doi: 10.1016/S0140-6736(20)32658-1

73. Wang X, Du B, Li J, Wang S, Wang X, Guo M, et al. D-Dimer surge and coagulation disorders in Covid-19 related pneumonia patients with cardiac injury: a case series. *Medicine*. (2020) 99:e21513. doi: 10.1097/MD.0000000000021513

74. Iba T, Levy JH, Connors JM, Warkentin TE, Thachil J, Levi M. The unique characteristics of Covid-19 coagulopathy. *Critical Care*. (2020) 24:360. doi: 10.1186/s13054-020-03077-0

75. Vital signs in accidental hypothermia. *High Alt Med Biol*. (2021) 22:142–7. doi: 10.1089/ham.2020.0179

76. Li N, Zhu L, Sun L, Shao G. The effects of novel coronavirus (SARS-CoV-2) infection on cardiovascular diseases and cardiopulmonary injuries. *Stem Cell Res*. (2021) 51:102168. doi: 10.1016/j.scr.2021.102168

77. Nash PB. Susceptibility to low dose influenza in mice is increased by administration of ketamine/xylazine. *J Immunol*. (2021) 206(1 Supplement):177–196.

78. Penna AM, Johnson KJ, Camilleri J, Knight PR. Alterations in influenza a virus specific immune injury in mice anesthetized with halothane or ketamine. *Intervirology*. (1990) 31:188–96. doi: 10.1159/000150153

79. Cummings KA. Alpha-2 adrenergic agonists. In: Silverstein DC, Rozanski EA, Hopper K, Drobatz KJ, editors. *Textbook of Small Animal Emergency Medicine*. Hoboken, NJ: John Wiley & Sons (2018), p. 1255–7. doi: 10.1002/9781119028994.ch195

80. Valverde A, Skelding AM. Alternatives to opioid analgesia in small animal anesthesia: alpha-2 agonists. *Vet Clin North Am*

Small Anim Pract. (2019) 49:1013–27. doi: 10.1016/j.cvsm.2019.07.010

81. Flanders CA, Rocke AS, Edwardson SA, Baillie JK, Walsh TS. The effect of dexmedetomidine and clonidine on the inflammatory response in critical illness: a systematic review of animal and human studies. *Crit Care.* (2019) 23:402. doi: 10.1186/s13054-019-2690-4

82. Jain A, Lamperti M, Doyle DJ. Dexmedetomidine: another arrow in the quiver to fight COVID-19 in intensive care units. *Br J Anaesth.* (2021) 126:e35–e8. doi: 10.1016/j.bja.2020.10.010

83. Yuki K. The immunomodulatory mechanism of dexmedetomidine. *Int Immunopharmacol.* (2021) 97:107709. doi: 10.1016/j.intimp.2021.107709

84. Wang K, Wu M, Xu J, Wu C, Zhang B, Wang G, et al. Effects of dexmedetomidine on perioperative stress, inflammation, and immune function: systematic review and meta-analysis. *Br J Anaesth.* (2019) 123:777–94. doi: 10.1016/j.bja.2019.07.027

85. Cheng HW. The immunomodulatory effects of clonidine, an alpha-2-adrenergic agonist, in laying hens. *Poult Sci.* (2006) 85:452–6. doi: 10.1093/ps/85.3.452

86. Bournazos S, Gupta A, Ravetch JV. The role of Igg Fc receptors in antibody-dependent enhancement. *Nat Rev Immunol.* (2020) 20:633–43. doi: 10.1038/s41577-020-00410-0

87. Wu Y, Liu Y, Huang H, Zhu Y, Zhang Y, Lu F, et al. Dexmedetomidine inhibits inflammatory reaction in lung tissues of septic rats by suppressing Tlr4/Nf-Kb pathway. *Mediators Inflamm.* (2013) 2013:562154. doi: 10.1155/2013/562154

88. Zhang JJ, Peng K, Zhang J, Meng XW, Ji FH. Dexmedetomidine preconditioning may attenuate myocardial ischemia/reperfusion injury by down-regulating the Hmgb1-Tlr4-Myd88-Nf-Kb signaling pathway. *PLoS ONE.* (2017) 12:e0172006. doi: 10.1371/journal.pone.0172006

89. Hamilton JL, Vashi M, Kishen EB, Fogg LF, Wimmer MA, Balk RA. The association of an alpha-2 adrenergic receptor agonist and mortality in patients with Covid-19. *Front Med.* (2021) 8:797647. doi: 10.3389/fmed.2021.797647

90. Moura E, Afonso J, Hein L, Vieira-Coelho MA. Alpha2-adrenoceptor subtypes involved in the regulation of catecholamine release from the adrenal medulla of mice. *Br J Pharmacol.* (2006) 149:1049–58. doi: 10.1038/sj.bjp.0706950

91. Giovannitti JA Jr, Thoms SM, Crawford JJ. Alpha-2 adrenergic receptor agonists: a review of current clinical applications. *Anesth Prog.* (2015) 62:31–9. doi: 10.2344/0003-3006-62.1.31

92. Herrera-García AM, Domínguez-Luis MJ, Arce-Franco M, Armas-González E, Álvarez de La Rosa D, Machado JD, et al. Prevention of neutrophil extravasation by A2-adrenoceptor-mediated endothelial stabilization. *J Immunol.* (2014) 193:3023–35. doi: 10.4049/jimmunol.1400255

93. Lankadeva YR, Shehabi Y, Deane AM, Plummer MP, Bellomo R, May CN. Emerging benefits and drawbacks of α -adrenoceptor agonists in the management of sepsis and critical illness. *Br J Pharmacol.* (2021) 178:1407–25. doi: 10.1111/bph.15363

94. Alonso B, Carregaro A, Cuypers C, Michielsen A, Gasthuys F, Schauvliege S. Effects of detomidine or romifidine during maintenance and recovery from isoflurane anaesthesia in horses. *Vet Anaesth Analg.* (2022) 49:624–33. doi: 10.1016/j.vaa.2022.07.004

95. Flaherty D. Alpha2-adrenoceptor agonists in small animal practice 1. Why they do what they do. *In Practice.* (2013) 35:524–30. doi: 10.1136/inp.f5826

96. Connell AR, Hookham MB, Fu D, Brazil DP, Lyons TJ Yu JY. Comparisons of A2-adrenergic agents, medetomidine and xylazine, with pentobarbital for anesthesia: important pitfalls in diabetic and nondiabetic rats. *J Ocul Pharmacol Ther.* (2022) 38:156–66. doi: 10.1089/jop.2021.0084

97. Zhu L, She ZG, Cheng X, Qin JJ, Zhang XJ, Cai J, et al. Association of blood glucose control and outcomes in patients with Covid-19 and pre-existing type 2 diabetes. *Cell Metab.* (2020) 31:1068–77.e3. doi: 10.1016/j.cmet.2020.04.021

98. Dollery C. *Therapeutic Drugs*. London: Churchill Lingstone (1991), p. 1.

99. Borba VV, Zandman-Goddard G, Shoenfeld Y. Prolactin and autoimmunity. *Front Immunol.* (2018) 9:73. doi: 10.3389/fimmu.2018.00073

100. Liu GL, Cui YF, Lu C, Zhao P. Ketamine a dissociative anesthetic: neurobiology and biomolecular exploration in depression. *Chem Biol Interact.* (2020) 319:109006. doi: 10.1016/j.cbi.2020.109006

101. Takahashi T, Kinoshita M, Shono S, Habu Y, Ogura T, Seki S, et al. The effect of ketamine anesthesia on the immune function of mice with postoperative septicemia. *Anesth Analg.* (2010) 111:1051–8. doi: 10.1213/ANE.0b013e3181ed12fc

102. Gao M, Jin W, Qian Y, Ji L, Feng G, Sun J. Effect of N-methyl-D-aspartate receptor antagonist on T helper cell differentiation induced by phorbol-myristate-acetate and ionomycin. *Cytokine.* (2011) 56:458–65. doi: 10.1016/j.cyto.2011.06.022

103. Braun S, Gaza N, Werdehausen R, Hermanns H, Bauer I, Durieux ME, et al. Ketamine induces apoptosis *via* the mitochondrial pathway in human lymphocytes and neuronal cells. *Br J Anaesth.* (2010) 105:347–54. doi: 10.1093/bja/aeq169

104. Zeng J, Xia S, Zhong W, Li J, Lin L. *In vitro* and *in vivo* effects of ketamine on generation and function of dendritic cells. *J Pharmacol Sci.* (2011) 117:170–9. doi: 10.1254/jphs.11113FP

105. Laudanski K, Qing M, Oszkiel H, Zawadka M, Lapko N, Nowak Z, et al. Ketamine affects *in vitro* differentiation of monocyte into immature dendritic cells. *Anesthesiology.* (2015) 123:628–41. doi: 10.1097/ALN.0000000000000783

106. Eldufani J, Nekoui A, Blaise G. Nonanesthetic effects of ketamine: a review article. *Am J Med.* (2018) 131:1418–24. doi: 10.1016/j.amjmed.2018.04.029

107. Jafarzadeh A, Hadavi M, Hassanshahi G, Rezaeian M, Vazirinejad R. General anesthetics on immune system cytokines: a narrative review article. *Anesth Pain Med.* (2020) 10:e103033. doi: 10.5812/aapm.103033

108. Li Y, Shen R, Wen G, Ding R, Du A, Zhou J, et al. Effects of ketamine on levels of inflammatory cytokines Il-6, Il-1β, and TNF-α in the hippocampus of mice following acute or chronic administration. *Front Pharmacol.* (2017) 8:139. doi: 10.3389/fphar.2017.00139

109. Patten KT, Valenzuela AE, Wallis C, Harvey DJ, Bein KJ, Wexler AS, et al. Hippocampal but not serum cytokine levels are altered by traffic-related air pollution in TgF344-Ad and wildtype Fischer 344 rats in a sex- and age-dependent manner. *Front Cell Neurosci.* (2022) 16:861733. doi: 10.3389/fncel.2022.861733

110. Banks WA. Peptides and the blood–brain barrier. *Peptides.* (2015) 72:16–9. doi: 10.1016/j.peptides.2015.03.010

111. Liu FL, Chen TL, Chen RM. Mechanisms of ketamine-induced immunosuppression. *Acta Anaesthesiol Taiwan.* (2012) 50:172–7. doi: 10.1016/j.aat.2012.12.001

112. Steffey EP, Mama KR, Brosnan RJ. Inhalation anesthetics. In: Grimm K, Lamont A, Tranquilli J, Greene S, Robertson S, editors. *Lumb & Jones' Veterinary Anesthesia*. Hoboken, NJ: John Wiley & Sons, Inc (2015). p. 297–329. doi: 10.1002/9781119421375.ch16

113. Stollings LM, Jia LJ, Tang P, Dou H, Lu B, Xu Y. Immune modulation by volatile anesthetics. *Anesthesiology.* (2016) 125:399–411. doi: 10.1097/ALN.0000000000001195

114. Kalimeris K, Christodoulaki K, Karakitsos P, Batistatou A, Lekka M, Bai M, et al. Influence of propofol and volatile anaesthetics on the inflammatory response in the ventilated lung. *Acta Anaesthesiol Scand.* (2011) 55:740–8. doi: 10.1111/j.1399-6576.2011.02461.x

115. Woo JH, Baik HJ, Kim CH, Chung RK, Kim DY, Lee GY, et al. Effect of propofol and desflurane on immune cell populations in breast cancer patients: a randomized trial. *J Korean Med Sci.* (2015) 30:1503–8. doi: 10.3346/jkms.2015.30.10.1503

116. Arruda NM, Braz LG, Nogueira FR, Souza KM, Aun AG, Figueiredo DBS, et al. Inflammation and DNA damage induction in surgical patients maintained with desflurane anesthesia. *Mutat Res Genet Toxicol Environ Mutagen.* (2019) 846:403073. doi: 10.1016/j.mrgentox.2019.07.003

117. Endo S, Yano A, Fukami T, Nakajima M, Yokoi T. Involvement of miRNAs in the early phase of halothane-induced liver injury. *Toxicology.* (2014) 319:75–84. doi: 10.1016/j.tox.2014.02.011

118. Khomich OA, Kochetkov SN, Bartosch B, Ivanov AV. Redox biology of respiratory viral infections. *Viruses.* (2018) 10:392. doi: 10.3390/v10080392

119. Kozlov EM, Ivanova E, Grechko AV, Wu WK, Starodubova AV, Orekhov AN. Involvement of oxidative stress and the innate immune system in SARS-CoV-2 infection. *Diseases.* (2021) 9:17. doi: 10.3390/diseases9010017

120. Erbas M, Demiraran Y, Yildirim HA, Sezen G, Iskender A, Karagoz I, et al. [Comparison of effects on the oxidant/antioxidant system of sevoflurane, desflurane and propofol infusion during general anesthesia]. *Rev Bras Anestesiol.* (2015) 65:68–72. doi: 10.1016/j.bjane.2014.05.004

121. Feng Y, He X, Yang Y, Chao D, Lazarus LH, Xia Y. Current research on opioid receptor function. *Curr Drug Targets.* (2012) 13:230–46. doi: 10.2174/138945012799201612

122. Pomorska DK, Gach K, Janecka A. Immunomodulatory effects of endogenous and synthetic peptides activating opioid receptors. *Mini Rev Med Chem.* (2014) 14:1148–55. doi: 10.2174/1389557515666150101095237

123. Chuang TK, Killam KF Jr, Chuang LF, Kung HF, Sheng WS, Chao CC, et al. Mu opioid receptor gene expression in immune cells. *Biochem Biophys Res Commun.* (1995) 216:922–30. doi: 10.1006/bbrc.1995.2709

124. Sacerdote P, Franchi S, Panerai AE. Non-analgesic effects of opioids: mechanisms and potential clinical relevance of opioid-induced immunodepression. *Curr Pharm Des.* (2012) 18:6034–42. doi: 10.2174/138161212803582496

125. Filipczak-Bryniarska I, Nazimek K, Nowak B, Kozlowski M, Wasik M, Bryniarski K. In contrast to morphine, buprenorphine enhances macrophage-induced humoral immunity and, as oxycodone, slightly suppresses the effector phase of cell-mediated immune response in mice. *Int Immunopharmacol.* (2018) 54:344–53. doi: 10.1016/j.intimp.2017.11.039

126. Allen AA, Kendall LV. Immunomodulation associated with sustained-release buprenorphine in female CD1 mice challenged with ovalbumin. *J Am Assoc Lab Anim Sci.* (2019) 58:577–82. doi: 10.30802/AALAS-JAALAS-18-000135

127. Anderson SL, Duke-Novakovski T, Singh B. The immune response to anesthesia: part 2 sedatives, opioids, and injectable anesthetic agents. *Vet Anaesth Analg.* (2014) 41:553–66. doi: 10.1111/vaa.12191

128. Luan G, Pan F, Bu L, Wu K, Wang A, Xu X. Butorphanol promotes macrophage phenotypic transition to inhibit inflammatory lung injury *via* K receptors. *Front Immunol.* (2021) 12:692286. doi: 10.3389/fimmu.2021.692286

129. Shapouri-Moghaddam A, Mohammadian S, Vazini H, Taghadosi M, Esmaeili SA, Mardani F, et al. Macrophage plasticity, polarization, and function in health and disease. *J Cell Physiol.* (2018) 233:6425–40. doi: 10.1002/jcp.26429

130. Widjaja G, Turki Jalil A, Sulaiman Rahman H, Abdelbasset WK, Bokov DO, Suksatan W, et al. Humoral immune mechanisms involved in protective and pathological immunity during Covid-19. *Hum Immunol.* (2021) 82:733–45. doi: 10.1016/j.humimm.2021.06.011

131. Sacerdote P, Bianchi M, Manfredi B, Panerai AE. Effects of tramadol on immune responses and nociceptive thresholds in mice. *Pain.* (1997) 72:325–30. doi: 10.1016/S0304-3959(97)00055-9

132. Saeed I, La Caze A, Hollmann MW, Shaw PN, Parat MO. New insights on tramadol and immunomodulation. *Curr Oncol Rep.* (2021) 23:123. doi: 10.1007/s11912-021-01121-y

133. Beilin B, Grinevich G, Yardeni IZ, Bessler H. Tramadol does not impair the phagocytic capacity of human peripheral blood cells. *Can J Anaesth.* (2005) 52:1035–9. doi: 10.1007/BF03021601

134. Boland JW, Foulds GA, Ahmedzai SH, Pockley AG. A preliminary evaluation of the effects of opioids on innate and adaptive human *in vitro* immune function. *BMJ Support Palliat Care.* (2014) 4:357–67. doi: 10.1136/bmjspcare-2013-000573

135. Wang ZY, Wang CQ, Yang JJ, Sun J, Huang YH, Tang QF, et al. Which has the least immunity depression during postoperative analgesia–morphine, tramadol, or tramadol with lornoxicam? *Clin Chim Acta.* (2006) 369:40–5. doi: 10.1016/j.cca.2006.01.008

136. Bianchi M, Rossoni G, Sacerdote P, Panerai AE. Effects of tramadol on experimental inflammation. *Fundam Clin Pharmacol.* (1999) 13:220–5. doi: 10.1111/j.1472-8206.1999.tb00342.x

137. Bastami S, Norling C, Trinks C, Holmlund B, Walz TM, Ahlner J, et al. Inhibitory effect of opiates on LPS mediated release of TNF and IL-8. *Acta Oncol.* (2013) 52:1022–33. doi: 10.3109/0284186X.2012.737932

138. MacFater WS, Xia W, Barazanchi A, Su'a B, Svirskis D, Hill AG. Intravenous local anaesthetic compared with intraperitoneal local anaesthetic in abdominal surgery: a systematic review. *World J Surg.* (2018) 42:3112–9. doi: 10.1007/s00268-018-4623-9

139. Taylor A, McLeod G. Basic pharmacology of local anaesthetics. *BJA Educ.* (2020) 20:34–41. doi: 10.1016/j.bjae.2019.10.002

140. Tavare AN, Perry NJ, Benzonana LL, Takata M, Ma D. Cancer recurrence after surgery: direct and indirect effects of anesthetic agents. *Int J Cancer.* (2012) 130:1237–50. doi: 10.1002/ijc.26448

141. Piegeler T, Votta-Velis EG, Liu G, Place AT, Schwartz DE, Beck-Schimmer B, et al. Antimetastatic potential of amide-linked local anesthetics: inhibition of lung adenocarcinoma cell migration and inflammatory SRC signaling independent of sodium channel blockade. *Anesthesiology.* (2012) 117:548–59. doi: 10.1097/ALN.0b013e3182661977

142. Cassuto J, Sinclair R, Bonderovic M. Anti-inflammatory properties of local anesthetics and their present and potential clinical implications. *Acta Anaesthesiol Scand.* (2006) 50:265–82. doi: 10.1111/j.1399-6576.2006.00936.x

143. Kolle G, Metterlein T, Gruber M, Seyfried T, Petermichl W, Pfaehler SM, et al. Potential impact of local anesthetics inducing granulocyte arrest and altering immune functions on perioperative outcome. *J Inflamm Res.* (2021) 14:1–12. doi: 10.2147/JIR.S275525

144. Cruz FF, Rocco PR, Pelosi P. Anti-inflammatory properties of anesthetic agents. *Crit Care.* (2017) 21:67. doi: 10.1186/s13054-017-1645-x

145. Sheil M, De Benedictis GM, Scollo A, Metcalfe S, Innocent G, Polkinghorne A, et al. Efficacy of intra-operative topical wound anaesthesia to mitigate piglet castration pain-a large, multi-centred field trial. *Animals*. (2021) 11:2763. doi: 10.3390/ani11102763

146. Milosavljevic SB, Pavlovic AP, Trpkovic SV, Ilić AN, Sekulic AD. Influence of spinal and general anesthesia on the metabolic, hormonal, and hemodynamic response in elective surgical patients. *Med Sci Monit.* (2014) 20:1833–40. doi: 10.12659/MSM.890981

147. Edwards SH. *Nonsteroidal Anti-Inflammatory Drugs in Animals. MSD Veterinary Manual*, Vol. 11. Rahway, NJ: Merck & Co, Inc. (2022).

148. Cashman JN. The mechanisms of action of nsaids in analgesia. *Drugs.* (1996) 52(Suppl 5):13–23. doi: 10.2165/00003495-199600525-00004

149. Schattenkirchner M. Meloxicam: a selective Cox-2 inhibitor non-steroidal anti-inflammatory drug. *Expert Opin Investig Drugs.* (1997) 6:321–34. doi: 10.1517/13543784.6.3.321

150. Michelin MA, Figueiredo F, Cunha FQ. Involvement of prostaglandins in the immunosuppression occurring during experimental infection by paracoccidioides brasiliensis. *Exp Parasitol.* (2002) 102:170–7. doi: 10.1016/S0014-4894(03)00053-5

151. Roth J, Hübschle T, Pehl U, Ross G, Gerstberger R. Influence of systemic treatment with cyclooxygenase inhibitors on lipopolysaccharide-induced fever and circulating levels of cytokines and cortisol in guinea-pigs. *Pflugers Arch.* (2002) 443:411–7. doi: 10.1007/s004240100718

152. Kalinski P. Regulation of immune responses by prostaglandin E2. *J Immunol.* (2012) 188:21–8. doi: 10.4049/jimmunol.1101029

153. de Grauw JC, van de Lest CH, Brama PA, Rambags BP, van Weeren PR. *In vivo* effects of meloxicam on inflammatory mediators, mmp activity and cartilage biomarkers in equine joints with acute synovitis. *Equine Vet J.* (2009) 41:693–9. doi: 10.2746/042516409X436286

154. Kolstad AM, Rodriguiz RM, Kim CJ, Hale LP. Effect of pain management on immunization efficacy in mice. *J Am Assoc Lab Anim Sci.* (2012) 51:448–57.

155. Fishback JE, Stronsky SM, Green CA, Bean KD, Froude JW. Antibody production in rabbits administered freund's complete adjuvant and carprofen concurrently. *Lab Anim.* (2016) 45:63–6. doi: 10.1038/laban.937

156. Kotiw M, Morgan M, Taylor SM, Shiels IA. Detection of anti-tnfalpha activity in canine hyperimmune serum using a tnfalpha inhibition assay. *Vet Clin Pathol.* (2010) 39:46–52. doi: 10.1111/j.1939-165X.2009.00166.x

157. Hish GA Jr, Diaz JA, Hawley AE, Myers DD Jr, Lester PA. Effects of analgesic use on inflammation and hematology in a murine model of venous thrombosis. *J Am Assoc Lab Anim Sci.* (2014) 53:485–93.

158. DeMarco GJ, Nunamaker EA. A review of the effects of pain and analgesia on immune system function and inflammation: relevance for preclinical studies. *Comp Med.* (2019) 69:520–34. doi: 10.30802/AALAS-CM-19-000041

159. Giraudel JM, Toutain PL, King JN, Lees P. Differential inhibition of cyclooxygenase isoenzymes in the cat by the nsaid robenacoxib. *J Vet Pharmacol Ther.* (2009) 32:31–40. doi: 10.1111/j.1365-2885.2008.01031.x

160. Bennett D, Eckersall PD, Waterston M, Marchetti V, Rota A, McCulloch E, et al. The effect of robenacoxib on the concentration of C-reactive protein in synovial fluid from dogs with osteoarthritis. *BMC Vet Res.* (2013) 9:42. doi: 10.1186/1746-6148-9-42

161. Risser A, Donovan D, Heintzman J, Page T. NSAID prescribing precautions. *Am Fam Physician.* (2009) 80:1371–8.

162. Mbah C, Ogbonna J, Nzekwe I, Ugwu G, Ezeh R, Builders P, et al. Nanovesicle formulation enhances anti-inflammatory property and safe use of piroxicam. *Pharm Nanotechnol.* (2021) 9:177–90. doi: 10.2174/2211738509666210129151844

163. Pinho-Ribeiro FA, Verri WA Jr, Chiu IM. Nociceptor sensory neuron-immune interactions in pain and inflammation. *Trends Immunol.* (2017) 38:5–19. doi: 10.1016/j.it.2016.10.001

164. Amodeo G, Bugada D, Franchi S, Moschetti G, Grimaldi S, Panerai A, et al. Immune function after major surgical interventions: the effect of postoperative pain treatment. *J Pain Res.* (2018) 11:1297–305. doi: 10.2147/JPR.S158230

165. Page GG. The immune-suppressive effects of pain. *Adv Exp Med Biol.* (2003) 521:117–25.

166. Peterson NC, Nunamaker EA, Turner PV. To treat or not to treat: the effects of pain on experimental parameters. *Comp Med.* (2017) 67:469–82.

167. Pezzone MA, Dohanics J, Rabin BS. Effects of footshock stress upon spleen and peripheral blood lymphocyte mitogenic responses in rats with lesions of the paraventricular nuclei. *J Neuroimmunol.* (1994) 53:39–46. doi: 10.1016/0165-5728(94)90062-0

168. Shavit Y, Martin FC, Yirmiya R, Ben-Eliyahu S, Terman GW, Weiner H, et al. Effects of a single administration of morphine or footshock stress on natural killer cell cytotoxicity. *Brain Behav Immun.* (1987) 1:318–28. doi: 10.1016/0889-1591(87)90034-1

169. Laudenslager ML, Fleshner M, Hofstadter P, Held PE, Simons L, Maier SF. Suppression of specific antibody production by inescapable shock: stability under varying conditions. *Brain Behav Immun.* (1988) 2:92–101. doi: 10.1016/0889-1591(88)90010-4

170. Dabrowska AM, Słotwiński R. Review paperthe immune response to surgery and infection. *Cent Eur J Immunol.* (2014) 39:532–7. doi: 10.5114/ceji.2014.47741

171. Brown EN, Pavone KJ, Naranjo M. Multimodal general anesthesia: theory and practice. *Anesth Analg.* (2018) 127:1246–58. doi: 10.1213/ANE.0000000000003668

172. Amaya V, Paterson MBA, Descovich K, Phillips CJC. Effects of olfactory and auditory enrichment on heart rate variability in shelter dogs. *Animals.* (2020) 10:1385. doi: 10.3390/ani10081385

173. Billman GE. The effect of heart rate on the heart rate variability response to autonomic interventions. *Front Physiol.* (2013) 4:222. doi: 10.3389/fphys.2013.00222

174. Turner PV, Pang DS, Lofgren JL. A review of pain assessment methods in laboratory rodents. *Comp Med.* (2019) 69:451–67. doi: 10.30802/AALAS-CM-19-000042

175. Klages C. IACUC and veterinary considerations for review of ABSL3 and ABSL4 research protocols. *ILAR J.* (2021) 61:3–9. doi: 10.1093/ilar/ilab009

176. Kendall LV, Owiny JR, Dohm ED, Knapek KJ, Lee ES, Kopanke JH, et al. Replacement, refinement, and reduction in animal studies with biohazardous agents. *ILAR J.* (2018) 59:177–94. doi: 10.1093/ilar/ily021

177. Mota-Rojas D, Olmos-Hernández A, Verduzco-Mendoza A, Hernández E, Martínez-Burnes J, Whittaker AL. The utility of grimace scales for practical pain assessment in laboratory animals. *Animals*. (2020) 10:1838. doi: 10.3390/ani10101838

178. Langford DJ, Bailey AL, Chanda ML, Clarke SE, Drummond TE, Echols S, et al. Coding of facial expressions of pain in the laboratory mouse. *Nat Methods.* (2010) 7:447–9. doi: 10.1038/nmeth.1455

179. Reijgwart ML, Schoemaker NJ, Pascuzzo R, Leach MC, Stodel M, de Nies L, et al. The composition and initial evaluation of a grimace scale in ferrets after surgical implantation of a telemetry probe. *PLoS ONE.* (2017) 12:e0187986. doi: 10.1371/journal.pone.0187986

180. Evangelista MC, Watanabe R, Leung VSY, Monteiro BP, O'Toole E, Pang DSJ, et al. Facial expressions of pain in cats: the development and validation of a feline grimace scale. *Sci Rep.* (2019) 9:19128. doi: 10.1038/s41598-019-55693-8

181. Navarro E, Mainau E, Manteca X. Development of a facial expression scale using farrowing as a model of pain in sows. *Animals*. (2020) 10:2113. doi: 10.3390/ani10112113

182. Benato L, Murrell J, Knowles TG, Rooney NJ. Development of the Bristol Rabbit Pain Scale (BRPS): a multidimensional composite pain scale specific to rabbits (*Oryctolagus cuniculus*). *PLoS ONE*. (2021) 16:e0252417. doi: 10.1371/journal.pone.0252417

183. Benato L, Murrell J, Rooney N. Bristol Rabbit Pain Scale (BRPS): clinical utility, validity and reliability. *BMC Vet Res*. (2022) 18:341. doi: 10.1186/s12917-022-03434-x

184. Watanabe R, Doodnaught GM, Evangelista MC, Monteiro BP, Ruel HLM, Steagall PV. Inter-rater reliability of the feline grimace scale in cats undergoing dental extractions. *Front Vet Sci*. (2020) 7:302. doi: 10.3389/fvets.2020.00302

185. Hernandez-Avalos I, Mota-Rojas D, Mora-Medina P, Martínez-Burnes J, Casas Alvarado A, Verduzco-Mendoza A, et al. Review of different methods used for clinical recognition and assessment of pain in dogs and cats. *Int J Vet Sci Med*. (2019) 7:43–54. doi: 10.1080/23144599.2019.1680044

186. Cleary SJ, Pitchford SC, Amison RT, Carrington R, Robaina Cabrera CL, Magnen M, et al. Animal models of mechanisms of SARS-CoV-2 infection and Covid-19 pathology. *Br J Pharmacol*. (2020) 177:4851–65. doi: 10.1111/bph.15143

187. Denayer T, Stöhr T, Van Roy M. Animal models in translational medicine: validation and prediction. *New Horiz Transl Med*. (2014) 2:5–11. doi: 10.1016/j.nhtm.2014.08.001

188. Wemelsfelder F, Mullan S. Applying ethological and health indicators to practical animal welfare assessment. *Rev Sci Tech*. (2014) 33:111–20. doi: 10.20506/rst.33.1.2259

189. Lilley E, Stanford SC, Kendall DE, Alexander SPH, Cirino G, Docherty JR, et al. Arrive 2.0 and the British Journal of Pharmacology: updated guidance for 2020. *Br J Pharmacol*. (2020) 177:3611–6. doi: 10.1111/bph.15178

190. Mei J, Riedel N, Grittner U, Endres M, Banneke S, Emmrich JV. Body temperature measurement in mice during acute illness: implantable temperature transponder versus surface infrared thermometry. *Sci Rep*. (2018) 8:3526. doi: 10.1038/s41598-018-22020-6

191. Niemeyer JE. Telemetry for small animal physiology. *Lab Anim*. (2016) 45:255–7. doi: 10.1038/laban.1048

192. Carbone L. Pain in laboratory animals: the ethical and regulatory imperatives. *PLoS ONE*. (2011) 6:e21578. doi: 10.1371/journal.pone.0021578

193. Relja B, Land WG. Damage-associated molecular patterns in trauma. *Eur J Trauma Emerg Surg*. (2020) 46:751–75. doi: 10.1007/s00068-019-01235-w

194. Jia R, Zhou M, Tuttle CSL, Maier AB. Immune capacity determines outcome following surgery or trauma: a systematic review and meta-analysis. *Eur J Trauma Emerg Surg*. (2020) 46:979–91. doi: 10.1007/s00068-019-01271-6

195. Huber-Lang M, Lambris JD, Ward PA. Innate immune responses to trauma. *Nat Immunol*. (2018) 19:327–41. doi: 10.1038/s41590-018-0064-8

196. González-Sánchez C, Fraile JC, Pérez-Turiel J, Damm E, Schneider JG, Zimmermann H, et al. Capacitive sensing for non-invasive breathing and heart monitoring in non-restrained, non-sedated laboratory mice. *Sensors*. (2016) 16:1052. doi: 10.3390/s16071052

197. Belda B, Enomoto M, Case BC, Lascelles BDX. Initial evaluation of petpace activity monitor. *Vet J*. (2018) 237:63–8. doi: 10.1016/j.tvjl.2018.05.011

198. Halachmi I, Guarino M, Bewley J, Pastell M. Smart animal agriculture: application of real-time sensors to improve animal well-being and production. *Annu Rev Anim Biosci*. (2019) 7:403–25. doi: 10.1146/annurev-animal-020518-114851

199. Hernández-Avalos I, Valverde A, Antonio Ibancovichi-Camarillo J, Sánchez-Aparicio P, Recillas-Morales S, Rodríguez-Velázquez D, et al. Clinical use of the parasympathetic tone activity index as a measurement of postoperative analgaesia in dogs undergoing ovariohysterectomy. *J Vet Res*. (2021) 65:117–23. doi: 10.2478/jvetres-2021-0004

200. Rowlison de Ortiz A, Belda B, Hash J, Enomoto M, Robertson J, Lascelles BDX. Initial exploration of the discriminatory ability of the petpace collar to detect differences in activity and physiological variables between healthy and osteoarthritic dogs. *Front Pain Res*. (2022) 3:949877. doi: 10.3389/fpain.2022.949877

201. Magawa S, Lear CA, Beacom MJ, King VJ, Kasai M, Galinsky R, et al. Fetal heart rate variability is a biomarker of rapid but not progressive exacerbation of inflammation in preterm fetal sheep. *Sci Rep*. (2022) 12:1771. doi: 10.1038/s41598-022-05799-3

202. Kézér FL, Kovács L, Tozsér J. Step behaviour and autonomic nervous system activity in multiparous dairy cows during milking in a herringbone milking system. *Animal*. (2015) 9:1393–6. doi: 10.1017/S1751731115000130

203. Paci P, Mancini C, Price BA. Designing for wearability in animal biotelemetry. In: *Proceedings of the Third International Conference on Animal-Computer Interaction*. Milton Keynes: Association for Computing Machinery (2016), p. 13. doi: 10.1145/2995257.3012018

204. Stygar AH, Gómez Y, Berteselli GV, Dalla Costa E, Canali E, Niemi JK, et al. A systematic review on commercially available and validated sensor technologies for welfare assessment of dairy cattle. *Front Vet Sci*. (2021) 8:634338. doi: 10.3389/fvets.2021.634338

205. Richardson CA. The power of automated behavioural homecage technologies in characterizing disease progression in laboratory mice: a review. *Appl Anim Behav Sci*. (2015) 163:19–27. doi: 10.1016/j.applanim.2014.11.018

206. Casas-Alvarado A, Mota-Rojas D, Hernández-Ávalos I, Mora-Medina P, Olmos-Hernández A, Verduzco-Mendoza A, et al. Advances in infrared thermography: surgical aspects, vascular changes, and pain monitoring in veterinary medicine. *J Therm Biol*. (2020) 92:102664. doi: 10.1016/j.jtherbio.2020.102664

207. Mota-Rojas D, Olmos-Hernández A, Verduzco-Mendoza A, Lecona-Butrón H, Martínez-Burnes J, Mora-Medina P, et al. Infrared thermal imaging associated with pain in laboratory animals. *Exp Anim*. (2021) 70:1–12. doi: 10.1538/expanim.20-0052

208. Verduzco-Mendoza A, Bueno-Nava A, Wang D, Martínez-Burnes J, Olmos-Hernández A, Casas A, et al. Experimental applications and factors involved in validating thermal windows using infrared thermography to assess the health and thermostability of laboratory animals. *Animals*. (2021) 11:3448. doi: 10.3390/ani11123448

209. Wang FK, Shih JY, Juan PH, Su YC, Wang YC. Non-invasive cattle body temperature measurement using infrared thermography and auxiliary sensors. *Sensors*. (2021) 21:2425. doi: 10.3390/s21072425

210. Rekant SI, Lyons MA, Pacheco JM, Arzt J, Rodriguez LL. Veterinary applications of infrared thermography. *Am J Vet Res*. (2016) 77:98–107. doi: 10.2460/ajvr.77.1.98

211. Loughin C, Marino D. Evaluation of thermographic imaging of the limbs of healthy dogs. *Am J Vet Res*. (2007) 68:1064–9. doi: 10.2460/ajvr.68.10.1064

212. Warren-Gash C, Blackburn R, Whitaker H, McMenamin J, Hayward AC. Laboratory-confirmed respiratory infections as triggers for acute myocardial infarction and stroke: a self-controlled case series analysis of national linked datasets from Scotland. *Eur Respir J*. (2018) 51:170179. doi: 10.1183/13993003.01794-2017

213. Schaefer AL, Cook N, Tessaro SV, Deregt D, Desroches G, Dubeski PL, et al. Early detection and prediction of infection using infrared thermography. *Can J Anim Sci*. (2004) 84:73–80. doi: 10.4141/A02-104

214. Pereira C, Kunczik J, Bleich A, Haeger C, Kiessling F, Thum T, et al. Perspective review of optical imaging in welfare assessment in animal-based research. *J Biomed Opt*. (2019) 24:1–11. doi: 10.1117/1.JBO.24.7.070601

215. Homer LC, Alderman TS, Blair HA, Brocard AS, Broussard EE, Ellis RP, et al. Guidelines for Biosafety training programs for workers assigned to BSL-3 research laboratories. *Biosecur Bioterror*. (2013) 11:10–9. doi: 10.1089/bsp.2012.0038

216. Oh DY, Barr IG, Hurt AC. A novel video tracking method to evaluate the effect of influenza infection and antiviral treatment on ferret activity. *PLoS ONE*. (2015) 10:e0118780. doi: 10.1371/journal.pone.0118780

217. Wu B, Abbott T, Fishman D, McMurray W, Mor G, Stone K, et al. Comparison of statistical methods for classification of ovarian cancer using mass spectrometry data. *Bioinformatics*. (2003) 19:1636–43. doi: 10.1093/bioinformatics/btg210

218. Price A, Okumura A, Haddock E, Feldmann F, Meade-White K, Sharma P, et al. Transcriptional correlates of tolerance and lethality in mice predict ebola virus disease patient outcomes. *Cell Rep*. (2020) 30:1702–13.e6. doi: 10.1016/j.celrep.2020.01.026

219. Feighelstein M, Shimshoni I, Finka LR, Luna SPL, Mills DS, Zamansky A. Automated recognition of pain in cats. *Sci Rep*. (2022) 12:9575. doi: 10.1038/s41598-022-13348-1

220. Mei J, Banneke S, Lips J, Kuffner MTC, Hoffmann CJ, Dirnagl U, et al. Refining humane endpoints in mouse models of disease by systematic review and machine learning-based endpoint definition. *ALTEX*. (2019) 36:555–71. doi: 10.14573/altex.1812231

221. Hughes GL, Lones MA, Bedder M, Currie PD, Smith SL, Pownall ME. Machine learning discriminates a movement disorder in a zebrafish model of Parkinson's disease. *Dis Model Mech*. (2020) 13:dmm045815. doi: 10.1242/dmm.045815

222. Ellmann S, Seyler L, Gillmann C, Popp V, Treutlein C, Bozec A, et al. Machine learning algorithms for early detection of bone metastases in an experimental rat model. *J Vis Exp*. (2020) 162. doi: 10.3791/61235

223. Carslake C, Vázquez-Diosdado JA, Kaler J. Machine learning algorithms to classify and quantify multiple behaviours in dairy calves using a sensor: moving beyond classification in precision livestock. *Sensors*. (2020) 21:88. doi: 10.3390/s21010088

224. Gu Y, Ge Z, Bonnington CP, Zhou J. Progressive transfer learning and adversarial domain adaptation for cross-domain skin disease classification. *IEEE J Biomed Health Inform*. (2020) 24:1379–93. doi: 10.1109/JBHI.2019.2942429

225. O'Malley CI, Hubley R, Tambadou H, Turner PV. Refining restraint techniques for research pigs through habituation. *Front Vet Sci*. (2022) 9:1016414. doi: 10.3389/fvets.2022.1016414

226. Chiesa OA, Gonzales R, Kouneski A, Lewandowski A, Rotstein D, Myers MJ. Minimally invasive ultrasound-guided technique for central venous catheterization *via* the external jugular vein in pigs. *Am J Vet Res*. (2021) 82:760–9. doi: 10.2460/ajvr.82.9.760

227. Ortmeyer HK, Robey L, McDonald T. Combining actigraph link and PetPace collar data to measure activity, proximity, and physiological responses in freely moving dogs in a natural environment. *Animals*. (2018) 8:230. doi: 10.3390/ani8120230

228. Taneja M, Byabazaire J, Jalodia N, Davy A, Olariu C, Malone P. Machine learning based fog computing assisted data-driven approach for early lameness detection in dairy cattle. *Comput Electron Agric*. (2020) 171:105286. doi: 10.1016/j.compag.2020.105286

frontiers | Frontiers in Veterinary Science

TYPE Original Research
PUBLISHED 10 February 2023
DOI 10.3389/fvets.2023.1112466

OPEN ACCESS

EDITED BY
Mikolaj Adamek,
University of Veterinary Medicine Hannover, Germany

REVIEWED BY
Xu-Jie Zhang,
Huazhong Agricultural University, China
Hoole,
Keele University, United Kingdom

*CORRESPONDENCE
Niccolò Vendramin
✉ niven@aqua.dtu.dk

SPECIALTY SECTION
This article was submitted to Veterinary Infectious Diseases, a section of the journal Frontiers in Veterinary Science

RECEIVED 30 November 2022
ACCEPTED 25 January 2023
PUBLISHED 10 February 2023

CITATION
Sørensen J, Cuenca A, Olsen AB, Skovgaard K, Iburg TM, Olesen NJ and Vendramin N (2023) Decreased water temperature enhance *Piscine orthoreovirus* genotype 3 replication and severe heart pathology in experimentally infected rainbow trout.
Front. Vet. Sci. 10:1112466.
doi: 10.3389/fvets.2023.1112466

Decreased water temperature enhance *Piscine orthoreovirus* genotype 3 replication and severe heart pathology in experimentally infected rainbow trout

Juliane Sørensen[1], Argelia Cuenca[1], Anne Berit Olsen[2], Kerstin Skovgaard[3], Tine Moesgaard Iburg[1], Niels Jørgen Olesen[1] and Niccolò Vendramin[1]*

[1]Section for Fish and Shellfish Diseases, National Institute for Aquatic Resources, Technical University of Denmark, Kgs. Lyngby, Denmark, [2]Section of Aquatic Biosecurity Research, Norwegian Veterinary Institute, Bergen, Norway, [3]Department of Biotechnology and Biomedicine, Technical University of Denmark, Kgs. Lyngby, Denmark

Piscine orthoreovirus genotype 3 (PRV-3) was first discovered in Denmark in 2017 in relation to disease outbreaks in rainbow trout (*Oncorhynchus mykiss*). While the virus appears to be widespread in farmed rainbow trout, disease outbreaks associated with detection of PRV-3 have only occurred in recirculating aquaculture systems, and has predominantly been observed during the winter months. To explore the possible effects of water temperature on PRV-3 infection in rainbow trout, an *in vivo* cohabitation trial was conducted at 5, 12, and 18°C. For each water temperature, a control tank containing mock-injected shedder fish and a tank with PRV-3 exposed fish were included. Samples were collected from all experimental groups every 2nd week post challenge (WPC) up until trial termination at 12 WPC. PRV-3 RNA load measured in heart tissue of cohabitants peaked at 6 WPC for animals maintained at 12 and 18°C, while it reached its peak at 12 WPC in fish maintained at 5°C. In addition to the time shift, significantly more virus was detected at the peak in fish maintained at 5°C compared to 12 and 18°C. In shedders, fish at 12 and 18°C cleared the infection considerably faster than the fish at 5°C: while shedders at 18 and 12°C had cleared most of the virus at 4 and 6 WPC, respectively, high virus load persisted in the shedders at 5°C until 12 WPC. Furthermore, a significant reduction in the hematocrit levels was observed in the cohabitants at 12°C in correlation with the peak in viremia at 6 WPC; no changes in hematocrit was observed at 18°C, while a non-significant reduction (due to large individual variation) trend was observed at cohabitants held at 5°C. Importantly, *isg15* expression was positively correlated with PRV-3 virus load in all PRV-3 exposed groups. Immune gene expression analysis showed a distinct gene profile in PRV-3 exposed fish maintained at 5°C compared to 12 and 18°C. The immune markers mostly differentially expressed in the group at 5°C were important antiviral genes including *rigi*, *ifit5* and *rsad2* (viperin). In conclusion, these data show that low water temperature allow for significantly higher PRV-3 replication in rainbow trout, and a tendency for more severe heart pathology development in PRV-3 injected fish. Increased viral replication was mirrored by increased expression of important antiviral genes. Despite no mortality being observed in the experimental trial, the data comply with field observations of clinical disease outbreaks during winter and cold months.

KEYWORDS

***Piscine orthoreovirus* genotype 3 (PRV-3), double stranded RNA (dsRNA) virus, temperature, immune response, rainbow trout, RAS**

1. Introduction

Piscine orthoreovirus is a double stranded RNA (dsRNA) virus, with a genome consisting of 10 segments (1–3). The virus is non-enveloped, with a double protein capsid in icosahedral structure (1).

Three genotypes of PRV have been described (4, 5), each with different host tropism:

PRV-1, which infects Atlantic salmon (*Salmo salar*), has been shown to be the causative agent of heart and skeletal muscle inflammation (HSMI) in Norway (6). Importantly, different strains representing different geographic regions or time of detection show different capabilities of inducing HSMI (6, 7). PRV-1 has also been linked to alteration in color of Atlantic salmon fillet (8).

PRV-2, which has been shown as the putative causative agent of erythrocytic inclusion body syndrome (EIBS) in coho salmon (*Oncorhynchus kisutch*) in Japan (9).

PRV-3, which primarily infects rainbow trout (*Oncorhynchus mykiss*), was first discovered in Norway in 2013 in a disease outbreak in farmed rainbow trout (10). It was then detected in Denmark in farmed rainbow trout in late 2017 and early 2018 in field cases with increased mortality and signs of abnormal swimming behavior (3, 11). As a result, a surveillance program was conducted in Denmark including 53 farms, both flow-through and recirculated aquaculture systems (RAS), in order to assess the spread of PRV-3 within Danish aquaculture (4). The study showed that ∼72% of the farms in the surveillance program were positive for PRV-3 at least once for the duration of the program (∼1.5 years). Notably, PRV-3 genotypes divide into two clades, which are geographically distinct. PRV-3a has so far only been detected in Norway, while PRV-3b has been detected in exchange and aeration, has shown no significant Europe and Chile (4). However, only RAS farms experienced cases of increased mortality in association with PRV-3 detection in Denmark (4). The occurrence of PRV-3 infection is often associated with other production pathogens [e.g., *Flavobacterium psychrophilum*, *Renibacterium salmoninarum*, and infectious pancreatic necrosis virus (IPNV); personal communication]. In the surveillance conducted in 2017–2019, while PRV-3 was detected at RAS farms throughout the year, all 14 disease outbreaks were recorded in December to April where the water temperature was low (4).

Experimental infection both with infected blood and purified viral particles have depicted the pathogenesis of the virus at the temperature of 12°C, and showed its capability of inducing heart pathology. However, private practitioners and farmers report more severe disease outbreaks where PRV-3 is detected during winter and spring, when the water temperature is lower (12, 13).

Experimental infection trials with PRV-1, -2, and -3 have yet to replicate the mortality observed in field cases despite observations of heart inflammation and anemia (6, 9, 13). In some instances, reduced survival is not observed experimentally even when fish are exposed to additional stressors beyond PRV challenge (6, 9, 14–20), pointing toward a complex host-pathogen-environment interaction to achieve clinical disease development.

Fish are poikilothermic organisms, with temperature having a measurable effect on energy metabolism (21). Notably, the host-pathogen interaction is also affected by temperature, either by the effect of temperature on the immune status of fish (22, 23), by affecting the capability of the pathogen to replicate at different environmental temperature, or a combination of both (24). Additionally, behavioral fever has been studied in fish; it induces fish to move to warmer areas as a response to infections (particularly viruses) (25). The increased water temperature has been shown to both improve immune response and modulate replication of the pathogen (26). This behavior has been reported for fish affected by HSMI (27, 28), and in a study which has reported epigenetic changes of the immune response in Atlantic salmon exposed to IPNV (29). Considering that disease outbreaks in Danish farms associated with PRV-3 have mostly been reported during winter, we attempt to dissect the host-pathogen-environment interaction by examining the effect of water temperature on PRV-3 infection kinetics.

By exposing rainbow trout to PRV-3 in a cohabitation trial at three different temperatures (5, 12, and 18°C), we have elucidated its effect on viral load kinetics, hematocrit, heart histopathology, and immune gene expression. The results of the experiment align with field observations, supporting the fact that low water temperature enhance PRV-3 replication and severe heart pathology.

2. Materials and methods

2.1. Production and preparation of inoculum

The experiment was conducted under license number 2019-15-0201-00159, and the experimental protocols were approved by the Danish Animal Research Authority. The PRV-3b isolate (DK/PRV315, accession number MW012855.1) used for inoculum was propagated *in vivo* following the procedure as previously described (3).

Briefly, Specific Pathogen Free (SPF) rainbow trout (average size of 30 g) were anesthetized in water containing benzocaine (80 mg/L, Sigma) and injected i.p. with 0.1 mL homogenized blood cell pellet from PRV-3b infected fish diluted 1:3 (v/v) in L-15 medium. The PRV-3 levels were monitored weekly by non-lethal blood sampling from five fish, which were marked by clipping of the adipose fin to avoid repeated sampling of the same fish. At 3 weeks post challenge (WPC), all of the fish were euthanized by immersing fish in water containing high concentration of benzocaine (800 mg/L). Blood was collected in heparin tubes, tested for PRV-3 levels by RT-qPCR (see below), and stored at 4°C.

The PRV-3 positive inoculum for the experiment consisted of 10 mL PRV-3b positive blood diluted in 10 mL L-15 medium and 500 μL gentamycin (Life technologies, Carlsbad, CA, USA). This inoculum was tested by RT-qPCR, with a Ct value of 29.4. The mock inoculum consisted of 5 mL blood from naive fish diluted in 15 mL L-15 medium and 500 μL gentamycin. Mock inoculum was confirmed negative by RT-qPCR.

2.2. Experimental Trial

The experiment was conducted under license as previously described.

Rainbow trout were obtained from eyed eggs provided by a Danish commercial fish farm registered officially free of infectious pancreatic necrosis virus (IPNV), infectious hematopoietic necrosis virus (IHNV), viral hemorrhagic septicemia virus (VHSV), and *Renibacterium salmoninarum* (bacterial kidney disease, BKD). After

10.3389/fvets.2023.1112466

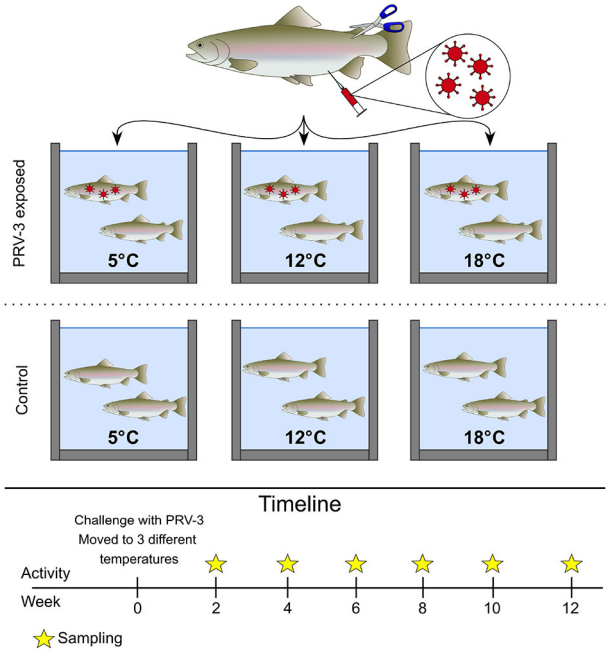

FIGURE 1
Experimental trial setup. The trial was conducted as a cohabitation trial, with one control and one PRV-3 exposed tank per temperature. The fish were kept at 12°C until i.p., injection, and were then moved to the respective temperatures (5, 12, and 18°C). Samples were collected every 2nd week post challenge according to the sampling table.

disinfection procedures using iodine, the eggs were hatched and grown in the wet laboratory facilities of section for fish and shellfish diseases, DTU Aqua, Kgs. Lyngby, Denmark) in recirculating and UV disinfected tap water (12°C).

Before beginning the trial, SPF rainbow trout were moved into the high containment infection facility at EURL. Six-hundred fish of ∼15 g were divided into six 180 L tanks run with 15 L/h flow-through fresh water renewal at the following conditions: L:D 12:12, stocking density below 60 kg/m3, and feeding at 1% of the biomass. The water temperature was set to 5, 12, and 18°C, with two tanks for each temperature (see Figure 1). The temperature was monitored throughout the trial (±2° in all temperatures). The experimental setting, including biomass, feeding ration, water exchange and aeration, has shown no significant difference in the level of oxygen and saturation in the water at the three temperatures. Fish were not acclimatized before the start of the experiment, but all started at 12°C before treatment.

The experimental trial was conducted as a cohabitation trial with a 50:50 distribution of shedders (intraperitoneal injection, i.p.) and cohabitants. Shedders were anesthetized by immersion in benzocaine-containing water (80 mg/L), and i.p. injected with 40 µL PRV-3b or mock inoculum. To later identify shedders, the adipose fin was clipped.

To confirm that the fish were infected with PRV-3b, RNA was extracted from the fish (heart tissue) at the peak of viral load at each temperature, with magnetic bead-based extraction using Indimag Pathogen Kit in an IndiMag48 automated extraction system (Indical Biosciences) according to manufacturer's recommendations.

RT-PCR targeting the S1 segment (10) of PRV-3 was performed using OneStep RT-PCR kit (Qiagen) according to manufacturer's recommendations. The PCR products were separated by electrophoresis using 1.2% E-gels (ThermoFisher Scientific) and E-gel powerbase version 4 (Invitrogen) as instructed by the manufacturer. PCR fragments were cleaned with the QIAquick PCR Purification kit (Qiagen) according to manufacturer's recommendations, and Sanger sequencing was performed by Eurofins Genomics (Ebersberg, Germany). Sequence analysis was done using CLC Main Workbench 8 (version 11.0.1) and subsequently run through nucleotide BLAST, confirming that the experimental fish were infected with PRV-3b.

2.3. Sample collection

Samples were collected every 2nd week post challenge from weeks 2 to 12. At each sampling point, 6:6 and 3:3 shedders:cohabitants from PRV-3b exposed and control groups, respectively, were euthanized in benzocaine-containing water (800 mg/L) and then sampled. Blood was collected from the caudal vein in heparin-coated 1.5 mL tubes (Eppendorf) from the cohabitants. From all experimental groups, heart, spleen, and kidney were collected in 1.5 mL tubes containing 500 µL RNAlater (Invitrogen). Additionally, heart, spleen, gill, brain, kidney, and intestine were collected in 10% neutral buffered formalin (4% formaldehyde (VWR International A/S) for histopathological examination. For further details, see sampling plan in Table 1.

2.4. Improved RT-qPCR assay for PRV-3 detection

Based on previous sequence analysis of isolates from Denmark, a mismatch was observed in the region of S1 segment targeted by the RT-qPCR developed by Olsen et al. (10). In order to ensure optimal detection, a new assay was designed targeting the L1 segment. See Table 2 for primer and probe sequences. The new assay was tested against a panel of fish pathogens for specificity, and against both PRV-3 subgenotypes (PRV-3a and -3b) and an artificial control (PRV-3 gBlock, IDT, see Supplementary Table S1) to ensure equal and efficient detection of both.

2.5. Virus detection by RT-qPCR

Approximately 25 mg of heart tissue was homogenized in 600 µL PBS with a 5 mm stainless steel bead (Qiagen) for 2 min at 25 Hz on TissueLyzer II (Qiagen). The samples were centrifuged at 14,000 x g for 5 min at 4°C, and total RNA was extracted from 200 µL supernatant using the IndiMag Pathogen extraction (Indical Biosciences) kit previously described.

Viral load was assessed by RT-qPCR using TaqPath 1-Step Master Mix (Applied Biosystems) according to manufacturer's recommendations, using 5 µL RNA template in a total volume of 25 µL. As the starting amount of RNA template was not standardized among samples, the L1PRV3 assay was multiplexed with ELF1a assay (30, 31) in the concentrations shown in Table 2, with the following

TABLE 1 Sampling plan for all experimental groups (5, 12, and 18°C).

Group	Number of fish	Fish sampled per time point	Sampling points (WPC)	Sample	Purpose
Negative control	50 shedders (mock injected)	3	2, 4, 6, 8, 10, 12	Heart	PRV-3 qPCR Viral load
	50 cohabitants	3		Spleen	Immune gene expression
PRV-3	50 shedders (PRV-3 exposed)	6		Kidney	Backup
				Blood	hematocrit
	50 cohabitants	6		Organs	Histopathology

TABLE 2 Sequences and final concentration of primers and probes for PRV-3 detection by RT-qPCR.

Primer/probe	Sequence	Concentration (nM)	References
L1PRV3-951F	TACAGGTCGTGTTCCCGTTG	700	This paper
L1PRV3-1042R	TCCAGCCACGAGGTAGATCA	700	This paper
L1PRV3-1003 probe	/56-FAM/TTCAGGTTG/ZEN/ GATGGAGCGCG/3IABkFQ/	200	This paper
ELF1a_FW	CCC CTC CAG GAT GTC TAC AAA	200	(30)
ELF1a_BW	CAC ACG GCC CAC GGG TAC T	200	(30)
ELF1a_P	/5HEX/-ATC GGC GGT/ZEN/ATT GGA AC-/3IABkFQ/	50	(31)

thermal profile: 30 min at 50°C, 15 min at 95°C, 50 cycles of 15 s at 94°C and 1 min at 60°C.

Data was collected and analyzed using mxPro–mx3005P v4.10 Build 389, Schema 85 (Stratagene). The threshold was set using an inter-plate callibrator (PRV-3 positive tissue PCR control) for both PRV-3 and ELF1A. Data was exported to Excel 2016 (Microsoft), and Ct values of PRV-3 were normalized:

$$Ct(PRV-3) - Ct(ELF1a) = dCt$$

Statistical analyses for virus RNA load was performed on log2 transformed data of PRV-3 positive samples at selected time points.

2.6. Immune gene expression by high throughput microfluidic qPCR

Samples for immune gene expression analyses were selected based on the virus load in each experimental group, selecting samples collected before, during, and after highest virus RNA load. For shedders, samples collected at all time points at 5°C were selected, and at 12 and 18°C samples collected at 2–6 WPC were selected. For cohabitants, 8–12 WPC was selected for 5°C, and 2–8 WPC was selected for 12 and 18°C.

For immune gene expression analyses, RNA was extracted from spleen with RNeasy Mini Kit (Qiagen) using QiaCube (Qiagen) according to manufacturer's recommendations. Briefly, ∼25 mg tissue was homogenized in 700 µL RLT buffer with a 5 mm stainless steel bead (Qiagen) for 2 min at 25 Hz on TissueLyzer II (Qiagen). The lysate was centrifuged for 5 min at 4°C at 14,000 x g, and 600 µL supernatant was transferred to a clean tube for automatic extraction on QiaCube.

The concentration was measured by Nanodrop (Nanodrop 1000, Thermo Scientific), and the quality of the RNA was checked on a Bioanalyzer 2100 (Agilent) using RNA 6000 Nano Kit (Agilent) according to manufacturer's recommendations with an input of ∼100 ng total RNA. RNA integrity number (RIN) above 6 was accepted for downstream applications.

cDNA synthesis was performed using QuantiTect Reverse Transcription Kit (Qiagen) according to manufacturer's recommendations and as previously described (32), with an input of 500 ng total RNA. As control for genomic DNA (gDNA) contamination, samples with high RIN value were chosen as non-reverse transcription controls. After cDNA synthesis, all samples were diluted 2 µL cDNA in 18 µL Low EDTA TE-buffer (VWR).

Pre-amplification was performed using TaqMan PreAmp Master Mix (Applied Biosystems) as previously described (32). Briefly, pre-amplification was performed with a 20 µM primer mix containing all assays as shown in Table 3, with the following thermal cycling conditions: 95°C for 10 min, 20 cycles: 95°C for 15 s and 60°C for 4 min. After pre-amplification, all samples were treated with Exonuclease 1 (4 units/µL, New England Biolabs).

High throughput microfluidic qPCR on the pre-amplified, exonuclease treated cDNA samples was performed using 192.24 Dynamic Array IFC (Fluidigm/Standard Biotools) as previously described (33).

Briefly, 21 genes of interest (GOI) were selected along with the references genes listed in Table 3. The 192.24 Dynamic Array combines 192 samples with 24 different assays, resulting in 4,608 individual qPCR reactions running simultaneously.

Raw data analysis was performed in the Fluidigm Real-Time PCR Analysis software (version 4.7.1, build 20200930.1707, Fluidigm Corporation), and then exported to GenEx (version 7, MultiD Analyses AB).

To calibrate for variation between IFCs (integrated fluidic circuits), four samples were selected as interplate calibrators and included in each IFC run. After interplate calibration, all data was efficiency corrected based on the efficiency for each individual assay. To identify the most suitable reference genes, GeNorm

10.3389/fvets.2023.1112466

TABLE 3 Primers used for immune gene expression in spleen tissue.

Target	Primer name	Sequence
mx	RBT_mx_OI_73F	CTCATCTCAGCACACTTTATGATG
	RBT_mx_OI_73R	GGCAGGGATTTCTCGATATG
cd4	RBT_cd4_OI_89_F	CACACTGAAGATCGAGCGAGT
	RBT_cd4_OI_89_R	GGATGAGGAGGAGGACGAAT
cd8	RBT_cd8A_77_F	CCACGACGACTACACCAATG
	RBT_cd8A_77_R	CTTTCCCACTTTGCACGACT
ifng	RBT_ifng_70_F	ACACCGGGAAGTTGATCTTG
	RBT_ifng_70_R	CTCCCCCAATCCTAACCTTC
rsad2	RBT_rsad2_OI_78_F	GCTGGAAGGTGTTCCAGTGT
	RBT_rsad2_OI_78_R	GGTCGCTGATGAGAAACCTC
ifnc3	RBT_ifnc3_OI_78_F	CACAGTTGAGCAGCAGTGGT
	RBT_ifnc3_OI_78_R	GGTCGTCAGCTCCAAACAAT
tnf	RBT_tnf_OI_88_F	CTGGCAACGATGCAGGA
	RBT_tnf_OI_88_R	CGGCAATCTGCTTCAATGTA
il1b	RBT_il1b_OI_82_F	CAGCAGCTACCACAAAGTGC
	RBT_il1b_OI_82_R	GGCTACAGGTCTGGCTTCAG
irf8	RBT_irf8_OI_90_F	CGACGCCTCTATCTTCAAGG
	RBT_irf8_OI_ 90_R	AGCCTGGTCTTCCATGTAGC
mhc class II	RBT_MHCclassII_ 100_F	CAGGTTTCTACCCCAGTGGA
	RBT_MHCclassII_ 100_R	CCATCATCGTTTGGGAGAGT
gzma	RBT_gzma_82_F	CAAGACCAGGGTGGACTCAT
	RBT_gzma_82_R	GAACGACACGACTCCCCTTA
rigi	RBT_DDX58_105_F	ACTGAGATGCTCCGCAAGAT
	RBT_DDX58_105_R	CTGGTAGCTGCCTTCAGTCC
isg15	RBT_isg15_85_F	ATCCTGAATGCAGGCCATAG
	RBT_isg15_85_R	CAGAGGCTGTCAGGTGTCAA
tlr3	RBT_tlr3_83_F	CTCTAACGGCAACCAGAAGC
	RBT_tlr3_83_R	CTCTCCCCAGCATCAGAGTC
cxcl10	RBT_cxcl10/IP-10/11-1_107_F	ATCCATGACCAACACGATGA
	RBT_cxcl10/IP-10/11-1_107_R	ACAGGCACCGAGCTTTAGAA
saa	RBT_saa_i_78_F	CCCTCGTTGTAGGAGCTCAA
	RBT_saa_i_78_R	CACGCCACATGTCTTTAGCA
hp	RBT_hp_84_F	GCCTTGATCTTGTAAAACTCTCTCAA
	RBT_hp_84_R	TCAACATCGGAAGACATACTCAATC
ifit5	RBT_ifit5_73_F	AGAGAGGTGGCAGGCTAACA
	RBT_ifit5_73_R	CCTCTCCTGTTTGAGGAACG
ifi44	RBT_ifi44_OI_76_F	GGAAAGCTGAGAGGAGAAAGG
	RBT_ifi44_OI_76_R	GCCTGACCCACAGAACTGAT
irf1	RBT_irf1_OI_96_F	CACCCCACAGACTATGAAGACAG
	RBT_irf1_OI_96_R	GCTCAGGAACCTCTTGTCGT
csf1	RBT_csf1r_OI_71_F	GCAGCCAAGAACTGTATTCACC
	RBT_csf1r_OI_71_R	TTAGCCACATGGAGGTCTGTC
actb	RBT_actb_OI_84_F	GAAGATGACCCAGATTATGTTTGAG
	RBT_actb_OI_84_R	GAGGCGTACAGGGACAACAC
hprt1	RBT_hprt1_OI_73_F	CCTTGACAGGACAGAGAGGCTA
	RBT_hprt1_OI_73_R	GCAGAGGGCCACGATATG
eef1a1	RBT_eef1a1_OI_76_F	CGGTGGTATTGGAACTGTACCT
	RBT_eef1a1_OI_76_R	GGCGAAGGTGACGATCATA

"OI" indicates that the forward primer has been designed to cross an intron.

and GeNormFinder in GenEx were used. Of the three reference genes, *hprt1* and *eef1a1* were selected and the geometric mean of the two selected reference genes was used to normalize all genes.

2.7. Hematocrit

Hematocrit (hct) was measured by centrifuging an aliquot of heparinized full blood in glass microhematocrit tubes (manufacturer) at 2,000 x g for 10 min. The hematocrit value (% red blood cells) was read on a visual analogue scale. The remaining blood was centrifuged at the same speed and time for separation of plasma and blood cells.

2.8. Histopathology of heart

According to Olsen et al. (10),the heart was the organ most consistently affected in diseased rainbow trout naturally infected with PRV-3. Accordingly, heart was chosen as the indicator of tissue effect visible by light microscopy. Heart sampled from all experimental groups (see Table 1) were fixed in 10% neutral buffered formalin, and processed as previously described (10). The slides were assessed blinded. Histopathological findings were scored as none or very sparse (0–0.5), mild (1), moderate (1.5), and severe (2) (see Supplementary Figure S5).

2.9. Statistical analysis

Statistical analyses and plots of virus RNA load, hematocrit, and histopathology was performed in Graphpad Prism 9 [version 9.4.1 (681)]. Kruskuall-Wallis and Mann-Whitney test was selected for comparison between groups where relevant. Area under the curve (AUC) was used to assess the differences in virus load in shedders at two to eight WPC, and cohabitants at four to ten WPC at 18 and 12°C.

Data analysis of immune gene expression data was performed as previously described (34). Briefly, for fold-change calculation of

immune genes between control and PRV-3 exposed groups, relative quantities (RQ) of the PRV-3 exposed groups were scaled according the control of the corresponding control group, setting the mean value of the controls to 1. Statistical analyses were performed in Excel 2016 on log2 transformed non-scaled RQ values. T-test was selected, as gene expression values are assumed to be normally distributed within the given groups. Only genes with both $p < 0.05$ in addition to fold change> 2.0 or < 0.5 were considered significantly up- or down-regulated. Heatmaps were created in R (version 4.0.5) with Rstudio (version 1.4.1106), using the pheatmap package, and were based on the median value of the log2 transformed RQ values for each group. Graphs of individual genes were made based on non-scaled RQ values in Graphpad Prism 9.

Pearson's correlation was calculated using GenEx (version 7, MultiD Analyses AB).

3. Results

3.1. New RT-qPCR assay performance

To assess the specificity and sensitivity of the newly developed PRV-3 qPCR assay targeting the L1 segment, the assay was tested against a series of pathogens, and standard curves based on both subgenotypes of PRV-3 along with the PRV-3 gblock (artificial control). Of the following pathogens, none besides PRV-3 were detected by the assay: *R. salmoninarum*, CEV, *A. invadans*, IHNV, IPNV, ISAV, KHV, MLO/RMS, NODA virus, OMV, PFRV, *P. salmonis*, *T. bryosalmonae*, PMCV, SGPV, PRV-1, PRV-2, SAV, SVCV, TSV, VHSV, and WSSV.

Limit of detection was 7.6 copies per reaction (tested in quadruplicates) at Ct 31.

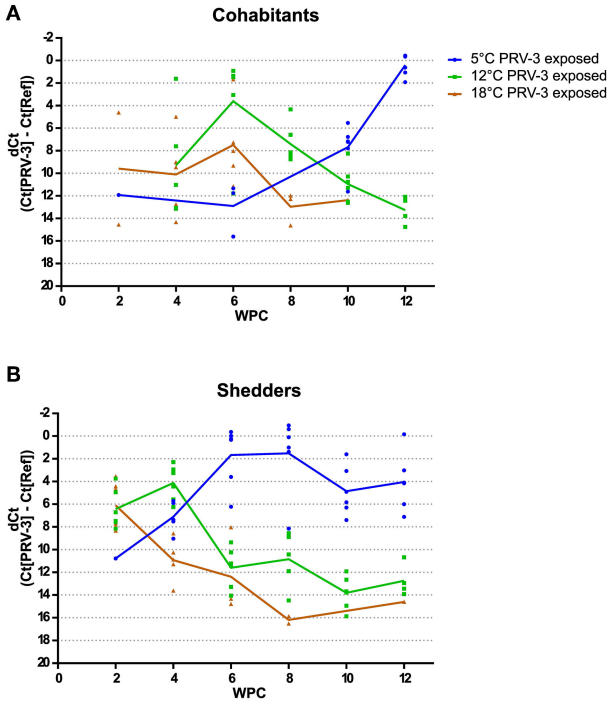

FIGURE 2
PRV-3 virus load shown as dCt [= Ct(PRV-3)-Ct(Reference gene)] for **(A)** cohabitants, and **(B)** shedders. Only individuals that tested positive are shown on the graphs. In cohabitants, a significant difference in virus load was detected at 5°C at 12 WPC compared to 6 WPC at 12 and 18°C (time point of highest virus load, $p = 0.024$ and $p = 0.009$, respectively). Similar tendency was observed in the shedders: at 5°C 8 WPC, a significantly higher amount of virus was detected compared to 2 WPC at 18°C and 4 WPC at 12°C ($p = 0.041$ and $p = 0.026$, respectively).

3.2. Virus load across temperatures

Figure 2 shows the dCt values of PRV-3 positive fish for both cohabitants (Figure 2A) and shedders (Figure 2B) measured in heart tissue. Table 4 shows the number of PRV-3 positive fish in the PRV-3 exposed groups at the different temperatures and time points.

In cohabitants (see Figure 2A), virus RNA load peaked at 6 weeks post challenge for both 12 and 18°C, with a lower amount at 18°C (not statistically different, $p = 0.16$ Mann-Whitney test). At this time point, six out of six and five out of six fish at 12 and 18°C, respectively, were positive for PRV-3. From 6 to 12 WPC, the virus RNA load steadily decreased in both groups; four and zero out of six fish were positive for PRV-3 at 12 WPC at 12 and 18°C, respectively (see Table 4).

At 5°C, only four cohabitant fish had tested positive up until 10 WPC, and at very low virus levels. However, at 10 weeks post challenge, all six fish were positive with medium-high virus load. At 12 WPC, six out of six fish were positive with high virus load. Comparing the time point with highest virus load at the three different temperature (6 WPC for 12 and 18°C, and 12 WPC for 5°C), there was significantly more virus detected at 5°C compared to 12 and 18°C ($p = 0.024$ and $p = 0.009$, respectively).

In shedders (see Figure 2B), fish kept at 18 and 12°C had high virus load with all six fish testing positive for PRV-3 at 2 and 4 WPC, respectively, after which the virus load decreases. At the end of the experiment, one and four fish at 18 and 12°C were PRV-3 positive at low virus levels, respectively.

Shedders at 5°C experienced a time delay in virus load. Here, high virus load is detected at 6 WPC where all six fish tested positive. Interestingly, for the remainder of the experiment, all shedders kept at 5°C were PRV-3 positive, and at high virus load. The fish seem unable to clear the infection, unlike what is typically observed at higher temperatures. Comparing the time points with highest virus load at the different conditions, fish kept at 5°C at 8 WPC had significantly higher virus load compared to fish at 18°C at 2 WPC ($p = 0.041$), and compared to 12°C at 4 WPC ($p = 0.026$). No significant difference was observed between shedders maintained at 12 and 18°C ($p = 0.818$).

3.3. Hematocrit fluctuations due to temperature and PRV-3 infection

Cohabitants exposed to PRV-3 kept at 12°C experienced a significant reduction in hct levels compared to cohabitants kept at 5 and 18°C at 6 weeks post challenge (p = 0,005 and $p = 0.026$, respectively), corresponding to the time of highest virus load in the 12°C group. Here, a reduction from ~50 to 30% hct was observed (see Figure 3).

TABLE 4 Number of PRV-3 positive fish at a given time-point and temperature.

WPC/ temperature	2	4	6	8	10	12	Total no. of positive fish
Cohabitants							
5°C	1	0	3	0	6	6	16/36
12°C	0	5	6	6	6	4	27/36
18°C	2	5	5	3	1	0	16/36
Shedders							
5°C	1	5	6	6	6	6	30/36
12°C	6	6	6	5	6	4	33/36
18°C	6	5	3	2	0	1	17/36

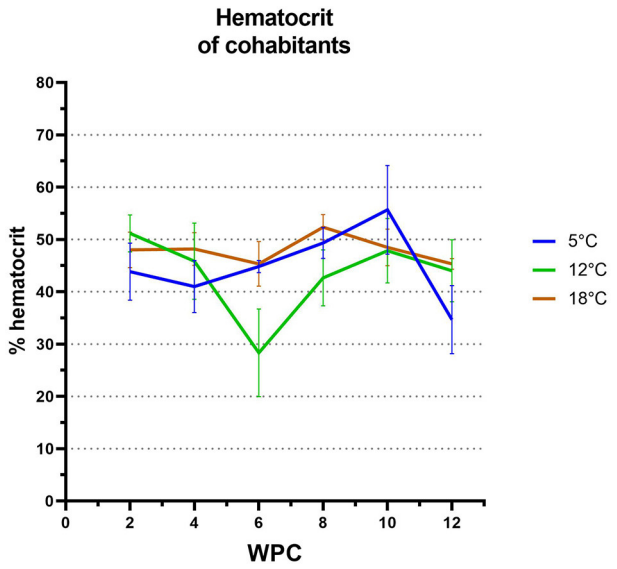

FIGURE 3
Hematocrit levels of cohabitants exposed to PRV-3. Significant difference observed in PRV-3 exposed cohabitants at 12°C compared to 5 and 18°C at six WPC (p = 0.05 and p = 0.026, respectively). Likewise, a significant difference was observed at 5°C compared to 12 and 18°C at 12 WPC (p = 0.026 and p = 0.0096, respectively). Error bars show SD.

Similar was observed for the cohabitants exposed to PRV-3 kept at 5°C: a significant reduction in hct occurred at 12 weeks post challenge, corresponding to the time point of highest virus load in this group (p = 0.0268 and p = 0.0096 for 12 and 18°C, respectively).

No reduction in hct was observed at 18°C in PRV-3 exposed cohabitants.

However, when comparing to non-infected control fish at each temperature, there was no significant difference from control to exposed at 5°C due to the large variation both within the control and the exposed group (data not shown). Additionally, the mock-infected fish at 18°C had a significantly lower hct at the time of highest virus load compared to the PRV-3 exposed fish at this temperature (data not shown).

3.4. Histopathology in the heart

Histopathological findings in hearts consistent with PRV-3 associated pathology described earlier (10, 12) were observed in the cohabitants at 12°C 2 weeks post peak load of virus. Six out of six fish had heart lesions at 8 WPC, with highest histoscore of 1.5 (see Figure 4B).

Cohabitants kept at 5°C did not show any signs of lesions in the heart (Figure 4A). However, heart lesions were seen in the shedders at 10 WPC, i.e., 4 weeks post peak virus load (five out of six fish, Figure 4D). At 12 WPC, all six 5°C shedders had heart lesions, and to severe degrees (3:3 with histoscores 1.5 and 2, Figure 4E). This is compared to shedders at 12°C at 8 WPC, at which three out of six fish had heart lesions, 1:1:1 with histoscores 1, 1.5, and 2. No statistically significant difference between heart lesions in the shedders at 12°C 8 WPC and 5°C 12 WPC was observed, however there was a trend toward more severe lesions at 5°C (p = 0.0563).

No heart histopathology was observed in cohabitants and shedders kept at 18°C during the experiment (see Figures 4C, F).

3.5. Immune gene profiles

In order to assess the impact of water temperature on the immune gene status of both control and PRV-3 exposed fish, 21 different immune genes covering both the innate and the adaptive immune system were selected for immune gene expression by microfluidic qPCR (see Table 3 for a full list of the genes and primer sequences). Typically, in our experimental facility, standard *in vivo* studies in rainbow trout are conducted at 12°C, and therefore this group was considered the baseline in this study.

3.5.1. Temperature induced regulation of anti-viral genes in non-infected control fish

In mock-injected shedders, fish at all three temperatures had a relatively similar immune gene expression profile forming a single cluster (see Figure 6). Overall, the immune profile of PRV-3 exposed fish differed from the relatively homogeneous profile of control fish regardless the temperature. However, significant differences in the immune profile expression of certain genes were observed between 5 and 18°C controls: Up-regulation of *cd4, rigi, isg15, saa, ifit5* and *ifi44*

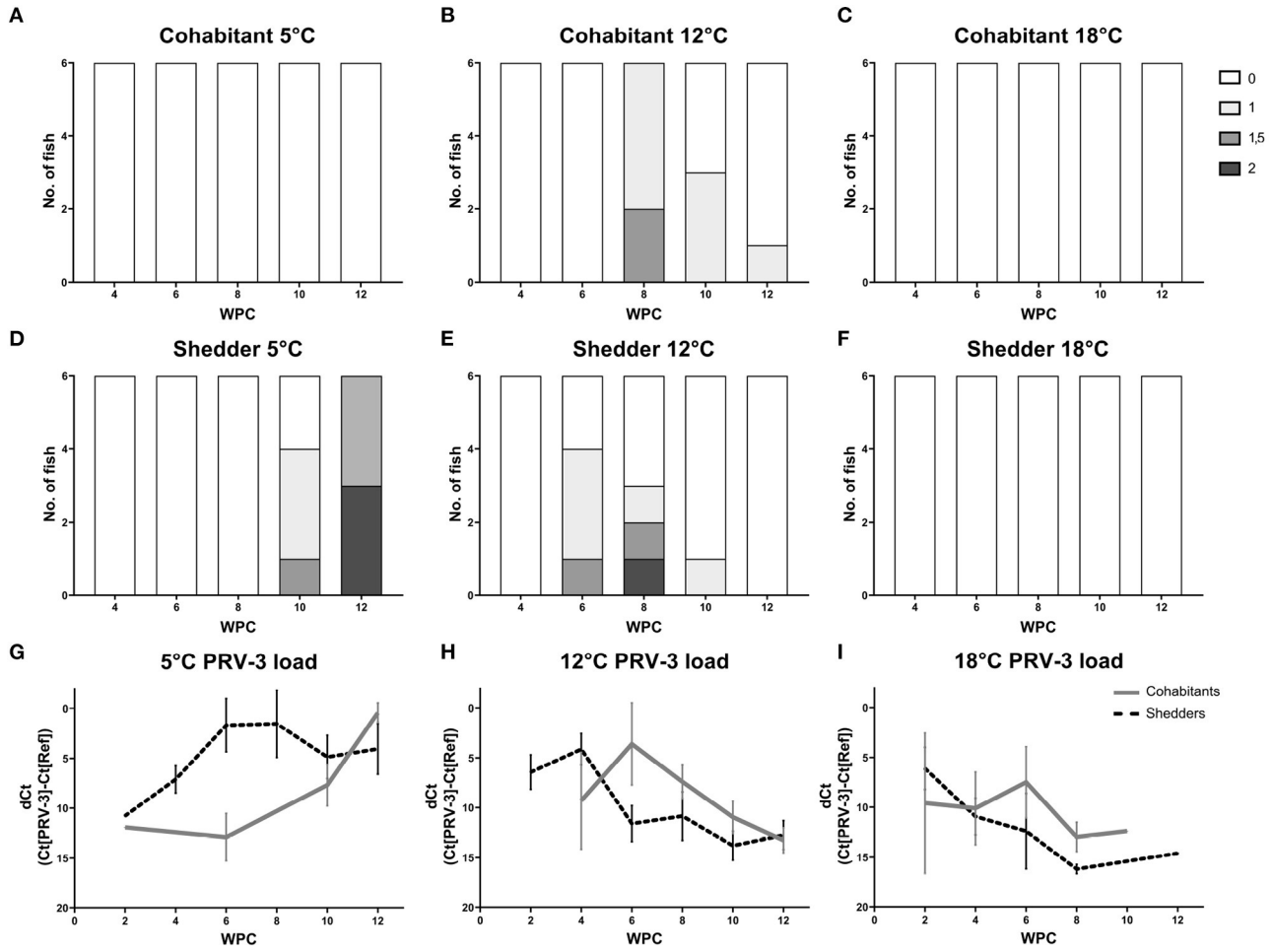

FIGURE 4
Heart histopathology of shedders **(A–C)** and cohabitants **(D–F)** of PRV-3 exposed fish in comparison to dCt values **(G–I)**. Histoscore 0 = no lesions, 1 = mild, 1.5 = moderate, 2 = severe. Error bars show SD.

was observed at 18°C compared to 5°C ($p < 0.01$). At 5°C, down-regulation of *ifnc3* was observed compared to 12°C ($p = 0.001$). No significant differences between 12 and 18°C were observed.

In cohabitant controls, fish maintained at 5 and 12°C showed similar gene expression profiles, while 18°C formed a separate group (see Figure 5). 18°C controls grouped together with PRV-3 exposed fish of the same temperature (with exception of 2 WPC), with only *mhc class II* and *saa* showing significant differences between the control and the exposed fish of 18°C ($p = 0.003$ with fold change of 2.03 and $p = 0.017$ with fold change 0.17, respectively).

Cohabitants control fish at 18°C had up-regulation of *mx, cd4, rsad2, gzma, rigi, isg15, cxcl10, saa* and *ifit5* compared to control fish at 12°C (fold change above 2.5 and $p < 0.05$ in all genes listed).

3.5.2. Temperature induced effect on immune profile of PRV-3 exposed fish

PRV-3 exposed shedder fish of all three temperatures grouped together with the exception of 5°C at 2 WPC (see Figure 6). Across the trial, significant differences were observed at 5°C in *saa* ($p = 0.002$ with fold change 4.6) and 18°C in *cxcl10* ($p = 0.02$ with fold change 0.18) compared to 12°C.

The temperature pattern of *saa* at 5°C changes after viral infection, probably reflecting high viral load and inflammation in the infected spleens at this low temperature.

In cohabitants, fish maintained at 5 and 12°C at the time of highest virus RNA load formed a separate group (10 and 12 WPC at 5°C and 6 WPC at 12°C, see Figure 5). 18°C PRV-3 exposed cohabitants (with the exception of 2 WPC) grouped together with controls of 12°C and 5°C. At the time point of highest virus load at the respective temperatures (6 WPC for both 12 and 18°C, 12 WPC for 5°C), significant differences were observed particularly at 18°C compared to 12°C: here, *mx, rsad2, ifnc3, gzma, rigi, isg15, saa*, and *ifit5* were significantly down-regulated ($p < 0.05$ in all genes), while *cd8* was up-regulated ($p < 0.05$). At 5°C, *ifnc3* and *cxcl10* were up-regulated compared to 12°C at time of high virus load ($p = 0.0008$ with fold change of 4.9 and $p = 0.018$ with fold change of 2.5, respectively).

By comparing the virus load to the immune gene expression of each individual fish, a positive correlation was found in the genes shown in Table 5. Importantly, *isg15* was positively correlated with PRV-3 virus load in all groups, and *rsad2* (viperin) was positively correlated in all groups except 18°C shedders (see Supplementary Figure S4).

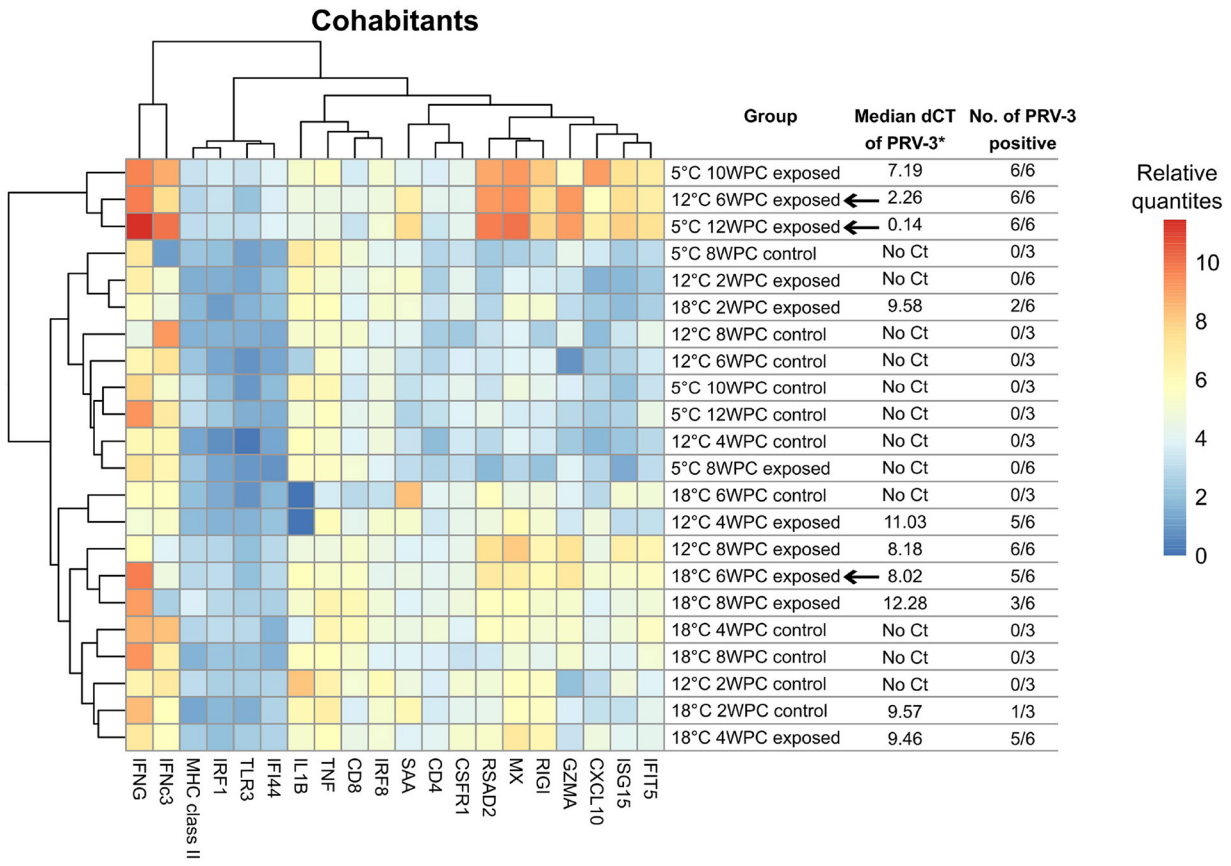

FIGURE 5
Heatmap of median log2 transformed relative quantities of immune gene expression analyses of selected cohabitant groups. Arrows indicate time point for peak in virus load. *Low value corresponds to high virus load (dCt = Ct[PRV-3] − Ct[Reference gene]). SD values of each group are shown in Supplementary material.

4. Discussion

RAS farms report to experience severe losses in association with PRV-3 infection, especially during winter and early spring with low water temperature. Hence, in this study, we set out to explore the effect of water temperature on PRV-3 infection in rainbow trout.

In this study, low water temperature (5°C) negatively impacted rainbow trout exposed to PRV-3, inducing a longer incubation period, and yielding higher virus load in shedders with more severe lesions in heart of exposed fish. Shedders at 5°C seemed unable to clear the infection during the course of the experiment: while there was a reduction in virus RNA at 10 weeks post challenge, high virus load persisted until the end of the trial at 12 weeks post challenge. This resembles the observations by Páez et al., showed that long virus persistence and higher long-term virulence was favored at cold water temperature (6°C) in steelhead trout (*Oncorhynchus mykiss*) infected with infectious hematopoietic necrosis virus (IHNV). Complementarily, that study showed that virus persisted for a shorter time and resulted in lower mortality at higher temperatures (10 and 15°C) (24).

Typically, changes in the heart due to PRV infection occur 2 weeks after viral peak under experimental conditions (6, 13). This was delayed in shedder fish at 5°C. Although high virus load (dCt value below 5) was measured starting at 6 WPC, heart lesions were not observed until 10 WPC. However, more severe lesions were found, with half of the fish having the highest histoscore and the other half the second highest histoscore at 12 WPC. Comparing the heart lesions at their respective peak across the three water temperatures (12 WPC at 5°C and 8 WPC at 12°C), there was a tendency toward worse lesions although not significant ($p = 0.0563$).

In cohabitants, low amount of virus was detected until 10 weeks post challenge in the 5°C group, and high virus load was not reached until 12 WPC. Despite the late detection of PRV-3 in this group, there was a significantly higher amount of virus RNA compared to the corresponding time point at 12°C (6 WPC). In contrast to fish at 18°C, fish at 5°C had a reduction of hematocrit at 12 WPC synchronized with the peak in virus RNA load. Heart pathology was not observed in the cohabitants at 5°C, but as changes in the heart are typically observed 2 weeks post highest virus load, it could be expected to show at a later time point which was not covered by the experiment. Additionally, the gene expression profile of the 5°C shedders at 12 WPC differed from the 12°C shedders at 6 WPC: This group had up-regulation of *saa* ($p = 0.002$ with a fold change at 4.6), and down-regulation of *cd8* and *cxcl10* ($p < 0.001$ and $p = 0.002$ at fold change 0.4 and 0.3, respectively).

The PRV-3 exposed shedder fish at 5°C at 2 WPC had immune gene expression profile more similar to the controls than the other exposed fish (see Figure 6). It seems that, despite the i.p. injection of

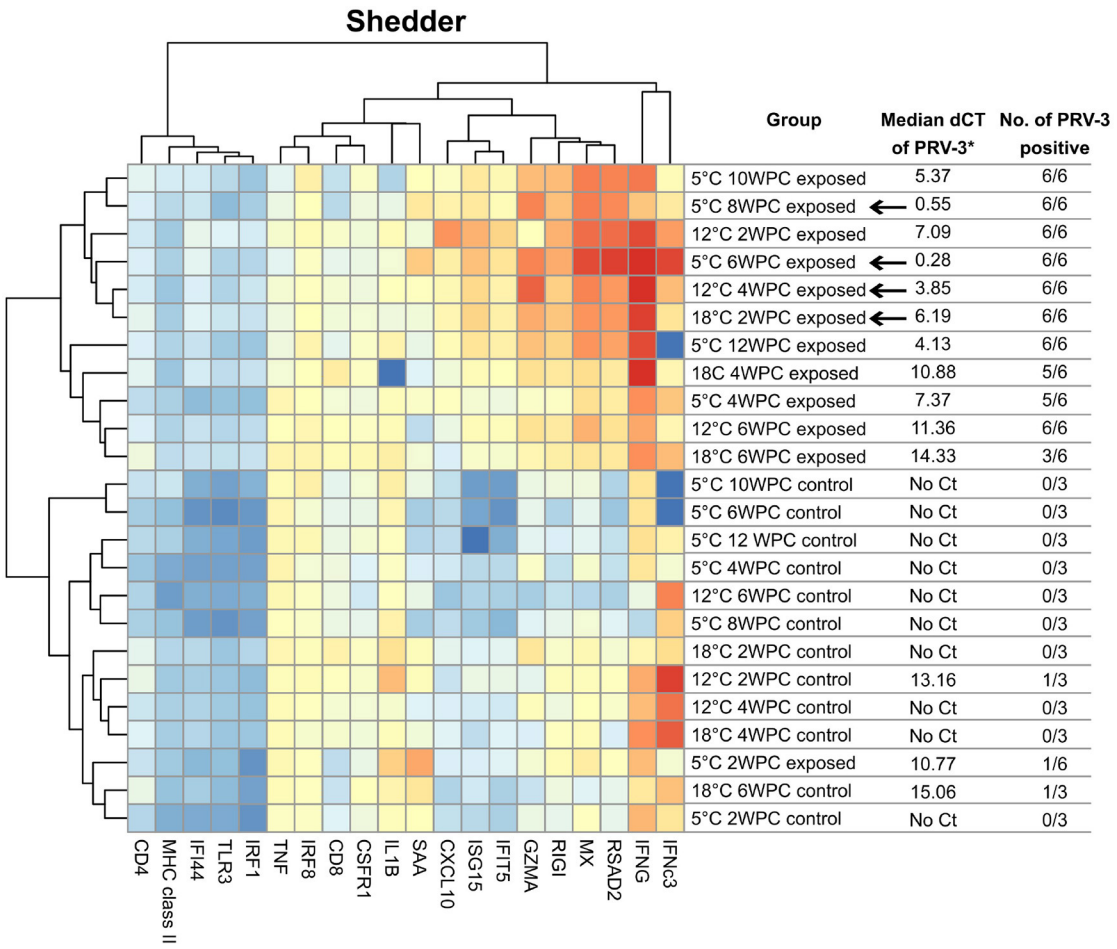

FIGURE 6
Heatmap of median log2 transformed relative quantities of immune gene expression profiles of selected cohabitant groups. Arrows indicate time point for peak in virus load. *Low value corresponds to high virus load (dCt = Ct[PRV-3] − Ct[Reference gene]). SD values of each group are shown in Supplementary material.

TABLE 5 Genes with positive Pearson's correlation to the PRV-3 virus load for all time points with $p < 0.05$.

Temperature	Group	Genes
5°C	Cohabitant	*mx, cd4, ifng, rsad2, irf8, gzma, rigi, isg15, tlr3, cxcl10, saa, ifit5, ifi44, irf1, csf1r*
	Shedder	*mx, rsad2, gzma, rigi, isg15, cxcl10, ifit5, ifi44, irf1*
12°C	Cohabitant	*mx, cd4, rsad2, ifnc3, gzma, rigi, isg15, tlr3, cxcl10, ifit5, ifi44, irf1*
	Shedder	*mx, rsad2, isg15, saa*
18°C	Cohabitant	*ifng, rsad2, gzma, isg15, cxcl10, ifit5, irf1*
	Shedder	*mx, gzma, isg15, cxcl10, ifit5*

PRV-3 positive inoculum, it took longer time to trigger the immune response due to the low water temperature.

Cohabitants at 10 and 12 weeks post challenge (high virus RNA load) at 5°C had a similar gene expression profile as fish in 12°C water at the corresponding time point (6 weeks post challenge), with up-regulation of *ifng*. However, comparing 5°C at 12 WPC to 12°C at 6 WPC, a significant up-regulation of *ifnc3* and *cxcl10* was observed at 5°C.

The protective effect of interferon C has already been shown in Atlantic salmon challenged with ISAV. By injecting *ifnc* encoding plasmid along with ISAV vaccine, it was possible to highlight the role of IFN in promoting ISG expression and boosting specific protection and antibody response (35, 36). Similarly, Zhang et al. (37) have shown that early activation of interferon pathway prevent second replication of the virus using as experimental model fish hirame rhabdovirus in flounders, a similar effect has also been shown for a number of fish viral infections [e.g., VHSV, IHNV, and RGNNV (red grouper nervous necrosis virus)] (38–41). In our experiment, we report significant overexpression of *ifnc3* in shedder fish at 12 and 18°C compared to 5°C (p = 6.1E-05 and p = 0.0132, respectively), when grouping together all time points. *ifnc3* overexpression likely limited the replication of PRV-3, preventing further shedding, and heart pathology development. Additionally, *cxcl10* is highly expressed in a wide range of tissues following viral infection, including influenza A virus and SARS-CoV-2 (42, 43). Expression of *cxcl10* is stimulated by *IFN* and involved in inflammation and chemotaxis of

lymphocytes including T lymphocytes and natural killer cells during viral infections.

cxcl10 is an important antiviral gene and is highly correlated with viral load in the present study (Table 5). *cxcl10* is expressed in a wide range of tissues following viral infection, including influenza A virus and SARS-CoV-2 (42, 43). Expression of *cxcl10* is stimulated by IFN and involved in inflammation and chemotaxis of lymphocytes including T lymphocytes and NK cells during viral infections. Thus, the high level of this anti-viral chemokine at 5°C might be explained by the high viral load found at the same temperature. In agreement with exposed shedders, cohabitant fish maintained at 5°C show a high expression of the ISG *cxcl10*, reflecting the high viral load. Type 1 interferon expression (*ifnc3*) was likewise found to be increased at low temperatures. *ifnc* has previously been shown to protect against Salmonid alphavirus 3 (SAV3), probably by inducing expression of the ISG *mx* also found to be correlated with viral titers in the present study (44).

Shedder control fish at 5°C showed down-regulation of *ifnc3* compared to 12°C group. The significant down-regulation of ifnc3 at 5°C could be a result of low levels of the pattern recognition receptor (PRR) *rigi* also found at 5°C. *rigi* is central in activating a wide range of IFNs after nucleic acid recognition from invading viral pathogens. Low levels of IFN including *ifnc3* will results in compromised activation of important interferon stimulated genes (ISG) including *isg15*, *ifit5* and *ifi44*. The combined action of these and other ISG are crucial in control and disease outcome after viral infections. Importantly, reduced expression of ISG at 5°C might affect the course and outcome of subsequent viral infections including PRV-3. Significant upregulation of the acute-phase protein (APP) saa at 18°C was also seen in the mock-injected shedders. APPs are normally produced in the liver and rises as a response to inflammation and tissue injury. Extra-hepatic changes of APPs upon viral infection has previously been reported during influenza A virus infection in pigs (34), but the link between saa, inflammation and water temperature still needs to be elucidated.

In this experiment, we observe little to no regulation of both *cd4* and *cd8*. In a previous experiment with PRV-3, these two genes have been up-regulated in relation to heart pathology (13). However, it is important to note that in the aforementioned study, immune gene expression was performed on heart tissue, while we here looked at the spleen. This may explain the lack of regulation of *cd4* and *cd8*.

Importantly, *isg15* was shown to be positively correlated with PRV-3 virus load in all PRV-3 exposed groups, while *rsad2* (viperin) and *mx* were positively correlated with PRV-3 virus load in all groups with exception of 18°C shedders and 18°C cohabitants, respectively (see Supplementary Tables S2–S14 and Supplementary Figure S4).

Rainbow trout are poikilothermic animals, which has significant effect on the kinetics of a large number of metabolic processes including immune response. To normalize the effect of temperature, we explored the data of viral load as function of degree days (Supplementary Figure S1). Overall, this approach shows an interesting alignment in degree days for reaching viral peak in shedders at 5 and 12°C. High PRV-3 virus load is detected earlier at 5°C than at 12 and 18°C in both cohabitants and shedders (see Supplementary Figure S1). This is likely to reflect slight changes in sampling point. Notably, worse heart pathology was observed at 5°C shedders at peak of infection.

In fish, the phenomenon of behavioral fever has been studied as a response to infections, particularly to viruses (25). Behavioral fever induces the fish to shift from optimal temperature moving to a warmer area with increased oxygen consumption and reduction of oxygen dissolved in the water. The increase of environmental temperature has a double effect both boosting the immune response and modulating the replication capacity of the pathogen (26). Induction of behavioral fever has been shown in zebra fish exposed to dsRNA (45). With regards to PRV infection in salmonids, it is reported that HSMI outbreaks tend to appear more frequently late spring-early summer (27), and it is documented that HSMI affected fish in sea cage are close to the surface (28). Similarly, rainbow trout suffer severe disease outbreak during winter, and during the outbreak tend to swim in close proximity of the surface, possibly searching for the warmest temperature available in the confined environment to develop a behavioral fever. Recent studies by Boltana and colleagues (29) highlight how behavioral fever modulates epigenetic expression of immune response, showing how Atlantic salmon exposed to another double stranded RNA virus (IPNV); by shifting to higher water temperature fish activates transcription of a specific subset of mRNA for innate and adaptive immune response, potentiating its mitigating effect on infection.

In our experiment, high water temperature (18°C) had a positive effect in mitigating the infection. At 18°C water temperature, both shedders and cohabitants had a tendency toward lower virus RNA load compared to 12°C (AUC, $p < 0.0001$). Although we demonstrated some PRV-3 replication, the reduction in hematocrit, which is normally observed at the same time point as peak in virus RNA, did not occur. Strikingly, these fish (18°C shedders and cohabitants) did not develop any heart pathology either. Cohabitants maintained at 18°C had an up-regulation of *cd8*, and down-regulation of immune genes of the innate response (*mx, rsad2, ifnc3, gzma, rigi, isg15*, and *saa*) compared to 12°C at 6 weeks post challenge ($p < 0.05$ in all genes) which mitigated the negative effect of PRV-3 infection in rainbow trout. Further studies will focus on how water temperature control could be practically implemented in future RAS farm design for mitigation of infectious diseases.

Taking into consideration the viral kinetics and heart pathology development both at 12 and 18°C, it appears that a threshold in virus load is required in order to trigger the development of heart pathology in rainbow trout due to PRV-3 infection. In shedder fish at 12°C, but not at 18°C, heart lesions were observed following high virus load. Here, a dCt value below 5 dCt at 12°C resulted in heart lesions, while a dCt value above 5 in 18°C did not trigger heart pathology. The same case can be observed in the cohabitants at 12 and 18°C; a dCt value above 5 did not result in histopathology in contrast to a dCt value below 5 (Figures 4G, H, I). Additionally, *rigi* appear to be a possible immune marker predictive of heart histopathology for PRV-3 infection. Within the pool of *rigi, ifit5,* and *rsad2*, this gene was highly expressed 2–4 weeks prior to the occurrence of lesions in the heart of both shedder and cohabitant fish at 5 and 12°C, but not at 18°C (see Supplementary Figure S2). In a study using human cardiac fibroblasts, *rigi* has been shown to be involved in cardiac cell pathology, as expression of *rigi* promoted production of pro-inflammatory cytokines which contributed to heart injury (46).

Fish were not acclimatized before the exposure to PRV-3, thus it is important to consider the potential impact of the sudden temperature shift on the fish. In cohabitants, controls of 5 and 12°C had a relatively

similar gene expression profile, while controls of 18°C formed a separate group (see Figure 5), primarily driven by the deferentially expression of *mx, cd4, rsad2, gzma, rigi, isg15, cxcl10, saa,* and *ifit5* (up-regulated in controls of 18°C compared to 12°C). However, these differences persisted throughout the trial, and should therefore not be attributed to the lack of acclimatization, but rather an impact of the temperature on the base level of immune gene expression. In shedders, all controls showed similar gene profile. In the shedder control fish of 12°C two and four WPC and 18°C four WPC, high expression of interferon's was observed. This short increase in interferon expression could be a reaction to the mock-injection. Nevertheless, the expression of both *ifng* and *ifnc3* decreased after some time.

In conclusion, low water temperature negatively impacts PRV-3 exposed fish, as virus replication persists for longer compared to higher temperatures. Additionally, heart pathology was indicated to be worsened by low temperature, while high temperature negates the negative impact of PRV-3 infection. It could be speculated, if the movement of at risk fish batches into warm water compartments could prevent disease outbreaks caused by PRV-3.

Data availability statement

The original contributions presented in the study are included in the article/Supplementary material, further inquiries can be directed to the corresponding author.

Ethics statement

The animal study was reviewed and approved by the Animal Experiments Inspectorate (Ministry of Food, Agriculture and Fisheries of Denmark).

Author contributions

NV, NO, AC, and JS contributed to the conceptualization and design of the study. Methodology, data analysis, and visualization done by JS, AC, NV, AO, and KS. Data curation done by JS and AO. Statistical analyses and writing of original draft done by JS. Review and editing done by JS, NV, NO, AC, AO, TI, and KS. Project administration done by NV and NO. Funding acquisition done by NV. All authors have read and agree to the published version of the manuscript.

Funding

The study was funded by the GUDP grant number: 34009-19-1510.

Acknowledgments

The authors would like to thank Anne Marie Nordvig Petersen at DTU Aqua for providing support in testing samples for PRV-3 by RT-qPCR, and Karin Tarp and Betina Lyngfeldt Henriksen at DTU Bioengineering for general support for testing of immune gene expression. Additional thanks to the animal caretakers at DTU Aqua. We also gratefully thank Henriette Kvalvik at the Norwegian Veterinary Institute Bergen for the preparation of slides for histopathology. Richard Hopewell for fruitful discussion on infection kinetics and degree/days.

Conflict of interest

The authors declare that the research was conducted in the absence of any commercial or financial relationships that could be construed as a potential conflict of interest.

Publisher's note

Supplementary material

The Supplementary Material for this article can be found online at: https://www.frontiersin.org/articles/10.3389/fvets.2023.1112466/full#supplementary-material

References

1. Markussen T, Dahle MK, Tengs T, Løvoll M, Finstad ØW, Wiik-Nielsen CR, et al. Sequence analysis of the genome of *Piscine orthoreovirus* (PRV) associated with heart and skeletal muscle inflammation (HSMI) in Atlantic salmon (*Salmo salar*). *PLoS ONE*. (2013) 8:e0070075. doi: 10.1371/journal.pone.0070075

2. Bohle H, Bustos P, Leiva L, Grothusen H, Navas E, Sandoval A, et al. First complete genome sequence of piscine orthoreovirus variant 3 infecting coho salmon (*Oncorhynchus kisutch*) farmed in southern Chile. *Genome Announ*. (2018) 6:e00484–18. doi: 10.1128/genomeA.00484-18

3. Dhamotharan K, Vendramin N, Markussen T, Wessel Ø, Cuenca A, Nyman IB, et al. Molecular and antigenic characterization of *Piscine orthoreovirus* (PRV) from rainbow trout (oncorhynchus orthoreovirumykiss). *Viruses*. (2018) 10:170. doi: 10.3390/v10040170

4. Sørensen J, Vendramin N, Priess C, Kannimuthu D, Henriksen NH, Iburg TM, et al. Emergence and spread of *Piscine orthoreovirus*genotype 3. *Pathogens*. (2020) 9:823. doi: 10.3390/pathogens9100823

5. Polinski MP, Vendramin N, Cuenca A, Garver KA. *Piscine orthoreovirus* : Biology and distribution in farmed and wild fish. *J Fish Dis*. (2020) 43:1331–52. doi: 10.1111/jfd.13228

6. Wessel Ø, Braaen S, Alarcon M, Haatveit H, Roos N, Markussen T, et al. Infection with purified *Piscine orthoreovirus* demonstrates a causal relationship with heart and skeletal muscle inflammation in Atlantic salmon. *PLoS ONE*. (2017) 12:e0183781. doi: 10.1371/journal.pone.0183781

7. Wessel Ø, Hansen EF, Dahle MK, Alarcon M, Vatne NA, Nyman IB, et al. *Piscine orthoreovirus*-1 isolates differ in their ability to induce heart and skeletal

muscle inflammation in atlantic salmon (*Salmo salar*). *Pathogens*. (2020) 9:1050. doi: 10.3390/pathogens9121050

8. Malik MS, Bjørgen H, Nyman IB, Wessel Ø, Koppang EO, Dahle MK, et al. PRV-1 infected macrophages in melanized focal changes in white muscle of Atlantic salmon (*Salmo salar*) correlates with a pro-inflammatory environment. *Front Immunol*. (2021) 12:664624. doi: 10.3389/fimmu.2021.664624

9. Takano T, Nawata A, Sakai T, Matsuyama T, Ito T, Kurita J, et al. Full-genome sequencing and confirmation of the causative agent of erythrocytic inclusion body syndrome in coho salmon identifies a new type of *Piscine orthoreovirus*. *PLoS ONE*. (2016) 11:e0165424. doi: 10.1371/journal.pone.0165424

10. Olsen AB, Hjortaas M, Tengs T, Hellberg H, Johansen R, Wessel Ø, et al. First description of a new disease in rainbow trout (Oncorhynchus mykiss (Walbaum)) similar to heart and skeletal muscle inflammation (HSMI) and detection of a gene sequence related to *Piscine orthoreovirus* (PRV). *PLoS ONE*. (2015) 10:e0131638. doi: 10.1371/journal.pone.0131638

11. Teige LH, Kumar S, Johansen GM, Wessel Ø, Vendramin N, Lund M, et al. Detection of salmonid IgM specific to the *Piscine orthoreovirus* outer capsid spike protein sigma 1 using lipid-modified antigens in a bead-based antibody detection assay. *Front Immunol*. (2019) 10:2119. doi: 10.3389/fimmu.2019.02119

12. Hauge H, Vendramin N, Taksdal T, Olsen AB, Wessel Ø, Mikkelsen SS, et al. Infection experiments with novel *Piscine orthoreovirus* from rainbow trout (*Oncorhynchus mykiss*) in salmonids. *PLoS ONE*. (2017) 12:e0180293. doi: 10.1371/journal.pone.0180293

13. Vendramin N, Kannimuthu D, Olsen AB, Cuenca A, Teige LH, Wessel Ø, et al. *Piscine orthoreovirus* subtype 3 (PRV-3) causes heart inflammation in rainbow trout (*Oncorhynchus mykiss*). *Vet Res*. (2019) 50:14. doi: 10.1186/s13567-019-0632-4

14. Garver KA, Marty GD, Cockburn SN, Richard J, Hawley LM, Thompson RL, et al. Piscine reovirus, but not Jaundice syndrome, was transmissible to Chinook salmon, *Oncorhynchus tshawytscha* (Walbaum), Sockeye salmon, *Oncorhynchus nerka* (Walbaum), and Atlantic salmon, *Salmo salar* L. *J Fish Dis*. (2016) 39:117–28. doi: 10.1111/jfd.12329

15. Polinski MP, Bradshaw JC, Inkpen SM, Richard J, Fritsvold C, Poppe TT, et al. De novo assembly of Sockeye salmon kidney transcriptomes reveal a limited early response to piscine reovirus with or without infectious hematopoietic necrosis virus superinfection. *BMC Genomics*. (2016) 17:848. doi: 10.1186/s12864-016-3196-y

16. Polinski MP, Garver KA. Characterization of *Piscine orthoreovirus* (PRV) and associated diseases to inform pathogen transfer risk assessments in British Columbia. *Can Sci Advis Sec Res Doc*. (2019) 35.

17. Purcell MK, Powers RL, Taksdal T, McKenney D, Conway CM, Elliott DG, et al. Consequences of *Piscine orthoreovirus* genotype 1 (PRV-1) infections in Chinook salmon (*Oncorhynchus tshawytscha*), coho salmon (*O. kisutch*), and rainbow trout (*O. mykiss*). *J Fish Dis*. (2020) 43:719–28. doi: 10.1111/jfd.13182

18. Zhang Y, Polinski MP, Morrison PR, Brauner CJ, Farrell AP, Garver KA. High-load reovirus infections do not imply physiological impairment in salmon. *Front Physiol*. (2019) 10:114. doi: 10.3389/fphys.2019.00114

19. Lund M, Røsæg MV, Krasnov A, Timmerhaus G, Nyman IB, Aspehaug V, et al. Experimental *Piscine orthoreovirus* infection mediates protection against pancreas disease in Atlantic salmon (*Salmo salar*). *Vet Res*. (2016) 47:107. doi: 10.1186/s13567-016-0389-y

20. Lund M, Dahle MK, Timmerhaus G, Alarcon M, Powell M, Aspehaug V, et al. Hypoxia tolerance and responses to hypoxic stress during heart and skeletal muscle inflammation in Atlantic salmon (*Salmo salar*). *PLoS ONE*. (2017) 12:e0181109. doi: 10.1371/journal.pone.0181109

21. Volkoff H, Rønnestad I. Effects of temperature on feeding and digestive processes in fish. *Temperature*. (2020) 7:307–20. doi: 10.1080/23328940.2020.1765950

22. Bowden TJ, Thompson KD, Morgan AL, Gratacap RML, Nikoskelainen S. Seasonal variation and the immune response: A fish perspective. *Fish Shellfish Immunol*. (2007) 22:695–706. doi: 10.1016/j.fsi.2006.08.016

23. Bowden TJ. Modulation of the immune system of fish by their environment. *Fish Shellfish Immunol*. (2008) 25:373–83. doi: 10.1016/j.fsi.2008.03.017

24. Páez DJ, Powers RL, Jia P, Ballesteros N, Kurath G, Naish KA, et al. Temperature variation and host immunity regulate viral persistence in a salmonid host. *Pathogens*. (2021) 10:855. doi: 10.3390/pathogens10070855

25. Rakus K, Ronsmans M, Vanderplasschen A. Behavioral fever in ectothermic vertebrates. *Dev Comparat Immunol*. (2017) 66:84–91. doi: 10.1016/j.dci.2016.06.027

26. Rakus K, Ronsmans M, Forlenza M, Boutier M, Piazzon MC, Jazowiecka-Rakus J, et al. Conserved fever pathways across vertebrates: A herpesvirus expressed decoy TNF-α receptor delays behavioral fever in fish. *Cell Host and Microbe*. (2017) 21:244–53. doi: 10.1016/j.chom.2017.01.010

27. Kongtorp RT, Kjerstad A, Taksdal T, Guttvik A, Falk K. Heart and skeletal muscle inflammation in Atlantic salmon, *Salmo salar* L.: A new infectious disease. *J Fish Dis*. (2004) 27:351. doi: 10.1111/j.1365-2761.2004.00549.x

28. Godoy MG, Kibenge MJT, Wang Y, Suarez R, Leiva C, Vallejos F, et al. First description of clinical presentation of *Piscine orthoreovirus* (PRV) infections in salmonid aquaculture in Chile and identification of a second genotype (Genotype II) of PRV. *Virol J*. (2016) 13:98. doi: 10.1186/s12985-016-0554-y

29. Boltana S, Aguilar A, Sanhueza N, Donoso A, Mercado L, Imarai M, et al. Behavioral fever drives epigenetic modulation of the immune response in fish. *Front Immunol*. (2018) 9:1241. doi: 10.3389/fimmu.2018.01241

30. Jonstrup SP, Kahns S, Skall HF, Boutrup TS, Olesen NJ. Development and validation of a novel Taqman-based real-time RT-PCR assay suitable for demonstrating freedom from viral haemorrhagic septicaemia virus. *J Fish Dis*. (2013) 36:9–23. doi: 10.1111/j.1365-2761.2012.01416.x

31. Snow M, McKay P, McBeath AJA, Black J, Doig F, Kerr R, et al. Development, application and validation of a Taqman real-time RT-PCR assay for the detection of infectious salmon anaemia virus (ISAV) in Atlantic salmon (*Salmo salar*). *Dev Biol*. (2006) 126:133–6.

32. Vreman S, Rebel JMJ, McCaffrey J, Ledl K, Arkhipova K, Collins D, et al. Early immune responses in skin and lymph node after skin delivery of Toll-like receptor agonists in neonatal and adult pigs. *Vaccine*. (2021) 39:1857–69. doi: 10.1016/j.vaccine.2021.02.028

33. Barington K, Jensen HE, Skovgaard K. Forensic age determination of human inflicted porcine bruises inflicted within 10 h prior to slaughter by application of gene expression signatures. *Res Vet Sci*. (2018) 120:47–53. doi: 10.1016/j.rvsc.2018.08.007

34. Skovgaard K, Cirera S, Vasby D, Podolska A, Breum SO, Dürrwald R, et al. Expression of innate immune genes, proteins and microRNAs in lung tissue of pigs infected experimentally with influenza virus (H1N2). *Innate Immunity*. (2013) 19:531–44. doi: 10.1177/1753425912473668

35. Robertsen B. The role of type I interferons in innate and adaptive immunity against viruses in Atlantic salmon. *Dev Comparat Immunol*. (2018) 80:41–52. doi: 10.1016/j.dci.2017.02.005

36. Langevin C, Boudinot P, Collet B. IFN signaling in inflammation and viral infections: New insights from fish models. *Viruses*. (2019) 11:302. doi: 10.3390/v11030302

37. Zhang J, Tang X, Sheng X, Xing J, Zhan W. The influence of temperature on viral replication and antiviral-related genes response in hirame rhabdovirus-infected flounder (*Paralichthys olivaceus*). *Fish Shellfish Immunol*. (2017) 68:260–5. doi: 10.1016/j.fsi.2017.07.029

38. Lapatra SE. Factors affecting pathogenicity of infectious hematopoietic necrosis virus (Ihnv) for salmonid fish. *J Aquatic Anim Health*. (1998) 10:121–31. doi: 10.1577/1548-8667(1998)010<0121:FAPOIH>2.0.CO;2

39. Goodwin AE, Merry GE, Noyes AD. Persistence of viral RNA in fish infected with VHSV-IVb at 15°C and then moved to warmer temperatures after the onset of disease. *J Fish Dis*. (2012) 35:523–8. doi: 10.1111/j.1365-2761.2012.01374.x

40. Ahne W. The influence of environmental temperature and infection route on the immune response of carp (*Cyprinus carpio*) to spring viremia of carp virus (SVCV). *Vet Immunol Immunopathol*. (1986) 12:383–6. doi: 10.1016/0165-2427(86)90144-3

41. Thanasaksiri K, Sakai N, Yamashita H, Hirono I, Kondo H. Influence of temperature on Mx gene expression profiles and the protection of sevenband grouper, Epinephelus septemfasciatus, against red-spotted grouper nervous necrosis virus (RGNNV) infection after poly (I:C) injection. *Fish Shellfish Immunol*. (2014) 40:441–5. doi: 10.1016/j.fsi.2014.07.035

42. Starbæk SMR, Andersen MR, Brogaard L, Spinelli A, Rapson V, Glud HA, et al. Innate antiviral responses in porcine nasal mucosal explants inoculated with influenza A virus are comparable with responses in respiratory tissues after viral infection. *Immunobiology*. (2022) 227:152192. doi: 10.1016/j.imbio.2022.152192

43. Brogaard L, Larsen LE, Heegaard PMH, Anthon C, Gorodkin J, Dürrwald R, et al. IFN-λ and microRNAs are important modulators of the pulmonary innate immune response against influenza A (H1N2) infection in pigs. *PLoS ONE*. (2018) 13:e0194765. doi: 10.1371/journal.pone.0194765

44. Gan Z, Chen SN, Huang B, Zou J, Nie P. Fish type I and type II interferons: Composition, receptor usage, production and function. *Rev Aquacult*. (2020) 12:773–804. doi: 10.1111/raq.12349

45. Rey S, Moiche V, Boltaña S, Teles M, MacKenzie S. Behavioural fever in zebrafish larvae. *Dev Comparat Immunol*. (2017) 67:287–92. doi: 10.1016/j.dci.2016.09.008

46. Wang H, Yin J, Gu X, Shao W, Jia Z, Chen H, et al. Immune regulator retinoic acid-inducible gene I (RIG-I) in the pathogenesis of cardiovascular disease. *Front Immunol*. (2022) 13:893204. doi: 10.3389/fimmu.2022.893204

frontiers | Frontiers in Veterinary Science

TYPE Original Research
PUBLISHED 22 September 2023
DOI 10.3389/fvets.2023.1264200

OPEN ACCESS

EDITED BY
Valeria Grieco,
University of Milan, Italy

REVIEWED BY
Claudio Pigoli,
Experimental Zooprophylactic Institute of Lombardy and Emilia Romagna (IZSLER), Italy
Stanislaw Dzimira,
Wrocław University of Environmental and Life Sciences, Poland
Claudio Counoupas,
Royal Prince Alfred Hospital, Australia

*CORRESPONDENCE
Francisco J. Salguero
✉ javier.salguero@ukhsa.gov.uk

†These authors have contributed equally to this work

RECEIVED 20 July 2023
ACCEPTED 08 September 2023
PUBLISHED 22 September 2023

CITATION
Larenas-Muñoz F, Ruedas-Torres I, Hunter L, Bird A, Agulló-Ros I, Winsbury R, Clark S, Rayner E and Salguero FJ (2023) Characterisation and development of histopathological lesions in a guinea pig model of *Mycobacterium tuberculosis* infection. *Front. Vet. Sci.* 10:1264200. doi: 10.3389/fvets.2023.1264200

Characterisation and development of histopathological lesions in a guinea pig model of *Mycobacterium tuberculosis* infection

Fernanda Larenas-Muñoz[1†], Inés Ruedas-Torres[1,2†], Laura Hunter[2,3], Alison Bird[2], Irene Agulló-Ros[1], Rebecca Winsbury[2], Simon Clark[2], Emma Rayner[2] and Francisco J. Salguero[2*]

[1]Department of Anatomy and Comparative Pathology and Toxicology, Pathology and Immunology Group (UCO-PIG), UIC Zoonosis y Enfermedades Emergentes ENZOEM, University of Córdoba, International Excellence Agrifood Campus 'CeiA3', Córdoba, Spain, [2]Pathology Department, UK Health Security Agency (UKHSA), Porton Down, Salisbury, United Kingdom, [3]School of Biosciences and Medicine, University of Surrey, Guildford, United Kingdom

Tuberculosis (TB) remains a very significant infectious disease worldwide. New vaccines and therapies are needed, even more crucially with the increase of multi-drug resistant *Mycobacterium tuberculosis* strains. Preclinical animal models are very valuable for the development of these new disease control strategies. Guinea pigs are one of the best models of TB, sharing many features with the pathology observed in human TB. Here we describe the development of TB lesions in a guinea pig model of infection. We characterise the granulomatous lesions in four developmental stages (I–IV), using histopathological analysis and immunohistochemical (IHC) techniques to study macrophages, T cells, B cells and granulocytes. The granulomas in the guinea pigs start as aggregations of macrophages and few heterophils, evolving to larger lesions showing central caseous necrosis with mineralisation and abundant acid-fast bacilli, surrounded by a rim of macrophages and lymphocytes in the outer layers of the granuloma. Multinucleated giant cells are very rare and fibrotic capsules are not formed in this animal model.

KEYWORDS

tuberculosis, guinea pig, granuloma, pathology, animal model, immunohistochemistry, cell marker, *Mycobacterium tuberculosis*

1. Introduction

Tuberculosis (TB) is a chronic disease which remains a significant global health threat, particularly to immunosuppressed individuals (1, 2). TB accounts for over 1.6 million human deaths worldwide (3), 191.000 of which were due to resistance to antibiotic treatment in 2021 (4). Because of this, animal models have been used historically to gain a better understanding of the disease and evaluate new therapies and vaccines (5).

The tuberculous granuloma is the hallmark lesion induced by *Mycobacterium tuberculosis* complex (MTBC) bacteria (6). These granulomas exhibit similar features in human disease, as

well as in both experimental and natural animal infections, with differences dependent on the animal species and type of MTBC bacteria involved. Granulomas are mainly composed of an accumulation of epithelioid macrophages, lymphocytes, some plasma cells and granulocytes which, depending on the chronicity, may include a necrotic centre with or without dystrophic mineralisation, and surrounded by a connective tissue capsule (7–16).

Guinea pigs have been widely used as an animal model for the study of various infectious diseases (17, 18) and have been found to be more susceptible to tuberculosis compared to other animal models (19, 20). Laboratory mice, for example, develop granulomatous lesions that differ significantly from those observed in humans, including the cellular composition as well as the progression to necrosis and lack of mineralisation (7, 19, 21). Non-human primates are very good models of human TB, showing many similarities with the granulomatous lesions observed in humans (15, 22). However, this animal model is costly and, due to its similarity to people and the ethical considerations alongside this, its use is strictly regulated (19, 23). Tuberculous granulomas in rabbits and guinea pigs share many similarities to those observed in humans (7, 20, 23); however, the number of reagents available to evaluate immune responses and cellular composition of granulomas in these species is scarce (19). Immunohistochemistry (IHC) provides additional information to conventional histopathological studies by using specific antibodies against MTBC antigens or cell markers, helping to understand the mechanisms of immune response, granuloma formation and the interaction of the bacteria with the host (8, 24).

It is believed that guinea pigs are thought to be the most susceptible animal model of TB (7) and previous reports have briefly described the development and characterisation of tuberculous granulomas in this species (11, 12, 25–28). Whilst much research has been focused on this model, currently, there is no robust scoring system for assessing the microscopic features of pulmonary granulomas to aid the evaluation of disease severity and progression in studies that assess new vaccines and therapeutics. Furthermore, there is scope to expand the understanding of cellular composition for each granuloma stage using various immunochemical markers, as well as investigating the presence and frequency of mycobacteria. In this study, we have used archived and new material from *Mycobacterium tuberculosis* (Mtb) infected guinea pigs, to characterise and categorise the development of pulmonary granulomas post-infection. Moreover, we have employed a panel of commercially available antibodies to study the different cell populations within the granulomas.

2. Materials and methods

2.1. Experimental animals

Wherever possible, analyses of existing, formalin-fixed paraffin-embedded (FFPE) lung tissues from an archive of historical experiments (equating to 44 animals), were used in this study to reduce the number of additional animals needed for analyses. Twelve additional adult, female Dunkin Hartley guinea pigs (*Cavia porcellus*), free from pathogen-specific infection, with a body weight of 300–400 g, were obtained from a UK Home Office accredited facility (Envigo, United Kingdom). Animals were randomly assigned to groups and identified using subcutaneously implanted microchips (Plexx, Netherlands) to enable blinding of the analyses. Animals were housed at ACDP (Advisory Committee on Dangerous Pathogens) level 3, post-infection in groups of up to eight, with access to food and water *ad libitum*. The housing environment was maintained within a temperature range of 15–21°C and a relative humidity range of 45 to 65%. Group sizes were determined by statistical power calculations (Minitab, version 16) performed using previous data (SD, approximately 0.5) to reliably detect a difference of 1.0 $\log_{10}$ in the median number of colony-forming units (cfu) per millilitre. All animal procedures were approved by the United Kingdom Health Security Agency, Porton Down Establishment Animal Welfare and Ethical Review Body and authorised under an appropriate UK Home Office project license. Animals' clinical and behavioural status were monitored daily.

2.2. Inoculum

The Mtb H37Rv strain was used for the challenge. National Collection of Type Cultures (NCTC) 7,416 challenge stock was generated from a chemostat grown to steady state under controlled conditions at 37°C ± 0.1, pH 7.0 ± 0.1 and a dissolved oxygen tension of 10% ± 0.1, in a defined medium, the details of which have been previously described (29). Aliquots were stored at −80°C. Titre of the stock suspension was determined from thawed aliquots by enumeration of Cfus cultured onto Middlebrook 7H11 OADC selective agar.

2.3. Infection

Challenge for each group of animals was by the aerosol route with Mtb strain H37Rv. Animals were challenged using a contained Henderson apparatus in conjunction with an AeroMP control unit as previously described (30, 31). Aerosol particles generated were delivered to the animals via both nares using a 3-jet Collison nebuliser, for an exposure time of 5 min. The challenge suspension in the nebuliser was adjusted by dilution in sterile water to a concentration of between 5×10^5 to 1×10^6 cfu/mL to deliver the required estimated, retained, inhaled, dose of 10–50 cfus to the lungs of each animal. The suspension of Mtb in the nebuliser was plated onto Middlebrook 7H11 OADC selective agar to measure the concentration and confirm retrospectively that the expected doses had been delivered (30).

Within this study, six guinea pigs were euthanised at each of day 5 and 10 days post-infection (dpi) by an overdose of sodium pentobarbital via the intraperitoneal route. Archived, FFPE lung tissues came from previously performed studies whereby the same strain of guinea pigs received the same dose, route of delivery and batch Mtb H37Rv but were euthanised at 3 weeks ($n = 8$), 4 weeks ($n = 8$), and 8 weeks ($n = 8$) post-infection. Guinea pigs necropsied at 24–27 weeks post-infection (wpi) ($n = 20$: $n = 2{,}167$ dpi; $n = 1{,}169$ dpi; $n = 1{,}178$ dpi; $n = 14{,}188$ dpi; $n = 2{,}189$ dpi), were given once daily (Monday to Friday) oral treatment of Rifampicin (10 mg/Kg) and Isoniazid (50 mg/Kg) drug regimen between 3–7 wpi to reduce bacterial load and induce relapse of disease between weeks 7 and 28 wpi.

2.4. Bacteriology

At necropsy, representative tissue from the lung of each animal (left: cranial lobe; right: cranial lobe and caudal lobe) were removed and placed into sterile Precellys tubes containing ceramic zirconium oxide beads were homogenised in 5 mL of phosphate buffered saline (PBS). Serial dilutions were plated (0.1 mL per plate, in duplicate) onto Middlebrook 7H11 OADC selective agar. After up to 4 weeks of incubation at 37°C, bacterial colonies were counted and duplicate data averaged to measure cfu/mL of viable Mtb in each lung sample homogenate. Where no colonies were observed, a minimum detection limit was set by assigning an average count of 0.5 colonies, equating to 5 cfu/mL.

2.5. Histopathology

At necropsy, lungs were removed and fixed by immersion in 10% neutral-buffered formalin [NBF] (Solmedia Ltd., Shrewsbury, United Kingdom). Tissue from pre-defined areas of each lung lobe (left: middle and caudal lung lobes; right: middle and accessory lung lobes) were sampled using a standard protocol to ensure consistency, routinely processed and embedded in paraffin blocks. All tissue blocks were sectioned at 4 µm and stained with haematoxylin and eosin (H&E).

Additionally, serial sections were stained with Ziehl-Neelsen (ZN) technique for the identification of acid-fast bacilli (AFB). Numbers of AFBs were quantified by light microscopy from ZN-stained slides, as previously described by Garcia-Jimenez et al. (2012) (8). The total number of AFBs present in each granuloma was counted and recorded using a scoring system as follows: 0 = no AFBs, 1 = 1–10 AFBs, 2 = 11–50 AFBs, and 3 ≥ 50 AFBs.

Martius Scarlet Blue (MSB) staining was performed on representative tissue sections containing lesions of different developmental stages to evaluate the presence of fibrous tissue. In sections where focally extensive pyogranulomatous lesions were observed, additional Gram staining was carried out to detect non-mycobacterial colonies.

H&E stained slides were scanned with a Hamamatsu S360 (Hamamatsu Photonics, Shizuoka, Japan) digital scanner and e-slides were evaluated using ndp.view2 software (v 2.9.29) (Hamamatsu Phonics, Japan). Slides stained with ZN or MSB special stains were evaluated using light microscopy.

2.6. Immunohistochemistry

Immunohistochemical staining (IHC) was performed to study different cell populations within the lung granulomas, including macrophages (Iba-1), myeloid cells (calprotectin positive; MAC387), heterophils (myeloperoxidase positive; MPO), B-cells (Specific Activator Protein; Pax-5) and T cells (CD3). Selected tissue sections from lungs at each time point were selected apart from those at 5 and 10 dpi, due to the very low number of lesions present. At 3, 4 and 8 wpi, tissues from three animals per group were included, whereas from 24–27 wpi, tissues from a total of 11 animals were included. Details of primary antibodies and IHC methods are summarised in Table 1. Briefly, in all cases, deparaffinisation and heat-induced epitope retrieval were performed on the Leica BOND-RXm using BOND Epitope Retrieval Solution 1 (ER1, pH 6.0) for 20 min at 95°C. After primary antibody incubation, immunostaining was performed with the Dako Real EnVision Detection System Peroxidase/DAB, Rabbit/Mouse (Agilent, CA, United States) and counterstained with Gill's haematoxylin. Finally, slides were routinely dehydrated and mounted using the Ecomount medium (Biocare Medical, CA, United States). Negative controls, consisting of replacement of primary antibody by blocking solution, were included in each run to detect potential non-specific binding. Likewise, IHC stained slides were scanned and subjected to digital image analysis to calculate the percentage of positively stained area in each granuloma (excluding the necrotic cores in all stains except for the MPO IHC runs) by using Nikon NIS-Ar software (Nikon Instruments Inc., NY, United States).

Histopathological and immunohistochemical evaluations were carried out in a ISO9001:2015 and GLP compliant laboratory and evaluated by two veterinary pathologists blinded to the animal details and methodology.

2.7. Statistical analysis

Differences between granuloma stages and time point were evaluated for statistical significance, which was set at 0.05, using the *X-sq* for trend test. Figures and data analyses were performed using GraphPad Prism 9.0 software (GraphPad Prism software 9.0, Inc., San Diego, CA, United States).

3. Results

3.1. Description of granuloma stages (I–IV)

In the lung, granulomatous lesions were differentiated into four distinct stages, broadly reflecting a temporal pattern of lesion development (Table 2). Lesions were located randomly within the parenchyma, or in the fibrous broncho-vascular connective tissue surrounding blood vessels and airways. In general, there was a tendency for granuloma size to increase through progression of the stages. A description of the morphological appearance of each stage is given below:

Stage I: these lesions comprised small, unorganised structures which lacked a distinct, circumscribed appearance, with borders that were poorly demarcated from the surrounding parenchyma. They consisted primarily of macrophages and interspersed lymphocytes, with occasional, scattered heterophils and eosinophils; these cells expanded alveolar walls and infiltrated alveolar spaces and/or broncho-vascular connective tissue. In some stage I granulomas, epithelioid macrophages (Figures 1A,B) and few Langhan's type multinucleated giant cells (MNGCs) were also observed (Figure 2A).

Stage II: these lesions were often larger than stage I, circumscribed, and contained well-demarcated borders. They represented a variable morphology, from round to any shape, that included poorly organised or non-necrotic granulomas with initial signs of organisation. Less organised stage II granulomas comprised primarily of scattered lymphocytes and macrophages, the latter often epithelioid, alongside variable numbers of centrally located heterophils (Figures 1C,D). Other more organised granulomas showed a prominent peripheral

TABLE 1 Summary of immunohistochemical methods: primary antibody details, source, dilution, and blocking solution.

Specificity/Clone	Type of antibody	Source	Blocking solution	Dilution
IBA1	mAb (clone, GT10312)	Invitrogen, MA, United States	Superblock[1]	1:100[2]
MAC387	pAb	Bio-techne, OX, United Kingdom	10% NGS	1:100[2]
MPO	pAb	Invitrogen, MA, United States	Superblock[1]	1:100[2]
CD3	mAb (clone, LN10)	Leica Microsystems, MK, United Kingdom	Superblock[1]	1:50[3]
B-Cell-SAP	mAb (clone, DAK-Pax5)	Agilent, CA, United States	Superblock[1]	1:50[3]

[1]Superblock (TBS) Blocking Buffer (Thermo Scientific, United States).
[2]Primary antibody incubation 1 h in the oven at 37°C.
[3]Primary antibody incubation overnight at 4°C. MAb, monoclonal antibody; pAb, polyclonal antibody; NGS, normal goat serum; MPO, myeloperoxidase; B-cell SAP, B-cell Specific Activator Protein.

TABLE 2 Total number of granulomas observed at each stage and time point in guinea pig lungs.

Days/weeks post-inoculation	Granuloma stage				Total count
	I	II	III	IV	
5 dpi ($n=6$)	12	0	0	0	12
10 dpi ($n=6$)	9	0	0	0	9
3 wpi ($n=8$)*	9	28	14	0	51
4 wpi ($n=8$)*	126	130	37	0	293
8 wpi ($n=8$)*,**	185	209	8	16	418
24–27 wpi ($n=20$)*,**	346	458	48	40	892

dpi, days post infection; wpi, weeks post infection. *X-sq for trend $p<0.05$ compared to 5 and 10 dpi and **X-sq for trend $p<0.05$ compared to 3 and 4 wpi.

rim of lymphocytes surrounding a central core of macrophages and variable numbers of heterophils. The majority of heterophils observed were viable, although a small number of degenerate cells were noted in the centre of the lesions. Occasional MNGCs were also present (Figure 2B).

Stage III: central necrosis, often mild to moderate, was the key feature observed in stage III lesions. This was characterised by numerous degenerate heterophils with concomitant nuclear pyknosis and karyorrhexis. Variable amounts of early, caseous necrosis were also presented, predominantly comprising homogenous, eosinophilic material. The necrotic core was surrounded by a rim of inflammatory cells, containing variable numbers of heterophils and encircled by epithelioid macrophages and variable numbers of MNGCs. Lymphocytes and plasma cells constituted the outer peripheral rim (Figures 1E,F).

Stage IV: these granulomas exhibited extensive, central, caseous necrosis and concomitant, dystrophic calcification (Figures 1G,H). The surrounding tissue comprised primarily of epithelioid macrophages and some lymphocytes. MNGCs were noted variably.

Reactive fibroplasia, with the formation of a fibrous capsule, was not observed in the examined lung tissue (Figure 3A). Occasionally, in some granulomas that developed adjacent to airways or blood vessels, pre-existing broncho-vascular connective tissue was incorporated into the granuloma structure, as confirmed by MSB staining (Figure 3B). This feature was also observed in granulomas located close to the pleural membrane, irrespective of the stage of the granuloma. Furthermore, local expansion of the pleura by inflammatory cells, was also noted. Gram staining did not reveal the presence of non-mycobacterial bacteria in the severe extensive lesions observed in some animals.

3.2. Time course development of disease

A temporal association was noted between the progression in the stage of lesion development and an increase in the total number of granulomas observed in the lung (Figure 4). The total number of granulomas at each developmental stage for each time point is summarised in Table 2 and plotted in Figure 4. At 5 and 10 dpi, only stage I granulomas were present ($n=12$ and $n=9$ respectively), representing early-stage granuloma formation. By contrast, at 3 wpi, the majority of granulomas were stage II ($n=28$), with fewer numbers of stage III ($n=14$) and stage I granulomas ($n=9$). By 4 wpi, there were abundant stage I granulomas ($n=126$) together with numerous stage II ($n=130$) and lesser numbers of stage III granulomas ($n=37$). A predominance of stage I ($n=185$) and stage II ($n=209$) granulomas were noted by 8 wpi. In addition, there were a small number of stage IV granulomas with partially to fully mineralised necrotic centres ($n=16$), as well as stage III granulomas ($n=8$). At the final time point of 24–27 wpi, some lung lobes showed extensive, coalescing pneumonia and marked consolidation affecting the majority of the parenchyma. Most of the granulomas observed were stage II ($n=458$); abundant stage I granulomas were also noted ($n=346$) and a smaller number of stage III ($n=48$) and stage IV granulomas ($n=40$).

The presence and frequency of AFB in each granuloma stage at different time points are summarised in Table 3. In the early time points (5 and 10 dpi), AFBs were not detected in the small number of observed lesions. However, by 3 and 4 wpi, AFBs were noted in stage II (Figure 2A) and III granulomas with a tendency for higher numbers of AFBs visible in stage III (Figure 2B); stage I lesions did not show any AFB at these time points. By 8 wpi, AFB were observed in low numbers in a small proportion of stage I and II granulomas. However, the majority of stage III and IV granulomas showed abundant AFBs. At 24–27 wpi, abundant AFBs were observed in all granuloma stages.

3.3. Viable *Mycobacterium tuberculosis* in lung

Bacterial load data measured as cfu/mL of *M. tuberculosis* measured in lung at 5 and 10 days, and 3, 4, 8, and 24–27 weeks post-infection, is represented in Figure 5. Although at 5 and 10 dpi expected low values (around 10^2 cfu/mL) of bacterial burden were detected, at 3 wpi, numbers of viable bacilli had more than doubled (around 10^5 cfu/mL). Peak bacterial loads were detected at 4 wpi with values around 10^6 cfu/mL. Similar values than found at 3 wpi were found at

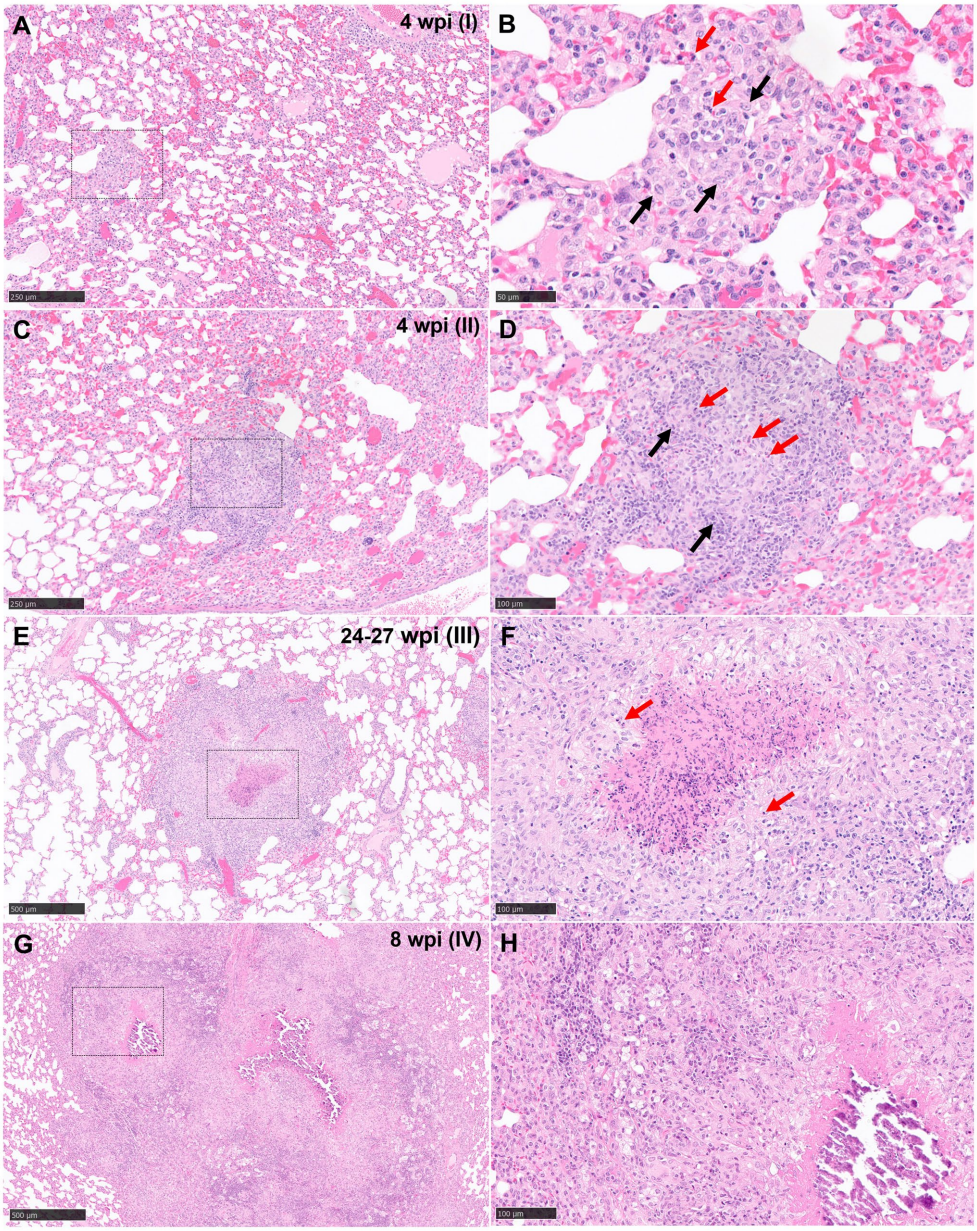

FIGURE 1
Representative microphotographs of the four stages of tuberculous granulomas in lungs from guinea pigs (H&E). (**A, B**) Stage I. Small with epithelioid macrophages (black arrows) with interspersed lymphocytes and heterophils (red arrows). (**C, D**) Stage II. Organised granulomas with heterophils (red arrows) in the centre and surrounded by epithelioid macrophages interspersed with polymorphonuclear cells (black arrows). (**E, F**) Stage III. Organised, with initial to caseous necrosis with degenerated and/or viable heterophils (red arrows). (**G, H**) Stage IV. Organised, advanced tuberculous lesion with extensive caseous necrosis and mineralisation. Scale bars = 250 µm (insets B, D, F, and H = 100 µm).

8 wpi to increase progressively until the end of the study (10^7 cfu/mL). A greater range of bacterial load (averaging at around 10^4 cfu/mL) were observed in animals at 24–27 weeks, following relapse from sub-optimal drug treatment (Figure 5).

3.4. Distribution of cell populations within granulomas

Iba1 was the most predominant marker in all stages of granulomas throughout the experiment (Figure 6). The staining was detected on the cell membrane of macrophages, including epithelioid and foamy macrophages and MNGCs, and diffusely extended in all the lesions, mainly from stage I and stage II granulomas (Figures 6B,C). In stage III and IV granulomas, the staining was also demonstrated in epithelioid macrophages surrounding the necrotic cores and central calcification, as well as in foamy macrophages at the periphery of the lesions (Figures 6D,E). No significant differences were observed in the percentage of Iba1+ staining between the different stages throughout the study.

Results from MAC387 positive staining quantification are represented in Figure 7A. MAC387+ staining was detected in the

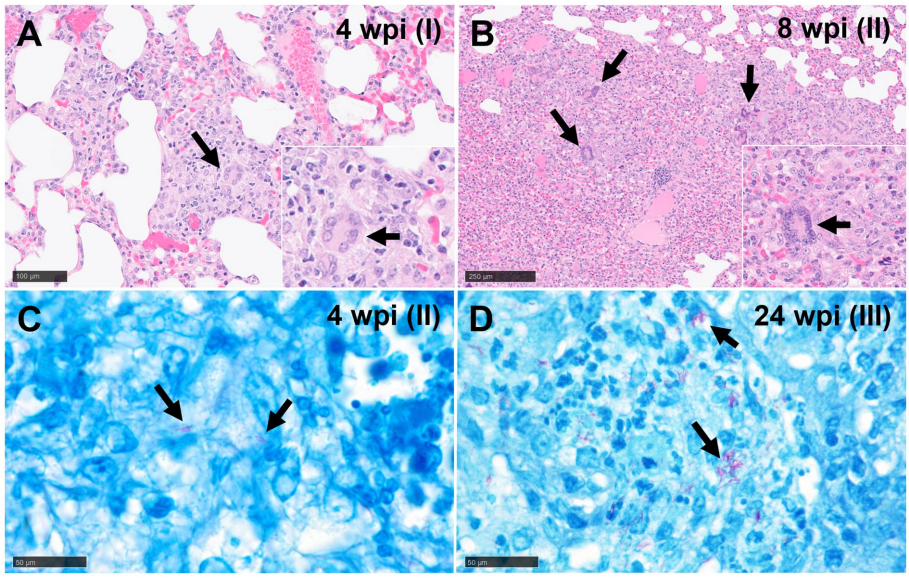

FIGURE 2
Representative microphotographs of multinucleated giant cells (MNGCs) (H&E) and Ziehl-Neelsen (ZN) staining. **(A)** Epithelioid macrophages forming an initial MNGC (arrows) in a stage I granuloma at 4 wpi and **(B)** several MNGCs (arrows) in a stage II granuloma at 8 wpi. **(C)** Acid-fast bacilli (AFBs, arrows) in lungs of guinea pigs with stage II (4 wpi) and **(D)** stage III (24 wpi) tuberculous granuloma (ZN staining). Scale bars A and B = 100 µm (insets, and C and D = 50 µm).

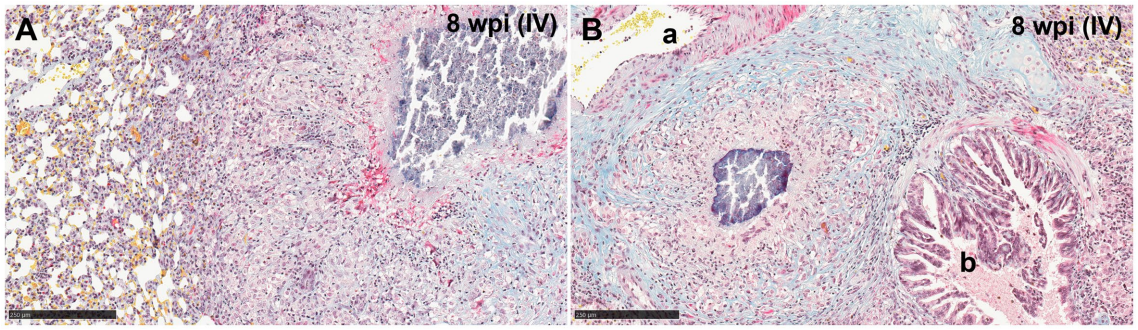

FIGURE 3
Representative microphotographs of Martius Scarlet Blue (MSB; blue for collagen) staining in lungs of guinea pigs with tuberculous granulomas. **(A)** Stage IV granuloma within the lung parenchyma, not showing a fibrotic capsule surrounding the lesion. **(B)** Stage IV granuloma located between an artery **(A)** and a bronchiole **(B)** showing normal collagen (blue stain) from the lung around the granuloma. Scale bars = 250 µm.

cytoplasm of scattered macrophages and granulocytes within the tuberculous granulomas (Figures 7B–E). An increase in MAC387+ staining was observed coinciding with the progression of the lesion, being the maximum percentage observed in stage III (Figures 7A,D). In this stage, MAC387+ cells formed a rim of inflammatory cells surrounding the necrotic core (Figure 7D). These differences were specially observed at 3 and 4 wpi (Figure 7A). At 8 and 24–27 wpi, no significant differences were found in the percentage of staining between the different stages of granulomas.

Similar kinetic expression pattern was observed for the myeloperoxidase (MPO) marker (Figure 8A). However, MPO was also highly expressed in stage IV granulomas at the late time points (8 and 24–27 wpi) (Figure 8E). MPO was expressed in scattered granulocyte-like cells of stage I and II granulomas (Figures 8B,C), as well as in the necrotic areas and inflammatory infiltrates of stage III and IV granulomas (Figures 8D,E).

Results from B-cell marker quantification are represented in Figure 9A. At 3, 4, and 8 wpi, a progressive increase in the percentage of this immunostaining was observed from stage I to stage IV (Figure 9). Higher expression of this marker was detected at 8 wpi in comparison with 4 and 24–27 wpi in stage I and II granulomas. Positive staining to B-cell SAP was found in the nuclei of B lymphocytes within multifocal inflammatory infiltrates in all granuloma stages (Figures 9B–E). In stage III and IV granulomas, the B-cell SAP$^+$ infiltrates were present in the outer rims of the granulomas and within the stage I and II "satellite" granulomas surrounding the larger lesions (Figures 9D,E).

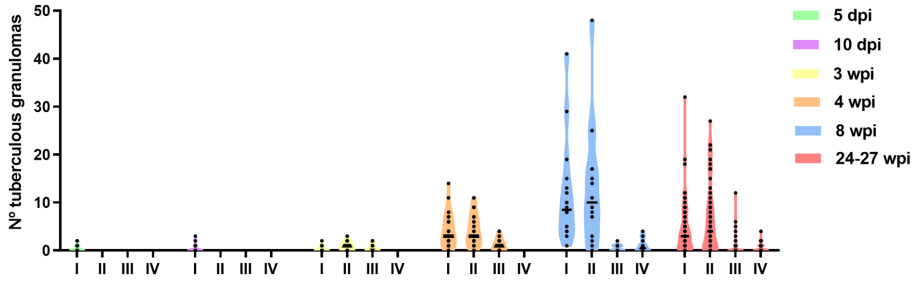

FIGURE 4
Number of different granulomas from different developmental stages (I–IV) observed in guinea pig lungs at different time points after inoculation (from 5 dpi to 24–27 wpi). Each dot represents a lung section and bars represent median values.

TABLE 3 Total score for the number of AFB in granulomas at each stage and time point in the guinea pig lungs.

Granuloma stage	5 dpi				10 dpi				3 wpi				4 wpi				8 wpi				24–27 wpi			
	0	1	2	3	0	1	2	3	0	1	2	3	0	1	2	3	0	1	2	3	0	1	2	3
Stage I	6	0	0	0	3	0	0	0	2	0	0	0	5	0	0	0	21	2	0	0	27	11	5	0
Stage II	0	0	0	0	0	0	0	0	0	2	1	0	2	8	0	0	17	9	0	0	24	23	3	10
Stage III	0	0	0	0	0	0	0	0	0	0	0	2	0	2	4	7	0	1	1	0	2	10	3	1
Stage IV	0	0	0	0	0	0	0	0	0	0	0	0	0	0	0	0	0	3	3	3	1	2	3	0
Total count	6	0	0	0	3	0	0	0	2	2	1	2	7	10	4	7	38	15	4	3	54	46	14	11

The total number of AFBs present in each granuloma were counted and recorded using a scoring system: 0 = no AFBs, 1 = 1–10 AFBs, 2 = 11–50 AFBs, and 3 ≥ 50 AFBs. AFB, acid fast bacilli; dpi, days post infection; wpi, weeks post infection.

Lower percentage of CD3+ staining was detected at 3 wpi in all granuloma stages compared to 4, 8, and 24–27 wpi, being the maximum expression observed at 8 wpi (Figure 10A). At 8 and 24–27 wpi, similar expression of CD3+ staining was detected in the different granuloma stages (Figure 10A). The staining was detected in the cytoplasm and cell membrane of T lymphocytes diffusely scattered within stage I and II granulomas and located at the periphery of stage III and IV granulomas (Figures 10B–E).

4. Discussion

The results describe the morphological features observed in the formation and progression of tuberculous granulomas in the lungs of guinea pigs and provide a clearly defined methodology for their classification into stages. These stages can be used to assess the severity and progression of tuberculosis in this animal model and aid in the evaluation of therapeutics and prophylactics against human disease.

The guinea pig model is widely used in tuberculosis research due to its similarities with human disease, specifically regarding disease progression and immunopathology (11). The pathology of tuberculous granuloma formation in the lung of the guinea pig has already been well documented in the literature (11, 12, 20, 30, 32–35). Microscopic evaluation of morphological changes using subjective scoring methodologies have been used for many years to evaluate disease severity and progression in multiple, pre-defined lung lobes; these include assessment of the percentage of lung parenchyma affected by tuberculous granulomatous inflammation, ranging from multifocal, discrete granulomas to consolidative changes, as well as microscopic features such as presence/absence of necrosis, dystrophic calcification and extent of lymphocytic infiltration of granulomas (36). Outputs, such as mean scores from lung lobes of individual animals, as well as group mean scores, can be compared alongside bacterial, immunological and other relevant data to discriminate between test and control groups. Similar scoring systems have been devised in other animal models of tuberculosis, such as macaques (15, 22, 37, 38), cattle (13, 39–41), badgers (42, 43), deer (8), swine (44), or mice (45). The current study aimed to enhance histopathological outputs through the provision of a semi-quantitative method characterising granuloma morphology. This approach provides additional discriminatory power, helping to overcome potential limitations associated with semi-quantitative scoring, such as experience and personal bias of the pathologist.

The granuloma developmental stages described here are similar to those described in cattle, from stage I (initial) to stage IV (necrotic and mineralised) (13, 39–41). The cellular composition of the granulomas is also similar to what is observed in other animal models of MTBC infection, with heavy presence of activated macrophages from the early stages, polymorphonuclear cells (neutrophils or heterophils), and rims of T and B cells surrounding the necrotic cores in the late stages of granuloma development. A large quantity of heterophils and activated macrophages is observed in late-stage granulomas, with high expression of MPO at the necrotic core and inner layers of the granulomas. The number of AFBs also increase concomitantly with lesion development, as seen in other animal models (37, 40). As expected, the viable bacterial burden in lung measured by plating homogenates onto selective medium, also increased concurrently with increased presence of AFBs and lesion development. The reduction of viable bacteria in lungs between 4 and

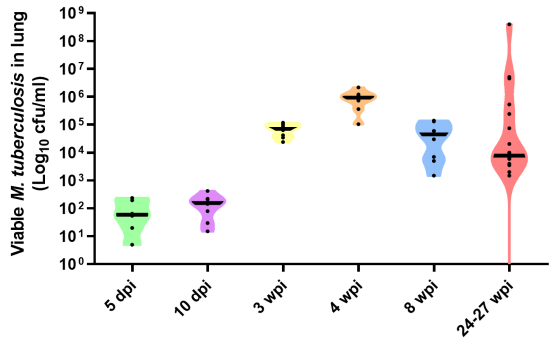

FIGURE 5
Number of viable Mtb H37Rv in lung at day 5 and 10, and weeks, 3, 4, and 8 weeks post-infection by the aerosol route of delivery. Bacterial load in lungs at 24–27 weeks post-infection represent the result of relapse of disease following sub-optimal delivery of drug treatment delivered between weeks 3–7 post-infection. Individual dots represent each animal in each group. Viable bacterial load are expressed as Log_{10} cfu/mL, each animal in the group represented as black circles, and group mean expressed as horizontal black bars, in violin plots.

8 weeks post-infection is commonly observed, and thought to be related to the switching of innate to adaptive host immune responses (20, 46, 47).

The presence of MNGCs is not prominent and only occasional in some granulomas, in contrast to what is observed in other models such as non-human primates (37, 48) or cattle (40, 41). MNGCs are normally formed by the fusion of macrophages responding to the intracellular persistence of mycobacteria. Their role in the different animal models of TB is under constant review, with some authors showing a possible correlation of vaccine protection with fewer presence of MNGCs (40).

The findings indicated that fibroplasia was not a feature in the formation of pulmonary granulomas in guinea pigs at this exposure dose and time points post-challenge. In general, the prominence of peripheral fibrosis in granuloma development varies between species, with non-human primates or cattle exhibiting prominent fibrous deposition (13, 37, 39–41, 48), whereas being sparse or absent in other animal models like mice, except for specific genetically modified strains (49). This fact represents a limitation of the guinea pig model for testing some potential therapies where fibrosis plays an important role.

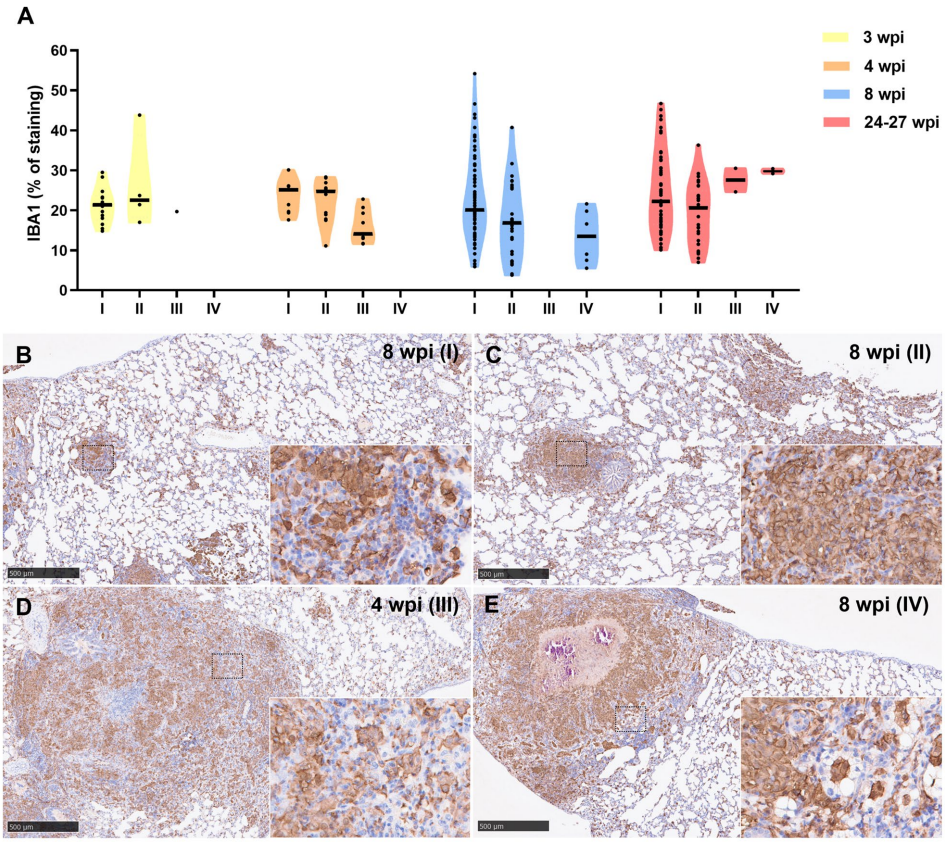

FIGURE 6
Iba1+ immunohistochemical detection in stage I, II, III, and IV granulomas throughout the experiment. **(A)** Percentage of $Iba1^+$ staining in stage I to IV granulomas at 3, 4, 8, and 24–27 wpi. Dots show the individual percentage of staining in each granuloma. Lines show the median value of the percentage of staining in the different stages throughout the study. **(B)** Iba1 expression in stage I granuloma at 8 wpi. **(C)** Iba1 expression in stage II granuloma at 8 wpi. **(D)** Iba1 expression in stage III granuloma at 4 wpi. **(E)** Iba1 expression in stage IV granuloma at 8 wpi. Insets show close-up images at higher magnification showing $Iba1^+$ macrophages. Scale bars = 500 μm (insets = 100 μm).

10.3389/fvets.2023.1264200

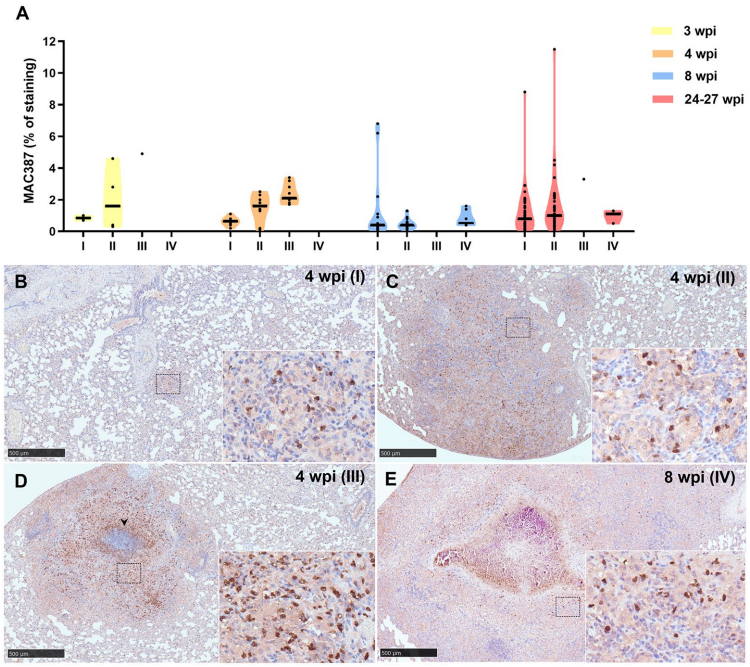

FIGURE 7
MAC387+ immunohistochemical detection in stage I, II, III, and IV granulomas throughout the experiment. **(A)** Percentage of MAC387$^+$ cells in stage I to IV granulomas at 3, 4, 8, and 24–27 wpi. Dots show the individual percentage of staining in each granuloma. Lines show the median value of the percentage of staining in the different stages throughout the study. **(B)** MAC387 expression in stage I granuloma at 4 wpi. **(C)** MAC387 expression in stage II granuloma at 4 wpi. **(D)** MAC387 expression surrounding a necrotic core (arrowhead) in stage III granuloma at 4 wpi. **(E)** MAC387 expression in stage IV granuloma at 8 wpi. Insets show close-up images at higher magnification showing MAC387$^+$ cells: macrophages and polymorphonuclear cells. Scale bars=500µm (insets=100µm).

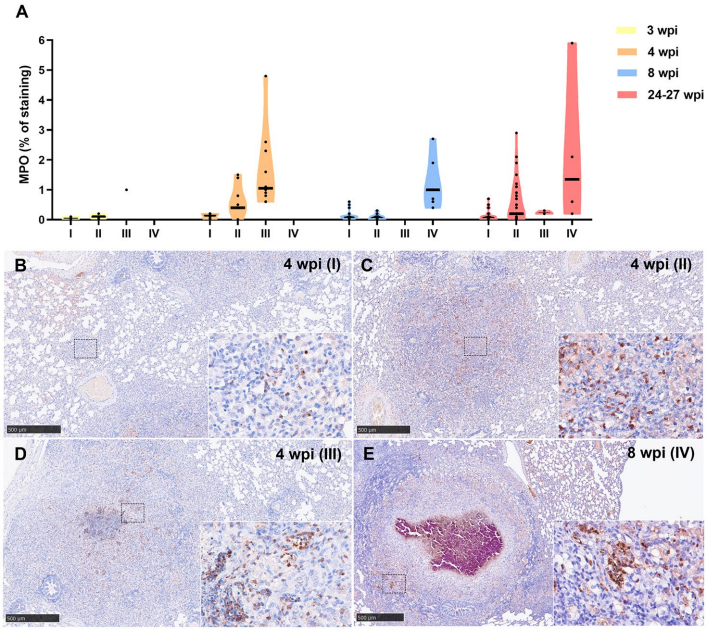

FIGURE 8
Myeloperoxidase (MPO) + immunohistochemical detection in stage I, II, III, and IV granulomas throughout the experiment. **(A)** Percentage of MPO$^+$ staining in stage I to IV granulomas at 3, 4, 8, and 24–27 wpi. Dots show the individual percentage of staining in each granuloma. Lines show the median value of the percentage of staining in the different stages throughout the study. **(B)** MPO expression in stage I granuloma at 4 wpi. **(C)** MPO expression in stage II granuloma at 4 wpi. **(D)** MPO expression in stage III granuloma at 4 wpi. **(E)** MPO expression in stage IV granuloma at 8 wpi. Insets show close-up images at higher magnification showing MPO$^+$ polymorphonuclear cells. Scale bars = 500 µm (insets = 100 µm).

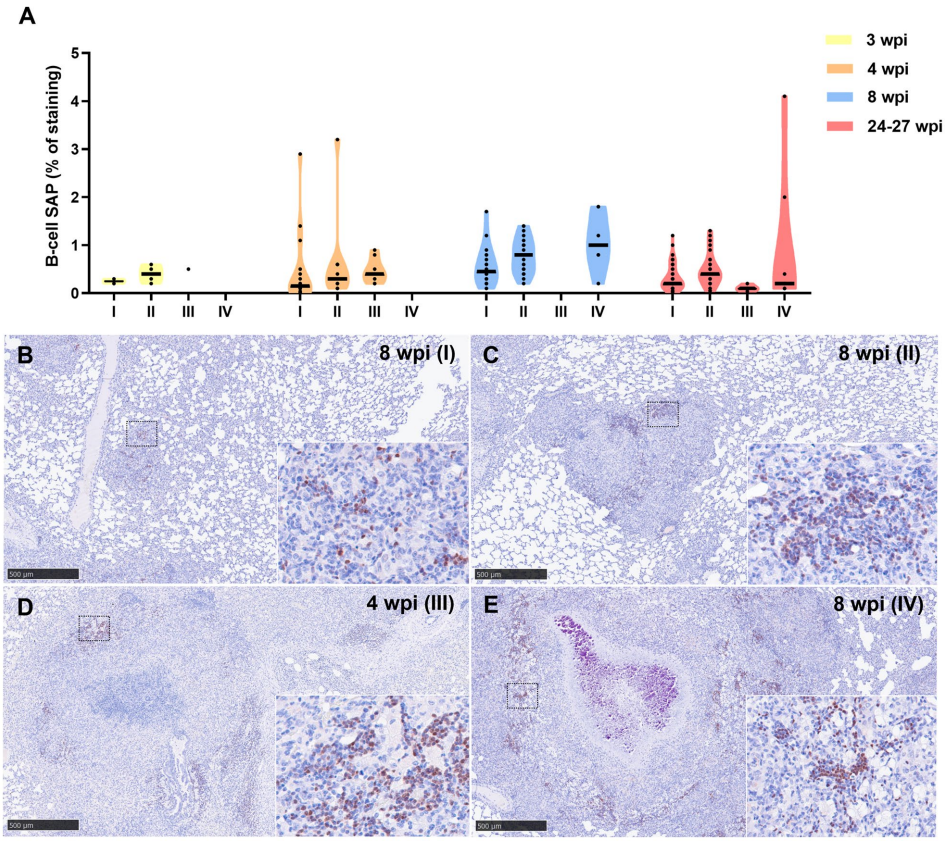

FIGURE 9
B-cell Specific Activator Protein+ (SAP+) immunohistochemical detection in stage I, II, III, and IV granulomas throughout the experiment. **(A)** Percentage of B-cell SAP+ staining in all stages granulomas at 3, 4, 8, and 24–27 wpi. Dots show the individual percentage of staining in each granuloma. Lines show the median value of the percentage of staining in the different stages throughout the study. **(B)** B-cell SAP expression in stage I granuloma at 8 wpi. **(C)** B-cell SAP expression in stage II granuloma at 8 wpi. **(D)** B-cell SAP expression in stage III granuloma at 4 wpi. **(E)** B-cell SAP expression in stage IV granuloma at 8 wpi. Insets show close-up images at higher magnification showing B cell SAP$^+$ lymphocytes. Scale bars = 500 µm (insets = 100 µm).

Conversely, the lack of a fibrotic capsule in late stages granulomas can be an advantage in this animal model for target therapies directed to advanced lesions where a xenobiotic can access the inner layers of the granuloma in the absence of a significant, fibrotic barrier.

Interestingly, the lesion development and cellular composition of granulomas observed in this study show many similarities to pulmonary TB granulomas in human patients, including the presence of solid non-necrotising early lesions to advanced necrotic granulomas categorised in four stages like in cattle and guinea pigs (50).

5. Conclusion

The guinea pig model provides a reliable, cost-effective method of evaluating potential new therapeutics and prophylactics in the treatment and prevention of human tuberculosis. This study demonstrates a refinement in the evaluation of the severity and extent of pulmonary tuberculous disease in the guinea pig model through the provision of a quantitative methodology for staging granuloma progression; this, in turn, can provide additional data to aid in the evaluation of future, potential drug and vaccine targets against human tuberculosis. Moreover, the IHC techniques developed may be valuable tools to characterise the local immune responses and lesions in other animal models of disease using guinea pigs.

Data availability statement

The raw data supporting the conclusions of this article will be made available by the authors, without undue reservation.

Ethics statement

The animal study was reviewed and approved by UK Health Security Agency, Animal Welfare and Ethical Review body, Porton Down, UK and authorised under an appropriate UK Home Office project license. The study was conducted in accordance with the local legislation and institutional requirements.

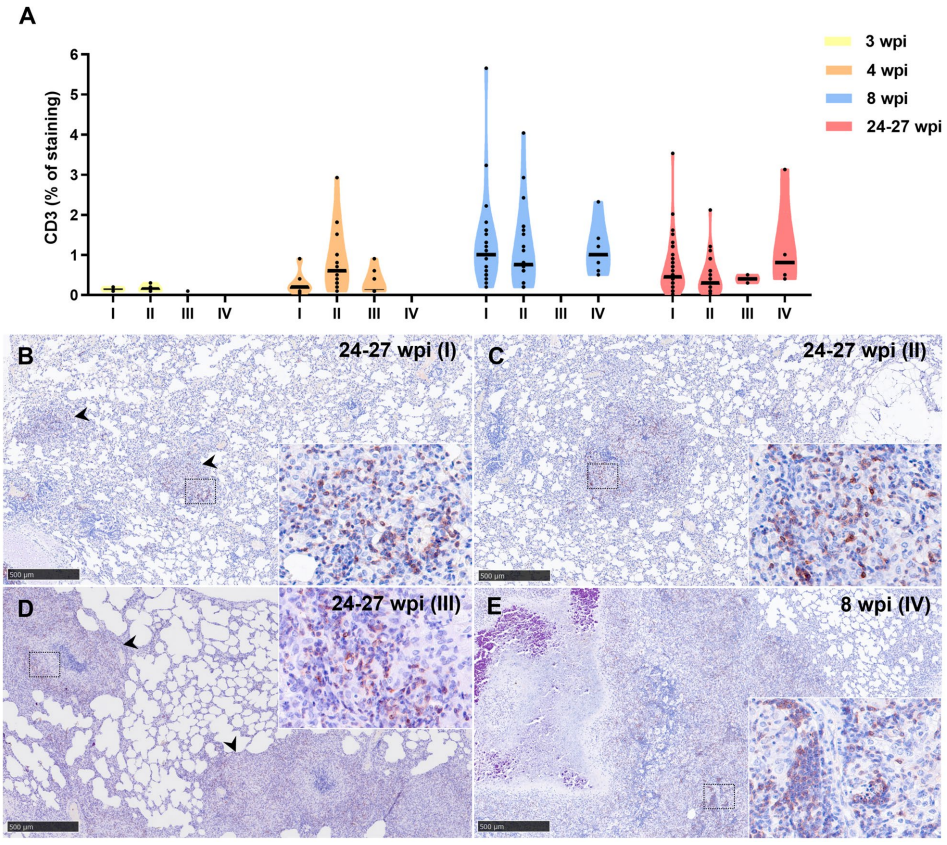

FIGURE 10
CD3+ immunohistochemical detection in stage I, II, III, and IV granulomas throughout the experiment. **(A)** Percentage of $CD3^+$ staining in stage I to IV granulomas at 3 to 24–27 wpi. Dots show the individual percentage of staining in each granuloma. Lines show the median value of the percentage of staining in the different stages throughout the study. **(B)** CD3 expression in stage I granuloma (arrowheads) at 24–27 wpi. **(C)** CD3 expression in stage II granuloma at 24–27 wpi. **(D)** CD3 expression in stage III granuloma (arrowheads) at 24–27 wpi. **(E)** CD3 expression in stage IV granuloma at 8 wpi. Insets show close-up images at higher magnification showing CD3+ T lymphocytes. Scale bars = 500 µm (insets = 100 µm).

Author contributions

FL-M: Formal analysis, Investigation, Writing – original draft, Writing – review & editing. IR-T: Data curation, Formal analysis, Investigation, Methodology, Validation, Writing – review & editing. LH: Data curation, Formal analysis, Methodology, Writing – review & editing. AB: Data curation, Methodology, Writing – review & editing. IA-R: Data curation, Formal analysis, Writing – review & editing. RW: Formal analysis, Methodology, Writing – review & editing. SC: Conceptualization, Data curation, Formal analysis, Funding acquisition, Project administration, Writing – review & editing. ER: Formal analysis, Validation, Writing – review & editing. FS: Conceptualization, Formal analysis, Funding acquisition, Investigation, Resources, Supervision, Writing – original draft, Writing – review & editing.

Funding

The author(s) declare financial support was received for the research, authorship, and/or publication of this article. This work has been funded by internal funds from UKHSA and in part with Federal funds from the National Institute of Allergy and Infectious Diseases, National Institutes of Health, Department of Health and Human Services, under Contract No. 75N93021C00029. The content is solely the responsibility of the authors and does not necessarily represent the official views of the National Institutes of Health. FL-M was supported by a doctoral grant from ANID (National Research and Development Agency) (Doctoral grant Chile/2019/72200324) and Call for applications of Grants for Line 2.3.1 International Mobility of Doctorate Students, included in the II Postgraduate Programme of the University of Córdoba. IR-T is supported by a "Margarita Salas" contract from the Spanish Ministry of Universities. IA-R is supported by the FPU grant of the Spanish Ministry of Education, Culture and Sport (FPU19/03969).

Acknowledgments

The authors would like to thank the staff in the Biological Investigation Group for their expert knowledge and help with this work. The authors would also like to thank Joanna Bacon for production and gift of *M. tuberculosis* H37Rv stock cultures used for infections, and to Vanessa Lucas for carrying out the bacteriology assays.

Conflict of interest

The authors declare that the research was conducted in the absence of any commercial or financial relationships that could be construed as a potential conflict of interest.

The author(s) declared that they were an editorial board member of Frontiers, at the time of submission. This had no impact on the peer review process and the final decision.

Publisher's note

References

1. Bermejo MC, Clavera I, Michel De La Rosa FJ, Marín B. Epidemiología de la tuberculosis epidemiology of tuberculosis. *An Sist Sanit Navar*. (2007) 30:7–19. doi: 10.4321/S1137-66272007000400002

2. Rook GAW, Hernandez-Pando R. The pathogenesis of tuberculosis. *Annu Rev Microbiol*. (1996) 50:259–84. doi: 10.1146/annurev.micro.50.1.259

3. WHO. Tuberculosis. World Health Organization (2023). Available at: https://www.who.int/news-room/fact-sheets/detail/tuberculosis (Accessed June 29, 2023)

4. WHO. Global Tuberculosis report 2022. (2022). Available at: http://apps.who.int/bookorders

5. Basaraba RJ. Experimental tuberculosis: the role of comparative pathology in the discovery of improved tuberculosis treatment strategies. *Tuberculosis (Edinb)*. (2008) 88:S35–47. doi: 10.1016/S1472-9792(08)70035-0

6. Ramakrishnan L. Revisiting the role of the granuloma in tuberculosis. *Nat Rev Immunol*. (2012) 12:352–66. doi: 10.1038/nri3211

7. Flynn JAL. Lessons from experimental Mycobacterium tuberculosis infections. *Microbes Infect*. (2006) 8:1179–88. doi: 10.1016/j.micinf.2005.10.033

8. García-Jiménez WL, Fernández-Llario P, Gómez L, Benítez-Medina JM, García-Sánchez A, Martínez R, et al. Histological and immunohistochemical characterisation of Mycobacterium bovis induced granulomas in naturally infected fallow deer (Dama dama). *Vet Immunol Immunopathol*. (2012) 149:66–75. doi: 10.1016/j.vetimm.2012.06.010

9. García-Jiménez WL, Benítez-Medina JM, Fernández-Llario P, Abecia JA, García-Sánchez A, Martínez R, et al. Comparative pathology of the natural infections by Mycobacterium bovis and by Mycobacterium caprae in wild boar (Sus scrofa). *Transbound Emerg Dis*. (2013) 60:102–9. doi: 10.1111/j.1865-1682.2012.01321.x

10. Hughes EJ, Tobin DM. Decoding the tuberculous granuloma. *Immunity*. (2022) 55:819–21. doi: 10.1016/j.immuni.2022.04.009

11. Orme IM, Ordway DJ. Mouse and guinea pig models of tuberculosis. *Tuberculosis and the tubercle Bacillus*: 2nd Edn. Eds. W. R. Jacobs, H. McShane, V. Mizrahi and I. M. Orme (2017)143–162.

12. Turner OC, Basaraba RJ, Orme IM. Immunopathogenesis of pulmonary granulomas in the guinea pig after infection with Mycobacterium tuberculosis. *Infect Immun*. (2003) 71:864–71. doi: 10.1128/IAI.71.2.864-871.2003

13. Wangoo A, Johnson L, Gough J, Ackbar R, Inglut S, Hicks D, et al. Advanced granulomatous lesions in Mycobacterium bovis-infected cattle are associated with increased expression of type I procollagen, γδ (WC1+) T cells and CD 68+ cells. *J Comp Pathol*. (2005) 133:223–34. doi: 10.1016/j.jcpa.2005.05.001

14. Pérez de Val B, Perea C, Estruch J, Solano-Manrique C, Riera C, Sanz A, et al. Generalised tuberculosis due to Mycobacterium caprae in a red fox phylogenetically related to livestock breakdowns. *BMC Vet Res*. (2022) 18:352. doi: 10.1186/s12917-022-03454-7

15. White AD, Laura S, Charlotte S, Alexandra M, Jennie G, Simon C, et al. MTBVAC vaccination protects rhesus macaques against aerosol challenge with M. tuberculosis and induces immune signatures analogous to those observed in clinical studies. *NPJ Vaccines*. (2021) 6:4. doi: 10.1038/s41541-020-00262-8

16. Hunter L, Hingley-Wilson S, Stewart GR, Sharpe SA, Salguero FJ. Dynamics of macrophage, T and B cell infiltration within pulmonary granulomas induced by Mycobacterium tuberculosis in two non-human primate models of aerosol infection. *Front Immunol*. (2022) 12:776913. doi: 10.3389/fimmu.2021.776913

17. Padilla-Carlin DJ, McMurray DN, Hickey AJ. The guinea pig as a model of infectious diseases. *Comp Med*. (2008) 58:324–40.

18. Kennedy EM, Dowall SD, Salguero FJ, Yeates P, Aram M, Hewson R. A vaccine based on recombinant modified vaccinia Ankara containing the nucleoprotein from Lassa virus protects against disease progression in a guinea pig model. *Vaccine*. (2019) 37:5404–13. doi: 10.1016/j.vaccine.2019.07.023

19. Silva Miranda M, Breiman A, Allain S, Deknuydt F, Altare F. The tuberculous granuloma: an unsuccessful host defence mechanism providing a safety shelter for the bacteria? *Clin Dev Immunol*. (2012) 2012:139127. doi: 10.1155/2012/139127

20. Clark S, Hall Y, Williams A. Animal models of tuberculosis: guinea pigs. *Cold Spring Harb Perspect Med*. (2015) 5:1–9. doi: 10.1101/cshperspect.a018572

21. Butler RE, Krishnan N, Garcia-Jimenez W, Francis R, Martyn A, Mendum T, et al. Susceptibility of Mycobacterium tuberculosis-infected host cells to phospho-MLKL driven necroptosis is dependent on cell type and presence of TNFα. *Virulence*. (2017) 8:1820–32. doi: 10.1080/21505594.2017.1377881

22. White AD, Sibley L, Gullick J, Sarfas C, Clark S, Fagrouch Z, et al. TB and SIV coinfection; a model for evaluating vaccine strategies against TB reactivation in Asian origin Cynomolgus macaques: a pilot study using BCG vaccination. *Vaccines*. (2021) 9:945. doi: 10.3390/vaccines9090945

23. Young D. Animal models of tuberculosis. *Eur J Immunol*. (2009) 39:2011–4. doi: 10.1002/eji.200939542

24. Kohli R, Punia RS, Singh R, Kundu R, Mohan H. Relative value of immunohistochemistry in detection of mycobacterial antigen in suspected cases of tuberculosis in tissue sections. *Indian J Pathol Microbiol*. (2014) 57:574–8. doi: 10.4103/0377-4929.142667

25. Orme IM, Basaraba RJ. The formation of the granuloma in tuberculosis infection. *Semin Immunol*. (2014) 26:601–9. doi: 10.1016/j.smim.2014.09.009

26. Basaraba RJ, Bielefeldt-Ohmann H, Eschelbach EK, Reisenhauer C, Tolnay AE, Taraba LC, et al. Tuberculosis (Edinb). *Tuberculosis*. (2008) 88:69–79. doi: 10.1016/j.tube.2007.09.002

27. Basaraba RJ, Smith EE, Shanley CA, Orme IM. Pulmonary lymphatics are primary sites of Mycobacterium tuberculosis infection in guinea pigs infected by aerosol. *Infect Immun*. (2006) 74:5397–401. doi: 10.1128/IAI.00332-06

28. Basaraba RJ, Dailey DD, McFarland CT, Shanley CA, Smith EE, McMurray DN, et al. Lymphadenitis as a major element of disease in the guinea pig model of tuberculosis. *Tuberculosis*. (2006) 86:386–94. doi: 10.1016/j.tube.2005.11.003

29. James BW, Williams A, Marsh PD. The physiology and pathogenicity of Mycobacterium tuberculosis grown under controlled conditions in a defined medium. *J Appl Microbiol*. (2000) 88:669–77. doi: 10.1046/j.1365-2672.2000.01020.x

30. Clark SO, Hall Y, Kelly DJF, Hatch GJ, Williams A. Survival of Mycobacterium tuberculosis during experimental aerosolization and implications for aerosol challenge models. *J Appl Microbiol*. (2011) 111:350–9. doi: 10.1111/j.1365-2672.2011.05069.x

31. Hartings JM, Roy CJ. The automated bioaerosol exposure system: preclinical platform development and a respiratory dosimetry application with nonhuman primates. *J Pharmacol Toxicol Methods*. (2004) 49:39–55. doi: 10.1016/j.vascn.2003.07.001

32. Clark S, Lanni F, Marinova D, Rayner E, Martin C, Williams A. Revaccination of Guinea pigs with the live attenuated Mycobacterium tuberculosis vaccine MTBVAC improves BCG's protection against tuberculosis. *J Infect Dis*. (2017) 216:525–33. doi: 10.1093/infdis/jix030

33. Creissen E, Izzo L, Dawson C, Izzo AA. Guinea pig model of Mycobacterium tuberculosis infection. *Curr Protoc*. (2021) 1:e312. doi: 10.1002/cpz1.312

34. Sander P, Clark S, Petrera A, Vilaplana C, Meuli M, Selchow P, et al. Deletion of zmp1 improves Mycobacterium bovis BCG-mediated protection in a guinea pig model of tuberculosis. *Vaccine*. (2015) 33:1353–9. doi: 10.1016/j.vaccine.2015.01.058

35. Larrouy-Maumus G, Layre E, Clark S, Prandi J, Rayner E, Lepore M, et al. Protective efficacy of a lipid antigen vaccine in a guinea pig model of tuberculosis. *Vaccine*. (2017) 35:1395–402. doi: 10.1016/j.vaccine.2017.01.079

36. Williams A, James BW, Bacon J, Hatch KA, Hatch GJ, Hall GA, et al. An assay to compare the infectivity of Mycobacterium tuberculosis isolates based on aerosol infection of guinea pigs and assessment of bacteriology. *Tuberculosis*. (2005) 85:177–84. doi: 10.1016/j.tube.2004.11.001

37. Rayner EL, Pearson GR, Hall GA, Gleeson F, McIntyre A, Smyth D, et al. Early lesions following aerosol challenge of rhesus macaques (Macaca mulatta) with Mycobacterium tuberculosis (Erdman strain). *J Comp Pathol*. (2015) 152:217–26. doi: 10.1016/j.jcpa.2014.10.002

38. Sibley L, Dennis M, Sarfas C, White A, Clark S, Gleeson F, et al. Route of delivery to the airway influences the distribution of pulmonary disease but not the outcome of Mycobacterium tuberculosis infection in rhesus macaques. *Tuberculosis*. (2016) 96:141–9. doi: 10.1016/j.tube.2015.11.004

39. Villarreal-Ramos B, Berg S, Whelan A, Holbert S, Carreras F, Salguero FJ, et al. Experimental infection of cattle with Mycobacterium tuberculosis isolates shows the attenuation of the human tubercle bacillus for cattle. *Sci Rep*. (2018) 8:894. doi: 10.1038/s41598-017-18575-5

40. Salguero FJ, Gibson S, Garcia-Jimenez W, Gough J, Strickland TS, Vordermeier HM, et al. Differential cell composition and cytokine expression within lymph node granulomas from BCG-vaccinated and non-vaccinated cattle experimentally infected with Mycobacterium bovis. *Transbound Emerg Dis*. (2017) 64:1734–49. doi: 10.1111/tbed.12561

41. Aranday-Cortes E, Bull NC, Villarreal-Ramos B, Gough J, Hicks D, Ortiz-Peláez Á, et al. Upregulation of IL-17A, CXCL9 and CXCL10 in early-stage granulomas induced by Mycobacterium bovis in cattle. *Transbound Emerg Dis*. (2013) 60:525–37. doi: 10.1111/j.1865-1682.2012.01370.x

42. Balseiro A, Prieto JM, Álvarez V, Lesellier S, Davé D, Salguero FJ, et al. Protective effect of oral BCG and inactivated Mycobacterium bovis vaccines in European badgers (Meles meles) experimentally infected with M. bovis. *Front Vet Sci*. (2020) 7:41. doi: 10.3389/fvets.2020.00041

43. Chambers MA, Aldwell F, Williams GA, Palmer S, Gowtage S, Ashford R, et al. The effect of oral vaccination with Mycobacterium bovis BCG on the development of tuberculosis in captive European badgers (Meles meles). *Front Cell Infect Microbiol*. (2017) 7:6. doi: 10.3389/fcimb.2017.00006

44. García-Jiménez WL, Salguero FJ, Fernández-Llario P, Martínez R, Risco D, Gough J, et al. Immunopathology of granulomas produced by Mycobacterium bovis in naturally infected wild boar. *Vet Immunol Immunopathol*. (2013) 156:54–63. doi: 10.1016/j.vetimm.2013.09.008

45. Irwin SM, Driver E, Lyon E, Schrupp C, Ryan G, Gonzalez-Juarrero M, et al. Presence of multiple lesion types with vastly different microenvironments in C3HeB/FeJ mice following aerosol infection with Mycobacterium tuberculosis. *DMM Disease Models Mech*. (2015) 8:591–602. doi: 10.1242/dmm.019570

46. Ordway D, Henao-Tamayo M, Shanley C, Smith EE, Palanisamy G, Wang B, et al. Influence of Mycobacterium bovis BCG vaccination on cellular immune response of guinea pigs challenged with Mycobacterium tuberculosis. *Clin Vaccine Immunol*. (2008) 15:1248–58. doi: 10.1128/CVI.00019-08

47. Converse PJ, Eisenach KD, Theus SA, Nuermberger EL, Tyagi S, Ly LH, et al. The impact of mouse passaging of Mycobacterium tuberculosis strains prior to virulence testing in the mouse and guinea pig aerosol models. *PLoS One*. (2010) 5:e10289. doi: 10.1371/journal.pone.0010289

48. Rayner EL, Pearson GR, Hall GA, Basaraba RJ, Gleeson F, McIntyre A, et al. Early lesions following aerosol infection of rhesus macaques (Macaca mulatta) with mycobacterium tuberculosis strain H37RV. *J Comp Pathol*. (2013) 149:475–85. doi: 10.1016/j.jcpa.2013.05.005

49. Cyktor JC, Carruthers B, Kominsky RA, Beamer GL, Stromberg P, Turner J. IL-10 inhibits mature fibrotic granuloma formation during Mycobacterium tuberculosis infection. *J Immunol*. (2013) 190:2778–90. doi: 10.4049/jimmunol.1202722

50. Sawyer AJ, Patrick E, Edwards J, Wilmott JS, Fielder T, Yang Q, et al. Spatial mapping reveals granuloma diversity and histopathological superstructure in human tuberculosis. *J Exp Med*. (2023) 220:e20221392. doi: 10.1084/jem.20221392

frontiers | Frontiers in Veterinary Science

TYPE Review
PUBLISHED 12 October 2023
DOI 10.3389/fvets.2023.1264833

OPEN ACCESS

EDITED BY
Cleverson D. Souza,
University of Florida, United States

REVIEWED BY
Christian Menge,
Friedrich-Loeffler-Institute, Germany
Amanda Jane Gibson,
Aberystwyth University, United Kingdom

*CORRESPONDENCE
Laura Hunter
✉ Laura.Hunter@ukhsa.gov.uk

RECEIVED 21 July 2023
ACCEPTED 22 September 2023
PUBLISHED 12 October 2023

CITATION
Hunter L, Ruedas-Torres I, Agulló-Ros I, Rayner E and Salguero FJ (2023) Comparative pathology of experimental pulmonary tuberculosis in animal models.
Front. Vet. Sci. 10:1264833.
doi: 10.3389/fvets.2023.1264833

Comparative pathology of experimental pulmonary tuberculosis in animal models

Laura Hunter[1,2]*, Inés Ruedas-Torres[1,3], Irene Agulló-Ros[1,3], Emma Rayner[1] and Francisco J. Salguero[1]

[1]Pathology Department, UK Health Security Agency (UKHSA), Porton Down, Salisbury, United Kingdom, [2]School of Biosciences and Medicine, University of Surrey, Guildford, United Kingdom, [3]Department of Anatomy and Comparative Pathology and Toxicology, UIC Zoonosis y Enfermedades Emergentes ENZOEM, University of Córdoba, International Excellence Agrifood Campus, Córdoba, Spain

Research in human tuberculosis (TB) is limited by the availability of human tissues from patients, which is often altered by therapy and treatment. Thus, the use of animal models is a key tool in increasing our understanding of the pathogenesis, disease progression and preclinical evaluation of new therapies and vaccines. The granuloma is the hallmark lesion of pulmonary tuberculosis, regardless of the species or animal model used. Although animal models may not fully replicate all the histopathological characteristics observed in natural, human TB disease, each one brings its own attributes which enable researchers to answer specific questions regarding TB immunopathogenesis. This review delves into the pulmonary pathology induced by *Mycobacterium tuberculosis* complex (MTBC) bacteria in different animal models (non-human primates, rodents, guinea pigs, rabbits, cattle, goats, and others) and compares how they relate to the pulmonary disease described in humans. Although the described models have demonstrated some histopathological features in common with human pulmonary TB, these data should be considered carefully in the context of this disease. Further research is necessary to establish the most appropriate model for the study of TB, and to carry out a standard characterisation and score of pulmonary lesions.

KEYWORDS

tuberculosis, animal models, pathology, granuloma, mycobacteria, lung

1. Introduction

Tuberculosis (TB) is the second leading infectious disease killer in humans after COVID-19 (SARS-2) (1). *Mycobacterium tuberculosis* (Mtb) is part of the *Mycobacterium tuberculosis* complex (MTBC), which consists of nine closely related species (*M. tuberculosis, M. bovis, M. africanum, M. canetti, M. microti, M. mungi, M. orygis, M. caprae, M. pinnipedii and M. suricattae*) that can cause TB in both humans and animals.

Although TB has been studied for many decades, there are still many aspects of the immunopathogenesis which are not fully understood. The only licenced vaccine, the Bacillus Calmette-Guérin (BCG), has variable efficacy dependant on various factors including the target population and the age at vaccination. Therefore, there is still much research ongoing to find new vaccines and therapeutics.

Research into human TB is limited by the availability of infected human tissues due to the challenges associated with obtaining serial lung biopsies throughout the progression of the

disease (2–4). Furthermore, pathogenic characteristics and severity is inherently altered by therapy and treatment, which is a major barrier (2, 3).

Whilst humans are the natural host for Mtb, infection and subsequent disease is observed in many animal species, making these good models in which to study the disease progression in a way that is prohibited in humans (3, 4). No animal model of TB fully replicates all the pathological characteristics observed in human TB disease progression; therefore, the vast majority of data is generated using many different animal models and must be considered carefully when relating to human disease (2, 3). Mycobacteria within the MTBC are also important pathogens for animal health, and animal models provide a useful tool for bovine TB (bTB) research (5–8).

Regardless of the species, the lung granuloma is the hallmark of pulmonary tuberculosis (9). Its first description was made by Anton Ghon, an Austrian pathologist, who made significant contributions to the understanding of primary TB and its anatomical pathology in humans (10, 11). It is known that Mtb infects alveolar macrophages, which release multiple cytokines to recruit additional macrophages, dendritic cells, and lymphocytes, leading to the formation of an early granuloma (9). This event triggers the recruitment of various types of immune cells, including neutrophils, which can produce chemokines and cytokines in response to the infection, attracting additional immune cells to the site of infection (9, 12). Infected macrophages play an important role during granuloma formation, serving as a central platform around where the rest of the immune cells are located, and giving rise to the typical, spherical morphology (9, 12). With the progression of the infection, mature macrophages undergo a morphological change, referred to as 'epithelioid differentiation' due to its capacity to form tight, interdigitated, cellular junctions, also known as epithelioid histiocytes (12–14). Macrophages can also fuse together to form multinucleated giant cells (MNGCs, also known as Langhans giant cells) or differentiate into foamy macrophages, characterised by the accumulation of lipids within their cytoplasm (9, 12–14).

This review paper will focus on the histopathological features of pulmonary granulomas in different animal models of experimental and natural MTBC infection (Table 1) and how they relate to the disease progression observed in humans.

2. Tuberculosis in humans

Early pulmonary granulomas induced by Mtb in human lungs are characterised by a central region of large epithelioid cells (CD68+ cells by immunohistochemistry [IHC]), surrounded by a mixture of macrophages and predominantly CD4+ T cells, with a smaller number of CD8+ T cells and MNGCs (15). The advanced model of human tuberculous granulomas describes well-structured and organised lesions, characterised by a central area of necrosis that harbours the mycobacteria (9, 11, 14–17) (Figure 1; Table 1). This necrosis is the result of the death of infected macrophages that form the central region of the granuloma and receives the name of caseum due to its 'cheese-like' consistency observed grossly (9, 12, 18). The necrotic core provides nutritional support and leads the mycobacteria to survive for decades in a latent state (9, 11). The initial layer surrounding the necrotic centre is populated with T lymphocytes (mainly CD4+ T cells), macrophages and MNGCs (CD68+ cells), diffusely distributed (9, 11, 14, 17, 19). These MNGCs are an important feature of human TB in lung tissue (17). In the outer layers there are large numbers of CD8+ T cells (15). Some authors also describe the presence of prominent, B cell aggregates which are located more distant to the necrotic core, and which are situated in a background of T lymphocytes and mycobacteria-containing macrophages diffusely distributed (15, 17). Whilst this leukocyte infiltration contributes to the local immune response, it can also lead to significant damage in the affected lung (11). As the disease progresses, the necrotic core can calcify (dystrophic mineralisation) and be encapsulated by a fibrotic rim (12, 16). Calcification is usually demonstrated with Von Kossa staining and fibrosis can be visualised with trichome stains such as Martius Scarlett Blue (MSB) or Masson's Trichrome (16). It is thought that the main function of the granuloma is to prevent the mycobacterial spread, but it could also serve as a physical barrier to prevent the penetration of anti-TB drugs (14).

Zieh-Neelsen (ZN) staining is the routine technique to detect the presence of acid-fast bacilli (AFB) in tissues (15, 16, 19–21). However, IHC and immunofluorescence (IF) are also applied to identify AFB in tissue specimens (11, 22–24).

During human disease where TB reactivation has occurred, it is typical to observe the formation of thin-walled cavities (2, 18). These derive from the replacement of large areas of necrosis in primary granulomas with an open space that often contains a high number of neutrophils and necrotic cellular debris (2). The wall of the cavity is composed of mixed inflammatory cells, resembling primary granulomas, and is separated from the surrounding normal parenchyma by a fibrous capsule (2). The underlying mechanisms of this phenomenon are still a subject of debate within the field of pathophysiology (25). However, the most widely accepted model proposes a central liquefaction of the necrotic centre, followed by erosion of the nearby airways and release of the liquefied contents resulting in the formation of an air-filled cavity (25). Whilst tuberculous bacilli do not multiply well in the cytoplasm of activated macrophages or in the solid caseous centres, both extracellular and intracellular bacilli can do so easily in an immunologically privileged location and be transmitted between individuals through aerosol spread (2, 14, 26). The advanced stage of post-primary disease in humans is likely the key aspect that animal models are unable to replicate in TB infections, creating a significant gap in our understanding of the disease (2). As well as the characteristics above, tissue hypoxia studies have revealed that areas of necrosis in pulmonary tissues from Mtb infected patients are developed in anaerobic conditions (17, 27–29). Hypoxia induces the secretion of matrix metalloproteinase-1 (MMP-1), which produce lung destruction mainly in areas of lung consolidation and around pulmonary cavities (29).

Lung samples from uncontrolled TB infections in humans are difficult to acquire so there is a lack of information regarding specific stages of granuloma development (17). For that reason, contrary to what happens in many TB animal models, there is not a clear classification of pulmonary granulomas from TB-infected humans. A first approach was performed by Canetti et al. (30), in 1955 and later by Ridley and Ridley (16) in 1987. Ridley and Ridley describe 6 groups of tuberculous granulomas: 1a, 1b, 2a, 2b, 3a and 3b, relating to the number of bacilli, the extension of the necrosis, and the cell

TABLE 1 Main histopathological features in pulmonary granulomas in the different TB models.

	Necrosis	Mineralisation	Fibrosis	MNGCs	AFB	Cavitary lesions	References and comments
Human	+	+	+	+	+	+	(8, 10, 13–30). Cavitary lesions are common (2, 17, 24). Liquefaction (necrosis) present (24).
Mouse	−/+	−/+	−/+	−	+	−/+	(8, 12, 19, 20, 31–43). Absence of central necrosis in common strains (8, 12, 19, 20, 31). MNGCs not present, only occasional (16, 19, 32). Fibrosis seen in C5BL/6 mice (19). Foamy macrophages essential in mice (19, 32). Central necrosis seen in C3HeB/FeJ and HIS-NSG mice (35, 37–39). Development of cavitary lesions in C3HeB/FeJ mice strain (37). Abundant AFBs
Rat	−/+	−/+	−/+	+	+	−	Absence of central necrosis in common rats (40, 41) F344/N-rnu rat strain develops central non-caseous necrosis (40) MNGCs are present (40, 41, 43). Cotton rats develop caseous necrosis and calcification (42)
Guinea Pig	+	+	−/+	+	+	−	(44–53). Fibrosis is occasional (45). Mineralisation is a key feature (47). Associated lymphadenopathy and lymphangitis are important (51).
NHP	+	+	+	+	+	+	(29, 33, 35, 36, 54–71). Cavitation is rare in Old World Monkeys but seen in New World Monkeys such as the common marmoset (36).
Rabbit	+	+	−/+	+	+	+	(25, 72–75, 88) Development of liquefaction is present (72–75). Good model for TB meningitis (75). Mineralisation and evidence of scant AFBs (91). Fibrosis is present (25, 88).
Zebrafish	+	−	+	+	+	−	(66, 92, 94, 95, 97, 101) Absence of mineralisation (76–78). Fewer lymphocytes than in other models (76–78).
Cattle	+	+	+	+	+	−	(6, 67, 93, 96, 98, 102) AFB abundant in more developed necrotic lesions (5, 66, 92) MNGCs and foamy macrophages are abundant (94)
Goats	+	+	+	+	+	+	(79, 80, 103, 105, 106). Liquefactive necrosis is observed (79, 80, 103). Cavitary lesions are present (79, 80, 103).

Key: +, presence of feature, −, absence of feature, +/−, differing results. MNGCs – Multinucleated giant cells. AFB – Acid fast bacilli.

composition. In samples from group 1a, neither necrosis nor AFB were present and mature epithelioid cells were the main cell type, whereas in samples from group 3b extensive necrosis, scanty macrophages and over 3 AFB per granuloma were observed (16). Fenhalls et al. (19) in 2002 classified the lesions from seven patients evaluated as necrotic and non-necrotic granulomas. Later, in 2016, Marakala et al. (18) described a different histopathological classification, including solid granulomas that lacked necrosis, caseous granulomas and cavitary granulomas. Further classification has been described by other authors, such as the following example for pulmonary granulomas: nascent, caseous, fibrocaseous and resolved granulomas (54).

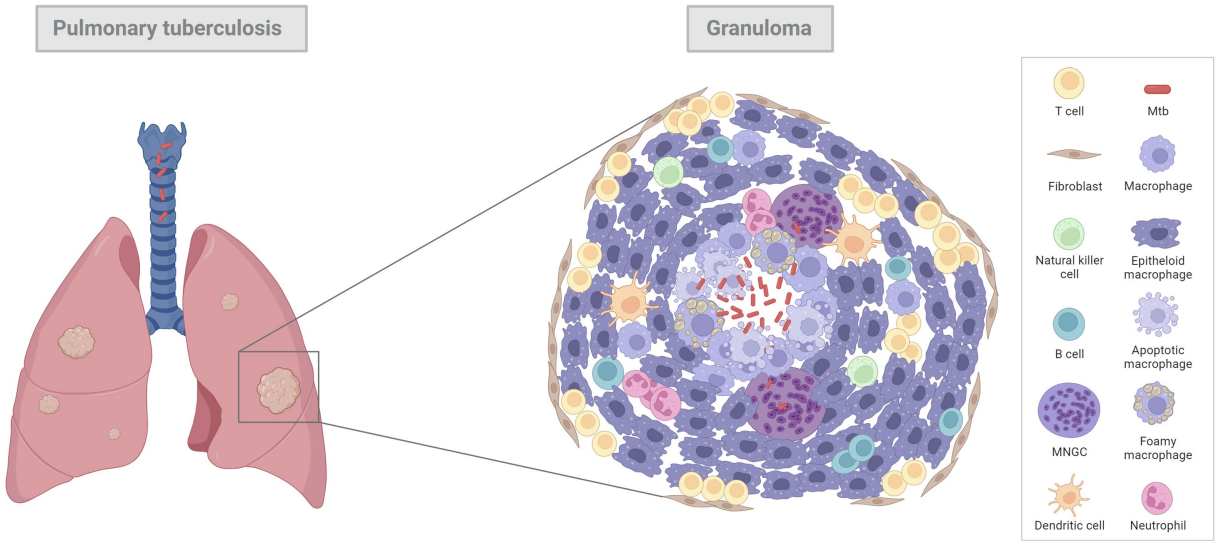

FIGURE 1
Diagram of a general pulmonary tuberculous granuloma. Mtb infects alveolar macrophages which release cytokines to attract additional macrophages, dendritic cells and lymphocytes, leading to an early granuloma. With the progression of the infection, tuberculous granulomas become bigger, more structured, and organised lesions, characterised by a central area of necrosis (infected macrophages) that harbours the mycobacteria. Surrounding this necrotic core there are mature macrophages, called "epithelioid macrophages" (due to its capacity to from interdigital junctions), multinucleated giant cells (MNGCs) and other immune cell types such as lymphocytes, neutrophils, natural killer cells, and dendritic cells to a less extent. In the outer layer there are large number of T cells and fibroblasts which try to encapsule the lesion. Image created with BioRender.com.

3. Comparative pathology of animal models

3.1. Non-human primates

Old World monkeys, including the rhesus (*Macaca mulatta*) and cynomolgus (*Macaca fascicularis*) macaques, and New World monkeys (*Callithrix jacchus*, the common marmoset), are used as experimental models of human TB disease. They all develop the full range of Mtb disease observed in humans, including children and immunosuppressed patients, ranging from solid lesions to caseation, calcification, and cavitation (30, 56–59, 81). Each NHP model has benefits for certain types of studies; for instance, rhesus macaques have been shown to be more susceptible to Mtb infection compared with cynomolgus macaques who can show active as well as latent TB infection (58, 60). Depending on the strain of Mtb used, different rates of disease progression, as well as varying degrees of cavitation, are observed in the common marmoset (59). Two different outcomes of infection from Mtb have been seen in the cynomolgus macaque, depending on the challenge dose. It has been shown that when high doses of Mtb are administered, severe disease develops (acute TB) (55); conversely, a low-dose can result in asymptomatic infection which is similar to latent TB in humans (56, 61, 62).

Varying the route of infection does not result in different outcomes in terms of clinical parameters and behavioural changes between the macaque subspecies (63); however, lesion distribution does vary in the lung, with diffuse lesions more commonly associated with the aerosol route as compared to the intra-bronchial route (63, 64).

A range of pulmonary granulomas are observed in active TB in all NHP models. These range from early lesions consisting of small aggregates of immune cells, mainly macrophages with variable numbers of lymphocytes and neutrophils, and lacking clearly defined boundaries (65); the classical, organised, 'solid' structured granulomas which comprise abundant, epithelioid macrophages, neutrophils and some MNGCs in the absence of necrosis; granulomas that have a central core of necrosis but are not caseous and are surrounded by a rim of epithelioid macrophages and a peripheral rim of lymphocytes; and, large, well-defined, caseous granulomas (57, 62, 65). Cavitary lesions are rarely observed in the Old World NHP models during active disease (62); however, they have been noted in the common marmoset between 58 and 70-days post-challenge (dpc) when infected with the CDC1551 strain (59). TB pneumonia is also observed during active TB in all NHP models, and it is usually surrounding multicentric, often coalescing, large, caseous granulomas (59, 62). A summary of the main histopathological features in NHPs is represented in Table 1.

The majority of more advanced lesions mentioned above are also observed during latent TB infection (LTBI); however, granulomas without necrotic centres have not been noted. Large caseous granulomas are observed although the caseous core has often been replaced by mineralisation and/or collagenous material (62) defined as 'fibro-calcified' lesions by some groups (62). Also observed are lesions that are termed 'sclerotic or fibrosing' granulomas; lack visible mineralisation and comprise compacted, sclerotic material (62).

Depending on the strain of Mtb used and the species of NHPs, microscopic granulomas can be seen as early as 2–5 weeks post-challenge (wpc) (57, 65, 66). In rhesus macaques, early granulomas often lack clearly defined boundaries, but by 3 wpc, more 'classical' granulomas are seen (66). Central necrosis is also seen this timepoint when infected with H37Rv (65, 66). In cynomolgus macaques, however, the earliest manifestations of granulomas within the lung are present at 4–5 wpc, comprising multifocal to

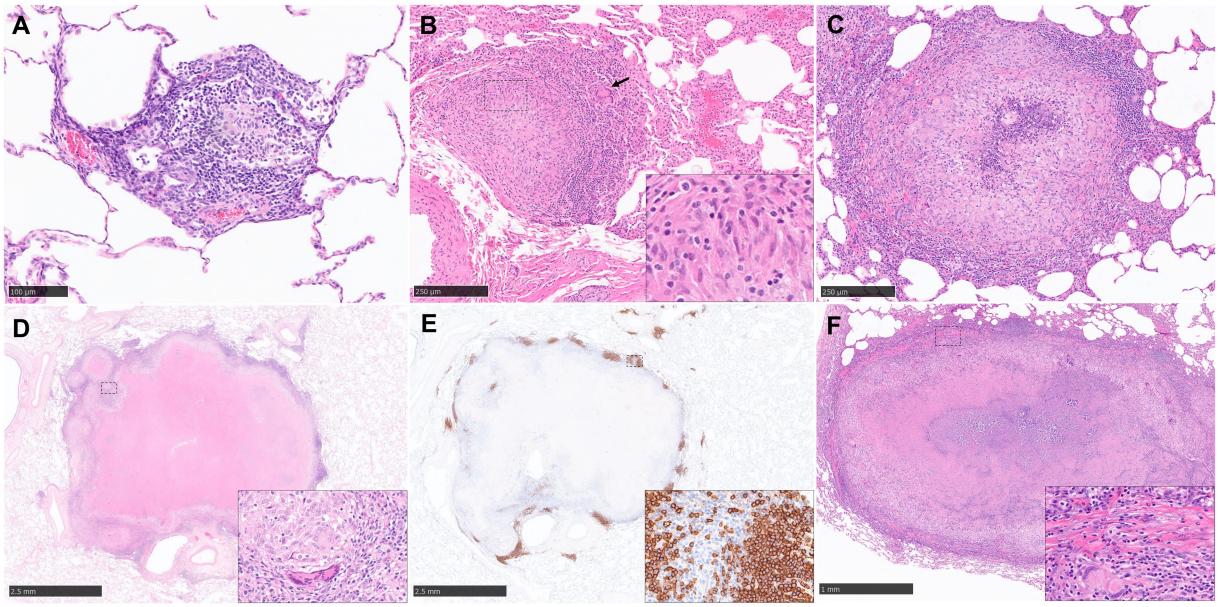

FIGURE 2
Representative histopathological images of the rhesus macaque (NHP) TB model in lung: (H&E) and CD20 staining (IHC). **(A)** Stage 1 granuloma characterized by the infiltration of the alveolar wall with macrophages and lymphocytes. **(B)** Stage 2 granuloma, well demarcated lesion composed by epithelioid macrophages (inset), macrophages and scattered MNGCs (arrow). **(C)** Stage 5 granuloma, larger lesion with a focal necrotic core composed of degenerated neutrophils and macrophages surrounded by viable cells. **(D, E)** Stage 6 granuloma, well demarcated lesion with central caseous necrosis surrounded by a layer of macrophages and an external rim of lymphocytes, with abundant B cells (CD20+) around the periphery forming "nests". Inset shows some MNGCs **(D)** and CD20+ B cells **(E)**. **(F)** Late stage 6 granuloma, partially encapsulated by a fibrotic capsule (inset), characterized by the presence of a necrotic centre with dystrophic mineralization surrounded by viable immune cells. MNGCs are also present (inset). Scale bars = A, 100 µm; B and C, 250 µm; D and E, 2.5 mm; F, 1 mm.

coalescing, caseous lesions (57). These granulomas are more like the 'classical' granuloma. A centre core of necrotic cells and amorphous material that is surrounded by a peripheral rim of epithelioid macrophages. In this zone, MNGCs may be observed where a number of macrophages have joined together to create a Langhan's type giant cell (67, 68). In smaller, unorganised granulomas, MNGCs tend to be scattered throughout the lesion rather than in an outer rim (68). MNGC's tend to be more abundant in the later, more advanced granulomas compared to the earlier manifestations (68). Beyond this there is rim of lymphocytes that consists of a mixture of B and T cells. It has been observed that as granulomas increase in size, B cell populations become more contained as 'follicle-like' structure in the lymphocyte rim, whereas in the smaller granulomas they tend to be scattered throughout this layer and the granuloma (15, 68–70). This is in contrast to findings from Fuller et al. (71) who state that B cells are only observed in follicle-like structures in caseous granulomas in cynomolgus macaques. Depending on the stage and extent of healing and containment of the granuloma a thin layer of fibrosis can develop around the external rim of lymphocytes (82). AFB are seen in most granulomas, but they are more abundant in larger granulomas with caseous necrosis (83).

The cellular composition of granulomas in NHPs used to distinguish between the type and severity of disease have been evaluated in various ways including semi-quantitative methods, for example, scoring systems (57, 65) as well as quantitative methods such as using image analysis to count the percentage of cells stained within a granuloma (31, 68). Scoring systems and lesion classifications have been used in NHP models in recent years and there are two that lead in the field; Lin et al. (57) whose system is based on 3 characteristics; the type of granulomas (caseous, solid, suppurative or mixed); the cellular composition (presence or absence of lymphocytic cuff, mineralisation, fibrosis, MNGCs and epithelioid macrophages) and the distribution pattern (focal, multifocal, coalescing and invasive). Lin et al. (57) have applied this to both active and latent TB experiments. The second is Rayner et al. (63, 65, 66) who published a more detailed description of the granulomas seen in active, early-stage TB infection which uses different stages of development to categorise the granulomas (stages 1–6). Briefly, stage 1 granulomas are small diffuse foci of cells including macrophages and lymphocytes and a few disperse neutrophils. They do not have clearly defined boundaries and they infiltrate alveolar walls and extend into the alveoli (Figure 2A). Stage 2 granulomas are unorganised but have a more defined boundary and they are larger than stage 1 but have the same mix of inflammatory cells (Figure 2B). Stage 3 granulomas are similar to stage 2, but they have a focal necrosis which is characterised by nuclear pyknosis and karyorrhexis with the loss of cellular architecture. Stage 4 lesions are circumscribed and primarily consist of macrophages mixed with neutrophils and other leucocytes and a few peripheral lymphocytes. Stage 5 granulomas are organised with a necrotic foci and degenerate neutrophils (Figure 2C). Finally, stage 6 is the classical, well demarcated granuloma that consists of central, caseous necrosis and has a variable rim of lymphocytes, mainly B cells, around the periphery (63, 65, 66) (Figures 2D–F). The use of this scoring system has been of great value evaluating vaccine candidates at the preclinical stage (32, 83).

3.2. Rodents

The mouse (*Mus musculus*) was one model utilised by Robert Koch to demonstrate that Mtb induced comparable lesions in mice to those observed in humans during natural infection (33, 34). The broad utilisation of mice in TB immunology research is attributed to the abundance of immunological tools and reagents, as well as the availability of inbred strains, which facilitate classical genetics and adoptive transfer experiments (13).

In general, mice tend to develop an acute rather than chronic infection with Mtb, and the granulomas formed in their lungs lack the structured and organised appearance observed in human granulomas (9) (Figure 3A). It should be noted that in most of the conventional strains of mouse models, granulomas do not develop the necrotic caseous centre, which is the primary characteristic of human TB (9, 13, 20, 35). Infected macrophages tend to show an enlarged cytoplasm with high lipidic content (foamy macrophages) that are interspersed with lymphocytes and neutrophils (Figure 3B). The presence of AFB is abundant within the macrophage cytoplasm and the necrotic cells (Figures 3C,D). Additionally, the lack of MNGCs in mice makes the tuberculous granulomas of mice histopathologically different from those observed in humans (17, 20, 36) (Figure 3). Table 1 summarises the main histopathological features in mice model observed during experimental pulmonary TB.

Numerous mouse models of infection have been developed, using mostly the intranasal infection route with the aim of mimicking pulmonary TB in humans as close to a natural infection route as possible (20, 24, 28, 36–41).

Rhoades et al. (20) infected C57BL/6 mice via the aerosol route with varying doses of three different Mtb strains and studied the development of a granuloma for a period of 1 year in the lung. Although the different conditions failed to induce a caseating necrosis, the mice developed a chronic form of pulmonary TB in all cases. Rhoades et al. (20) described five histopathological stages of granuloma development; category 1: small, isolated lesions diffusely distributed throughout infected lungs, composed of a few adjacent alveoli with thickened septae, consisting primarily of mononuclear phagocytes, alveolar macrophages and occasional lymphocytes; category 2: scattered, discrete foci of alveolitis filled with mononuclear phagocytes and a few epithelioid and foamy macrophages, with perivascular and peribronchiolar lymphocytes; category 3: moderate lesions characterised by sheets of epithelioid and foamy macrophages that fill the alveoli, with mild interstitial fibrosis and tight associations of lymphocytes. In this case, while evidence of irreversible cell degeneration and death was noticed, no central necrosis was detected. In category 4 enlarged, coalescing granulomatous lesions were detected, consisting mainly of the presence of macrophages, epithelioid macrophages, and large foamy macrophages. Small foci of

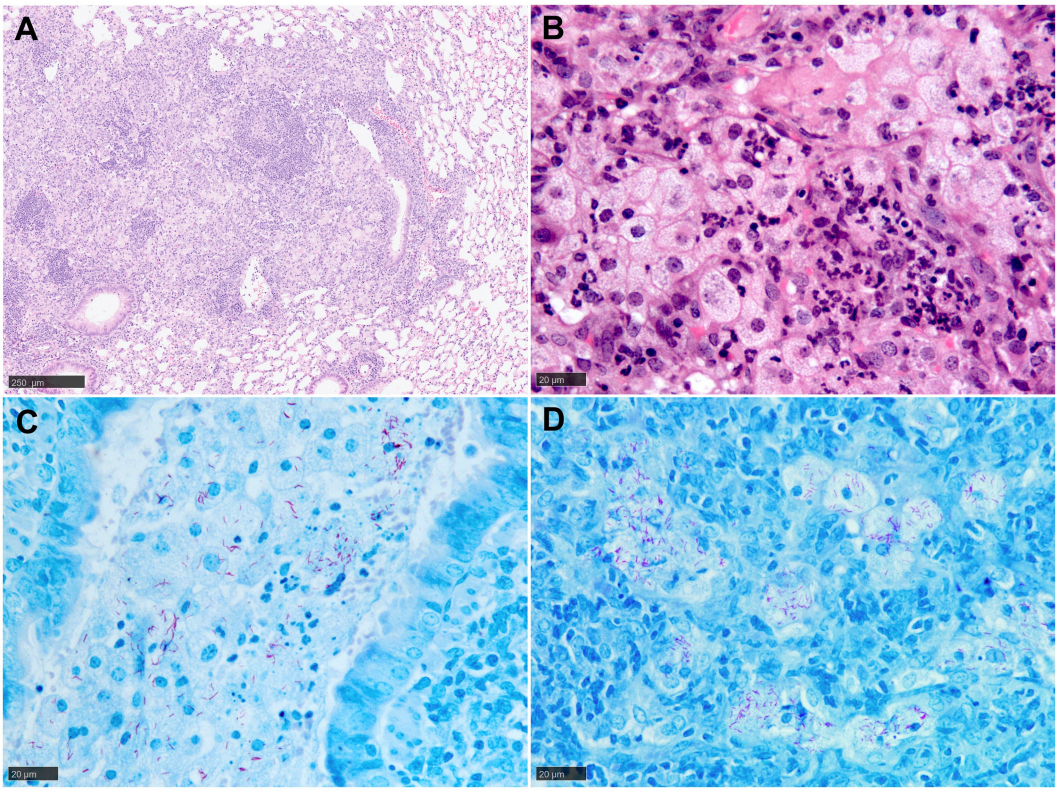

FIGURE 3
Representative histopathological images of the mouse (Balb/C) TB model in lung: (H&E) and Ziehl-Neelsen (ZN) staining. **(A)** Early-stage granuloma, non-demarcated and non-encapsulated, consisting mainly of macrophages, aggregates of lymphocytes and scattered polymorphonuclear cells. **(B)** Large foamy macrophages and polymorphonuclear cells in a late-stage granuloma. **(C)** Abundant AFB in the cytoplasm of foamy macrophages and cell debris within a bronchiolar lumen. **(D)** Large foamy macrophages with abundant intracellular AFB in a late-stage granuloma. Scale bars = A, 250 µm; B, C and D, 20 µm.

necrosis and polymorphonuclear cells were associated with cleft of cholesterol and fibrosis of alveolar septae was more advanced. Finally, lesions in category five are defined as extensive chronic, interstitial fibrosing granulomas, characterised by thickened alveolar septae demarcated areas filled with dead/dying epithelioid and foamy macrophages (20). With high doses of Mtb, single AFB were detected by ZN stain in several alveolar macrophages and polymorphonuclear cells of category 2 granulomas after 20 dpc. Multiple AFB were more apparent after 60 dpc in epithelioid cells and foamy macrophages and no differences between categories 3 and 4 were found (20).

Cardona et al. (36) also used the same mouse model, although with different conditions, and they proposed a new histopathological approach in the development of pulmonary lesions: primary, secondary, and tertiary granulomas. Primary granulomas (category 3 in Rhoades et al. (20) classification) consisted of an initially poorly structured lesion with neutrophils, lymphocytes and infected macrophages surrounded by a thick mantle of lymphocytes, in which periphery foamy macrophages filled the alveolar spaces. By day 220 post-challenge, macrophages are the predominant cellular element at the core of granulomas. In secondary granulomas, small numbers of infected macrophages are surrounded by lymphocytes. On day 60 post-challenge, peripheral lymphocytes formed a thick mantle which is surrounded by foamy macrophages. Tertiary granulomas consist of several neighbouring granulomas coalescing and remain confined within the alveolar spaces and did not elicit any significant fibrous reaction. Tertiary granulomas could be considered as categories 2, 4 and 5 from Rhoades et al. (20) classification because they may represent primary and/or secondary granulomas linked with foamy macrophages (36). Although Cardona et al. (36) remarked on the absence of MNGCs and the scarcity of epithelioid cells, both authors agree that foamy macrophages are a fundamental cell in mouse tuberculous granulomas (20, 36). Indeed, the continued enlargement of granulomas is heavily reliant on the presence of this particular cell type, as its proliferation plays a major role in the merging of lesions and the subsequent formation of large-sized granulomas (36).

Tsai et al. (17) evaluated significant differences as well as common characteristics in lung granulomas from humans and C57BL/6 mice with TB. A common feature observed in both human and mouse granulomas was the presence of B lymphocyte aggregates (17). However, some differences were observed between the two species. While in mouse lungs B cell aggregates were surrounded by macrophages, in human tissues this was not observed. In the latter, a characteristic association of B cells and T cells was observed, with two different patterns of expression (17).

Other groups have used the Balb/C mouse model for the study of pulmonary tuberculosis (28, 39–41). This model showed two histopathological phases of the disease. The first one or acute phase was characterised by an infiltrate of inflammatory cells in the alveoli, blood vessel and bronchiole with the formation of granulomas. The second phase was chronic pneumonia characterised by focal necrosis (40). Using the same mouse strain, Irwin et al. (39) demonstrated similar lesions to category two described by Rhoades et al. (20) at 3 wpc which became multifocal to coalescing with the progression of the disease. No evidence of necrosis or fibrosis was described with this model (28, 39–42). Pan et al. (43) demonstrated that C3HeB/FeJ mice (commonly referred to as the Kramnik mouse model) displayed lung pathology with a central caseous necrosis and encapsulation, similar to what is observed in human tissues (43). Using the same model, it had been observed that these lesions were also hypoxic (pimidazole+ by IHC), another key feature of human TB lesion, as previously mentioned (27, 28). C3HeB/FeJ mice develop three different pulmonary lesions following aerosol infection; type I is the one that most resembles classical human TB granulomas. They become evident after 35–45 dpc and are characterised by acellular caseum in the centre of the lesion, karyorrhectic debris and a distinct band of darkly stained intact neutrophils. This band is surrounded by a rim of foamy macrophages and a fibrotic capsule (24, 28, 39, 41). In humans, the central core is composed primarily of macrophages and foamy macrophages, however, in this mouse model it appears to be composed mainly of neutrophils and, to a lesser extent, foamy macrophages (24). SYBR Gold acid-fast stain, revealed large number of intracellular bacilli in the foamy macrophages and intact neutrophils and extracellular bacilli within the necrotic caseum (24). The type II lesions in infected C3HeB/FeJ mice presented fulminant granulocytic pneumonia and type III were similar to lesions found in Balb/c mice following aerosol infection (24). Occasionally, this model demonstrated the development of central cavities, like the ones observed in human tuberculosis (28, 41). Recently, a 'humanised' mouse model generated by transplanted human foetal liver derived haematopoietic stem cells have been proposed (HIS-NSG mice) (42). TB granulomas in these HIS-NSG mice comprised solid non-necrotic granulomas, tuberculoid pneumonia, and caseous necrotic granulomas, having the ability to model human-like pulmonary granuloma initiation and formation (42).

In contrast to mice, the use of rats (*Rattus* spp.) for the study of human tuberculosis is less common. However, this species could also represent a good model due to the well documented immunology and the number of monoclonal antibodies which are commercially available (84). Studies before 2006 described lung granulomas as histologically similar to classic murine models, with the absence of central necrosis (21, 84, 85). In the Lewis rat strain, Sugawara et al. (85) described granulomas of various sizes from 3 wpc, observing foamy macrophages and MNGCs with the progression of the disease (84, 85). Sugawara et al. (84) described a model of TB in F344/N-rnu nude rat strain which developed granulomas with central necrosis and encapsulated by thick collagen fibres, mimicking those observed in humans. However, unlike humans, the central necrosis was not caseous (84).

The American cotton rat (*Sigmodon hispidus*) is a useful model in many human respiratory diseases such as respiratory syncytial virus (RSV) or influenza virus (86). In 2007, Elwood et al. also demonstrated its value as a model for pulmonary TB (21). Cotton rats developed a granulomatous inflammation, which was visible macroscopically, demonstrating multiple white nodules in the lung parenchyma. At 8 wpc, localised and discrete granulomas surrounded by healthy lung tissue and composed of epithelioid macrophages in the centre and lymphocytes at the periphery were observed. Caseous necrosis was frequently observed which became calcified with disease progression. Multiple AFB were noted within the cytoplasm of epithelioid cells and intracellular and extracellular in necrotic granulomas (21). Later, Singhal et al. proposed another model in Wistar rats endotracheally infected with different strains and doses of Mtb, which revealed some similarities with human TB (44). Histopathological analysis of lung from rats infected with high dose of W4 Mtb strain revealed granulomas with a central area of epithelioid macrophages and a cuff

of lymphocytes, together with small peribronchial aggregates from 28 dpc onwards. At 60 dpc, well organised granulomas with many lymphocytes, foamy macrophages and occasional MNGCs were observed, although necrosis and fibrosis were seldom seen (44).

3.3. Guinea pigs

Guinea pigs have been used extensively in TB research; they share many features of disease with humans, making this species a popular choice as an animal model of TB model of human disease. The histopathological features of the TB lesions in the guinea pig, represented in Table 1 and Figure 4, have been well documented. Small lesions comprising mainly macrophages, with some neutrophils and lymphocytes, arise after a few days post aerosol challenge with Mtb. These lesions are often located close to large airways (45) and it has been suggested that these initial lesions are more likely to originate in the interstitium rather than alveolar spaces (46). This occurs through a process whereby bacilli escape from macrophages adhered to the alveolar epithelial surface and subsequently infiltrate into the surrounding, pulmonary tissue. Furthermore, neutrophils are thought to facilitate early lesion growth via degranulation and release of hydrolytic enzymes. At these early time points, the pulmonary lymphatics are also affected, with lymphangitis observed as early as 5–15 dpc and involving the connective tissue supporting delicate, peribronchial and perivascular, lymphatic vessels (47). These lymphangio-centric lesions continue to develop into granulomas in parallel with those located in the parenchyma. Macrophages, both epithelioid and foamy, and lymphocytes, continue to infiltrate lesions, resulting in larger, circumscribed 'solid' granulomas by days 15–20 post-challenge. As the granuloma enlarges, it compresses adjacent blood vessels, causing tissue hypoxia (48, 49). Although collagen deposition may form around the periphery of the granuloma as part of its progressive, structural development, fibrosis does not play as prominent a role as in other animal models such as NHPs or cattle with bTB; furthermore, pre-existing collagen in broncho-vascular connective tissue can be incorporated into the periphery of lesions that develop in these areas.

In addition, around days 15–20 post-challenge, signs of necrosis become evident; alongside this are increased numbers of granulocytes. Around this time point, the number of acid-fast bacilli observed in lesions also plateaus, coincident with the development of adaptive immunity (50).

This process rapidly progresses to prominent, central necrosis by around day 30 post-challenge (Figure 4A). It has been proposed that neutrophils are likely to be the key cells that initiate necrosis formation (46), as opposed to macrophage 'softening' and degradation. Dystrophic mineralisation, mainly calcification, of the necrotic core, a key feature in disease progression in this species, follows shortly afterwards (Figure 4B). Advanced staining techniques have identified numerous clumps of over 15 AFB within the necrotic core and its periphery, the latter of which is often observed as highly eosinophilic rim (51). Moreover, special stains have identified accumulation of extracellular ferric iron in areas of lesion necrosis, and iron accumulation in macrophages at the periphery of granulomas (52); this is commensurate with the requirement of Mtb for host iron to facilitate growth and promote increased virulence.

A prominent feature of pulmonary TB in guinea pigs is the formation of secondary lesions which may arise from a number of scenarios and reflect fundamental differences in host environments (53). Orme and Basaraba (46), propose that those located in a subpleural location may arise from the passive transportation of bacilli from primary lesions through pulmonary lymphatics towards the pleura where they lodge and develop lesions. Haematogenous spread can also result in secondary lung lesions; this has been demonstrated to occur within 2–3 wpc (53). As an adaptive immune response is likely to have established by the time secondary lesions are developing, their structure differs from their primary counterparts. In general, they are small, predominantly lymphocytic, lack the discrete granuloma morphology as well as neutrophils, necrosis and calcification; the number of intra-lesional bacilli are also reduced (53). This microscopic appearance is akin to primary lesions that form in the lungs of guinea pigs vaccinated with BCG prior to infection with Mtb (53); this results in partial protection from the adaptive immune response stimulated by the vaccine, and a reduction in the severity of the inflammatory response. Infection invariably leads to progressive disease, with the time taken to reach humane endpoints dependent on variables such as the mycobacterial strain and dose (87).

Many of the features described for guinea pigs are observed in TB infection in people. Both species develop large, pulmonary granulomas

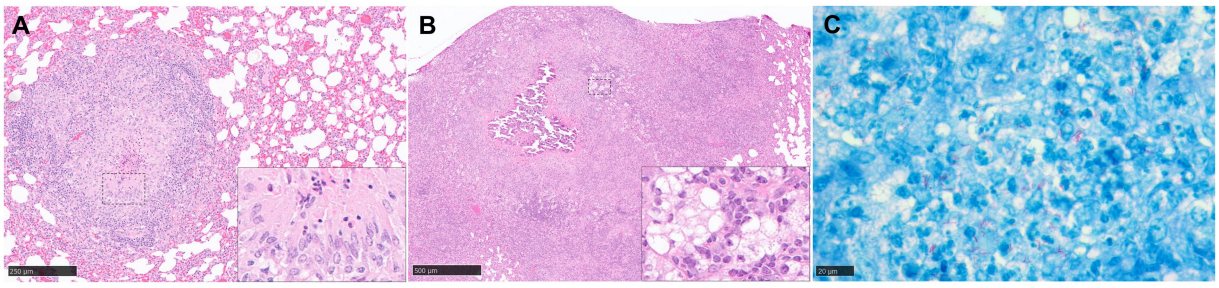

FIGURE 4
Representative histopathological images of the guinea pig TB model in lung: (H&E) and Ziehl-Neelsen (ZN) staining. **(A)** Stage III granuloma. Circumscribed and well demarcated granuloma, characterised by the presence of central necrosis surrounded by epithelioid macrophages and a peripheral rim of lymphocytes and plasma cells. Insets shows epithelioid macrophages and few necrotic heterophils. **(B)** Stage IV granuloma. Large non-encapsulated granuloma with central necrosis and dystrophic mineralisation, surrounded by epithelioid macrophages, foamy macrophages, and diffuse aggregates of lymphocytes. Inset shows foamy macrophages and lymphocyte aggregates. **(C)** Abundant intracellular and extracellular AFB in a stage II granuloma. Scale bars = A, 250 µm; B, 500 µm; C, 20 µm.

with central, caseating necrosis and surrounded by epithelioid macrophages, occasional MNGCs and a rim of lymphocytes and chronic, fibrous encapsulation (Table 1). Furthermore, prominent lymphadenopathy and lymphangitis are also shared features, as well as disease dissemination. Despite the paucity of other key morphological features noted in human disease, such as post-primary, cavitating lesions that facilitate rapid spread but that are observed uncommonly in the guinea pig, this species is considered the gold standard for the preclinical evaluation of both potential new vaccines and therapeutics (88).

Evaluation of differences in the type and severity of disease has traditionally seen the employment of semi-quantitative methods, such as subjective scoring systems (72, 73) which estimate extent of disease and numeration of particular features such as number of foci of necrosis or calcification. Quantitative analysis, determining percentage of lung affected by disease, such as consolidation, can also be estimated using proprietary software packages. Lesion classification systems have been devised to grade granuloma type in the lung of the guinea pig model (45). Our group has recently developed a new scoring system to differentiate morphological characteristics in a temporal pattern and which have been observed in both parenchyma and broncho-vascular, connective tissue (74). Briefly, stage I lesions incorporate small, poorly demarcated collections of inflammatory cells, primarily macrophages, with some lymphocytes and granulocytes. Larger, circumscribed and well demarcated, non-necrotic lesions comprising macrophages (mainly epithelioid), scattered lymphocytes and variable numbers of neutrophils, are considered stage II lesions; and these progress to stage III lesions when central necrosis is visible, often with a degree of caseation. The final stage, stage IV, contains granulomas with variable but often extensive, central, dystrophic calcification and caseating necrosis (Figure 4).

Reports on immunostaining of granulomas have enabled further characterisation of granulomas; Turner et al. (45) describe the lymphocytic population in the non-necrotic, solid granulomas, comprising of significant numbers of CD4+ cells with fewer CD8+ cells; interestingly, in contrast to mice, these cells were distributed randomly within the lesions without aggregating. By 30 dpc, numbers of these cell numbers decrease prominently and an increase in B cells and granulocytes is seen, with a concomitant worsening of pathology (75). More recently, our group have used a number of cell markers (CD3, CD4, Iba1, myeloperoxidase, Mac387) to describe presence and frequency of inflammatory and immune cells in granulomas up to 27 wpc. We have identified macrophages (Iba1+) as the predominant cell marker visible in all granuloma stages. By contrast, MAC387+ (calprotectin) staining in macrophages and granulocytes was noted in scattered granulomas, with an increase in staining correlating with lesion progression up to stage III and noted early in between weeks 3–4 post-challenge. Similar changes were reported for myeloperoxidase (MPO) in granulocytes, with particularly strong staining noted in stage IV granulomas between 8 and 27 wpc. Percentage of CD3+ staining was lowest in all granulomas at the early time point of 3 wpc, whilst maximum at 8 wpc, and similar expression of staining in all granuloma types noted at the later time points, up to 27 wpc. A progressive increase in B-cell marker quantification was observed from stage I to IV. Higher expression of this marker was detected at 8 wpc in comparison with weeks 4 and 24–27 wpc in stage I and II granulomas. As more markers become available for use in the guinea pig model, further characterisation is likely to occur.

3.4. Rabbits

Some consider the rabbit model good as a model of immunopathogenesis and rabbits can be experimentally infected with Mtb or *M. bovis* and they show similar characteristics as human TB disease, for example, caseous necrosis, liquefaction and cavitary disease (79, 80, 89, 90). Kaplan et al. also have developed a model of mycobacterial meningitis that closely resembles TB meningitis in people (90). The different strains of mycobacteria cause different manifestations of disease, for example, when infected with Mtb strain CDC1551, rabbits show similarities to latent TB infection when compared to humans as they can clear the bacilli and granulomas disappear (89). However, an infection with *M. bovis* creates a progressive TB disease that can lead to death (80, 91).

In the 1920's, Lurie and their team bred rabbits that had different susceptibilities to Mtb strains, and these were used to look at the pathogenesis of TB in rabbits (92, 93). Unfortunately, these inbred rabbits no longer exist, and the outbred strains of rabbits tend to be resistant to Mtb. However, in 2004, Dorman et al. evaluated a new inbred strain of New Zealand White rabbits that appeared to be more susceptible to Mtb infection when compared to the outbred strains (79).

After experimental challenge, lesions can be seen as early as 2 wpc with increased cellularity within the alveolar spaces (89). The strain of Mtb used can affect the outcome of disease. CDC1551 strain has a different outcome when compared to HN878 strain and Erdman strain. Multiple granulomas are observed with strain HN878 at 4 wpc which consist of scattered lymphocytes, neutrophils, and macrophages. These lymphoid aggregates are often perivascular and peribronchial. MNGCs are frequently observed in macrophage abundant areas (89). However, by 4 wpc with strain CDC1551, small, scattered aggregates of cells are observed (89).Inbred rabbits have large granulomas with frequent caseous necrosis and obvious AFB by 5 wpc with Erdman strain, whereas in outbred rabbits the granulomas tend to be smaller with less caseous necrosis and few viable AFB (79). By 8 wpc with HN878 strain, granulomas are more abundant and central necrosis is present with abundant AFB (89), and in rabbits with CDC1551 infection the granulomas have increased in size, started to coalesce, and have become organised structures similar to the classical granulomas in humans; with a central core of necrosis, macrophage layer and an outer rim of lymphocytes (89, 94). At 12–16 wpc in HN878 infection, central necrosis increases, liquefaction can be seen in some granulomas, and cavities can also form. Some granulomas, however, have been observed to reduce in size an become mineralised. It has been noted that the mineralised granulomas have only a few AFB (94). At 12–16 wpc in CDC1551 infection, it has been observed that granulomas are organised and some have no AFB present. It is also not uncommon for granulomas to have been reabsorbed to a point where only increased cellularity in the parenchyma is seen (89).

Infection with Mtb Erdman strain produces coalescing granulomas with some lesions developing cavities at 16–18 wpc. It has been observed that some rabbits have 'healed' granulomas at this time point whilst others have a mixture of small and large granulomas (80). Rabbits challenged with *M. bovis* tend to have a chronic infection with TB pneumonia, fibrotic granulomas and cavitary disease (26, 91). These histological features are summarised in Table 1.

3.5. Ruminants

3.5.1. Cattle

Bovine tuberculosis (bTB) is one of the most economically important disease in animal health worldwide. bTB is also a very important zoonosis and a major Public Health concern in low-income countries. For those reasons, bTB has been studied extensively and very valuable information about the pathogenesis of the disease and vaccination trails has been gathered over the past decades.

M. bovis is the main pathogen inducing bTB, and infected bovines (for example, *Bos taurus* and *Bos indicus*) show similar characteristics to Mtb infected humans (95). Other members of the MTBC can also infect bovines, e.g. *Mycobacterium caprae* showing very similar pathology when compared to *M. bovis* (96), or Mtb, showing a less pathogenic outcome in experimentally infected animals (6).

The main features of pulmonary granulomas in bTB are necrosis, mineralisation, a fibrous capsule, and presence of MNGCs (Table 1). AFB are present in higher numbers in more developed granulomas that show necrosis (5, 70, 95).

The earliest lesions described in lungs of experimentally infected cattle are at 15 dpc following an aerosol challenge with 1.12×10^4 cfu (97). Granulomas at this timepoint are not organised. This early stage in granuloma development is characterised by an increase of perivascular cuffing of lymphocytes around lymph and blood vessels, an increase of macrophages as well as granulocytes within the congested interstitum (97). Palmer et al. (97) have described observing the alveoli filled with homogenous eosinophilic, fibrillar material that is consistent with oedema fluid and fibrin. Foamy macrophages are abundant, and a variable number of AFB are observed. No necrosis is observed at this stage. At day 30 post-challenge, as the infection progresses, these early lesions start to grow and accumulate more lymphocytes, macrophages, MNGCs and neutrophils which fill the alveolar spaces. Lymphocytes also form small, circle-like shapes. Some will have small areas of contained necrosis (97). After 90 days post-challenge, granulomas have become more organised structures.

Wangoo et al. (5) developed a scoring system for TB granulomas in cattle experimentally infected with *M. bovis* which many research groups have since used to evaluate their work. The scoring system characterises granulomas into 4 stages. Briefly, stage I (initial) granulomas consist of irregular clusters of epithelioid macrophages with few neutrophils and Langhan's MNGCs with scattered lymphocytes, no necrosis observed at this stage. Stage II (solid) granulomas have either a complete or partial thin capsule. They primarily consist of epithelioid macrophages with minimal necrotic areas with infiltrates of lymphocytes, neutrophils and MNGCs as well as some haemorrhage. Stage III (minimal necrosis) granulomas are fully encapsulated, with central caseous necrosis and mineralisation. Surrounding the central necrosis are epithelioid macrophages and MNGCs. Towards the fibrous capsule, in the peripheral zone there are clusters of macrophages, lymphocytes, neutrophils and MNGCs. Finally, Stage IV (necrotic and mineralised) granulomas are large and irregular in shape, they are multicentric with prominent caseous necrosis. They have a thick capsule with an abundance of mineralisation which covers the majority of the lesion. MNGCs and epithelioid macrophages surround the necrotic core and there are dense clusters of lymphocytes towards the fibrotic capsule (5). Palmer et al. (97), looked at granulomas in cattle as early as day 15 and 30 post-challenge and proposed that the scoring system developed by Rayner et al. (65) for rhesus macaques was more suitable for these early timepoints than the commonly used Wangoo et al. (5) system.

There have been many studies that have looked at the cellular composition of bovine granulomas experimentally infected with *M. bovis*. Using techniques such as IHC and *in-situ* hybridisation (ISH) it has allowed us to characterise, visualise and locate different cell types within the granuloma (5, 7, 70, 97–99). CD68 is commonly used to identify macrophages, epithelial cells and MNGCs to help differentiate the different stages of granuloma development (70). CD68+ cells are most abundant in the early stages of lesion development (stage I and II) where they are scattered throughout the granuloma, whereas, by the more developed stages (III and IV) they are less abundant and are only located around the rim of the necrotic centre (70). IHC/ISH has allowed characterisation of MNGCs further by assessing the expression of cytokines including TNF-α, IFN-γ, TGF-β, IL-17A, and IL-10 (70, 100). From this characterisation it was observed that stage I early granulomas expressed more IL-17A and IL-10 when compared to late-stage granulomas (stage IV) (100). MNGCs have been observed in all studies of pulmonary granulomas infected with *M. bovis*, however, their role is still not fully understood. It has been suggested that they are used as a measure of lesion severity, with higher numbers associated with increased inflammation, more severe disease, and greater antigen persistence (101).

In the early stages of granulomas development (stages I/II) B cells tend to be scattered throughout the granuloma moving to follicle-like satellite nests around the outside of the fibrous capsule in the more advanced lesions (stages III/IV) (70, 102, 103). This is similar to what is seen with B cells during granuloma development in humans and NHPs (15, 68).

CD3+ T cells have been observed in a similar distribution to CD68+ cells as they are seen scattered throughout the lesion at stage I/II and then they are observed mainly in outer rim of the lesion at stage III/IV (70, 98). CD3+ T cells have further been identified to distinguish CD4+ T cells, CD8+ T cells and gamma/delta (γδ) T cells. This has shown that the predominant T cell subtype in all stage of granulomas is CD4+ T cells (98). Gamma/delta T cells appear to be predominantly in the early-stage granulomas with several studies showing that their presence decreases in the later stage of development (76, 98), however, some studies have shown that they are more abundant in the later stages of granuloma development (5, 70).

Neutrophils are thought to play an important role, especially in the early granuloma formation and are associated with the earliest signs of necrosis (104). Necrosis has been observed as early as 14–28 days post-challenge and studies have shown evidence of neutrophil infiltrates at day 14 (76, 104).

3.5.2. Goats

Goats (*Capra hircus*) are considered valuable animal models and potential target species for studying TB due to their natural susceptibility to tuberculous mycobacteria such as *M. bovis, M. caprae* and Mtb (105, 106). Goat TB closely resembles bovine and human TB in terms of immune response and pathological characteristics. They exhibit comparable patterns of disease progression, with a predominant anatomical localisation within the respiratory tract and the formation of caseous granulomas (77, 107). In addition, goats demonstrate notable similarities in the anatomical structure of their respiratory tract, as well as a comparable size and body weight to that of humans (107). These shared features present a unique opportunity

to bridge the gap between murine preclinical studies and subsequent human investigations (77, 105), thereby providing valuable insights into the intricate mechanisms of host-mycobacteria interaction (77).

In natural infections, as in cattle and humans, granulomas in goats are characterised by the presence of central caseous necrosis with varying degrees of mineralisation, surrounded by epithelioid macrophages, foamy macrophages, MNGCs, lymphocytes and a fibrotic capsule (78, 108, 109) (Table 1). Lymphocytes were mainly CD4+ T cells and B cells, located within the fibrotic capsule of the granuloma and the peripheric margin, respectively [reference (79)]. AFB are usually located inside the epithelioid macrophages and MNGCs [reference (79)]. Additionally, goats show a prominent tendency for the development of liquefactive necrosis and the formation of cavities within tuberculous granulomas, closely resembling the features observed in active TB cases in humans (78, 105, 108, 109). In the study performed by Sanchez et al. (78), the section of the cavitary lesions revealed the accumulation of intact and degenerate neutrophils and numerous intra- and extracellular AFB at the luminal surface [reference (79)]. The periphery was formed by granulation tissue with some macrophages and lymphocytes (mostly CD8+ T cells by IHC) and surrounded by a thick fibrotic capsule [reference (79)]. These cavitary lesions have been linked to high transmission rates, attributed to the higher abundance of AFB and a greater concentration of mycobacterial antigen detected within them (78, 109). These typical granulomatous lesions have also been reproduced in experimental conditions in goats, using low/middle doses (1,300–1,500 CFUs) of *M. bovis* or *M. caprae* through various inoculation routes, including intratracheal (105), transthoracic (110), and endobronchial (107, 108).

The gross pathology and histopathological scoring system developed by Vordermeier et al. (111) in 2002 and Wangoo et al. (5) in 2005 have also been adapted for use in goats (108, 112–115). The macroscopic evaluation categorises the pulmonary lung lesions in four different groups according to the percentage of the lobe affected, being 0 no evident TB-compatible lesions and 4 > 75% of the percentage affected (112, 113). Another gross approximation involves the meticulous sectioning of lung and lung-associated lymph nodes into thin sections measuring 0.5 to 4 mm in thickness. Through thorough observation, this approach allows for a semi-quantitative assessment of lesion size and distribution (108, 114). Histologically, the four granuloma developmental stages are the ones described in bovine: stage I (initial), stage II (solid), stage III (minimal necrosis) and stage IV (necrosis and mineralisation). Moreover, the detection of mycobacteria and the identification and quantification of AFB are conducted using IHC and ZN staining, as in the other animal species and in human beings (78, 96, 109, 116, 117). This standardised approach facilitates the quantification and characterisation of lesions, enabling consistent comparisons across different individuals and research studies. IHC has also been widely used to characterise the course of pulmonary TB infection in goats detecting the mycobacteria or host immune markers, including macrophages, neutrophils, T and B cells (78, 117, 118) within the lesions, providing insights into the host-pathogen interactions and local immune response during TB infection.

3.5.3. Other ruminants

The infection by *M. bovis* has been extensively described in domestic and wild ruminants of importance for animal or public health, mostly linked to bTB (95). The in-depth study of the pathology and pathogenesis of *M. bovis* infection in these species has been of great value to understand the dynamics of infection in natural and experimental conditions. We have described the goat model as a good model for some pathological features of human TB such as the liquefactive necrosis and the formation of cavernous lesions (105). In contrast, sheep (*Ovis aries*), considered a rare host for MTBC infection, show lesions similar to those observed in cattle infected with *M. bovis*. Sheep have been used experimentally to evaluate vaccine efficacy against the infection (119).

In contrast, cervids with natural MTBC infection show more caseous granulomas with a very soft centre that can resemble abscesses macroscopically; these caseous lesions show histologically a central necrotic core, an outer layer of lymphocytes, activated macrophages, abundant MNGCs and AFB and, in many occasions, poor encapsulation (120).

White-tailed deer (*Odocoileus virginianus*) can be naturally infected with *M. bovis* and this has been replicated in experimentally challenged white-tailed deer. Whilst the lymph nodes are the most common organ to observe tuberculous granulomas in this species due to the route of natural transmission, the lungs of a small percentage of deer also show tuberculous granulomas (121). When experimentally challenged via the intratonsilar route with *M. bovis* strain 1,315, lungs lesions are first observed 42 dpc. According to a study by Palmer et al. (121), the left caudal, right middle and caudal lobes were observed to be the main lung lobes affected. Granulomas were often small, solitary and approximately 3 – 10 mm in size. Granulomas by 56 and 89 dpc showed some mineralisation of the necrotic core as well as some evidence of mild peripheral fibrosis. Liquefaction and abscess-like centres of lesions have been commonly observed in lymph nodes however, this has not been observed in lung lesions (121). Palmer et al. (121), have observed that lung lesions follow a similar development as lymph node lesions in this species. MNGCs can be observed from 42 dpc in the lung with low numbers of AFB present in lesions.

3.6. Zebrafish

Over the past few decades, the zebrafish (*Danio rerio*) has emerged as a widely utilised alternative vertebrate animal model in the study of mycobacterial disease (122). This species can be infected with *Mycobacterium marinum* (*M. marinum*), a genetically close relative of MTBC and a natural pathogen affecting poikilothermic species, in which it induces a systemic TB-like disease (106). Fish mycobacteriosis, resembling human TB, can manifest as either an acute infection or a chronic progressive disease characterised by the containment of mycobacteria in well-organised granulomas structurally similar to those caused by Mtb in humans (123–125). Remarkably, despite lacking lungs, zebrafish exhibit high genomic homology with humans, and possess innate and adaptive immunity systems that are comparable to mammals (122, 126, 127). Furthermore, this species displays disease phases observed in humans, including latency and reactivation (125). These shared features make zebrafish an exceptional model for understanding the disease progression and host responses involved (122, 126, 127).

In the natural environment, *M. marinum* spreads through water and primarily enters the host through the oral route, whereas in experimental conditions, zebrafish are commonly infected through intraperitoneal or intramuscular inoculation (124, 128, 129). The

initial mycobacterial dose plays a critical role in determining the outcome of infection (125). Parenteral high-doses (>500 CFUs) lead to a more progressive and active disease with higher bacterial burden and mortality rates, while lower doses (~5–90 CFUs) can result in a chronic process with latent disease characterised by a stable numbers of granulomas (124, 128, 129). Following a successful *M. marinum* challenge, both larval and adult zebrafish models develop granulomas consistent with those reported in human TB, which can be found in various organs such as pancreas, gonads, kidney, liver, and occasionally the brain (106, 129). In embryos and larvae, early granuloma formation initiated by the innate immune response, can be visualised using *in vivo* real-time imaging within a few days post-challenge due to their transparency. These early lesions primarily consist of aggregated macrophages, few recruited neutrophils, epithelioid cells and MNGCs surrounding mycobacteria (123, 125, 130, 131). In adult zebrafish, initial TB-like granulomas characterised by cellular and bacterial aggregation have been reported at 2 wpc using both high and low infection doses. In advanced stages of the disease (16–20 wpc), mature granulomas are observed, featuring a caseous necrotic core surrounded by infected macrophages, epithelioid cells, neutrophils, infiltrating T and B lymphocytes, and a fibrous capsule (124, 129, 132–135). However, unlike mammalian tuberculous granulomas, zebrafish lesions contain fewer lymphocytes, and the presence of mineralisation has not been reported (124, 129, 131). Table 1 summarises the main histopathological features in zebrafish model observed during experimental pulmonary TB.

Various evaluation methods have been employed to study the TB-like lesions in zebrafish, enabling a comprehensive analysis of disease progression and the involvement of innate and adaptive immune responses. The transparency exhibited during the embryo and larval stages, offers a distinctive feature for investigating the initial stages of mycobacterial pathogenesis *in vivo* (131). Several authors have employed advanced *in vivo* real-time imaging techniques, including the utilisation of diverse immunofluorescence techniques to mark leukocytes and macrophages *in situ* (130, 136, 137). These techniques have demonstrated the ability of embryonic macrophages to phagocytose *M. marinum* within 1 h post-challenge, followed by the development of early granulomatous lesions 3–4 dpc (136).

Histopathological characterisation of the lesions has also been described using conventional histopathology and scoring systems. Risalde et al. (135) and López et al. (138) classified the granulomas into four histopathological stages based on their extent and cellular composition. Type I involved an infiltrate of epithelioid macrophages surrounding scattered mycobacteria, without necrotic areas or fibrous capsules. Type II represented partially encapsulated granulomas with a cluster of epithelioid macrophages and initial signs of necrosis. Type III consisted of encapsulated and well-organised granulomas containing regions of partial and complete necrosis, along with the presence of AFB. Type IV depicted encapsulated granuloma with an extensive necrotic core with a high mycobacteria concentration. Additionally, ZN staining revealed the presence of AFBs in both low and high infection dose experiments, primarily associated to necrotic areas (129, 132, 135, 138). In this context, Risalde et al. (135) and López et al. (138) developed a semi-quantitative assessment method to evaluate the presence of AFBs within the granulomas, categorised as: absent (0), very scarce (1–9), scarce (10–29), moderate (30–36, 54–71, 81–83), intense (36–53, 72–75, 84–100), very intense (>100).

Although the zebrafish has its limitations as a TB animal model, its distinctive characteristics have made significant contributions to our understanding of TB and mycobacterial disease in general. By providing valuable insights into host-pathogen interactions, immune responses, and the complex dynamics of TB granuloma formation, the zebrafish model serves as a crucial bridge between *in vitro* cell cultures and mammalian models, facilitating the translation of research findings to human clinical trials.

3.7. Other animal models

Many other animal species can be infected by MTBC bacteria. Natural TB in wildlife species such as badgers and wild boar (*Sus scrofa*) have been extensively studied due to its epidemiological importance in bTB, representing major reservoirs of infection for domestic livestock (139).

The histopathological features of granulomas in wild boar and domestic swine are similar to those observed in cattle and the differentiation of granulomas by developmental stages (stages I-IV) has been used in this species (140). Interestingly, wild boar can also show small lesions with heavy mineralisation and thick encapsulation, with very few immune cells and AFBs (95). The scoring system used for pulmonary lesion characterisation has been very valuable in this species to study the effect of different therapies against MTBC infection (141). Minipigs (*Sus domesticus*) have also been proposed as an excellent experimental model for the study of human TB, mimicking some histopathological characteristics observed in humans, such as granuloma encapsulation, and other parameters related with the immune response (142).

The Eurasian badger (*Meles meles*) is the main reservoir for bTB in the British Isles (143), and have been targeted for experimental vaccination to reduce the prevalence of bTB in these territories. The pulmonary lesions in naturally or experimentally infected badgers are typically solid, composed mainly of epithelioid macrophages with fewer lymphocytes, no apparent MNGCs and limited areas of necrosis and mineralisation (144). BCG has been licensed as a vaccine for TB in badgers after extensive experimental work, having used a version of the four developmental stages of the granulomas described by Wangoo et al. (5) in 2005 as a base for a histopathological scoring system principles (145, 146).

Following the 3Rs recommendations (replacement, reduction, and refinement), other less-conventional animal models have been used to study MTBC infection. For example, wax moth (*Galleria mellonella*) larvae, a well characterised model of infection for enterobacteria (147) has been recently used to study Mtb infection (148). It has been shown that phagocytic haemocytes can show internalisation of AFBs and cell aggregation towards a rudimentary 'granuloma-like' structure. Even though the model does not show many features of the typical pathology after mycobacterial infection, it can serve as a valuable tool to study the innate responses and identifying MTBC virulence genes (149). Moreover, novel *in vitro* models like the lung-on-chips are being developed to study the MTBC pathogenesis and will serve in the future to screen potential therapies against the disease reducing the number of animals used (150).

M. orygis has also been isolated in both humans and animals in S Asia and India. There are ongoing studies to evaluate whether this MTBC subspecies is a proxy for zoonotic TB. Currently, there is no

consensus as to whether *M. orygis* should be identified as zoonotic TB along with *M. bovis* which is presently the only zoonotic MTBC subspecies defined by the WHO (151).

4. Conclusion and future considerations

TB continues to be a major Public Health concern in the post-COVID19 era. The emergence of multidrug resistant strains and the high prevalence in immunosuppressed individuals, mainly due to HIV infection, makes TB one of the top ranked infectious diseases causing death in the human population. The only licensed vaccine against TB is the BCG, with a variable degree of protection. Many new vaccines are in the preclinical and clinical pipeline with the hope to have novel tools to control this disease. Preclinical animal models are crucial to evaluate the safety and efficacy of these new vaccine candidates, as well as new therapeutics.

The in-depth knowledge of the pathology and pathogenesis of TB infection in these animal models has been of great value to advance in the fight against TB. However, these data should be considered carefully in the context of this disease and more studies are necessary to establish the best and most appropriate model for the study of TB, and to carry out a standard characterisation and score of pulmonary lesions.

With the development of new molecular tools used in pathology like multiplex staining linked to quantitative analysis or spatial transcriptomics, new valuable knowledge will be gathered from these animal models of TB and the new generation of alternative models to reduce and replace animals following the 3Rs.

Data availability statement

The original contributions presented in the study are included in the article. Further inquiries can be directed to the corresponding author.

Ethics statement

All animal studies reviewed in this article were reviewed and approved by the correspondent Animal Welfare and Ethical Review body.

Author contributions

LH: Conceptualization, Writing – original draft, Writing – review & editing. IR-T: Writing – original draft, Writing – review & editing. IA-R: Writing – original draft. ER: Writing – original draft. FS: Conceptualization, Writing – original draft, Writing – review & editing.

Funding

The author(s) declare financial support was received for the research, authorship, and/or publication of this article. The authors have been supported by internal funding from the United Kingdom Health Security Agency (UKHSA) to produce this review article. IR-T is funded with a contract 'Margarita Salas' from the Spanish Ministry of Universities. IA-R is supported by the FPU grant of the Spanish Ministry of Education, Culture and Sport (FPU19/03969).

Acknowledgments

Authors would like to acknowledge UKHSA Porton Down histology technical team, Biological Investigation Group and TB research group as well as many colleagues in the TB research community that have collaborated with the authors over the years.

Conflict of interest

The authors declare that the research was conducted in the absence of any commercial or financial relationships that could be construed as a potential conflict of interest.

The author(s) declared that they were an editorial board member of Frontiers, at the time of submission. This had no impact on the peer review process and the final decision.

Publisher's note

References

1. WHO. Tuberculosis Fact Sheet (2023). Available from: https://www.who.int/news-room/fact-sheets/detail/tuberculosis.

2. Basaraba RJ, Hunter RL. Pathology of tuberculosis: how the pathology of human tuberculosis informs and directs animal models. *Microbiol Spectr*. (2017) 5. doi: 10.1128/microbiolspec.TBTB2-0029-2016

3. Hunter RL, Jagannath C, Actor JK. Pathology of Postprimary tuberculosis in humans and mice: contradiction of long-held beliefs. *Tuberculosis (Edinb)*. (2007) 87:267–78. doi: 10.1016/j.tube.2006.11.003

4. Ravimohan S, Kornfeld H, Weissman D, Bisson GP. Tuberculosis and lung damage: from epidemiology to pathophysiology. *Eur Respir Rev*. (2018) 27:2017. doi: 10.1183/16000617.0077-2017

5. Wangoo A, Johnson L, Gough J, Ackbar R, Inglut S, Hicks D, et al. Advanced granulomatous lesions in *Mycobacterium Bovis*-infected cattle are associated with increased expression of type I procollagen, Gammadelta (Wc1+) T cells and cd 68+ cells. *J Comp Pathol*. (2005) 133:223–34. doi: 10.1016/j.jcpa.2005.05.001

6. Villarreal-Ramos B, Berg S, Whelan A, Holbert S, Carreras F, Salguero FJ, et al. Experimental infection of cattle with *Mycobacterium Tuberculosis* isolates shows the attenuation of the human tubercle Bacillus for cattle. *Sci Rep*. (2018) 8:894. doi: 10.1038/s41598-017-18575-5

7. Salguero FJ, Gibson S, Garcia-Jimenez W, Gough J, Strickland TS, Vordermeier HM, et al. Differential cell composition and cytokine expression within lymph node granulomas from Bcg-vaccinated and non-vaccinated cattle experimentally infected with *Mycobacterium Bovis*. *Transbound Emerg Dis*. (2017) 64:1734–49. doi: 10.1111/tbed.12561

8. Palmer MV, Kanipe C, Boggiatto PM. The bovine Tuberculoid granuloma. *Pathogens*. (2022) 11:1. doi: 10.3390/pathogens11010061

9. Silva Miranda M, Breiman A, Allain S, Deknuydt F, Altare F. The tuberculous granuloma: an unsuccessful host Defence mechanism providing a safety shelter for the Bacteria? *Clin Dev Immunol*. (2012) 2012:139127. doi: 10.1155/2012/139127

10. Donald PR, Diacon AH, Thee S. Anton Ghon and his colleagues and their studies of the primary focus and complex of tuberculosis infection and their relevance for the twenty-first century. *Respiration*. (2021) 100:557–67. doi: 10.1159/000509522

11. Ulrichs T, Kaufmann SH. New insights into the function of granulomas in human tuberculosis. *J Pathol*. (2006) 208:261–9. doi: 10.1002/path.1906

12. Cronan MR. In the thick of it: formation of the tuberculous granuloma and its effects on host and therapeutic responses. *Front Immunol*. (2022) 13:820134. doi: 10.3389/fimmu.2022.820134

13. Ramakrishnan L. Revisiting the role of the granuloma in tuberculosis. *Nat Rev Immunol*. (2012) 12:352–66. doi: 10.1038/nri3211

14. Scriba TJ, Coussens AK, Fletcher HA, Jacobs WR Jr, McShane H, Mizrahi V, et al. Human immunology of tuberculosis. Microbiology. *Spectrum*. (2017) 5:1. doi: 10.1128/microbiolspec.TBTB2-0016-2016

15. Ulrichs T, Kosmiadi GA, Trusov V, Jörg S, Pradl L, Titukhina M, et al. Human tuberculous granulomas induce peripheral lymphoid follicle-like structures to orchestrate local host Defence in the lung. *J Pathol*. (2004) 204:217–28. doi: 10.1002/path.1628

16. Ridley DS, Ridley MJ. Rationale for the histological Spectrum of tuberculosis. A basis for classification. *Pathology*. (1987) 19:186–92. doi: 10.3109/00313028709077132

17. Tsai MC, Chakravarty S, Zhu G, Xu J, Tanaka K, Koch C, et al. Characterization of the tuberculous granuloma in murine and human lungs: cellular composition and relative tissue oxygen tension. *Cell Microbiol*. (2006) 8:218–32. doi: 10.1111/j.1462-5822.2005.00612.x

18. Marakalala MJ, Raju RM, Sharma K, Zhang YJ, Eugenin EA, Prideaux B, et al. Inflammatory signaling in human tuberculosis granulomas is spatially organized. *Nat Med*. (2016) 22:531–8. doi: 10.1038/nm.4073

19. Fenhalls G, Stevens L, Moses L, Bezuidenhout J, Betts JC, Helden Pv P, et al. In situ detection of *Mycobacterium Tuberculosis* transcripts in human lung granulomas reveals differential gene expression in necrotic lesions. *Infect Immun*. (2002) 70:6330–8. doi: 10.1128/IAI.70.11.6330-6338.2002

20. Rhoades ER, Frank AA, Orme IM. Progression of chronic pulmonary tuberculosis in mice Aerogenically infected with virulent *Mycobacterium Tuberculosis*. *Tuber Lung Dis*. (1997) 78:57–66. doi: 10.1016/s0962-8479(97)90016-2

21. Elwood RL, Wilson S, Blanco JC, Yim K, Pletneva L, Nikonenko B, et al. The American cotton rat: a novel model for pulmonary tuberculosis. *Tuberculosis (Edinb)*. (2007) 87:145–54. doi: 10.1016/j.tube.2006.07.001

22. Wiley EL, Mulhollan TJ, Beck B, Tyndall JA, Freeman RG. Polyclonal antibodies raised against Bacillus Calmette-Guerin, Mycobacterium Duvalii, and *Mycobacterium Paratuberculosis* used to detect mycobacteria in tissue with the use of Immunohistochemical techniques. *Am J Clin Pathol*. (1990) 94:307–12. doi: 10.1093/ajcp/94.3.307

23. Ulrichs T, Lefmann M, Reich M, Morawietz L, Roth A, Brinkmann V, et al. Modified Immunohistological staining allows detection of Ziehl-Neelsen-negative *Mycobacterium Tuberculosis* organisms and their precise localization in human tissue. *J Pathol*. (2005) 205:633–40. doi: 10.1002/path.1728

24. Irwin SM, Driver E, Lyon E, Schrupp C, Ryan G, Gonzalez-Juarrero M, et al. Presence of Multiple lesion types with vastly different microenvironments in C3heb/Fej mice following aerosol infection with *Mycobacterium Tuberculosis*. *Dis Model Mech*. (2015) 8:591–602. doi: 10.1242/dmm.019570

25. Ihms EA, Urbanowski ME, Bishai WR. Diverse cavity types and evidence that mechanical action on the necrotic granuloma drives tuberculous cavitation. *Am J Pathol*. (2018) 188:1666–75. doi: 10.1016/j.ajpath.2018.04.006

26. Converse PJ, Dannenberg AM, Estep JE, Sugisaki K, Abe Y, Schofield BH, et al. Cavitary tuberculosis produced in rabbits by aerosolized virulent tubercle Bacilli. *Infect Immun*. (1996) 64:4776–87. doi: 10.1128/iai.64.11.4776-4787.1996

27. Harper J, Skerry C, Davis SL, Tasneen R, Weir M, Kramnik I, et al. Mouse model of necrotic tuberculosis granulomas develops hypoxic lesions. *J Infect Dis*. (2012) 205:595–602. doi: 10.1093/infdis/jir786

28. Driver ER, Ryan GJ, Hoff DR, Irwin SM, Basaraba RJ, Kramnik I, et al. Evaluation of a mouse model of necrotic granuloma formation using C3heb/Fej mice for testing of drugs against *Mycobacterium Tuberculosis*. *Antimicrob Agents Chemother*. (2012) 56:3181–95. doi: 10.1128/AAC.00217-12

29. Belton M, Brilha S, Manavaki R, Mauri F, Nijran K, Hong YT, et al. Hypoxia and tissue destruction in pulmonary Tb. *Thorax*. (2016) 71:1145–53. doi: 10.1136/thoraxjnl-2015-207402

30. Canetti G. *The tubercle Bacillus in the pulmonary lesion of man: Histobacteriology and its bearing on the therapy of pulmonary tuberculosis*. New York: Springer Publishing Company (1955).

31. Wong EA, Joslyn L, Grant NL, Klein E, Lin PL, Kirschner DE, et al. Low levels of T cell exhaustion in tuberculous lung granulomas. *Infect Immun*. (2018) 86. doi: 10.1128/iai.00426-18

32. White AD, Sibley L, Gullick J, Sarfas C, Clark S, Fagrouch Z, et al. Tb and Siv coinfection; a model for evaluating vaccine strategies against Tb reactivation in Asian origin Cynomolgus macaques: a pilot study using Bcg vaccination. *Vaccines (Basel)*. (2021) 9. doi: 10.3390/vaccines9090945

33. Orme IM, Collins FM. Mouse model of tuberculosis. in *Tuberculosis*. Ed. Bloom BR (1994):111–34.

34. Gupta UD, Katoch VM. Animal models of tuberculosis. *Tuberculosis (Edinb)*. (2005) 85:277–93. doi: 10.1016/j.tube.2005.08.008

35. Cosma CL, Sherman DR, Ramakrishnan L. The secret lives of the pathogenic mycobacteria. *Annu Rev Microbiol*. (2003) 57:641–76. doi: 10.1146/annurev.micro.57.030502.091033

36. Cardona PJ, Llatjos R, Gordillo S, Diaz J, Ojanguren I, Ariza A, et al. Evolution of granulomas in lungs of mice infected Aerogenically with *Mycobacterium Tuberculosis*. *Scand J Immunol*. (2000) 52:156–63. doi: 10.1046/j.1365-3083.2000.00763.x

37. Huynh KK, Joshi SA, Brown EJ. A delicate dance: host response to mycobacteria. *Curr Opin Immunol*. (2011) 23:464–72. doi: 10.1016/j.coi.2011.06.002

38. Gonzalez-Juarrero M, Turner OC, Turner J, Marietta P, Brooks JV, Orme IM. Temporal and spatial arrangement of lymphocytes within lung granulomas induced by aerosol infection with *Mycobacterium Tuberculosis*. *Infect Immun*. (2001) 69:1722–8. doi: 10.1128/iai.69.3.1722-1728.2001

39. Irwin SM, Gruppo V, Brooks E, Gilliland J, Scherman M, Reichlen MJ, et al. Limited activity of Clofazimine as a single drug in a mouse model of tuberculosis exhibiting Caseous necrotic granulomas. *Antimicrob Agents Chemother*. (2014) 58:4026–34. doi: 10.1128/AAC.02565-14

40. Hernández-Pando R, Orozcoe H, Sampieri A, Pavón L, Velasquillo C, Larriva-Sahd J, et al. Correlation between the kinetics of Th1, Th2 cells and pathology in a murine model of experimental pulmonary tuberculosis. *Immunology*. (1996) 89:26–33.

41. Lanoix JP, Lenaerts AJ, Nuermberger EL. Heterogeneous disease progression and treatment response in a C3heb/Fej mouse model of tuberculosis. *Dis Model Mech*. (2015) 8:603–10. doi: 10.1242/dmm.019513

42. Arrey F, Lowe D, Kuhlmann S, Kaiser P, Moura-Alves P, Krishnamoorthy G, et al. Humanized mouse model mimicking pathology of human tuberculosis for in vivo evaluation of drug regimens. *Front Immunol*. (2019) 10:89. doi: 10.3389/fimmu.2019.00089

43. Pan H, Yan BS, Rojas M, Shebzukhov YV, Zhou H, Kobzik L, et al. Ipr1 gene mediates innate immunity to tuberculosis. *Nature*. (2005) 434:767–72. doi: 10.1038/nature03419

44. Singhal A, Aliouat el M, Herve M, Mathys V, Kiass M, Creusy C, et al. Experimental tuberculosis in the Wistar rat: a model for protective immunity and control of infection. *PloS One*. (2011) 6:e18632. doi: 10.1371/journal.pone.0018632

45. Turner OC, Basaraba RJ, Orme IM. Immunopathogenesis of pulmonary granulomas in the Guinea pig after infection with *Mycobacterium Tuberculosis*. *Infect Immun*. (2003) 71:864–71. doi: 10.1128/IAI.71.2.864-871.2003

46. Orme IM, Basaraba RJ. The formation of the granuloma in tuberculosis infection. *Semin Immunol*. (2014) 26:601–9. doi: 10.1016/j.smim.2014.09.009

47. Basaraba RJ, Smith EE, Shanley CA, Orme IM. Pulmonary lymphatics are primary sites of *Mycobacterium Tuberculosis* infection in Guinea pigs infected by aerosol. *Infect Immun*. (2006) 74:5397–401. doi: 10.1128/IAI.00332-06

48. Lenaerts AJ, Hoff D, Aly S, Ehlers S, Andries K, Cantarero L, et al. Location of persisting mycobacteria in a Guinea pig model of tuberculosis revealed by R207910. *Antimicrob Agents Chemother*. (2007) 51:3338–45. doi: 10.1128/aac.00276-07

49. Via LE, Lin PL, Ray SM, Carrillo J, Allen SS, Eum SY, et al. Tuberculous granulomas are hypoxic in Guinea pigs, rabbits, and nonhuman Primates. *Infect Immun*. (2008) 76:2333–40. doi: 10.1128/IAI.01515-07

50. Creissen E, Izzo L, Dawson C, Izzo AA. Guinea pig model of *Mycobacterium Tuberculosis* infection. *Current Protocols*. (2021) 1:e312. doi: 10.1002/cpz1.312

51. Ryan GJ, Hoff DR, Driver ER, Voskuil MI, Gonzalez-Juarrero M, Basaraba RJ, et al. Tuberculosis phenotypes in mouse and Guinea pig lung tissue revealed by a dual-staining approach. *PloS One*. (2010) 5:e11108. doi: 10.1371/journal.pone.0011108

52. Basaraba RJ. Experimental tuberculosis: the role of comparative pathology in the discovery of improved tuberculosis treatment strategies. *Tuberculosis*. (2008) 88:S35–47. doi: 10.1016/s1472-9792(08)70035-0

53. McMurray DN. Hematogenous reseeding of the lung in low-dose, aerosol-infected Guinea pigs: unique features of the host-pathogen Interface in secondary tubercles. *Tuberculosis (Edinb)*. (2003) 83:131–4. doi: 10.1016/s1472-9792(02)00079-3

54. Kim MJ, Wainwright HC, Locketz M, Bekker LG, Walther GB, Dittrich C, et al. Caseation of human tuberculosis granulomas correlates with elevated host lipid metabolism. *EMBO Mol Med*. (2010) 2:258–74. doi: 10.1002/emmm.201000079

55. Pena JC, Ho WZ. Non-human primate models of tuberculosis. *Microbiol Spectr*. (2016) 4. doi: 10.1128/microbiolspec.TBTB2-0007-2016

56. Capuano SV, Croix DA, Pawar S, Zinovik A, Myers A, Lin PL, et al. Experimental *Mycobacterium Tuberculosis* infection of Cynomolgus macaques closely resembles the various manifestations of human *M. tuberculosis Inf Inf Immun*. (2003) 71:5831–44. doi: 10.1128/iai.71.10.5831-5844.2003

57. Lin PL, Pawar S, Myers A, Pegu A, Fuhrman C, Reinhart TA, et al. Early events in *Mycobacterium Tuberculosis* infection in Cynomolgus macaques. *Infect Immun*. (2006) 74:3790–803. doi: 10.1128/IAI.00064-06

58. Sharpe SA, Eschelbach E, Basaraba RJ, Gleeson F, Hall GA, McIntyre A, et al. Determination of lesion volume by Mri and stereology in a macaque model of tuberculosis. *Tuberculosis (Edinb)*. (2009) 89:405–16. doi: 10.1016/j.tube.2009.09.002

59. Via LE, Weiner DM, Schimel D, Lin PL, Dayao E, Tankersley SL, et al. Differential virulence and disease progression following *Mycobacterium Tuberculosis* complex infection of the common marmoset (*Callithrix Jacchus*). *Infect Immun*. (2013) 81:2909–19. doi: 10.1128/IAI.00632-13

60. Sharpe S, White A, Sarfas C, Sibley L, Gleeson F, McIntyre A, et al. Alternative Bcg delivery strategies improve protection against *Mycobacterium Tuberculosis* in non-human Primates: protection associated with mycobacterial antigen-specific Cd4 effector memory T-cell populations. *Tuberculosis*. (2016) 101:174–90. doi: 10.1016/j.tube.2016.09.004

61. Walsh GP, Tan EV, Dela Cruz EC, Abalos RM, Villahermosa LG, Young LJ, et al. The Philippine Cynomolgus monkey (Macaca Fasicularis) provides a New nonhuman primate model of tuberculosis that resembles human disease. *Nat Med*. (1996) 2:430–6.

62. Lin PL, Rodgers M, Smith L, Bigbee M, Myers A, Bigbee C, et al. Quantitative comparison of active and latent tuberculosis in the Cynomolgus macaque model. *Infect Immun*. (2009) 77:4631–42. doi: 10.1128/IAI.00592-09

63. Sibley L, Dennis M, Sarfas C, White A, Clark S, Gleeson F, et al. Route of delivery to the airway influences the distribution of pulmonary disease but not the outcome of *Mycobacterium Tuberculosis* infection in Rhesus macaques. *Tuberculosis (Edinb)*. (2016) 96:141–9. doi: 10.1016/j.tube.2015.11.004

64. Cepeda M, Salas M, Folwarczny J, Leandro AC, Hodara VL, de la Garza MA, et al. Establishment of a neonatal Rhesus macaque model to study *Mycobacterium Tuberculosis* infection. *Tuberculosis (Edinb)*. (2013) 93:S51–9. doi: 10.1016/S1472-9792(13)70011-8

65. Rayner EL, Pearson GR, Hall GA, Basaraba RJ, Gleeson F, McIntyre A, et al. Early lesions following aerosol infection of Rhesus macaques (*Macaca Mulatta*) with *Mycobacterium Tuberculosis* strain H37rv. *J Comp Pathol*. (2013) 149:475–85. doi: 10.1016/j.jcpa.2013.05.005

66. Rayner EL, Pearson GR, Hall GA, Gleeson F, McIntyre A, Smyth D, et al. Early lesions following aerosol challenge of Rhesus macaques (*Macaca Mulatta*) with *Mycobacterium Tuberculosis* (Erdman strain). *J Comp Pathol*. (2015) 152:217–26. doi: 10.1016/j.jcpa.2014.10.002

67. Queval CJ, Fearns A, Botella L, Smyth A, Schnettger L, Mitermite M, et al. Macrophage-specific responses to human- and animal-adapted tubercle Bacilli reveal pathogen and host factors driving multinucleated cell formation. *PLoS Pathog*. (2021) 17:e1009410. doi: 10.1371/journal.ppat.1009410

68. Hunter L, Hingley-Wilson S, Stewart GR, Sharpe SA, Salguero FJ. Dynamics of macrophage, T and B cell infiltration within pulmonary granulomas induced by *Mycobacterium Tuberculosis* in two non-human primate models of aerosol infection. *Front Immunol*. (2022) 12:776913. doi: 10.3389/fimmu.2021.776913

69. Phuah JY, Mattila JT, Lin PL, Flynn JL. Activated B cells in the granulomas of nonhuman Primates infected with *Mycobacterium Tuberculosis*. *Am J Pathol*. (2012) 181:508–14. doi: 10.1016/j.ajpath.2012.05.009

70. Aranday-Cortes E, Bull NC, Villarreal-Ramos B, Gough J, Hicks D, Ortiz-Pelaez A, et al. Upregulation of Il-17a, Cxcl9 and Cxcl10 in early-stage granulomas induced by *Mycobacterium Bovis* in cattle. *Transbound Emerg Dis*. (2013) 60:525–37. doi: 10.1111/j.1865-1682.2012.01370.x

71. Fuller CL, Flynn JL, Reinhart TA. In situ study of abundant expression of Proinflammatory chemokines and cytokines in pulmonary granulomas that develop in Cynomolgus macaques experimentally infected with *Mycobacterium Tuberculosis*. *Infect Immun*. (2003) 71:7023–34. doi: 10.1128/IAI.71.12.7023-7034.2003

72. Williams A, James BW, Bacon J, Hatch KA, Hatch GJ, Hall GA, et al. An assay to compare the infectivity of *Mycobacterium Tuberculosis* isolates based on aerosol infection of Guinea pigs and assessment of bacteriology. *Tuberculosis (Edinb)*. (2005) 85:177–84. doi: 10.1016/j.tube.2004.11.001

73. Palanisamy GS, Smith EE, Shanley CA, Ordway DJ, Orme IM, Basaraba RJ. Disseminated disease severity as a measure of virulence of *Mycobacterium Tuberculosis* in the Guinea pig model. *Tuberculosis (Edinb)*. (2008) 88:295–306. doi: 10.1016/j.tube.2007.12.003

74. Larenas-Munoz F, Ruedas-Torres I, Hunter L, Bird A, Agullo-Ros I, Winsbury R, et al. Characterisation and development of histopathological lesions in a Guinea pig model of *Mycobacterium Tuberculosis* infection. *Front Vet Sci*. (2023) 10:4200. doi: 10.3389/fvets.2023.1264200

75. Ordway D, Palanisamy G, Henao-Tamayo M, Smith EE, Shanley C, Orme IM, et al. The cellular immune response to *Mycobacterium Tuberculosis* infection in the Guinea pig. *J Immunol*. (2007) 179:2532–41. doi: 10.4049/jimmunol.179.4.2532

76. Palmer MV, Thacker TC, Kanipe C, Boggiatto PM. Heterogeneity of pulmonary granulomas in cattle experimentally infected with *Mycobacterium Bovis*. *Front Vet Sci*. (2021) 8:671460. doi: 10.3389/fvets.2021.671460

77. Figl J, Köhler H, Wedlich N, Liebler-Tenorio EM, Grode L, Parzmair G, et al. Safety and immunogenicity of recombinant Bacille Calmette-Guérin strain Vpm1002 and its derivatives in a goat model. *Int J Mol Sci*. (2023) 24. doi: 10.3390/ijms24065509

78. Sanchez J, Tomás L, Ortega N, Buendía AJ, del Rio L, Salinas J, et al. Microscopical and immunological features of Tuberculoid granulomata and Cavitary pulmonary tuberculosis in naturally infected goats. *J Comp Pathol*. (2011) 145:107–17. doi: 10.1016/j.jcpa.2010.12.006

79. Dorman SE, Hatem CL, Tyagi S, Aird K, Lopez-Molina J, Pitt ML, et al. Susceptibility to tuberculosis: clues from studies with inbred and outbred New Zealand White rabbits. *Infect Immun*. (2004) 72:1700–5. doi: 10.1128/iai.72.3.1700-1705.2004

80. Manabe YC, Dannenberg AM, Tyagi SK, Hatem CL, Yoder M, Woolwine SC, et al. Different strains of *Mycobacterium Tuberculosis* cause various spectrums of disease in the rabbit model of tuberculosis. *Infect Immun*. (2003) 71:6004–11. doi: 10.1128/iai.71.10.6004-6011.2003

81. Lewinsohn DM, Tydeman IS, Frieder M, Grotzke JE, Lines RA, Ahmed S, et al. High resolution radiographic and fine immunologic definition of Tb disease progression in the Rhesus macaque. *Microbes Infect*. (2006) 8:2587–98. doi: 10.1016/j.micinf.2006.07.007

82. Flynn JL, Klein E. Pulmonary tuberculosis in monkeys In: FJ Leong, V Dartois and T Dick, editors. *A color atlas of comparative pathology of pulmonary tuberculosis*. Florida: CRC Press (2011). 83–106.

83. White AD, Sibley L, Sarfas C, Morrison A, Gullick J, Clark S, et al. Mtbvac vaccination protects Rhesus macaques against aerosol challenge with M. tuberculosis and induces immune signatures analogous to those observed in clinical studies. *NPJ Vaccines*. (2021) 6:4. doi: 10.1038/s41541-020-00262-8

84. Sugawara I, Yamada H, Mizuno S. Nude Rat (F344/N-Rnu) Tuberculosis. *Cell Microbiol*. (2006) 8:661–7. doi: 10.1111/j.1462-5822.2005.00658.x

85. Sugawara I, Yamada H, Mizuno S. Pathological and immunological profiles of rat tuberculosis. *Int J Exp Pathol*. (2004) 85:125–34. doi: 10.1111/j.0959-9673.2004.00379.x

86. Blanco JC, Boukhvalova MS, Perez DR, Vogel SN, Kajon A. Modeling human respiratory viral infections in the cotton rat (*Sigmodon Hispidus*). *J Antivir Antiretrovir*. (2014) 6:40–2. doi: 10.4172/jaa.1000093

87. Clark S, Hall Y, Williams A. Animal models of tuberculosis: Guinea pigs. *Cold Spring Harb Perspect Med*. (2014) 5:a018572. doi: 10.1101/cshperspect.a018572

88. Flynn JL. Lessons from experimental *Mycobacterium Tuberculosis* infections. *Microbes Infect*. (2006) 8:1179–88. doi: 10.1016/j.micinf.2005.10.033

89. Kaplan G, Tsenova L. Pulmonary tuberculosis in the rabbit In: FJDV Leong and T Dick, editors. *A color atlas of comparative pathology of pulmonary tuberculosis Boca Raton*. Florida: CRC Press (2011). 107–30.

90. Tsenova L, Sokol K, Freedman VH, Kaplan G. A combination of thalidomide plus antibiotics protects rabbits from mycobacterial meningitis-associated death. *J Infect Dis*. (1998) 177:1563–72. doi: 10.1086/515327

91. Jassal MS, Nedeltchev GG, Osborne J, Bishai WR. A modified scoring system to describe gross pathology in the rabbit model of tuberculosis. *BMC Microbiol*. (2011) 11:49. doi: 10.1186/1471-2180-11-49

92. Lurie MB. The fate of tubercle Bacilli in the organs of Reinfected rabbits. *J Exp Med*. (1929) 50:747–65. doi: 10.1084/jem.50.6.747

93. Lurie MB. The correlation between the histological changes and the fate of living tubercle Bacilli in the organs of tuberculous rabbits. *J Exp Med*. (1932) 55:31–54. doi: 10.1084/jem.55.1.31

94. Subbian S, Tsenova L, Yang G, O'Brien P, Parsons S, Peixoto B, et al. Chronic pulmonary Cavitary tuberculosis in rabbits: a failed host immune response. *Open Biol*. (2011) 1:110016. doi: 10.1098/rsob.110016

95. Salguero FJ. The pathology and pathogenesis of Mycobacterium bovis infection. *CABI Books*. CABI. (2018):122–39. doi: 10.1079/9781786391520.0122

96. García-Jiménez WL, Benítez-Medina JM, Fernández-Llario P, Abecia JA, García-Sánchez A, Martínez R, et al. Comparative pathology of the natural infections by Mycobacterium Bovis and by *Mycobacterium Caprae* in wild boar (*Sus Scrofa*). *Transbound Emerg Dis*. (2013) 60:102–9. doi: 10.1111/j.1865-1682.2012.01321.x

97. Palmer MV, Wiarda J, Kanipe C, Thacker TC. Early pulmonary lesions in cattle infected Via aerosolized *Mycobacterium Bovis*. *Vet Pathol*. (2019) 56:544–54. doi: 10.1177/0300985819833454

98. Palmer MV, Waters WR, Thacker TC. Lesion development and Immunohistochemical changes in granulomas from cattle experimentally infected with *Mycobacterium Bovis*. *Vet Pathol*. (2007) 44:863–74. doi: 10.1354/vp.44-6-863

99. Kanipe C, Boggiatto PM, Putz EJ, Palmer MV. Histopathologic differences in granulomas of *Mycobacterium Bovis* Bacille Calmette Guerin (Bcg) vaccinated and non-vaccinated cattle with bovine tuberculosis. *Front Microbiol*. (2022) 13:1048648. doi: 10.3389/fmicb.2022.1048648

100. Palmer MV, Thacker TC, Waters WR. Multinucleated Giant cell cytokine expression in pulmonary granulomas of cattle experimentally infected with *Mycobacterium Bovis*. *Vet Immunol Immunopathol*. (2016) 180:34–9. doi: 10.1016/j.vetimm.2016.08.015

101. Menin A, Fleith R, Reck C, Marlow M, Fernandes P, Pilati C, et al. Asymptomatic cattle naturally infected with *Mycobacterium Bovis* present exacerbated tissue pathology and bacterial dissemination. *PloS One*. (2013) 8:e53884. doi: 10.1371/journal.pone.0053884

102. Johnson LK, Liebana E, Nunez A, Spencer Y, Clifton-Hadley R, Jahans K, et al. Histological observations of bovine tuberculosis in lung and lymph node tissues from British deer. *Vet J*. (2008) 175:409–12. doi: 10.1016/j.tvjl.2007.04.021

103. Cassidy JP, Bryson DG, Gutiérrez Cancela MM, Forster F, Pollock JM, Neill SD. Lymphocyte subtypes in experimentally induced early-stage bovine tuberculous lesions. *J Comp Pathol*. (2001) 124:46–51. doi: 10.1053/jcpa.2000.0427

104. Cassidy JP, Bryson DG, Pollock JM, Evans RT, Forster F, Neill SD. Early lesion formation in cattle experimentally infected with *Mycobacterium Bovis*. *J Comp Pathol*. (1998) 119:27–44. doi: 10.1016/S0021-9975(98)80069-8

105. Gonzalez-Juarrero M, Bosco-Lauth A, Podell B, Soffler C, Brooks E, Izzo A, et al. Experimental aerosol *Mycobacterium Bovis* model of infection in goats. *Tuberculosis (Edinb)*. (2013) 93:558–64. doi: 10.1016/j.tube.2013.05.006

106. Gong W, Liang Y, Wu X. Animal models of tuberculosis vaccine research: an important component in the fight against tuberculosis. *Biomed Res Int*. (2020) 2020:4263079. doi: 10.1155/2020/4263079

107. Wedlich N, Figl J, Liebler-Tenorio EM, Köhler H, von Pückler K, Rissmann M, et al. Video endoscopy-guided Intrabronchial spray inoculation of *Mycobacterium Bovis* in goats and comparative assessment of lung lesions with various imaging methods. Frontiers in veterinary. *Science*. (2022):9. doi: 10.3389/fvets.2022.877322

108. de Val PB, López-Soria S, Nofrarías M, Martín M, Vordermeier HM, Villarreal-Ramos B, et al. Experimental model of tuberculosis in the domestic goat after endobronchial infection with *Mycobacterium Caprae*. *Clin Vaccine Immunol*. (2011) 18:1872–81. doi: 10.1128/cvi.05323-11

109. Seva J, Menchén V, Navarro JA, Pallarés FJ, Villar D, Vásquez F, et al. Caprine tuberculosis eradication program: an Immunohistochemical study. *Small Rumin Res*. (2002) 46:107–14. doi: 10.1016/S0921-4488(02)00174-8

110. Bezos J, de Juan L, Romero B, Álvarez J, Mazzucchelli F, Mateos A, et al. Experimental infection with *Mycobacterium Caprae* in goats and evaluation of immunological status in tuberculosis and Paratuberculosis co-infected animals. *Vet Immunol Immunopathol*. (2010) 133:269–75. doi: 10.1016/j.vetimm.2009.07.018

111. Vordermeier HM, Chambers MA, Cockle PJ, Whelan AO, Simmons J, Hewinson RG. Correlation of Esat-6-specific gamma interferon production with pathology in cattle following *Mycobacterium Bovis* Bcg vaccination against experimental bovine tuberculosis. *Infect Immun*. (2002) 70:3026–32. doi: 10.1128/iai.70.6.3026-3032.2002

112. Roy Á, Risalde MA, Bezos J, Casal C, Romero B, Sevilla I, et al. Response of goats to intramuscular vaccination with heat-killed Mycobacterium Bovis and natural challenge. *Comp Immunol Microbiol Infect Dis*. (2018) 60:28–34. doi: 10.1016/j.cimid.2018.09.006

113. Roy A, Tomé I, Romero B, Lorente-Leal V, Infantes-Lorenzo JA, Domínguez M, et al. Evaluation of the immunogenicity and efficacy of Bcg and Mtbvac vaccines using a natural transmission model of tuberculosis. *Vet Res*. (2019) 50:82. doi: 10.1186/s13567-019-0702-7

114. Domingo M, Vidal E, Marco A. Pathology of bovine tuberculosis. *Res Vet Sci*. (2014) 97:S20–9. doi: 10.1016/j.rvsc.2014.03.017

115. Neila C, Rebollada-Merino A, Bezos J, de Juan L, Domínguez L, Rodríguez-Bertos A. Extracellular matrix proteins (fibronectin, collagen iii, and collagen I) Immunoexpression in goat tuberculous granulomas (*Mycobacterium Caprae*). *Vet Res Commun*. (2022) 46:1147–56. doi: 10.1007/s11259-022-09996-3

116. Carrisoza-Urbina J, Morales-Salinas E, Bedolla-Alva MA, Hernández-Pando R, Gutiérrez-Pabello JA. Atypical granuloma formation in *Mycobacterium Bovis*-infected calves. *PloS One*. (2019) 14:e0218547. doi: 10.1371/journal.pone.0218547

117. di Marco Lo Presti V, Capucchio MT, Fiasconaro M, Puleio R, la Mancusa F, Romeo G, et al. *Mycobacterium Bovis* tuberculosis in two goat farms in multi-host ecosystems in Sicily (Italy): epidemiological, diagnostic, and regulatory considerations. *Pathogens*. (2022) 11. doi: 10.3390/pathogens11060649

118. Liebler-Tenorio EM, Heyl J, Wedlich N, Figl J, Kohler H, Krishnamoorthy G, et al. Vaccine-induced subcutaneous granulomas in goats reflect differences in host-Mycobacterium interactions between Bcg- and recombinant Bcg-derivative vaccines. *Int J Mol Sci*. (2022) 23. doi: 10.3390/ijms231910992

119. Balseiro A, Altuzarra R, Vidal E, Moll X, Espada Y, Sevilla IA, et al. Assessment of Bcg and inactivated *Mycobacterium Bovis* vaccines in an experimental tuberculosis infection model in sheep. *PloS One*. (2017) 12:e0180546. doi: 10.1371/journal.pone.0180546

120. Garcia-Jimenez WL, Fernandez-Llario P, Gomez L, Benitez-Medina JM, Garcia-Sanchez A, Martinez R, et al. Histological and Immunohistochemical characterisation of *Mycobacterium Bovis* induced granulomas in naturally infected fallow deer (*Dama Dama*). *Vet Immunol Immunopathol*. (2012) 149:66–75. doi: 10.1016/j.vetimm.2012.06.010

121. Palmer MV, Waters WR, Whipple DL. Lesion development in White-tailed deer (*Odocoileus Virginianus*) experimentally infected with *Mycobacterium Bovis*. *Vet Pathol*. (2002) 39:334–40. doi: 10.1354/vp.39-3-334

122. Bouz G, Al HN. The zebrafish model of tuberculosis - no lungs needed. *Crit Rev Microbiol*. (2018) 44:779–92. doi: 10.1080/1040841X.2018.1523132

123. Ramakrishnan L. Looking within the zebrafish to understand the tuberculous granuloma. *Adv Exp Med Biol*. (2013) 783:251–66. doi: 10.1007/978-1-4614-6111-1_13

124. Meijer AH. Protection and pathology in Tb: learning from the zebrafish model. *Semin Immunopathol*. (2016) 38:261–73. doi: 10.1007/s00281-015-0522-4

125. Myllymaki H, Bauerlein CA, Ramet M. The zebrafish breathes New life into the study of tuberculosis. *Front Immunol*. (2016) 7:196. doi: 10.3389/fimmu.2016.00196

126. Zon LI, Peterson RT. In vivo drug discovery in the zebrafish. *Nat Rev Drug Discov*. (2005) 4:35–44. doi: 10.1038/nrd1606

127. Varela M, Meijer AH. A fresh look at mycobacterial pathogenicity with the zebrafish host model. *Mol Microbiol*. (2022) 117:661–9. doi: 10.1111/mmi.14838

128. Prouty MG, Correa NE, Barker LP, Jagadeeswaran P, Klose KE. Zebrafish-*Mycobacterium Marinum* model for mycobacterial pathogenesis. *FEMS Microbiol Lett*. (2003) 225:177–82. doi: 10.1016/S0378-1097(03)00446-4

129. Swaim LE, Connolly LE, Volkman HE, Humbert O, Born DE, Ramakrishnan L. *Mycobacterium Marinum* infection of adult zebrafish causes Caseating granulomatous tuberculosis and is moderated by adaptive immunity. *Infect Immun*. (2006) 74:6108–17. doi: 10.1128/IAI.00887-06

130. Davis JM, Clay H, Lewis JL, Ghori N, Herbomel P, Ramakrishnan L. Real-time visualization of Mycobacterium-macrophage interactions leading to initiation of granuloma formation in zebrafish embryos. *Immunity*. (2002) 17:693–702. doi: 10.1016/s1074-7613(02)00475-2

131. van Leeuwen LM, van der Sar AM, Bitter W. Animal models of tuberculosis: zebrafish. *Cold Spring Harb Perspect Med*. (2014) 5:a018580. doi: 10.1101/cshperspect.a018580

132. Parikka M, Hammaren MM, Harjula SK, Halfpenny NJ, Oksanen KE, Lahtinen MJ, et al. *Mycobacterium Marinum* causes a latent infection that can be reactivated by gamma irradiation in adult zebrafish. *PLoS Pathog*. (2012) 8:e1002944. doi: 10.1371/journal.ppat.1002944

133. Yoon S, Alnabulsi A, Wang TY, Lee PT, Chen T-Y, Bird S, et al. Analysis of interferon gamma protein expression in zebrafish (*Danio Rerio*). *Fish Shellfish Immunol*. (2016) 57:79–86. doi: 10.1016/j.fsi.2016.08.023

134. Saralahti AK, Uusi-Makela MIE, Niskanen MT, Ramet M. Integrating fish models in tuberculosis vaccine development. *Dis Model Mech*. (2020) 13. doi: 10.1242/dmm.045716

135. Risalde MA, López V, Contreras M, Mateos-Hernández L, Gortázar C, de la Fuente J. Control of Mycobacteriosis in zebrafish (*Danio Rerio*) Mucosally vaccinated with heat-inactivated *Mycobacterium Bovis*. *Vaccine*. (2018) 36:4447–53. doi: 10.1016/j.vaccine.2018.06.042

136. Tobin DM, Ramakrishnan L. Comparative pathogenesis of Mycobacterium Marinum and *Mycobacterium Tuberculosis*. *Cell Microbiol*. (2008) 10:1027–39. doi: 10.1111/j.1462-5822.2008.01133.x

137. Stoop EJ, Schipper T, Rosendahl Huber SK, Nezhinsky AE, Verbeek FJ, Gurcha SS, et al. Zebrafish embryo screen for mycobacterial genes involved in the initiation of granuloma formation reveals a newly identified Esx-1 component. *Dis Model Mech*. (2011) 4:526–36. doi: 10.1242/dmm.006676

138. López V, Risalde MA, Contreras M, Mateos-Hernández L, Vicente J, Gortázar C, et al. Heat-inactivated *Mycobacterium Bovis* protects zebrafish against Mycobacteriosis. *J Fish Dis*. (2018) 41:1515–28. doi: 10.1111/jfd.12847

139. Fitzgerald SD, Kaneene JB. Wildlife reservoirs of bovine tuberculosis worldwide: hosts, pathology, surveillance, and control. *Vet Pathol*. (2013) 50:488–99. doi: 10.1177/0300985812467472

140. Garcia-Jimenez WL, Salguero FJ, Fernandez-Llario P, Martinez R, Risco D, Gough J, et al. Immunopathology of granulomas produced by *Mycobacterium Bovis* in naturally infected wild boar. *Vet Immunol Immunopathol*. (2013) 156:54–63. doi: 10.1016/j.vetimm.2013.09.008

141. Risco D, Salguero FJ, Cerrato R, Gutierrez-Merino J, Lanham-New S, Barquero-Pérez O, et al. Association between vitamin D supplementation and severity of tuberculosis in wild boar and Red Deer. *Res Vet Sci*. (2016) 108:116–9. doi: 10.1016/j.rvsc.2016.08.003

142. Gil O, Diaz I, Vilaplana C, Tapia G, Diaz J, Fort M, et al. Granuloma encapsulation is a key factor for containing tuberculosis infection in Minipigs. *PloS One*. (2010) 5:e10030. doi: 10.1371/journal.pone.0010030

143. Chambers MA, Aldwell F, Williams GA, Palmer S, Gowtage S, Ashford R, et al. The effect of Oral vaccination with *Mycobacterium Bovis* Bcg on the development of tuberculosis in captive European badgers (*Meles Meles*). *Front Cell Infect Microbiol*. (2017) 7:6. doi: 10.3389/fcimb.2017.00006

144. Corner LA, Murphy D, Gormley E. *Mycobacterium Bovis* infection in the Eurasian badger (*Meles Meles*): the disease, pathogenesis. *Epidemiol Control J Comp Pathol*. (2011) 144:1–24. doi: 10.1016/j.jcpa.2010.10.003

145. Lesellier S, Palmer S, Gowtage-Sequiera S, Ashford R, Dalley D, Davé D, et al. Protection of Eurasian badgers (*Meles Meles*) from tuberculosis after intra-muscular vaccination with different doses of Bcg. *Vaccine*. (2011) 29:3782–90. doi: 10.1016/j.vaccine.2011.03.028

146. Balseiro A, Prieto JM, Álvarez V, Lesellier S, Davé D, Salguero FJ, et al. Protective effect of Oral Bcg and inactivated *Mycobacterium Bovis* vaccines in European badgers (*Meles Meles*) experimentally infected with *M. bovis Front Vet Sci*. (2020) 7:41. doi: 10.3389/fvets.2020.00041

147. Senior NJ, Bagnall MC, Champion OL, Reynolds SE, La Ragione RM, Woodward MJ, et al. Galleria Mellonella as an infection model for *Campylobacter Jejuni* virulence. *J Med Microbiol*. (2011) 60:661–9. doi: 10.1099/jmm.0.026658-0

148. Li Y, Spiropoulos J, Cooley W, Khara JS, Gladstone CA, Asai M, et al. Galleria Mellonella - a novel infection model for the *Mycobacterium Tuberculosis* complex. *Virulence*. (2018) 9:1126–37. doi: 10.1080/21505594.2018.1491255

149. Asai M, Li Y, Spiropoulos J, Cooley W, Everest DJ, Kendall SL, et al. Galleria Mellonella as an infection model for the virulent *Mycobacterium Tuberculosis* H37rv. *Virulence*. (2022) 13:1543–57. doi: 10.1080/21505594.2022.2119657

150. Thacker VV, Dhar N, Sharma K, Barrile R, Karalis K, McKinney JD. A lung-on-Chip model of early *Mycobacterium Tuberculosis* infection reveals an essential role for alveolar epithelial cells in controlling bacterial growth. *Elife*. (2020) 9:9961. doi: 10.7554/eLife.59961

151. Duffy SC, Srinivasan S, Schilling MA, Stuber T, Danchuk SN, Michael JS, et al. Reconsidering *Mycobacterium Bovis* as a proxy for zoonotic tuberculosis: a molecular epidemiological surveillance study. *Lancet Microbe*. (2020) 1:e66–73. doi: 10.1016/S2666-5247(20)30038-0

frontiers | Frontiers in Veterinary Science

TYPE Original Research
PUBLISHED 02 November 2023
DOI 10.3389/fvets.2023.1249833

OPEN ACCESS

EDITED BY
Francisco Javier Salguero,
UK Health Security Agency (UKHSA),
United Kingdom

REVIEWED BY
Rodrigo Otávio Silveira Silva,
Federal University of Minas Gerais, Brazil
Stefano Cortellini,
Royal Veterinary College (RVC),
United Kingdom
Rafael Gariglio Clark Xavier,
Federal University of Minas Gerais, Brazil

*CORRESPONDENCE
Rene Dörfelt
✉ r.doerfelt@medizinische-kleintierklinik.de

RECEIVED 29 June 2023
ACCEPTED 09 October 2023
PUBLISHED 02 November 2023

CITATION
Dörfelt S, Mayer C, Wolf G, Straubinger RK, Fischer A, Hartmann K and Dörfelt R (2023) Retrospective study of tetanus in 18 dogs—Causes, management, complications, and immunological status.
Front. Vet. Sci. 10:1249833.
doi: 10.3389/fvets.2023.1249833

Retrospective study of tetanus in 18 dogs—Causes, management, complications, and immunological status

Stefanie Dörfelt[1], Christine Mayer[1], Georg Wolf[2], Reinhard K. Straubinger[2], Andrea Fischer[1], Katrin Hartmann[1] and Rene Dörfelt[1]*

[1]Ludwig-Maximilians-University (LMU) Small Animal Clinic, Centre for Clinical Veterinary Medicine, Ludwig-Maximilians-University (LMU), Munich, Germany, [2]Department of Veterinary Sciences, Institute for Infectious Diseases and Zoonoses, Ludwig-Maximilians-University (LMU), Munich, Germany

Objective: Tetanus is a severe neurologic disease caused by *Clostridium tetani,* resulting in spastic paralysis. Canine tetanus is associated with serious complications such as aspiration and a high mortality rate of up to 50%.

Materials and methods: Medical records of all dogs diagnosed with tetanus over 8 years (2014–2022) were analyzed for severity grade, treatment protocols, nutritional management, and complications, as well as outcome, vaccination, and antibody production in some dogs. No medical records were excluded. Normality was analyzed by the D'Agostino–Pearson test. Parametric, normally distributed data were presented as mean ± standard deviation. Non-parametric, non-normally distributed data were presented as median (m) and range (minimum–maximum). The association between tetanus grade, progression of diseases, and duration of hospitalization was analyzed using the *t*-test, Mann–Whitney U test, and Kruskal–Wallis test. A $P \leq 0.05$ was considered significant.

Results: Eighteen dogs were identified. Most affected dogs were classified into severity grade II (66.7%, 12 of 18). Clinical signs deteriorated in 55.6% of dogs (10 of 18). A source was identified in 88.9% of dogs (16 of 18). Nine dogs required surgical wound revision. A percutaneous endoscopic gastropexy tube was placed in 83.3% of dogs (15 of 18) for nutritional support. Medical treatment included metronidazole, methocarbamol, and combinations of different sedatives adapted to the patient's requirements. Tetanus antitoxin was used in 72.2% of dogs (13 of 18) without reported adverse events. The survival rate was 88.9% (16 of 18). Complications, such as hypertension, aspiration pneumonia, and laryngeal spasm occurred in 12 of 18 dogs. Median hospitalization time (8 days; range 0–16 days) was associated with the maximum tetanus severity grade ($p = 0.022$). Rapid eye movement behavior disorder was observed in 72.2% of dogs (13 of 18). In 5 dogs, antibodies were measured after recovery, and in 4 of 5 dogs, no antibodies were detectable despite generalized tetanus disease. Vaccination with tetanus toxoid was performed in five dogs following the disease.

Conclusion: In the present study, the mortality rate was lower than previously reported. Tetanus is still a life-threatening disease, but the prognosis may be good if adequate management and monitoring can be ensured.

KEYWORDS

***Clostridium tetani*, canine, outcome, tetanospasmin, tetanus toxoid, treatment, vaccination**

1. Introduction

Tetanus commonly presents as a life-threatening neurologic disease. This clinical syndrome is caused by tetanospasmin, a neurotoxin (TeNT) released by *Clostridium (C.) tetani*, a ubiquitous, anaerobic, spore-forming, gram-positive bacterium, which replicates mainly in infected wounds (1, 2). In a suitable anaerobic environment, such as tissue necrosis and cell lysis, *C. tetani* produces the toxin TeNT, which attaches to the presynaptic membrane of demyelinated nerve endings and migrates retrogradely to the neuronal cell body of inhibitory interneurons within the central nervous system (3). The toxin cleaves synaptobrevin, a vesicle-associated membrane protein required for the release of inhibitory neurotransmitters, such as glycine and gamma-aminobutyric acid (GABA) (4). The consequence is the lack of release of these inhibitory neurotransmitters, resulting in overstimulation of motor neurons with focal or generalized increased muscle tone that can worsen with excitement and other stimuli (5). The sensitivity to TeNT differs between species, with dogs and cats being much less sensitive compared with horses and humans. The minimal lethal dose of tetanus toxin *via* the intramuscular route of inoculation is 0.2 ng/kg in horses and humans. As the minimal lethal dose is higher in dogs (150 ng/kg) and cats (600 ng/kg) (6), vaccination is currently recommended in humans and horses but not in dogs and cats (7).

The most common initial clinical signs in affected dogs include oculofacial signs with trismus, risus sardonicus, dysphagia, and vomitus (5, 8). In more than half of the dogs, clinical signs progress to generalized rigidity with tonic, involuntary, prolonged muscle contractions with or without autonomic dysfunction (3, 5). Potential complications during the disease are (I) respiratory compromise due to laryngeal spasm, aspiration pneumonia, and central respiratory arrest; (II) autonomic dysfunction with brady-/tachycardia, hypotension, and urine retention; and (III) others, such as malnutrition, hyperthermia, hiatal hernia, megaesophagus, and urinary tract infection (5, 9, 10). Coxofemoral luxation and systemic inflammatory response syndrome may occur on rare occasions (5, 9, 11). Reported mortality rates in dogs are between 8% and 50% (5, 12–15).

Treatment strategies include the removal of the source of infection (if still ongoing), antitoxin, adequate antimicrobial therapy, control of rigidity and tetanic spasms with muscle relaxants and sedatives, and long-term intensive supportive care (5, 16). Any stimuli that could exacerbate spasms, e.g., pain, noise, manipulation, and light, should be avoided. Adequate analgesia is mandatory to control pain from muscle spasms and if procedures such as toe amputation are performed. Dogs that are dysphagic due to pharyngeal spasms and trismus, or dogs with deep sedation, need adequate nutritional support.

To date, no definitive antemortem laboratory test has been established to diagnose tetanus (15, 17). Before the onset and compatible clinical signs, history or suspicion of previous wound infection in the days or weeks prior usually indicate a clinical diagnosis of tetanus (1). Hematology and serum biochemistry panels are unspecific, often without any deviations, and only mild changes in the complete blood count, elevated creatine kinase, and increased serum creatinine levels can be observed (14, 18). Isolation of *C. tetani* from wounds often fails, as it requires anaerobic conditions and special culture media and may no longer be present on rare occasions (11). Measurement of serum antibodies to tetanus toxoid has been suggested to provide further support for the diagnosis of tetanus in case of positive results (1, 8). However, no information is available on the course of the production of antibodies in these dogs. In human medicine, a small quantity of TeNT already causes clinical disease but is insufficient to stimulate antibody production (7). Nowadays, the diagnosis of tetanus in dogs is still based on clinical signs and history.

This retrospective analysis aimed to evaluate the outcome of dogs with tetanus and summarize intensive care treatment protocols. The secondary aim was to describe the course of tetanus toxoid antibody production after the development of the disease and after vaccination in some of the dogs.

2. Materials and methods

Medical records of dogs diagnosed with tetanus that were presented between August 2014 and February 2022 to the Clinic of Small Animal Medicine, Center for Clinical Veterinary Medicine of the LMU Munich, were reviewed. Dogs with supportive history and characteristic clinical oculofacial signs consistent with tetanus, such as risus sardonicus, trismus, prolapse of the third eyelid with or without dysphagia, and generalized stiff gait, without evidence of other central nervous system or neuromuscular diseases, were included. Medical records were evaluated for signalment, age, body weight, presence of underlying source of infection, onset of clinical signs, clinical signs at presentation, bacteria isolated from wounds, surgical interventions, treatment protocols including sedation and muscle relaxation protocols, time points of placement of percutaneous endoscopic gastrostomy tube (PEG tube) during disease, course of disease, time until adequate food uptake and time when PEG tube was removed, duration of hospitalization, and complications. For the evaluation of clinical signs, an established tetanus severity classification system was used (Table 1) (5). Follow-up data were obtained on the presence of rapid eye movement sleep behavior disorder (RBD) (13). In addition, after disease and vaccination with subsequent antibody titer development, the course of tetanus toxoid antibody titer was evaluated. Antibody titers were controlled within 3 months after infection and 1 and 2 years after vaccination.

2.1. Data analysis

Statistical analysis was performed using commercial software.[1] Normality was analyzed by the D'Agostino–Pearson test. Parametric, normally distributed data were presented as mean ± standard deviation. Non-parametric, non-normally distributed data were presented as median (m) and range (minimum–maximum). The association between tetanus grade, progression of diseases, and duration of hospitalization was analyzed using the

1 Prism 5 for Windows (Graph Pad Software, Inc. San Diego, USA).

TABLE 1 Tetanus severity classification modified from Burkitt JM, Sturges BK, Jandrey KE, Kass PH. Risk factors associated with outcome in dogs with tetanus: 38 cases (1987–2005).

Grade	Clinical signs
I	Any or all of the following signs (ambulatory dogs): • Oculofacial signs: miosis, enophthalmus, *risus sardonicus*, erected ears, trismus • Hypersensitivity to noise, light, touch
II	Any or all of the following signs (ambulatory dogs): • Dysphagia • Stiff gait, sawhorse stance, erected tail • May have any or all grade I signs
III	Any or all of the following signs (recumbent dogs): • Muscle fasciculations or spasms • Seizures • Must have grade I or II signs
IV	Any or all of the following signs: • Autonomic signs (brady-/tachycardia, brady-/tachyarrhythmia; hypo-/hypertension, apnea, respiratory arrest) • Must have grade I, II or III signs

t-test, Mann–Whitney *U* test, and Kruskal–Wallis-test. A $P \leq 0.05$ was considered significant.

3. Results

3.1. Signalment of dogs with tetanus

Eighteen dogs aged 34.5 ± 40.6 months, with a median body weight of 25.0 kg (5.0–50.0 kg), met the inclusion criteria of the study (Supplementary File 1). Breeds included mixed-breed dogs ($n = 6$), Labrador Retriever ($n = 2$), and one each of American Staffordshire Terrier, American Pocket Bully, Border Collie, Collie, Boxer, Dutch Shepherd, Elo, Great Dane, Jack Russel Terrier, and Rhodesian Ridgeback. Six dogs were male intact, three dogs were male neutered, four dogs were female intact, and five dogs were female neutered.

3.2. Source of infection and isolation of *C. tetani*

In 16 of 18 (88.9%) dogs, a potential site of infection could be identified (Supplementary File 2). Nine dogs had a wound in one digit of the thoracic limb, five dogs had a wound in one digit of the pelvic limb, one dog had a wound at the proximal pelvic limb, and one dog developed clinical signs of tetanus during teething. In total, 8 of 18 (44.4%) dogs with nail injuries, 2 of 18 (11.1%) dogs with footpad wounds, and 4 of 18 (22.2%) dogs with digit lacerations could be identified at the time of presentation. Radiographic evaluation of the injured paws was performed in 12 cases. Radiographs showed osteomyelitis of one distal phalanx in 6 of 12 (50.0%) dogs, soft tissue swelling in 9 of 12 (75.0%) dogs, and a fracture of one distal phalanx in 3 of 12 (25.0%) dogs. In the remaining two dogs, the source of infections remained unknown.

In 8 of 18 (44.4%) dogs, samples from the infected site were submitted for bacterial culture (Supplementary File 2). In 2 of 8 (25.0%) dogs, no bacteria could be isolated during surgery (quality control swab). All dogs received antibiotic treatment at that time point. In the remaining six dogs, different bacteria including *Staphylococcus simulans, Staphylococcus pseudintermedius*, *Enterococcus faecium,* and *Citrobacter freundii* could be isolated (Supplementary File 2). *Clostridium tertium* was identified in one dog, and *Clostridium sporogenes* was identified in two dogs.

3.3. Clinical signs and progression

Overall, 2 of 18 (11.1%) dogs presented with tetanus grade I, and both dogs showed miosis, strabismus, risus sardonicus, one with mild trismus and one without trismus, and no dysphagia or stiff gait (Supplementary File 1). The majority of dogs (12 of 18, 66.7%) presented with tetanus grade II. Clinical signs in all these dogs included a combination of miosis, strabismus, enophthalmos, risus sardonicus, erected ears, and hypersensitivity to noise. All grade II dogs showed dysphagia and generalized stiff, but ambulatory gait. In total, 4 of 18 dogs (22.2 %) displayed signs consistent with grade III on presentation. In addition to signs of grade II, these dogs displayed generalized muscle fasciculations ($n = 3$) or muscle spasms ($n = 1$).

A possible source of infection was reported in 13 of 18 (72.2%) dogs (in 4 dogs, no wound was identified; in 1 dog, no information was available). The median time from the occurrence of the wound to the first clinical signs was 6 days (range 1–27 days), and the median time to presentation was 12 days (range 4–28 days; Supplementary File 1). Clinical signs progressed after the presentation in 10 of 18 (55.6%) hospitalized dogs within a median time of 2 days (range 1–5 days; Supplementary File 1), with 6 dogs progressing to tetanus grade IV. In these six dogs, autonomic signs occurred, including ventricular arrhythmia ($n = 2$), bradycardia ($<$ 35 bpm; $n = 3$), tachycardia ($>$ 150 bpm; $n = 2$), hypertension (systolic blood pressure range 189–220 mmHg; $n = 4$), and death of unknown cause in two dogs (Supplementary Files 1, 3).

3.4. Surgical treatment

Surgical wound revision was performed within 48 h after hospitalization of 9 of 18 (50.0%) dogs (Supplementary File 2). All nine dogs required amputation of the injured digit. All these digits showed soft tissue swelling, with purulent secretion (2 of 9, 22.2%) and panaritium (4 of 9, 44.4%). Radiologic evidence of osteomyelitis was observed in 6 of 9 (66.7%) dogs. The degree of amputation was determined by the visual or radiographic extent. In nine cases, the entire digit was amputated at the level of the metacarpophalangeal joint (1/9 dogs, 11.1%) or the distal level within the distal metacarpal bones via an osteotomy (8/9 dogs, 88.9%), all including removal of the sesamoid bones. Additionally, in one dog, the distal phalanx of two digits was amputated. Before starting surgery, in 8 of 9 dogs (88.9%), 1,000 I.U. tetanus antitoxin was injected locally along the line to healthy tissue. A soft-padded bandage was applied, the wound was cleaned, and the bandage was changed once daily.

3.5. Medical treatment and side effects

All but one dog (17 of 18, 94.4%) were hospitalized to manage the existing signs and to monitor clinical progression. One dog with initial tetanus grade I was treated as an outpatient. Standard management included shielding in a dark and quiet room with additional ear plugs or cotton wool placed into the outer ear canal to reduce auditory stimuli, cleaning the mouth and external ear canals once daily, application of eye drops, changing the dog's position every 4 h if the dog was recumbent, and manual bladder expression or placement of an indwelling urinary catheter if required. The individual sedation was increased and adapted to individual needs before handling and manipulation, depending on respiratory and cardiovascular status and side effects and reactions to the drug.

Standard medical treatment for all dogs included 10 mg/kg IV metronidazole (Fresenius Kabi AG, Bad Homburg Germany) every 8 h for at least 14 days and methocarbamol (Ortoton Recordali, Recordali Pharma GmbH, Ulm, Germany; dose, interval, and route adapted to the dog's requirement; Supplementary File 3).

Equine serum tetanus antitoxin (TAT, Tetanus Serum, WDT, Garbsen, Germany; Supplementary File 3) was used in 13 of 18 (72.2%) dogs. A test dose of 0.2 ml was injected subcutaneously 30 min before intravenous TAT application. No signs of hypersensitivity to TAT were observed in any dog. In 11 of 13 (84.6%) dogs, TAT was given once undiluted for 20 min as a slow intravenous injection (median 300 IU/kg, range 200–375 IU/kg). In two dogs, TAT was applied subcutaneously (1/13, 690 IU/kg) or intramuscularly (1 of 13, 250 IU/kg) by a veterinarian. No signs of hypersensitivity occurred in any dog.

Crystalloid fluids (Ringer-Lactat-Lösung nach Hartmann, B.Braun Vet Care; Sterofundin Iso, B.Braun Vet Care) were given intravenously as continuous rate infusion (CRI) to prevent dehydration and ongoing losses and fulfill maintenance requirements in all hospitalized dogs. A central venous catheter (CVC) was placed in 61.1% of the cases (11 of 18). Acepromazine was used for baseline sedation in all but four dogs. One of these four dogs had tetanus grade I (case No. 11), and no sedation was necessary. For the other three dogs, parenteral acepromazine product was not available on the German market at that time. Acepromazine was given as CRI combined with intermittent boli ($n = 9$) or as repeated boli every 6 to 8 h ($n = 5$; Supplementary File 3). Other drugs included in the sedation protocols were dexmedetomidine CRI ($n = 9$), midazolam CRI ($n = 2$), and opioids (fentanyl, butorphanol, and methadone) administered as a CRI ($n = 4$) or as an intravenous bolus ($n = 14$) and propofol CRI ($n = 4$) or bolus ($n = 4$). In the cases of a propofol CRI, intermittent boli were injected for the adaptation of sedation. In 44.4% of cases (8 of 18), different CRIs had to be combined to achieve adequate sedation and muscle relaxation (Supplementary File 3). Additional treatment included antibiotics ($n = 11$; 61%), such as amoxicillin/clavulanic acid alone ($n = 6$; 33%), amoxicillin/clavulanic acid in combination with marbofloxacin ($n = 3$; 17%), and ampicillin alone ($n = 2$; 11%) if concurrent infection or pneumonia was present; antiseizure drugs, such as phenobarbital ($n = 3$), gabapentin ($n = 3$), or levetiracetam ($n = 5$) for sedation; and antiemetic and gastro-protectant drugs, such as metoclopramide ($n = 8$), maropitant ($n = 12$), ranitidine ($n = 2$), omeprazole ($n = 7$), and chlorphenamine ($n = 2$), and magnesium sulfate ($n = 2$).

If additional sedatives besides acepromazine were started, a small test dose (half of the lowest recommended dose) was given intravenously, and side effects were evaluated. In one dog (case No. 7), escape beats and bradycardia (<35 bpm) were provoked by administration of 5 µg/kg buprenorphine and did not resolve after discontinuation. In another dog (case No. 10), respiratory depression was provoked by 1.5 µg/kg dexmedetomidine IV, which necessitated intubation and mechanical ventilation for 30 min. Dysphoria was observed after the application of benzodiazepines in two dogs. In two other dogs, hypoxemia occurred during the administration of propofol CRI, which was corrected by oxygen supplementation (flow by, nasal oxygen tube). In one of these dogs, hypoxemia was no longer evident after discontinuation of propofol. In the second dog, hypoxemia occurred due to brachycephalic syndrome (case No. 12) and deteriorated with propofol. After injecting dexmedetomidine CRI at a minimal dose, one dog (case No. 12) vomited. A generalized body tremor occurred with intravenous butorphanol administration (0.2 mg/kg) in another dog (case No. 14). The tremor stopped with midazolam treatment. One dog (case No. 7) started vomiting during metoclopramide CRI, which was given due to its prokinetic properties. The vomiting stopped with the subcutaneous administration of metoclopramide.

3.6. PEG tube placement and nutrition

In 83.3% of dogs (15 of 18), a PEG tube with additional gastropexy (PEG Feeding Tube PT20XL, Smith Medical 13/15; Freka PEG CH/Fr 15 ENFit, Fresenius Kabi AG 2/15) was placed under general anesthesia for enteral nutrition within 48 h after presentation due to dysphagia, decreasing the risk of aspiration during feeding (Supplementary File 3). In 7 of 8 dogs that had wound surgery, this procedure was combined with surgical wound management.

The PEG tube was cleaned daily with hypochloric acid (Vetericyn, Ecuphar) or polyhexanide (Prontovet Gel, B. Braun Vet Care) and covered with gauze. Nutrition *via* PEG tube was started 24 h after placement to fulfill one-third of the resting energy requirement (RER). The tube insertion site was controlled macroscopically in all cases and also *via* ultrasonography in 11 of 15 dogs (cases 7 to 18, 73.3%). Gastropexy sutures were left in place for a minimum of 10 days. As soon as an improvement in clinical signs was noticed and the dog was ambulatory again (in tetanus grade III and higher), oral water and food uptake were encouraged gradually. For this, a few drops of water were given into the mouth to evaluate the presence of adequate swallowing. When no salivation or vomiting occurred and the dog swallowed the water without any problem, the amount of water was increased slowly. If no salivation or vomiting was observed, a small amount of food was given and the amount was stepwise increased. The mean duration of spontaneous and physiologic oral food intake (physiologic mouth opening, normal swallowing, no salivation, no regurgitation, or vomiting) was 17.6 ± 6.7 days (recorded in 11 of 18 dogs), and the time of the removal of the PEG tube was 23.8

± 6.4 days (recorded in 13 of 18 dogs). The earliest time for the removal of the PEG tube was 14 days after placement.

The removal of the PEG tube was performed in non-sedated dogs in a standing position in all but three dogs (12 of 15). In two dogs (case Nos. 15 and 18), the low-profile PEG tube was removed endoscopically under general anesthesia. For one dog (case No. 17), sedation was needed for removal. After removal of the PEG tube, water was withheld for 12 h and food was withheld for 24 h.

3.7. Complications

Non-invasive, oscillometric blood pressure recordings were available in 12 of 18 (66.7%) dogs (Supplementary File 3). In 4 of 12 (33.3%) dogs, severe hypertension with a mean systolic blood pressure of 201 mmHg (189–220 mmHg) was developed and treated with amlodipine once or twice daily. The remaining eight dogs were normotensive, or only mild increases in blood pressure occurred (systolic blood pressure range 120–156 mmHg). None of the dogs was hypotensive.

Aspiration pneumonia was a complicating feature in 5 of 18 dogs and was treated with beta-lactam antibiotics (amoxicillin/clavulanic acid and ampicillin) or fluoroquinolone (marbofloxacin). One of these dogs (case No. 7) developed moderate hypalbuminemia (18.2 g/l), and a parenteral amino acid solution (Aminoplasmal B. Braun 10% E, B. Braun AG) was administered.

In 16.7% of the dogs (3 of 18), life-threatening laryngeal spasms occurred due to excitement during examination (n = 1), manipulation for premedication for anesthesia (n = 1), and after recovery from anesthesia (n = 1), necessitating orotracheal intubation. The last dog also developed swelling at the tongue and larynx and required oxygen supplementation *via* a nasal tube. In all three dogs, aspiration pneumonia was observed.

In two dogs (case Nos. 1 and 7), a low heart rate and escape beats, suspected to be triggered by opioid administration, occurred.

In total, 15 of the 18 dogs received nutritional support *via* PEG tube. Reduced gastrointestinal motility was evident in 3 of 15 dogs. After 4 h of feeding twice, the amount given could be removed from the stomach via a PEG tube. In these dogs, metoclopramide CRI or subcutaneous bolus injection was initiated.

Complications such as urine retention (n = 2), bacterial cystitis (n = 1), and disseminated intravascular coagulation due to initial hyperthermia (n = 1) were further observed during hospitalization.

3.8. Duration of hospitalization

The median hospitalization time of the 16 surviving dogs was 8 days (0–26 days; Supplementary File 1). The two non-survivors were hospitalized for 3 days. No difference in hospitalization time was observed for dogs with different initial tetanus grades (p = 0.163). However, a significant association between maximum tetanus grades and duration of hospitalization was observed in surviving dogs (p = 0.022). Dogs with a maximum tetanus grade III or IV had a significantly longer hospitalization time (18 days; 5–26 days) compared with dogs with grades I to II (4 days; 0–9 days; p = 0.004). Hospitalization time in the eight dogs with progression in their tetanus severity grade was also longer (18.5 ± 6.7 days) compared with those eight dogs without progression (4.5 ± 2.9 days; p < 0.001). Time to improvement in clinical signs was available for 13 of 18 dogs that were successfully treated. The median time to first improvement in clinical signs was 11 days (range 4–15 days).

3.9. Outcome

The 28-day survival rate was 88.9%. In total, 17 of the 18 dogs were discharged (94.4%). Respiratory complications occurred in 5 of 18 (27.8%) dogs (aspiration pneumonia, upper airway obstruction) but were managed successfully and had no negative impact on the outcome as described elsewhere (9). Two dogs with grade III tetanus died, one in the hospital (death before discharge, case No. 3) and the other one at home, after being discharged at an early stage of the disease due to the owner's request (1 of 18, case No. 5). This dog was only hospitalized for 3 days and showed progressive signs. The two non-survivors and three surviving dogs did not receive TAT. Necropsy was not performed in any of the non-surviving dogs.

3.10. Development of rapid eye movement sleep behavior disorder

In 13 of 18 (72.2%) dogs, the occurrence of rapid eye movement sleep behavior disorder (RBD) was already documented during hospitalization. In all 13 dogs, RBD was transient and began on the first day after presentation and resolved within weeks to months after recovery from generalized tetanus. RBD ranged from mild (n = 7) to severe (n = 6). In mild cases, probable RBD presented with facial twitching, jaw chomping, and rapid eye movements during sleep (movements under the eyelids or movement of the head). In severe cases, dogs showed episodes with running movements of the limbs, paddling, biting objects lying around them (e.g., towels), jaw chomping, and growling. Episodes could be interrupted. Immediately after approaching these dogs, they woke up and the episodes stopped. No salivation or urination occurred during these episodes. In one dog (case No. 7), these episodes lasted for 3 h and resembled generalized tonic–clonic epileptic seizures. The dog did not wake up when approached. It received levetiracetam (30 mg/kg IV) and phenobarbital (5 mg/kg IV) once, which intensified the episodes. During this period, electroencephalography was performed, and no epileptiform paroxysmal discharges could be detected, classifying these episodes as non-epileptiform RBD.

3.11. Tetanus toxoid antibodies and vaccination

In five dogs, antitoxoid antibody production was evaluated after a successful recovery from tetanus disease (case Nos. 7, 10, 12, 16, and 18). Three of these five dogs recovered from tetanus

grade IV (case Nos. 7, 10, and 12), one dog from tetanus grade III (case No. 18), and one dog from tetanus grade II (case No. 16). Serum tetanus toxoid antibody concentrations were measured 36–149 days after initial presentation (lateral flow assay, Miprolab Microbiologic Diagnostic, Göttingen, Germany). The test evaluates antibody titer against tetanus neurotoxin and is not species-specific. The matching of international units was performed with equine tetanus reference antitoxin from the National Institute for Biological Standards and Control, UK. The results were reported as "+" (equivalent to 0.1–0.9 IU/ml; Miprolab Microbiologic Diagnostic, Göttingen, Germany; (19)) in one dog (case No. 7) and "–" (no antibody titer present, equivalent to < 0.1 IU/ml) in four other dogs (case Nos. 10, 12 16, and 18). In line with current recommendations in human medicine recommending vaccination after recovery from disease,[2] and in line with the owners' wish to protect their dogs from this deadly disease, all five dogs were offered vaccination. The dogs were then vaccinated subcutaneously with tetanus toxoid (Equilis® Te, tetanus toxoid 40 FL, MSD, Germany) (Table 2). In horses, an intramuscular route is recommended,[3] whereas, in ruminants and small ruminants, tetanus vaccination is performed via a subcutaneous route.[4] A subcutaneous route was chosen for dogs in the present study. Before vaccination, informed consent was obtained from the pet owners and documented in the medical records. In line with the recommendations in horses, ruminants, and humans, a second vaccination was performed in each dog after 4 weeks. Tetanus toxoid antibodies were measured 4 weeks and 1 year after the first vaccination in all dogs ($n = 5$, case No. 7, 10, 12, 16, 18) and 2 years after the first vaccination in two dogs ($n = 2$, case No. 7, 10) (Table 2). In all dogs, serum antitoxoid antibody concentration increased. Antibodies were still present after 1 year in all five dogs ($n = 3$ with ++, equivalent to 1.0–5.0 IU/ml, case No. 7, 10, 16; $n = 2$ with + + +, equivalent to > 5.0 IU/ml, case No. 12 and 18) and were measured after 2 years in two dogs ($n = 1$ with ++, equivalent to 1.0–5.0 IU/ml, case No. 7; $n = 1$ with + + +, equivalent to > 5.0 IU/ml, case No. 10, Miprolab Microbiologic Diagnostic, Göttingen, Germany). Adverse effects of vaccination, such as local pain and swelling at the injection site, fever, and anorexia, were observed in one dog (case No. 10). These adverse effects were treated with an anti-histaminic drug (cetirizine 1 mg/kg q 12 h, PO) and metamizole (50 mg/kg q 8 h, PO) for 3 days. Two dogs had no side effects. In two other dogs, this treatment was initiated prophylactically before or immediately after vaccination. One of these dogs developed pain at the injection site and was anorectic for 1 day (case No. 12).

4. Discussion

The present retrospective study evaluated the clinical course and outcome of 18 dogs with tetanus. The survival rate (88.9%) in the present study is in the upper range of previous studies (12–92%) (5, 12–15). In the current study, dogs were managed intensively with individually adapted treatment protocols, intense monitoring to recognize any deterioration as early as possible, and early introduction of enteral nutrition. Despite this intensive care, two dogs died. In previous case reports and studies, dogs with generalized tetanus and higher severity scores, especially with autonomic dysfunction and respiratory complications (classification ≥ III upon admission) were more likely to have a poor outcome compared with those with less severe signs (5, 10, 14). The two non-surviving dogs in the present study had a tetanus severity score of III without obvious autonomic dysfunctions. Respiratory complications, which were associated with poor outcomes in previous studies, were also not evident in these two cases (10, 12, 14).

The potential source of infection was identified in 16 of 18 dogs with 14 dogs having paw lesions. Some were obvious and others were challenging to detect. Radiographic evidence of osteomyelitis was a frequent finding, which highlights the need for radiographic evaluation of injured digits. Therefore, clinicians should screen dogs with tetanus thoroughly for any paw or digit lesions, including radiographs (Supplementary File 2). Different sources of *C. tetani* infection, such as deep penetrating wounds (e.g., interdigital abscesses, bite wounds), broken or deciduous teeth, omphalitis, or surgical site infection, are documented in the veterinary literature (12, 15, 20). As the infection could originate from a small puncture wound and can no longer be visible when signs of tetanus develop, a missing source of infection does not rule out tetanus if typical clinical signs are present (9).

The data in this study highlight that tetanus frequently presents initially as a progressive disease. Signs of tetanus occurred in the reported cohort within a median time interval of 6 days after a wound was observed. After injury, the previously reported range of onset is 3 to 18 days (1, 5, 12). Other studies reported that tetanus can progress to complete body rigidity within 2 to 3 days after the initial hospitalization (12). In our cohort, tetanus progressed in 55.6% of the dogs for a median time of 2 days. Progression to grade III was observed in 17%, and progression to grade IV was observed in 33% of the dogs, which agrees with previously reported progression to grade III or IV with rates of 45–50% (5, 13). In the present study, more dogs with surgical treatment progressed to a higher severity score (6 of 9 dogs) compared with dogs without surgery (3 of 9 dogs). Surgical stimulation is a potential risk factor that could not be determined and is not evaluated in the present study.

In all dogs, specific treatment protocols, which were adapted to the specific needs of the individual dog, were used in combination with standard baseline medication including acepromazine, metronidazole, and methocarbamol. Equine serum TAT was given intravenously to 11 of 18 dogs and 2 dogs by another route (intramuscular, subcutaneous). The TAT which was used in our dogs is a purified high-titer antiserum which is obtained from horses immunized with *C. tetani* (9). The application of TAT aims to neutralize unbound toxins that might spread hematogenously after wound infection, but its use is still discussed controversially, and its effect is unproven (9, 16). No statistically significant difference in survival, severity, and duration of signs is reported between dogs treated with TAT and those not receiving TAT. There is no reported relationship between the timing of TAT

2 https://www.rki.de/DE/Content/Infekt/EpidBull/Merkblaetter/Ratgeber_Tetanus.html#doc2398266bodyText10

3 https://www.noahcompendium.co.uk/?id=-454714

4 https://www.openagrar.de/servlets/MCRFileNodeServlet/openagrar_derivate_00011385/Impfleitlinie_Wiederkaeuer_2018-03-01.pdf

TABLE 2 Tetanus toxoid antibody production after tetanus and vaccination in four dogs.

Case No.	Antibody titer after tetanus	Timepoint of measurement of antibody titer and first vaccination after presentation (days after presentation)	Antibody titer after vaccination		
			Four weeks after first vaccination (+ second vaccination was performed)	One year after first vaccination (no further vaccination)	Two years after first vaccination (no further vaccination)
7	+	109	++	++	++
10	–	149	+	++	+++
12	–	36	+	+++	Not yet performed∫∫
16	–	47	++	++	Not yet performed ∫∫
18	–	53	+	+++	Not yet performed ∫∫

Tetanus toxoid antibodies*.
- → no antibodies detected.
+ → 0.1–0.9 IU/ml.
++ → 1.0–5.0 IU/ml.
+++ → >5.0 IU/l.
*Miprolab Microbiologic Diagnostic, Göttingen, Germany, 19; ∫∫ 2 years not finished.

administration, clinical course, and outcome (5, 12, 15). In 5 of 18 dogs, no TAT was given (case Nos. 3, 4, 5, 7, and 8). Due to the retrospective nature of this study, the cause for this decision could not be determined for earlier cases (case Nos. 3 and 4). In one dog (case No. 5), a wound could not be detected, and the timetable between a potential infection and presentation at the clinic was unknown. In two other dogs (case Nos. 7 and 8), the time between the wound (case No. 7) and potential wound (case No. 8) was 28 days and 20 days, respectively. For these cases (case Nos. 5, 7, and 8), TAT was not given, as there was a high risk that the tetanus toxin was already internalized. TeNT attaches to the presynaptic membrane of nerve endings after wound infection or hematogenous spread and internalizes and migrates retrogradely within axons to the neuronal cell body, making TeNT not accessible to TAT once it is internalized (18). After proximal and transsynaptic migration, TeNT is localized and exerts its effect on the gray matter of the central nervous system (e.g., spinal cord, brainstem) in inhibitory interneurons, interfering with neurotransmitter release. Passive immunization with TAT has limited effects, as the large immunoglobulin TAT does not cross the blood–brain barrier due to its size (9). Intrathecal administration of TAT could bypass the blood–brain barrier. In dogs and horses, intrathecal administration is reported (21–23). However, conflicting evidence of intrathecal TAT compared with other routes exists in human medicine. No definite benefit over parenteral administration is proven in human patients (24–27). Even though we observed a lower mortality rate, it is of interest that two dogs that died had not received TAT (case No. 3 and 5). The effect of parenteral TAT administration could not be evaluated in the present study due to the low mortality rate. The fatal outcomes were probably not related to the lack of TAT application.

Antibiotic therapy with coverage against anaerobic bacteria is commonly recommended for the treatment of tetanus to address any potential ongoing infection with *C tetani*. Nevertheless, deep wound infections and osteomyelitis might not be amenable to antibiotic treatment alone and can also require a surgical approach. Penicillin G has been suggested for a long time to be the antibiotic of choice against anaerobic gram-positive bacteria (15). It is documented that metronidazole penetrates the tissue with vascular compromise more effectively (15). People treated with metronidazole require lower doses of muscle relaxants and sedatives compared with people treated with penicillin G (28). In addition, potential GABA antagonistic properties of penicillin G are discussed to potentiate the effects of tetanospasmin, which might worsen rigidity and reduce the effect of benzodiazepines (29, 30). However, metronidazole can also exert neurotoxic effects, and signs of tremor, rigidity, ataxia, head tilt, and nystagmus can potentially occur if given in high doses or for a prolonged time period (31), although this has so far not been described in dogs treated for tetanus. However, caution should be exerted when metronidazole is administered at recommended dose (31).

In addition to resting in quiet surroundings and minimization of pain and manipulations, adequate sedation and muscle relaxation are important therapeutic goals in patients with tetanus. Acepromazine was used for baseline sedation and muscle relaxation in 14 of 18 dogs, and none of the dogs developed adverse effects from acepromazine. The two dogs with lethal outcomes did not receive acepromazine. In contrast with the result of a previous study, these findings reported a decreased survival of dogs treated with acepromazine (14). This finding could not be confirmed in the present study as most dogs were treated with acepromazine. A potential cause for worse outcomes in the previous study could be an institution of acepromazine treatment, especially in more severely affected dogs. As mentioned above, for the management of the dogs in the present study, individually adapted sedation and analgesic protocols were used, depending on individual efficacy and observed adverse effects. Typically, dogs were managed by clinicians who were dedicated at all hours to those dogs with tetanus, with additional support from the emergency and critical care team to be able to titrate medication and recognize complications in time. Magnesium sulfate was only used in two dogs in the present case series. In human studies, magnesium sulfate reduced the requirements for other muscle relaxants and sedatives and improved autonomic dysfunction (32). In a recent case series with two dogs, the time interval between acepromazine administration and muscle relaxation could be increased with

magnesium supplementation (16). However, in animals, the dose range is empirical, and care should be taken to avoid adverse effects such as hypotension and arrhythmias.

In six dogs, signs of autonomic dysfunctions, such as hypertension, arrhythmias, bradycardia, or tachycardia, were present. Dysautonomia is a common complication of tetanus in human patients and is found in 11.8% of hospitalized patients in a cross-sectional study (33). In human patients with generalized tetanus, autonomic dysfunction is associated with poor prognosis (32). In the present study, cardiovascular autonomic dysfunction, such as premature ventricular contractions ($n = 1$), bradycardia ($n = 1$), or intermittent tachycardia ($n = 2$), was rarely observed. Autonomic dysfunction is rarely reported in animals with tetanus (11, 18, 34). However, autonomic dysfunction could be underrecognized due to inadequate monitoring and might be the unknown cause of death and was also suspected in the fatal cases in the present study. In the present study, the results from blood pressure measurements were available in 12 of 18 (66.7%) dogs with 41.7% of the dogs (5 of 12) showing severe hypertension. In contrast to this finding, primarily hypotension is described in previous case reports (9, 16). In human patients, clinical signs of autonomic dysfunction range from profound hypertension and tachycardia to bradycardia, arrhythmia, and hypotension (35). Elevated serum levels of norepinephrine, with spikes of epinephrine levels, cause a hyperdynamic circulatory state. These spikes increase up to 100 times normal, resembling levels occurring with pheochromocytoma in human patients (36). Excess acetylcholine may contribute to this autonomic dysfunction (37). Possible mechanisms of bradycardia are sudden withdrawal of catecholamines or increased vagal tone (35). In human patients, autonomic storms are often followed by severe resistant hypotension, bradycardia, and asystole and result in massive fluctuations in systemic vascular resistance index, with little change in cardiac index (37). In the present study, hypotension was not observed. Nevertheless, it is mandatory to continuously monitor electrocardiography for arrhythmia and control blood pressure regularly.

Respiratory complications occurred in 5 of 18 dogs (28%) with two dogs with aspiration pneumonia and three dogs with both aspiration pneumonia and laryngeal spasm. In a previous study, respiratory complications occurred at a similar rate and were observed in 26.4% of dogs with tetanus. In this study, poor outcome was associated with 14.2% of dogs that survived with respiratory complications compared with 94.8% of dogs without respiratory complications (10). Other studies also describe a poor outcome in cases with evidence of aspiration pneumonia (12, 14). In the present study, the management of dogs with aspiration pneumonia or laryngeal spasm required much more intensive care than the other dogs, and none of these dogs with respiratory compromise died.

Other rare complications in the present study were disseminated intravascular coagulation, urine retention, cystitis, and reduced gastrointestinal motility. Urinary tract infection is a known problem in cases with a long duration of catheterization, which might be necessary in dogs with urinary retention (38). Other rarely reported complications, such as coxo-femoral luxation (15) and hiatal hernia (11, 38, 39), were not observed in the present study. Reduced gastrointestinal motility, which was present in 3 of 18 (16.7%) dogs, has not been described in dogs with tetanus so far. In human patients, increased abdominal pressure and gastrointestinal stasis, even in patients who are awake, are known complications increasing the risk of aspiration (36).

The median hospitalization time of 8 days in the 16 surviving dogs is comparable to previous reports ranging from 0 to 30 days (12, 13). Median hospitalization time in surviving dogs was significantly associated with the grade of tetanus disease. Dogs with higher tetanus grade classification had a significantly longer median hospitalization time (18 days for grades III and IV).

The median time of improvement in clinical signs (11 days) was in a similar range compared with another retrospective analysis of 20 dogs (9.5 days and 5–12 days) (11). It has to be noted that the median time of improvement was slightly longer than the duration of hospitalization in the present study because dogs with milder and non-progressive signs of tetanus were discharged before clear improvement was observed. As TeNT binds irreversibly to axonal terminals and recovery is dependent on the synthesis of new presynaptic components and their transport to the distal axon, it is known that the duration of clinical improvement is approximately 2 weeks, and full recovery can require weeks to months (15, 40, 41). Muscle spasms can even be the result of permanent damage to inhibitory circuits within the CNS with unknown etiology (5). Long-term complications in humans after recovery, such as physical and psychological problems, are rarely reported (2, 42). In the present study, all surviving dogs recovered fully without any permanent deficits.

The binding of TeNT to neurons inhibits the release of inhibitory neurotransmitters, causing rigid muscle contractions (2). As TeNT can reach higher motor centers within the brain (the brainstem, midbrain, and hypothalamus) via retrograde intraneuronal transport, the subsequent prevention of GABA release can result in inappropriate activation of these motor centers and cause rapid eye movement (REM) sleep without characteristic muscle atonia, called rapid eye movement sleep behavior disorder (RBD) (13). In the present study, RBD was reported in all dogs in which information about sleep period was available. As electroencephalography (EEG) was not performed in all dogs, epileptic activity as a differential diagnosis to RBD cannot be excluded completely. As antiseizure drugs were used in 6/13 dogs and no improvement in episodes was reported, and indeed in one dog episodes deteriorated with a loading dose of levetiracetam and phenobarbital and episodes stopped when approaching and stimulating the dog, RBD was most likely. In one dog with severe episodes of RBD, an EEG was evaluated for confirmation. During a 3-h EEG, no epileptic paroxysmal discharges were observed, categorizing this disorder as non-epileptiform. RBD has been mentioned as "abnormal movements during sleep" in three dogs with tetanus (5). Sleep disturbances have also been reported by other authors (43, 44). A recent case series reported abnormal sleep behavior with violent epileptic-seizure-like RBD in 40% of dogs during recovery from tetanus (13). In a previous study, "abnormal movements during sleep" were already reported (5). In the present study, antiseizure drugs were ineffective in stopping these events, while RBD started during hospitalization; in previous reports, 75% of the RBDs started after discharge (13). The episodes of RBD stopped within weeks to months in all dogs in the present report.

Four dogs were immunized with tetanus toxoid subcutaneously. In human medicine, tetanus itself commonly does not induce antibody development (17). One older study on the Galápagos Islands describes the production of a naturally acquired antibody to tetanus toxin >0.01 IU/ml in humans and animals including four cows, two horses, two mules, and one dog (45). To the best of the authors' knowledge, no further reports evaluating antitoxoid antibodies, after disease or vaccination, are available in dogs. In the reported cases, 4 of 5 (80.0%) dogs did not develop an adequate amount of antitoxoid antibodies when tested within 36–149 days after the presentation at the clinic. It can be speculated that tetanus toxin alone is of low immunogenicity and that the neuronal receptor causes endocytosis of free toxin into the cells via the "A component" causing decreased contact of the toxin with the immune system. However, after 4 weeks of vaccination and booster vaccination, a rise in antibodies and adequate antibody concentration was present in all five dogs. As an adequate antibody titer, a serum antibody titer of > 0.01 IU/ml was considered, as this concentration is shown to be protective against tetanus in human medicine (46). After a second booster vaccination, a further rise in antibody titer was present in 3 of 5 dogs after 12 months, and the titer remained unchanged in the other two dogs. After 24 months, the antibody titer still rose in one dog and remained unchanged in the other dog (Table 2). In human medicine, the duration of immunity after vaccination was 11–14 years with antibodies being present for 64–74 years, measured using a double-antigen tetanus enzyme-linked immunosorbent assay (46). In dogs, the timing of further booster vaccinations has to be determined. The current guidelines of the World Small Animal Veterinary Association for the vaccination of dogs and cats currently do not list tetanus toxoid as a recommended vaccine but mention that tetanus is becoming more common, and "vaccine might be justified and commercially available" (47).

5. Limitations

The main limitation is the retrospective nature of the study. Therefore, not all data, such as on blood pressure and RBD, were available in all dogs, Furthermore, dogs were treated by different veterinarians. A standard operating procedure for tetanus patients was developed and adapted during the study period.

6. Conclusion

Tetanus is still a life-threatening disease but is also associated with a good prognosis if adequate management and monitoring can be ensured. In the present study with intensive, individual management and early institution of enteral nutrition, the mortality rate was in the lower range compared with previous publications. The benefit of vaccination is still questionable as tetanus is a rare disease in dogs, as this species is relatively resistant. After recovery from the disease, vaccination with a second booster dose 4 weeks later did result in an antibody increase. However, the usefulness of vaccination is still debatable.

Data availability statement

The original contributions presented in the study are included in the article/Supplementary material, further inquiries can be directed to the corresponding author.

Ethics statement

Ethical approval was not required for the studies involving animals in accordance with the local legislation and institutional requirements because the study involved medical records of the patients only. Written informed consent was not obtained from the owners for the participation of their animals in this study because the study involved medical records of the patients only.

Author contributions

SD: conception and design of the study, data analysis, and manuscript preparation. CM and GW: data analysis, critical revision of the manuscript, and approved the submitted version. RS, AF, and KH: critical revision of the manuscript and approved the submitted version. RD: conception and design of the study, data analysis, statistical analysis, critical revision of the manuscript, and approved the submitted version. All authors contributed to the article and approved the submitted version.

Conflict of interest

The authors declare that the research was conducted in the absence of any commercial or financial relationships that could be construed as a potential conflict of interest.

Publisher's note

Supplementary material

The Supplementary Material for this article can be found online at: https://www.frontiersin.org/articles/10.3389/fvets.2023.1249833/full#supplementary-material

References

1. Greene CE. Tetanus. In: Greene CE, editor. *Infectious Diseases of the Dog and Cat (4th ed.* Amsterdam: Elsevier Saunders. (2012). p. 423–31.

2. Cook TM, Protheroe RT, Handel JM. Tetanus: a review of the literature. *Br J Anaesth*. (2001) 87:477–87. doi: 10.1093/bja/87.3.477

3. Popoff MR. Tetanus in animals. *J Vet Diagn Invest*. (2020) 32:1–8. doi: 10.1177/1040638720906814

4. Humeau Y, Doussau F, Grant NJ, Poulain B. How botulinum and tetanus neurotoxins block neurotransmitter release. *Biochemie*. (2000) 82:427–46. doi: 10.1016/S0300-9084(00)00216-9

5. Burkitt JM, Sturges BK, Jandrey KE, Kass PH. Risk factors associated with outcome in dogs with tetanus: 38 cases (1987–2005). *J Am Vet Med Assoc*. (2007) 230:76–83. doi: 10.2460/javma.230.1.76

6. Rossetto O., Montecucco C. Tables of toxicity of botulinum and tetanus neurotoxins. *Toxins*. (2019) 11:686. doi: 10.3390/toxins11120686

7. Galazka AM. *The Immunological Basis for Immunization, Module 3*. Tetanus: WHO. (2001). Available online at: https://apps.who.int/iris/bitstream/handle/10665/58891/WHO-EPI-GEN-93.13-mod3-eng.pdf?sequence=51&isAllowed=y

8. Coleman ES. Clostridial neurotoxins: tetanus and botulism. *Comp Cont Educ Small Anim Pract*. (1998) 20:1089.

9. Fawcett A, Irwin P. Diagnosis and treatment of generalized tetanus in dogs. *In Pract*. (2014) 36:482–93. doi: 10.1136/inp.g6312

10. Guedra M, Humm K, Cortellini S. Respiratory complications in dogs with tetanus: a retrospective study of 53 cases. *Can Vet J*. (2021) 62:1202–6.

11. Acke E, Jones BR, Breathnach R, McAllister H, Mooney CT. Tetanus in the dog: review and a case-report of concurrent tetanus with hiatal hernia. *Ir Vet J*. (2004) 57:593–97. doi: 10.1186/2046-0481-57-10-593

12. Bandt C, Rozanski E, Steinberg T, Shaw S. Retrospective study of tetanus in 20 dogs: 1988–2004. *J Am Anim Hosp Assoc*. (2007) 43:143–148. doi: 10.5326/0430143

13. Shea A, Hatch A, Risico L, Beltran E. Association between clinically probable REM sleep behavior disorder and tetanus in dogs. *J Vet Intern Med*. (2018) 32:2029–36. doi: 10.1111/jvim.15320

14. Zitzl J, DyckersJ, Güssow A, Hazuchova K, Lehmann H. Survival in canine tetanus: retrospective analysis of 42 cases (2006–2020). *Front Vet Sci*. (2022) 15:1015569. doi: 10.3389/fvets.2022.1015569

15. Adamantos S, Boag A. Thirteen cases of tetanus in dogs. *Vet Rec*. (2007) 161:298–302. doi: 10.1136/vr.161.9.298

16. Papageorgiou V, Kazakos G, Anagnostou T, Polizopoulou Z. The role of magnesium in the management of acute and long-term symptoms caused by tetanus in two dogs. *Topics Comp Animal Med*. (2021) 44:100535. doi: 10.1016/j.tcam.2021.100535

17. Peter R, Nunley MK, Demetriades D, Velmahos G, Doucet JJ. Tetanus and trauma: a review and recommendations. *J Trauma*. (2005) 58:1082–8. doi: 10.1097/01.TA.0000162148.03280.02

18. Linnenbrink T, McMichael M. Tetanus: pathophysiology, clinical signs, diagnosis, and update on new treatment modalities. *J Vet Emerg Crit Care*. (2006) 16:199–207. doi: 10.1111/j.1476-4431.2006.00192.x

19. Medicine and Healthcare Products Regulatory Agency. *Non WHO Material, Tetanus Antitoxin, Equine, For Bioassay, 3rd British Standard*. (2012) Available online at: https://www.nibsc.org/documents/ifu/60-013.pdf

20. Mayousse V, Soete C, Jeandel A. Suspected generalized neonatal tetanus in a litter of puppies. *J Am Anim Hosp Assoc*. (2023) 59:51–5. doi: 10.5326/JAAHA-MS-7246

21. Firor WM. Intrathecal administration of tetanus antitoxin. *Arch Surg*. (1940) 41:299–307. doi: 10.1001/archsurg.1940.01210020095011

22. Soubasis N, Koutinas AF, Saridomichelakis MN, Polizopoulou ZS. Tetanus in the dog: a study of 6 cases. *Eur J Comp Animal Pract*. (2002) 12:19–23.

23. Steinman A, Haik R, Elad D, Sutton GA. Intrathecal administration of tetanus antitoxin to three cases of tetanus in horses. *Equine Vet Educ*. (2000) 12:237–40. doi: 10.1111/j.2042-3292.2000.tb00049.x

24. Sedaghatian MR. Intrathecal serotherapy in neonatal tetanus - controlled trial. *Arch Dis Child*. (1979) 54:623–5. doi: 10.1136/adc.54.8.623

25. Vakil BJ, Armitage P, Clifford RE, Laurence DR. Therapeutic trial of intracisternal human tetanus immunoglobulin in clinical tetanus. *T Roy Soc Trop Med H*. (1979) 73:579–83. doi: 10.1016/0035-9203(79)90058-0

26. Bhandari B, Ajmera NK, Jagetiya PR. Intrathecal anti-tetanus serum in management of tetanus neonatorum. *Indian J Med Res*. (1980) 72:685–7.

27. Abrutyn E, Berlin JA. Intrathecal therapy in tetanus. A meta-analysis. *J Am Med Assoc*. (1991) 226:2262–7. doi: 10.1001/jama.1991.03470160094039

28. Farrar JJ, Yen LM, Cook T, Fairweather N, Binh N, Parry J, et al. Tetanus. *J Neurol Neurosurg Psychiat*. (2000) 69:292–301. doi: 10.1136/jnnp.69.3.292

29. Bruce RB, Turnbull LB, Newman JH. Metabolism of methocarbamol in rat, dog and human. *J Pharm Sci*. (1971) 60:104–6. doi: 10.1002/jps.2600600120

30. Sahal M, Haydardedeoglu AE, Cingi CC. Generalized tetanus in a dog after ovariohysterectomy. *Kafkas Univ Vet Fak Derg*. (2011) 17:877.

31. Taruo A, Beltran E, Cherubini GB, Coelho AT, Wessmann A, Driver CJ, et al. Metronidazole-induced neurotoxicity in 26 dogs. *Aust Vet J*. (2018) 96:495–501. doi: 10.1111/avj.12772

32. Thwaites CL, Yen LM, Loan HT, Thuy TTD, Thwaites GE, Stepniewska K, et al. Magnesium sulphate for treatment of severe tetanus: a randomize controlled trial. *Lancet*. (2006) 368:1436–43. doi: 10.1016/S0140-6736(06)69444-0

33. Derbie A, Amdu A, Alamneh A, et al. Clinical profile of tetanus patients attended at Felege Hiwot Referral Hospital, Northwest Ethiopia: a retrospective cross-sectional study. *Springerplus*. (2016) 5:892. doi: 10.1186/s40064-016-2592-8

34. Panciera DL, Baldwin CJ, Keene BW. Electrocardiographic abnormalities associated with tetanus in two dogs. *J Am Vet Med Assoc*. (1988) 192:225–7.

35. Sharma N, Li S, Sravanthi MV, Kazmierski D, Wang Y, Sharma A, et al. Tetanus complicated by dysautonomia: a case report and review of management. *Case Rep Crit Care*. (2021) 88:42522.

36. Freshwater-Turner D, Udy A, Lipman J, et al. Autonomic dysfunction in tetanus - what lessons can be learned with specific reference to alpha-2 agonists? *Anaesthesia*. (2007) 62:1066–70. doi: 10.1111/j.1365-2044.2007.05217.x

37. Dolar D. The use of continuous atropine infusion in the management of severe tetanus. *Intens Care Med*. (1992) 18:26–31. doi: 10.1007/BF01706422

38. Ham L, Van Bree H. Conservative treatment of tetanus associated with hiatal hernia and gastro-oesophageal reflux. *J Small Anim Pract*. (1992) 33:289–94. doi: 10.1111/j.1748-5827.1992.tb01146.x

39. Dieringer TM, Wolf AM. Esophageal hiatal hernia and megaesophagus complicating tetanus in two dogs. *J Am Vet Med Assoc*. (1991) 199:87–9.

40. Bleck TP, Brauner JS. Tetanus. In: Eds Scheld WM, Whitley RJ, Durack DT, editor. *Infections of the Central Nervous System, 2nd ed*. Philadelphia: Lippincourt-Raven. (1997). p. 629–653.

41. Verma A, Solbrig MV. Infections of the nervous system. In: Bradley WG, Daroff RB, Fenichel GM, Jankovic J, editors. *Neurology in Clinical Practice: The Neurological Disorders, 4th ed*. Philadelphia: Butterworth Heinemann. (2004) p. 1510.

42. Illis LS, Taylor FM. Neurological and electroencephalographic sequelae of tetanus. *Lancet*. (1971) 7704:826–30. doi: 10.1016/S0140-6736(71)91496-6

43. Hanson CJ. Tetanus in a dog: a case report. *Vet Rec*. (1982) 110:336–7. doi: 10.1136/vr.110.14.336

44. Zontine WJ, Uno T. Tetanus in a dog. (A case report). *Vet Med Small Anim Clin*. (1968) 63:341–4.

45. Veronesi R, Bizzini B, Focaccia R, et al. Naturally acquired antibodies to tetanus toxin in humans and animals from the galapagos islands. *J Infect Dis*. (1983) 147:308–11. doi: 10.1093/infdis/147.2.308

46. Hammarlund E, Thomas A, Poore EA, Amanna IJ, Rynko AE, Mori M, et al. Durability of vaccine-induced immunity against tetanus and diphtheria toxins: a cross-sectional analysis. *Clin Infect Dis*. (2016) 62:1111–8. doi: 10.1093/cid/ciw066

47. Day JM, Horzinek MC, Schultz RD, Squires RA, WSAVA. Guidelines for vaccination of dogs and cats. *JSAP*. (2016) 57:E1–E45. doi: 10.1111/jsap.2_12431

frontiers | Frontiers in Veterinary Science

TYPE Review
PUBLISHED 11 December 2023
DOI 10.3389/fvets.2023.1270064

OPEN ACCESS

EDITED BY
Francisco Javier Salguero,
UK Health Security Agency (UKHSA),
United Kingdom

REVIEWED BY
Mihaela Niculae,
University of Agricultural Sciences and Veterinary Medicine of Cluj-Napoca, Romania
Peter Geldhof,
Ghent University, Belgium

*CORRESPONDENCE
Verónica Molina-Hernández
✉ vmolina@uco.es

†These authors have contributed equally to this work

RECEIVED 31 July 2023
ACCEPTED 30 October 2023
PUBLISHED 11 December 2023

CITATION
Flores-Velázquez LM, Ruiz-Campillo MT, Herrera-Torres G, Martínez-Moreno Á, Martínez-Moreno FJ, Zafra R, Buffoni L, Rufino-Moya PJ, Molina-Hernández V and Pérez J (2023) Fasciolosis: pathogenesis, host-parasite interactions, and implication in vaccine development.
Front. Vet. Sci. 10:1270064.
doi: 10.3389/fvets.2023.1270064

Fasciolosis: pathogenesis, host-parasite interactions, and implication in vaccine development

Luis Miguel Flores-Velázquez[1†], María Teresa Ruiz-Campillo[2†], Guillem Herrera-Torres[2], Álvaro Martínez-Moreno[3], Francisco Javier Martínez-Moreno[3], Rafael Zafra[3], Leandro Buffoni[3], Pablo José Rufino-Moya[3], Verónica Molina-Hernández[2]* and José Pérez[2]

[1]Unidad de Anatomía, Histología y Patología Veterinaria, Escuela de Medicina Veterinaria, Facultad de Ciencias Naturales, Universidad San Sebastián, Campus Puerto Montt, Puerto Montt, Chile, [2]Departamento de Anatomía y Anatomía Patológica Comparadas y Toxicología, UIC Zoonosis y Enfermedades Emergentes ENZOEM, Universidad de Córdoba, Córdoba, Spain, [3]Departamento de Sanidad Animal (Área de Parasitología), UIC Zoonosis y Enfermedades Emergentes ENZOEM, Universidad de Córdoba, Córdoba, Spain

Fasciola hepatica is distributed worldwide, causing substantial economic losses in the animal husbandry industry. Human fasciolosis is an emerging zoonosis in Andean America, Asia, and Africa. The control of the disease, both in humans and animals, is based on using anthelmintic drugs, which has resulted in increased resistance to the most effective anthelmintics, such as triclabendazole, in many countries. This, together with the concerns about drug residues in food and the environment, has increased the interest in preventive measures such as a vaccine to help control the disease in endemic areas. Despite important efforts over the past two decades and the work carried out with numerous vaccine candidates, none of them has demonstrated consistent and reproducible protection in target species. This is at least in part due to the high immunomodulation capacity of the parasite, making ineffective the host response in susceptible species such as ruminants. It is widely accepted that a deeper knowledge of the host-parasite interactions is needed for a more rational design of vaccine candidates. In recent years, the use of emerging technologies has notably increased the amount of data about these interactions. In the present study, current knowledge of host-parasite interactions and their implication in *Fasciola hepatica* vaccine development is reviewed.

KEYWORDS

***Fasciola hepatica*, pathogenesis, host-pathogen interaction, immunomodulation, vaccine, livestock, onehealth, zoonosis**

1 Introduction

Fasciolosis is a parasitic disease with worldwide distribution, excluding Antarctica. In livestock, it has major economic implications with estimated worldwide economic losses amounting to USD 3,200 million, including anthelmintic treatments, control of intermediate hosts (molluscicides), research, and the implication of economic losses in dairy and meat livestock production (1, 2).

Human fasciolosis has persisted since prehistoric times (3), and currently, it has a significant global health impact in specific geographic locations. The World Health Organization (WHO) has classified fasciolosis as a neglected tropical disease (4), and it is the most geographically distributed parasitic zoonosis (5, 6). *F. hepatica* human infections range between 2.4 and 17 million people (7), with 91 to 180 million people at risk of infection annually (8, 9).

Currently, the control of fasciolosis in ruminants continues to be based on management measures such as pasture rotation and the use of anthelmintics (10). The continued use of anthelmintics has resulted in an increase in parasite-resistant strains for the most effective and widely used flukicides, such as triclabendazole and albendazole (11, 12). Over the past three decades, there has been a rising interest in obtaining vaccines that help prevent and control fasciolosis in ruminants (13). However, the development of vaccines against fasciolosis has been slow, partly due to the great immunomodulatory capacity of the parasite. Hence, a better understanding of the parasite-host interactions is necessary for a more rational design of new vaccine candidates (14, 15).

2 Etiology and biological cycle of the parasite

Fasciolosis is caused by flukes of the genus Fasciola, known as liver flukes. The two species most implicated as the etiologic agents of fasciolosis are *F. hepatica,* which is distributed mainly in temperate climate regions, and *F. gigantica,* which is located in tropical regions. Further, hybrid forms have been described in regions where the two species coexist (16, 17). Real-time PCR (qPCR) targeting ITS1 rDNA, ITS2 rDNA, and 28S rDNA have been used to differentiate the two distinct genetic signatures representing each species (18–20). The epidemiological potential of hybridization and introgression between *F. hepatica* and *F. gigantica* remains unknown; therefore, it is important to use the correct terminology consistently and not use the two terms interchangeably (21).

The life cycle of *Fasciola spp.* is quite complex, involving several variations. In general, it involves one or more intermediate hosts, which are the mollusks. At least 20 species of the Lymnaeidae family have been reported as intermediate hosts (22, 23). The asexual larvae undergo several multiplications (24–26) before finally infecting a definitive host in which sexual reproduction occurs.

3 Pathogenesis

The penetration, migration, and localization of the parasites in the bile ducts exert a traumatic action that causes a series of lesions in the liver parenchyma and in the bile ducts (27). The newly excysted juveniles (NEJs) of *Fasciola spp.* penetrate the intestinal mucosa and can be found in the abdominal cavity 72 h after metacercaria ingestion. NEJs migrate through the peritoneum to the liver surface and present no clinical sinology in animals (28). The destination of the majority of NEJs is the left hepatic lobe, probably due to its anatomical proximity to the duodenum and the fact that they reach less of the other hepatic lobes. Sometimes, due to massive infestations, these juveniles can have an aberrant migration to other organs, such as the diaphragm and the lung, causing pneumonia and fibrinous pleurisy (29).

Fasciolosis pathogenesis occurs in two phases—the parenchymal and biliary phases. The parenchymal phase begins when the NEJs cross the liver capsule (Glisson's capsule), continuing with the migration of the juvenile stages through the liver parenchyma. This migration causes mechanical damage through abrasion by the tegument that presents spines that help maintain the parasite's position within the liver tissues and probably by-products secreted by migrating larvae. Several pathological processes occur simultaneously within the liver parenchyma, including the migration of juvenile stages that cause necrotic and hemorrhagic lesions, which, in turn, cause inflammatory reactions activating the immune system (30). This response can be found throughout the tortuous migrating trajectory of the parasites, suggesting that the excretion and secretion of these products remain in the tissue, attracting more infiltration of inflammatory cells of an immune nature (31). The biliary phase begins when the parasites enter the bile ducts, where they exert a combined mechanical and chemical action. Through the oral sucker, adult parasites cause mechanical damage while feeding on blood and the liver parenchyma adjacent to the duct. Macerated hepatocytes have been observed inside the sucker and pharynx (27), leading to erosion of the epithelium, trauma, focal rupture of the duct, and puncture of small blood vessels. The enlargement of the bile duct can be chemically induced (32), and it has been suggested that the amino acid proline, which is essential for the synthesis of collagen by fibroblasts, is also released in large quantities by the parasite (33, 34). These two actions exerted by the adult parasite cause a severe eosinophilic and granulomatous inflammatory response, particularly when eggs reach hepatic parenchyma (35), and marked hyperplasia of the bile ducts in which the parasites lodge (36).

The effect of these two phases causes a series of lesions in the liver parenchyma, which is widely correlated with the infective dose; a high dose causes more severe lesions that are more acute and even fatal. However, different studies carried out in sheep (35) and goats (37) have also shown that small repetitive doses (trickle infections) caused more severe hepatic damage than a single dose using the same total number of metacercariae. These findings suggest that the mechanical and enzymatic activities of the parasite may be the initial cause of liver damage. Therefore, the immune response or healing, as well as simultaneous infection at different stages and the immune response to the first infection, play an important role in the pathogenesis of fasciolosis (31).

4 Host immune response

4.1 Innate immune response

The initial recognition of NEJs takes place within the epithelial mucosa of the intestinal tract with extensive activation. The response to NEJs can occur through the recognition of glycosylated protein and carbohydrate residues that behave as tegumental antigens and induce T-cell proliferation through dendritic cell activation (38, 39). Excretory secretory products containing antigens released by *F. hepatica* (FhESP) can also induce a response of bovine macrophages, which is partially TLR4-dependent (40, 41).

The function of mast cells is not really defined, nor is there evidence that it is protective (42). These cells are residents of tissues that respond to activation of both the innate and acquired immune systems by producing and releasing different inflammatory mediators present in their cytoplasmic granules, prostaglandins, leukotrienes, and certain cytokines such as tumor necrosis factor-alpha (TNF-α) or interleukin-4 (IL-4) (43). In addition, they can release certain active substances against parasites by binding the parasite antigen-IgE complexes with their high-affinity IgE receptors (44, 45). It is estimated that its role is more decisive in the initial stages (peritoneum) of the infection (42, 46, 47). However, it has been described in cattle that after getting infected by *F. hepatica,* there is little evidence of an increase in the percentage of basophils and mast cells (48, 49) and in peritoneal fluid in sheep (50). In contrast, *F. gigantica* infection in buffaloes induces increases in the number of mast cells in the hepatic inflammatory infiltrate (51). In numerous parasitic processes, we can find a population of resident intraepithelial mast cells responsible for rapid parasite rejection phenomena at the epithelial level (52–54). However, these cells have neither been described in the intestine after the migration of *F. hepatica* (30, 36) nor in bile cells such as macrophages and neutrophils, whose function is phagocytic and can release substances such as reagents derived from nitric oxide or active oxygen species that act directly against the parasite (55, 56). On the other hand, infection by *F. hepatica* provokes a Th2-type immune response with IgE production (57) and infiltration of eosinophils and mast cells in the liver (48).

Human neutrophils from patients with acute fasciolosis showed a greater phagocytic function compared to those in the chronic stage of infection (58). Similarly, neutrophils from chronically infected goats showed a poor phagocytic response compared to those from uninfected goats. This poor phagocyte response was correlated with fluke burdens (59). The role of neutrophils in protective responses has not been reported yet in fluke infections.

In cattle, sheep, and goats, *F. hepatica* induces liver and blood eosinophilia, and *F. gigantica* infection in sheep gives the same profile (60–62). However, vaccination of calves and goats showing protection had reduced eosinophil counts (30, 63), which may be due to the lower fluke burdens and hepatic lesions in partially protected animals. In acute stages of *F. hepatica* infection, a dramatic increase of eosinophils has been described in the peritoneal cavity (50, 64) as well as in hepatic lesions, both during the migratory stage (30, 36, 65, 66) and during the chronic stage (35). Eosinophils have been shown to mediate antibody-dependent cell cytotoxicity (ADCC) against *F. hepatica* in rats (42). In Indonesian thin-tailed (ITT) sheep which display resistance to *F. gigantica* but not *F. hepatica,* it has been observed that ADCC by eosinophils plays a role (*ex vivo*) in killing *F. gigantica* but not *F. hepatica* newly excysted juveniles (NEJs) (56). However, peripheral eosinophilia was not related to resistance to *F. gigantica*, suggesting that this cell type is effective only within the gut or peritoneal cavity but not the liver, at least in ITT sheep (67).

Peritoneal macrophages from ITT sheep have also been shown to kill *F. gigantica* but not *F. hepatica* by ADCC (56, 68). This mechanism occurs by attaching effector cells with NEJs in the presence of serum from infected sheep. Macrophages participating in the effective ADCC mechanism against *F. gigantica* showed increased levels of superoxide radicals than those participating in ineffective ADCC against *F. hepatica*, suggesting oxygen radicals play a role in killing *F. gigantica* NEJs (56). It has been reported that in calves protected by experimental vaccination, ADCC mediated by macrophages is nitric oxide-mediated and induces a Th1 cytokine response relying on IgG2a (69). *In vitro* studies have revealed that bovine macrophages were able to kill NEJs in the presence of serum from infected animals. However, NEJs were able to produce molecules such as a family of TGF-like molecules (FhTLM) that significantly reduces ADCC. These macrophages showed features of alternative activation with the expression of high levels of IL-10 (70). In non-protected animals, it has been observed that NEJs induce alternative (M2) activation of macrophages and secrete the regulatory cytokines IL-10 and transforming growth factor-beta (TGF-β) during the peritoneal migration (71–73). M2-activated macrophages have an important role in tissue repair, but they have a reduced capacity to kill NEJs (41, 70).

4.2 Adaptive immune response

B-cells have shown importance in *Fasciola spp.*-infected animals as well as in those that have been previously vaccinated (74), highlighting the increase in CD19+ B-cells at the level of hepatic lymph nodes, increasing the recruitment of these cells (66). In cattle, sheep, and goats, IgG1 is the dominant antibody, raising at 4–5 weeks post-infection (wpi) and reaching peaks at 12–15 wpi (37, 75, 76). An increase in specific IgG2 has been shown to correspond to vaccine-induced protection, and an increase in IgG1 has been associated with a non-protective Th2 response (76–78). IgA specific for fluke antigens has not been detected in serum (75), but it has been found in the bile and liver of infected cattle (51), where this immunoglobulin may participate in activating eosinophils to kill NEJs by ADCC (49). Despite this interesting suggestion, few studies have investigated the presence of IgA in bile and liver in both experimental and natural infections.

The immune response exerted during the early stages of fasciolosis is generally regarded as a mixed Th1/Th2 response displaying an increase of certain cytokines such as IFN-γ, IL-4, IL-10, and TGF-β. As the infection progresses, a Th2 response is amplified in conjunction with suppression of Th1 inflammation, thus allowing a prolonged infection that may be dependent on IL-4 (79). In the early stages of sheep and cattle *F. hepatica* infection, both IFN-γ and IL-10 are increased, confirming the initial mixed immune response (75, 80, 81). When the infection progresses, a Th2 response is amplified in conjunction with suppression of Th1 response with reduced IFN-γ and increased IL-4 levels (79). In the early stages of bovine *F. hepatica* infection, both IFN-γ and IL-10 are increased, corroborating the idea that the initial immune response is mixed (75). Buffaloes with both primary and secondary infection of *F. gigantica* also showed a mixed Th1/Th2 response in serum with elevated IFN-γ, IL-4, IL-5, and TGF-β during the early stages of infection. In contrast, when the infection progressed, the Th2 response was dominant (82). The Th1/Th2 response was not the same in different compartments—in sheep liver, IFN-γ increased during the early stages of infection (80, 81), and it remained high during chronic states of infections (81). At the

same time, in the hepatic lymph nodes, IFN-γ was reduced both in infected and reinfected animals in acute and chronic stages of infections (81). The high levels of IFN-γ reported in the liver during acute and chronic stages of *F. hepatica* infections contrast with the downregulation of this cytokine in PBMC (83) and hepatic lymph nodes (80, 81) and could be due to a response to hepatic necrosis caused by migrating or adult flukes and granulomata formation.

5 Immunomodulation strategies

The inflammatory reaction in fasciolosis is one of the points to be treated primarily to understand the immune response and its evasion. Since metacercariae are excysted in the gut lumen, NEJs are exposed to the host immune response to kill the parasite. However, *Fasciola spp.* has developed a variety of strategies to evade the host response in the different compartments where they stay during the early and late stages of infection, which allows the parasite to live for years within the host. Some of these strategies may be considered passive, as the protection conferred by the tegument, which consists of a syncytial layer covering the entire body of the parasite, formed by a plasma membrane that serves as a support for the outer glycocalyx and a basement membrane that is connected through channels. These structures allow the passage of the components needed for the replacement of the tegument. The rapid replacement of the glycocalyx that covers the tegument—which takes place every 2 to 3 h—may also be an obstacle for products released by inflammatory cells to reach the parasite tegument (84), which is composed of at least 369 proteins. Additionally, the presence of abundant N-glycosylated proteins and glycolipids has made it difficult to characterize its physiological and immune regulatory functions (85).

The majority of strategies used by the parasite to evade the host response may be considered active since they imply the release of a large amount of parasite molecules into the parasite vicinity. These molecules can be released free or within extracellular vesicles (EVs) that are covered by a membrane, and they can be internalized by the host cells, causing their modulation (84, 85). EVs are produced by all developmental stages of *F. hepatica,* and they are considered efficient transporters of parasite molecules to different host compartments, preventing the action of antibodies due to the membrane surrounding the parasite molecules contained in EVs (86). In EVs from *F. hepatica,* up to 618 proteins have been identified, which gives us an idea of how important EVs are for the parasite to interact with the host (87).

Fasciola spp. not only use proteins to modulate the host immune response, but EVs also contain microRNAs (miRNAs), molecules with modulating gene expression capacity. miRNAs are abundant in both metacercariae, juvenile and adult *F. hepatica* worms and may play a main role in regulating the developmental and metabolic processes of the parasite, as well as in host-parasite interactions (88–90). The miRNA content in the EVs is different when they are produced by adult or juvenile parasites, leading to different influences in the host cells. These data support the hypothesis that miRNAs are the mediators of the previously demonstrated immune modulatory function of the EVs. However, current data do not allow a fundamental understanding of their regulatory mechanisms in different processes of host-parasite interaction (88–91).

Another mechanism used by liver fluke to survive, migrate, obtain nutrients, and evade the immune response of the host, is the release of excretory secretory products (ESP) (92). FhESP from adult *F. hepatica* contains up to 160 different proteins, including proteases such as cathepsins B and L (FhCB and FhCL), leucine aminopeptidase and carboxypeptidase, fatty acid-binding protein (FABP), and the *F. hepatica* saposin-like protein (FhSAP), all of them necessary for its metabolism (93) (Table 1). FhESP also contains numerous antioxidant enzymes to protect the parasite from reactive oxygen species released by eosinophils and macrophages, such as superoxide dismutase (SOD), glutathione-S-transferase (GST), thioredoxin peroxidase (TPx), and peroxiredoxin (Px) (Table 1). These enzymes not only participate in inactivating reactive oxygen species but also in several important metabolic processes important for parasite survival, such as the excyst of the metacercariae, tissue migration, feeding, and immune evasion (92, 105, 106). Some strategies that *Fasciola spp.* use to evade the host response are discussed below.

5.1 Parasite movement

During the hepatic migration, it has been reported that some larvae show a heavy inflammatory infiltrate, mainly composed of eosinophils attached to the parasite cuticula and in the vicinity of the parasite. However, in other larvae, no inflammatory reaction was found in their vicinity, but necrotic tract and inflammation were observed 2–3 mm behind them (30, 36). It has been suggested that when the parasites are disturbed by the inflammatory reaction, they move ahead, leaving the inflammatory cells behind them (66).

5.2 Apoptosis of effector and immune cells

There is an intimate connection between the inflammatory response and the immune response when suffering from fasciolosis. The innate immune response determines the cell populations involved in the inflammatory response by attracting and activating inflammatory cells (107). Eosinophils play a key role in the host response to *Fasciola spp* infection, as suggested by the rapid increase of this cell type in blood, peritoneum, and liver during the early migration of juveniles in sheep (35, 60), cattle (48), and rodents (108). *In vitro* studies have reported that FhESP antigens from *F. hepatica* induce apoptosis of rat eosinophils and macrophages (109, 110). *In vivo* studies have described apoptosis in eosinophils in the liver inflammatory infiltrate during the acute and chronic phases of infection in sheep (65) and the migratory stage in a relevant percentage of peritoneal macrophages, eosinophils, and lymphocytes (50). Increased expression of the pro-apoptotic gene in peripheral blood mononuclear cells of infected sheep and cattle has also been reported (111, 112). More recently, the role of a variety of *F. hepatica* molecules in the induction of apoptosis has been investigated; some of them have been identified as glutathione S-transferase Omega type (GSTO1), which down-regulated the ratio of Bcl-2/Bax and induced increased expression of caspase-3

TABLE 1 *F. hepatica* molecules involved in host immune modulation/evasion.

Molecule	Actions	References
Antioxidants:		
Peroxiredoxins	Antagonizes actions of ROS and induces M2 activation of macrophages	(71)
Thioredoxins		(72)
Glutathione-S- transferase		
Superoxide dismutase		
Glutathione-S-transferase	Induces IL-1β, IL-6, and TNF-α production	(94)
Omega type (GSOT1)	Reduces IL-10 production	
	Induces of macrophage	
Cysteine proteases		
Cathepsins L, B	Reduced eosinophils attachment	(95)
Leucine aminopeptidase	Suppression of Th1, Th17	(96)
	Responses, anticoagulants	
Protease inhibitors:		
Kunitz type molecule	Suppression of Th1, Th17 responses	(97)
Other molecules:		
Fatty binding proteins	Reduction of pro-inflammatory cytokines	(93, 98)
	Induces apoptosis of dendritic cells	(99)
Helminth defense molecule-1	Inhibits APC antigen presentation	(100)
	Inhibits release of IL-1β	
Mucin-like peptides	Increases Th1-type response	(101, 102)
TGF-like molecule	Induces M2-activated macrophages	(70)
Serpin	Prevents the activation of the Lectin complement pathway	(103)
Cystatin	Inhibits NO, IL-6, TNF-α, and promotes the expression of TNF-β and IL-10	(104)
	Induces apoptosis of murine macrophages	(104)

and apoptosis of macrophages *in vitro* (94). Recombinant cystatin from *F. hepatica* (rFhCystatin) has been shown to induce apoptosis of murine macrophages (104), and fatty acid binding protein (Fh12) induced apoptosis of murine dendritic cells in *in vitro* studies (99).

5.3 Modulation of Th1/Th2 and Th17 responses

The immune response mounted during the early stages of fasciolosis is generally a mixed Th1/Th2 response with elevated levels of cytokines such as IFN-γ, IL-4, IL-10, and TGF-β. As the infection progresses, a Th2 response is amplified in conjunction with the suppression of Th1 cytokine production, particularly IFN-γ, which facilitates parasite survival in mice, cattle, and sheep infected with *F. hepatica* (41, 79–81, 113). A similar Th1/Th2 dynamic has been reported in buffaloes infected with *F. gigantica* (82). It has been reported that a variety of parasitic molecules are able to produce modulation of the Th1/Th2 host response; thus, rFhCystatin induced reduced production of IL-6 and TNF-α and increased production of IL-10 and TGF-β in murine macrophages (104). *F. hepatica* Kunitz-type molecule induced suppression of the Th1 and Th17 responses in murine and human dendritic cells (DC) in *in vitro* studies (97).

5.4 Modulation of macrophage and antigen-presenting cell functions

In the early stages of *F. hepatica* infection, the recruitment of macrophages and alternative (M2) activation in the peritoneal cavity has been reported in rats at 24 h post-infection (hpi) (71) and at 48 hpi in mice (114). Moreover, FhESP induced M2 activation of peritoneal macrophages in mice (114). In sheep, marked M2 activation has been described by gene expression in PBMC at 7 dpi (83), although peritoneal sheep macrophages showed M2 activation at 24 hpi (73). In cattle, *F. hepatica* also induced M2-activation of macrophages (115, 116). M2-activated macrophages participate in tissue repair, but they show limited ability to control helminth infections (117). *F. hepatica* possesses FhTLM, which is highly expressed in NEJs and unembryonated

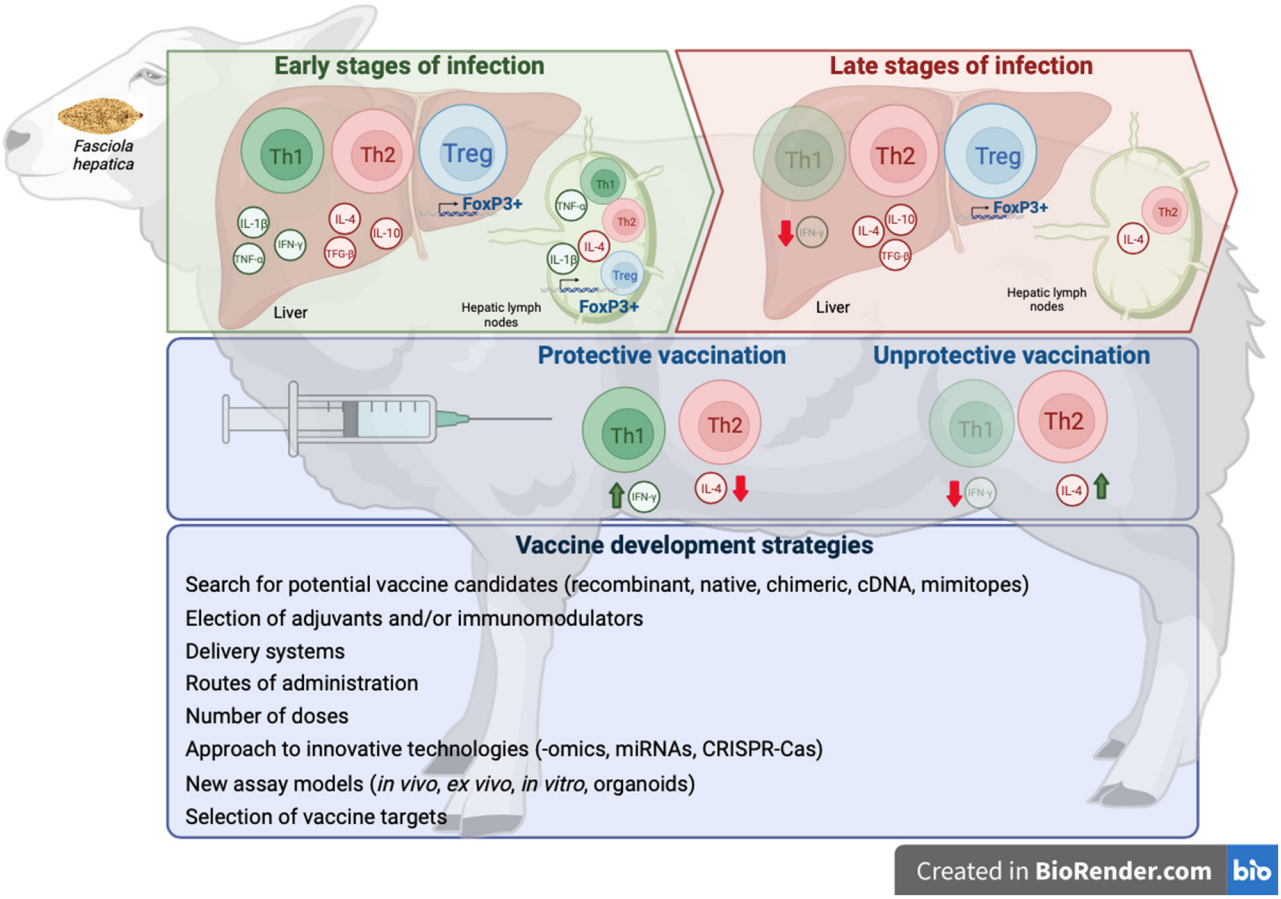

FIGURE 1
Scheme of immune responses exerted at early and late stages of *F. hepatica* infections, immune responses induced by protective and unproductive vaccines against *F. hepatica,* and strategies to develop effective vaccines. Created with BioRender.com.

eggs. It has been reported that FhTLM induces the differentiation of the monocyte-derived macrophages to M2 activation with increased production of IL-10, arginase-1, mannose receptor, and PD-L1 (70).

It has been reported that different antigenic preparations of this parasite, such as total extract, *F. hepatica* tegumental antigen (FhTeg), and *Fasciola hepatica* ESP, decrease the activation state of dendritic cells (DCs) in mice (118–121), and *F. gigantica* ESP induces the modulation of buffalo DCs (122). More specifically, it has been reported that FhTeg induces DC modulation, provoking the absence of T-cell Th1 cytokine response and proliferative activity (38). Glycan products produced by *F. hepatica* have also been reported to induce modulation of DC maturation, resulting in increased production of IL-10 and IL-4 during infection, inducing a Th2/regulatory-polarized immune response (40, 79, 113, 123, 124). In addition, *F. hepatica* cathepsin L1 (FhCL1), glutathione S-transferase (FhGST), and Kunitz-type molecule participate in the modulation of DCs, leading to the suppression of the adaptive immune responses, Th1, and/or Th17 (40, 97). *F. hepatica*-infected sheep showed increased numbers of DCs in the hepatic lymph nodes but reduced expression of MHC class II and CD83, suggesting suppression of the antigen-presentation process in lymphocytes both in the early and late stages of infection (125).

5.5 Expansion of T regulatory cells

F. hepatica-infected sheep and goats showed expansion of T regulatory cells (Treg) Foxp3+ during early and late stages of infection in the liver and hepatic lymph nodes (50, 81, 126). Moreover, the increase of Foxp3+ cells was more severe in the vicinity of hyperplastic bile ducts during chronic states of infections (50). This expansion of Foxp3+ Treg has been related to IL-10 and parasite survival (127, 128).

6 Vaccine development

Over the past two decades, there have been considerable advances in identifying potential vaccine molecules for the control of fasciolosis in livestock. However, despite some promising results with some vaccine candidates in ruminants, a consistent efficacy required for commercialization has not yet been reached (13). A major obstacle to developing vaccines for fasciolosis is the immune suppression/modulation induced by *Fasciola spp*. that prevents the induction of a protective immune response (Figure 1), evidenced by the lack of immunity observed in naturally and experimentally infected sheep (31, 70, 129). In cattle, natural or experimental infections have been shown to induce certain protection against

TABLE 2 Summary of fasciolosis single vaccines in livestock.

Antigen (μg per dose)	Species (sex_age)/No. per group	Admin. Route (no. doses)/time	Adjuvant	Efficacy†	References
Cathepsin L					
rFhCL1 (200)	Cattle (m_3-8mo.)/13	s.c.(2)/3w	Montanide™ ISA 70VG or 206VG	48%	(69)
rFhCL1 (100)	Goat (m_4mo.)/10	s.c.(2)/4w	QuilA	ns	(30)
rFhpCL1 (100)	Sheep (f_4-6mo.)/5	s.c.(2)/4w	QuilA	ns	(138)
CL1 mimitopes (§)	Sheep (nd_9mo.)/5	s.c.(2)/2w	None	51%	(139)
CL1 mimitopes (§)	Sheep (m_9mo.)/5	s.c.(2)/4w	QuilA	57.5%	(140)
CL2 mimitopes (§)	Sheep (m_9mo.)/5	s.c.(2)/4w	QuilA	ns	(140)
CL1 mimitopes (§)	Goat (m_9mo.)/5	s.c.(2)/4w	QuilA	55.4%	(141)
CL1 mimitopes (§)	Goat (m_9mo.)/5	s.c.(2)/4w	QuilA	70.4%	(141)
CL2 mimitopes (§)	Goat (m_9mo.)/5	s.c.(2)/4w	QuilA	ns	(141)
CL1 mimitopes (§)	Goat (nd_6mo.)/6	s.c.(2)/4w	QuilA	46.9-79.5%	(134)
Cathepsin					
rCPFhW (300)	Sheep (m&f_5mo.)/6	oral(2)/4w	None	35.5%	(142)
rCPFhW (500)	Cattle (m&f_5-7mo.)/6	oral(2)/4w	None	56.2%	(142)
Leucine Amino-Peptidase (LAP)					
rFhLAP (100)	Sheep (m_12mo.)/10	s.c.(2)/4w	FCA/FIA, Adyuvac 50, Alum, DEAE-D, or Ribi	49–89%	(143)
rFgLAP (150&300)	Buffalo (nd_8-10mo.)/7	i.m.(3)/3w	Montanide™ M-70 VG	ns	(144)
Fatty acid binding protein (FABP)					
rFh15 (150)	Sheep (nd_nd)/6	s.c.(2)/5d	ADAD (Qs, PAL, Montanide™ ISA763A)	43%	(145)
rFgFABP (400)	Buffalo (nd_8-10 mo.)/5	s.c.(3)/3w	FCA/FIA	35%	(146)
rFgFABP (400)	Buffalo (nd_8-10 mo.)/7	i.m.(3)/3w	Montanide™ M-70 VG	ns	(147)
rSm14 (100)	Goat (m_6mo.)/7	s.c.(2)/4w	QuilA	ns	(148)
Glutathione S transferase					
rFgGST (400)	Buffalo (nd_8-10 mo.)/7	i.m.(3)/3w	Montanide™ M-70 VG	ns	(147)
rFhGST (100)	Goat (m_4mo.)/10	s.c.(2)/4w	QuilA	ns	(36)
Helminth defense molecule					
sMF6p/FhHDM1 (100)	Sheep (f_4-6mo.)/5	s.c.(2)/4w	QuilA	6%	(138)
nMF6p/FhHDM1 (100)	Sheep (f_4-6mo.)/5	s.c.(2)/4w	QuilA	15%	(138)
Thioredoxin					
rFhTGR (300)	Cattle (nd_nd)/8	s.c.(3)/4w	FIA	8.2%	(149)
rFhTGR (400)	Cattle (nd_nd)/6	s.c.(2)/4w	Adyuvac50	3.8%	(149)
rFhTGR (400)	Cattle (nd_nd)/6	s.c.(2)/4w	Alum	23%	(149)
Glutathione reductase phospho-glicerate kinase					
cFhPGK/pCMV (100)	Sheep (m_5mo.)/8	i.m. (3)/4w	Montanide™ ISA 206	ns	(150)
cFhPGK/pCMV (100)	Sheep (m_5mo.)/6	i.m. (3)/4w	CTLA-4	ns	(150)
14-3-3z					
r14-3-3z (100)	Sheep (f_6mo.)/8	s.c.(2)/4w	Montanide™ ISA 71 VG	ns	(151)
Tetraspanin					
rFhTSP2 (200)	Cattle (f_6mo.)/6	s.c.(2)/4w	FCA/FIA	ns	(152)

†percentage expressing only significant efficacy; §1 × 10^{13} phage particles; ADAD, Adaptation adjuvant (ADAD) system; c, cDNA; d, days; DEAE-D, Diethylaminoethyl-dextran; f, female; FCA/FIA, Freund's complete adjuvant and Freund's incomplete adjuvant; Fh, *Fasciola hepatica*; Fg, *Fasciola gigantica*; i.m., intramuscular; m, male; mo., months; n, native; nd, not defined; ns, non-significant; PAL, the hydroalcoholic extract of *P. leucotomos*; Qs, saponin from *Q. saponaria*; r, recombinant; Ribi, MPL + TDM + CWS Adjuvant System (Sigma–Aldrich); s, synthetic; s.c., subcutaneous; w, weeks apart between doses.

TABLE 3 Summary of fasciolosis combined vaccines in livestock.

Antigens (μg each per dose)	Species (sex_age)/No. per group	Admin. Route (no. doses)/time	Adjuvant	Efficacy†	References
CL1 + CL2 mimitopes (§)	Sheep (m_9mo.)/5	s.c.(2)/4w	QuilA	ns	(140)
CL1 + CL2 mimitopes (§)	Goat (m_9mo.)/5	s.c.(2)/4w	QuilA	32.4%	(141)
rmFhCL1 + rmFhCL3 (200)	Cattle (m_6-8mo.)/5	s.c.(2)/3w	ZA1	37.6%	(153)
rmFhCL1 + rmFhCL3 (200)	Cattle (m_5-11mo.)/5	s.c.(2)/2w	ZA1	ns	(153)
rCatL5 + rCatB2 (150)	Sheep (m_5mo.)/8	i.m.(3)/4w	QuilA	20.9%	(154)
rCatL5 + rCatB2 (75)	Sheep (m_5mo.)/8	i.n.(3)/4w	CpG-ODN + ISC-adjuvant	40.5%	(154)
rFhLAP + chCL1(100)	Sheep (m_8mo.)/5	s.c.(2)/2w	QuilA	25.5%	(155)
rFhLAP + chCL1(200)	Sheep (m_8mo.)/5	s.c.(2)/2w	QuilA	30.7%	(155)
rFhLAP + chCL1(400)	Sheep (m_8mo.)/5	s.c.(2)/2w	QuilA	40.6%	(155)
rFhTeg1 + rFhTeg5 (200)	Cattle (f_6mo.)/7	nd(2)/4w	FCA/FIA	ns	(156)
rFhCL1 + rFhHDM + rFhLAP + rFhPrx (100)	Sheep (m_8mo.)/10	s.c.(2)/4w	Montanide™ ISA 61	37.2%	(157)
rFhCL1 + rFhHDM + rFhLAP + rFhPrx (100)	Sheep (m_8mo.)/10	s.c.(2)/4w	Alum	ns	(157)
rFhStf1 + rFhStf2 + rFhStf3 + rFhKT1 (100)	Sheep (f&m_8mo.)/14	s.c.(3)/3w	Montanide™ ISA 61	17.4%	(15)
rFhStf1 + rFhStf2 + rFhStf3 + rFhKT1 (100)	Sheep (m_8mo.)/13	s.c.(3)/3w	Montanide™ ISA 61+CpG	0%	(15)
rLTB-rFhTSP2 (451)	Cattle (f_6mo.)/6	i.n.(2)/4w	None	ns	(152)

†percentage expressing only significant efficacy; §1 × 10^{13} phage particles; CatL5, Cathepsin L5; CatB2, Cathepsin B2; CL1, Cathepsin L1; CL2, Cathepsin L2; CpG-ODN, CpG-oligodeoxynucleotide; ch, chimeric; d, days; f, female; FCA/FIA, Freund's complete adjuvant and Freund's incomplete adjuvant; Fh, *Fasciola hepatica*; HDM, helminth defense molecule; i.m., intramuscular; i.n., intranasal; ISC-adjuvant by Zoetis; KT1, K unit 1; LAP, Leucin aminopeptidase; LTB, Heat labile enterotoxin B subunit; m, male; mo., months; nd, not defined; ns, non-significant; Prx, Peroxiredoxin; r, recombinant; rm, recombinant mutant; s, synthetic; s.c., subcutaneous; Stf, Stefin; Teg1, Tegumental glycoprotein 1; Teg5, Tegumental glycoprotein 5; TSP2, Tretaspanin 2; w, weeks apart between doses.

reinfection, which is maintained long-term (up to 26 weeks post-infection). It has been attributed to the severe fibrosis induced by the primary infection that makes the hepatic migration difficult during the secondary infection (130) or by an increase of intestinal eosinophil and mucosal mast cells (47). Some studies have also reported evidence that protection against *F. hepatica* is inducible in rats, sheep, or cattle by passive transfer of immune sera and cells (131). However, other studies have reported no resistance to reinfection measured by fluke burdens (75). Moreover, no differences in fluke burdens, fecal egg counts, humoral response (specific IgG1 and IgG2), and cell-mediated immune response (IFN-γ production) were reported in calves challenged with *F. hepatica* after single or trickle infection (48, 57, 75) suggesting that reinfections do not induce protection. Experimental studies reported no protection against reinfection in sheep (35, 81, 132) and goats (37), although the host response was different; thus, primo-infected sheep showed a mixed Th1/Th2/Th17 response while reinfected ones presented a more Th2 polarized response (81) and a lower humoral response (132).

It has been reported that in protective vaccines in sheep (133) and goats (134), a mixed Th1/Th2 response was found with higher levels of IFN-γ and lower levels of IL-4 in vaccinated groups than in the infected control group (133). In sheep immunized with a non-protective vaccine, the host immune response showed a predominantly Th2 profile during chronic stages of the infection, similar to that found in non-vaccinated and infected animals (80). The challenge is to identify the specific antigens that are the targets of this protective immunity and incorporate these in vaccine

formulations that induce a mixed Th1/Th2 response to enhance vaccine efficacy (135). It has been estimated that a vaccine with an efficacy of 50–60% in fluke reduction would likely be beneficial in numerous countries to significantly reduce economic losses, and it also would have a positive impact on epidemiology by reducing eggs in pasture (13).

Several strategies have been used to design vaccine candidates for fasciolosis in livestock. The first vaccine trials used native proteins isolated using conventional biochemical methods from the excreted/secreted (ES) proteins of adult parasites (136, 137). Despite good protection being found in sheep and cattle in these trials using native FhCL1 and FhGST, the use of native proteins in a commercial vaccine for fasciolosis in livestock is not feasible, which is why the majority of subsequent vaccine trials have been carried out using recombinant proteins of different stages of the parasite (13). Some vaccine trials using recombinant proteins reported high protection of up to 89% in fluke reduction (Tables 2, 3); however, this high protection has not been reproducible in different labs and conditions. A combination of recombinant vaccines (cocktail vaccines) has also been used recently with variable efficacy (Table 3). The majority of vaccine trials have used the subcutaneous or intramuscular administration route. However, a few trials have used mucosal vaccine delivery with promising results. For instance, Norbury et al. (154) administered a cocktail vaccine containing FhCL5 and FhCB2 by an intranasal method in sheep, obtaining a 40.5% fluke reduction and a 92% egg viability reduction, while the same vaccine administered intramuscularly did not induce protection. The oral route has also been used to administer freeze-dried transgenic lettuce expressing the cysteine proteinase of *F. hepatica* (CPFhW) in sheep and cattle, inducing significant protection in cattle (56.2%) and 35.5% fluke reduction (not significant) in sheep (142).

Most vaccine trials in ruminants have used proteases, antioxidant enzymes, or fatty acid-binding proteins as antigens (Tables 2, 3). However, these proteins are quite abundant in *Fasciola* spp, and blocking one or several of them by a vaccine probably does not cause serious problems to the worm since it has other proteins with similar functions. This might be a reason for the limited efficacy obtained in the numerous vaccine trials conducted with these antigens in ruminants.

7 Conclusion and remarks

The slow progress to date in developing a protective vaccine to be used in the control of fasciolosis in livestock suggests that new approaches should be investigated, such as the use of new antigens, evaluation of immunity induced by recombinant proteins, use of different adjuvants, formulations, and delivery systems. Despite important advances in the knowledge of host-parasite interactions in fasciolosis, a more rational vaccine candidate design requires a deeper knowledge of the mechanisms and molecules involved in host-parasite cross-talk in relevant target host species (sheep, cattle, goats, buffalo). The progress of the -omics technologies and the immunoinformatic/immunoproteomic approaches should provide useful data in the next few years. An example is the new proteomic technologies applied to NEJs after crossing the gut (158) or during the early stages of hepatic migration, which may be useful to select new vaccine candidates directed against NEJs, a stage of the parasite that it is more exposed to the host immune system than adult ones located within the bile ducts.

Author contributions

LF-V: Writing—original draft. MR-C: Writing—original draft. GH-T: Writing—review & editing. ÁM-M: Writing—review & editing. FM-M: Writing—review & editing. RZ: Writing—review & editing. LB: Writing—review & editing. PR-M: Writing—review & editing. VM-H: Conceptualization, Writing—original draft, Writing—review & editing. JP: Conceptualization, Writing—original draft, Writing—review & editing.

Funding

The author(s) declare that financial support was received for the research, authorship, and/or publication of this article. The work has been supported by National Grant PID2019-108782RB-C21. VM-H was supported by the financial support of the Regional Government of Andalusia (Junta de Andalucía, Consejería de Conocimiento, Investigación y Universidad)-FEDER (project P18-RTJ-1956).

Conflict of interest

The authors declare that the research was conducted in the absence of any commercial or financial relationships that could be construed as a potential conflict of interest.

Publisher's note

References

1. Mehmood K, Zhang H, Sabir AJ, Abbas RZ, Ijaz M, Durrani AZ, et al. A review on epidemiology, global prevalence and economical losses of fasciolosis in ruminants. *Microb Pathog.* (2017) 109:253–62. doi: 10.1016/j.micpath.2017.06.006

2. Hayward AD, Skuce PJ, McNeilly TN. The influence of liver fluke infection on production in sheep and cattle: a meta-analysis. *Int J Parasitol.* (2021) 51:913–24. doi: 10.1016/j.ijpara.2021.02.006

3. Dittmar K, Teegen WR. The presence of *Fasciola hepatica* (liver-fluke) in humans and cattle from a 4,500 year old archaeological site in the Saale-Unstrut valley, Germany. *Mem Inst Oswaldo Cruz.* (2003) 98(Suppl 1):141–3. doi: 10.1590/S0074-02762003000900021

4. WHO. *Neglected Tropical Diseases.* Geneva: World Health Organization (2017). Available online at: http://www.who.int/neglected_diseases/diseases/en/ (accessed May 30, 2020).

5. Cabada MM, White AC Jr. New developments in epidemiology, diagnosis, and treatment of fascioliasis. *Curr Opin Infect Dis.* (2012) 25:518–22. doi: 10.1097/QCO.0b013e3283567b7e

6. Nyindo M, Lukambagire AH. Fascioliasis: an ongoing zoonotic trematode infection. *Biomed Res Int.* (2015) 2015:786195. doi: 10.1155/2015/786195

7. Mas-Coma S, Valero MA, Bargues MD. Fascioliasis. *Adv Exp Med Biol.* (2019) 1154:71–103. doi: 10.1007/978-3-030-18616-6_4

8. Mas-Coma S. Epidemiology of fascioliasis in human endemic areas. *J Helminthol.* (2005) 79:207–16. doi: 10.1079/JOH2005296

9. Keiser J, Utzinger J. Food-borne trematodiases. *Clin Microbiol Rev.* (2009) 22:466–83. doi: 10.1128/CMR.00012-09

10. Carson A, Jones B, Grove-White D. Managing liver fluke on hill farms. *Vet Rec.* (2022) 191:115–7. doi: 10.1002/vetr.2105

11. Fairweather I. Reducing the future threat from (liver) fluke: realistic prospect or quixotic fantasy? *Vet Parasitol.* (2011) 180:133–43. doi: 10.1016/j.vetpar.2011.05.034

12. Carmona C, Tort JF. Fasciolosis in South America: epidemiology and control challenges. *J Helminthol.* (2017) 91:99–109. doi: 10.1017/S0022149X16000560

13. Spithill TW, Toet H, Rathinasamy V, Zerna G, Swan J, Cameron T, et al. Vaccines for fasciola: new thinking for an old problem. In: Dalton, JP, editor. *Fasciolosis 2nd edn*. Cambridge: CABI Publishing (2022). p. 379–422. doi: 10.1079/9781789246162.0012

14. Beesley NJ, Caminade C, Charlier J, Flynn RJ, Hodgkinson JE, Martinez-Moreno A, et al. Fasciola and fasciolosis in ruminants in Europe: identifying research needs. *Transbound Emerg Dis.* (2018) 65(Suppl 1):199–216. doi: 10.1111/tbed.12682

15. Cwiklinski K, Drysdale O, López Corrales J, Corripio-Miyar Y, De Marco Verissimo C, Jewhurst H, et al. Targeting secreted protease/anti-protease balance as a vaccine strategy against the helminth *Fasciola hepatica*. *Vaccines.* (2022) 10:155. doi: 10.3390/vaccines10020155

16. Agatsuma T, Arakawa Y, Iwagami M, Honzako Y, Cahyaningsih U, Kang SY, et al. Molecular evidence of natural hybridization between *Fasciola hepatica* and F. gigantica. *Parasitol Int.* (2000) 49:231–8. doi: 10.1016/S1383-5769(00)00051-9

17. Lotfy WM, Brant SV, DeJong RJ, Le TH, Demiaszkiewicz A, Rajapakse RP, et al. Evolutionary origins, diversification, and biogeography of liver flukes (Digenea, Fasciolidae). *Am J Trop Med Hyg.* (2008) 79:248–55. doi: 10.4269/ajtmh.2008.79.248

18. Marcilla A, Bargues MD, Mas-Coma S. A PCR-RFLP assay for the distinction between *Fasciola hepatica* and *Fasciola gigantica*. *Mol Cell Probes.* (2002) 16:327–33. doi: 10.1006/mcpr.2002.0429

19. Alasaad S, Soriguer RC, Abu-Madi M, El Behairy A, Jowers MJ, Baños PD, et al. A TaqMan real-time PCR-based assay for the identification of *Fasciola* spp. *Vet Parasitol.* (2011) 179:266–71. doi: 10.1016/j.vetpar.2011.01.059

20. Calvani NED, Ichikawa-Seki M, Bush RD, Khounsy S, Šlapeta J. Which species is in the faeces at a time of global livestock movements: single nucleotide polymorphism genotyping assays for the differentiation of *Fasciola* spp. *Int J Parasitol.* (2020) 50:91–101. doi: 10.1016/j.ijpara.2019.12.002

21. Calvani NED, Šlapeta J. *Fasciola gigantica* and Fasciola Hybrids in Southeast Asia. In: Dalton, JP, editor. *Fasciolosis 2nd edn*. Cambridge: CABI Publishing (2022). p. 423–60. doi: 10.1079/9781789246162.0013

22. Torgerson P, Claxton J. Epidemiology and control. In: Dalton JP, editor. *Fasciolosis.* Wallingford: CAB International (1999). p. 113–49.

23. Correa AC, Escobar JS, Durand P, Renaud F, David P, Jarne P, et al. Bridging gaps in the molecular phylogeny of the Lymnaeidae (Gastropoda: Pulmonata), vectors of Fascioliasis. *BMC Evol Biol.* (2010) 10:381. doi: 10.1186/1471-2148-10-381

24. Wilson RA, Pullin R, Denison J. An investigation of the mechanism of infection by digenetic trematodes: the penetration of the miracidium of *Fasciola hepatica* into its snail host Lymnaea truncatula. *Parasitology.* (1971) 63:491–506. doi: 10.1017/S003118200008001X

25. Thomas AP. The natural history of the liver-fluke and the prevention of rot. *J R Agric Soc.* (1883) 19:276–305.

26. Thomas AP. The life history of the liver-fluke (*Fasciola hepatica*). *Q J Microsc Sci.* (1883) 23:99–133. doi: 10.1242/jcs.s2-23.89.99

27. Dawes B, Hughes DL. Fascioliasis: the invasive stages of *Fasciola hepatica* in mammalian hosts. *Adv Parasitol.* (1964) 2:97–168. doi: 10.1016/S0065-308X(08)60587-4

28. Dow C, Ross JG, Todd JR. The histopathology of *Fasciola hepatica* infections in sheep. *Parasitology.* (1968) 58:129–35. doi: 10.1017/S0031182000073480

29. Boray JC. Experimental fascioliasis in Australia. *Adv Parasitol.* (1969) 7:95–210. doi: 10.1016/S0065-308X(08)60435-2

30. Zafra R, Pérez-Écija RA, Buffoni L, Moreno P, Bautista MJ, Martínez-Moreno A, et al. Early and late peritoneal and hepatic changes in goats immunized with recombinant cathepsin L1 and infected with *Fasciola hepatica*. *J Comp Pathol.* (2013) 148:373–84. doi: 10.1016/j.jcpa.2012.08.007

31. Molina-Hernández V, Mulcahy G, Pérez J, Martínez-Moreno Á, Donnelly S, O'Neill SM, et al. *Fasciola hepatica* vaccine: we may not be there yet but we're on the right road. *Vet Parasitol.* (2015) 208:101–11. doi: 10.1016/j.vetpar.2015.01.004

32. Lopez P, Tuñon MJ, Gonzalez P, Diez N, Bravo AM, Gonzalez-Gallego J. Ductular proliferation and hepatic secretory function in experimental fascioliasis. *Exp Parasitol.* (1993) 77:36–42. doi: 10.1006/expr.1993.1058

33. Isseroff H, Sawma JT, Reino D. Fascioliasis: role of proline in bile duct hyperplasia. *Science.* (1977) 198:1157–9. doi: 10.1126/science.929191

34. Modavi S, Isseroff H. *Fasciola hepatica*: collagen deposition and other histopathology in the rat host's bile duct caused by the parasite and by proline infusion. *Exp Parasitol.* (1984) 58:239–44. doi: 10.1016/0014-4894(84)90040-7

35. Pérez J, Ortega J, Moreno T, Morrondo P, López-Sández C, Martínez-Moreno A. Pathological and immunohistochemical study of the liver and hepatic lymph nodes of sheep chronically reinfected with *Fasciola hepatica*, with or without triclabendazole treatment. *J Comp Pathol.* (2002) 127:30–6. doi: 10.1053/jcpa.2002.0561

36. Zafra R, Pérez-Écija RA, Buffoni L, Pacheco IL, Martínez-Moreno A, LaCourse EJ, et al. Early hepatic and peritoneal changes and immune response in goats vaccinated with a recombinant glutathione transferase sigma class and challenged with *Fasciola hepatica*. *Res Vet Sci.* (2013) 94:602–9. doi: 10.1016/j.rvsc.2012.10.026

37. Martínez-Moreno A, Jiménez-Luque V, Moreno T, Redondo ES, de las Mulas JM, Pérez J. Liver pathology and immune response in experimental *Fasciola hepatica* infections of goats. *Vet Parasitol.* (1999) 82:19–33. doi: 10.1016/S0304-4017(98)00262-3

38. Aldridge A, O'Neill SM. *Fasciola hepatica* tegumental antigens induce anergic-like T cells via dendritic cells in a mannose receptor-dependent manner. *Eur J Immunol.* (2016) 46:1180–92. doi: 10.1002/eji.201545905

39. Garcia-Campos A, Ravidà A, Nguyen DL, Cwiklinski K, Dalton JP, Hokke CH, et al. Tegument glycoproteins and cathepsins of newly excysted juvenile *Fasciola hepatica* Carry mannosidic and paucimannosidic N-glycans. *PLoS Negl Trop Dis.* (2016) 10:e0004688. doi: 10.1371/journal.pntd.0004688

40. Dowling DJ, Hamilton CM, Donnelly S, La Course J, Brophy PM, Dalton J, et al. Major secretory antigens of the helminth *Fasciola hepatica* activate a suppressive dendritic cell phenotype that attenuates Th17 cells but fails to activate Th2 immune responses. *Infect Immun.* (2010) 78:793–801. doi: 10.1128/IAI.00573-09

41. Flynn RJ, Mulcahy G. Possible role for Toll-like receptors in interaction of *Fasciola hepatica* excretory/secretory products with bovine macrophages. *Infect Immun.* (2008) 76:678–84. doi: 10.1128/IAI.00732-07

42. van Milligen FJ, Cornelissen JB, Gaasenbeek CP, Bokhout BA. A novel ex vivo rat infection model to study protective immunity against *Fasciola hepatica* at the gut level. *J Immunol Methods.* (1998) 213:183–90. doi: 10.1016/S0022-1759(98)00026-X

43. Prussin C, Metcalfe DD. 4. IgE, mast cells, basophils, and eosinophils. *J Allergy Clin Immunol.* (2003) 111:S486–94. doi: 10.1067/mai.2003.120

44. Gurish MF, Bryce PJ, Tao H, Kisselgof AB, Thornton EM, Miller HR, et al. IgE enhances parasite clearance and regulates mast cell responses in mice infected with trichinella spiralis. *J Immunol.* (2004) 172:1139–45. doi: 10.4049/jimmunol.172.2.1139

45. Yoshimoto T, Nakanishi K. Roles of IL-18 in basophils and mast cells. *Allergol Int.* (2006) 55:105–13. doi: 10.2332/allergolint.55.105

46. Doy TG, Hughes DL, Harness E. Hypersensitivity in rats infected with *Fasciola hepatica*: possible role in protection against a challenge infection. *Res Vet Sci.* (1981) 30:360–3. doi: 10.1016/S0034-5288(18)32558-X

47. Wicki P, Schwalbach B, Charbon JL, Steiner A, Lang M, Loup F, et al. Intestinal cellular reaction of cattle after infection by *Fasciola hepatica*. *Schweiz Arch Tierheilkd.* (1991) 133:429–37.

48. Bossaert K, Jacquinet E, Saunders J, Farnir F, Losson B. Cell-mediated immune response in calves to single-dose, trickle, and challenge infections with *Fasciola hepatica*. *Vet Parasitol.* (2000) 88:17–34. doi: 10.1016/S0304-4017(99)00200-9

49. McCole DF, Doherty ML, Baird AW, Davis WC, McGill K, Torgerson PR. Concanavalin a-stimulated proliferation of T cell subset-depleted lymphocyte populations isolated from *Fasciola hepatica*-infected cattle. *Vet Immunol Immunopathol.* (1998) 66:289–300. doi: 10.1016/S0165-2427(98)00207-4

50. Escamilla A, Pérez-Caballero R, Zafra R, Bautista MJ, Pacheco IL, Ruiz MT, et al. Apoptosis of peritoneal leucocytes during early stages of *Fasciola hepatica* infections in sheep. *Vet Parasitol.* (2017) 238:49–53. doi: 10.1016/j.vetpar.2017.03.015

51. Molina EC, Skerratt LF. Cellular and humoral responses in liver of cattle and buffaloes infected with a single dose of *Fasciola gigantica*. *Vet Parasitol.* (2005) 131:157–63. doi: 10.1016/j.vetpar.2005.04.028

52. Huntley JF, Newlands G, Miller HR. The isolation and characterization of globule leucocytes: their derivation from mucosal mast cells in parasitized sheep. *Parasite Immunol.* (1984) 6:371–90. doi: 10.1111/j.1365-3024.1984.tb00809.x

53. Stankiewicz M, Jonas WE, Douch PC, Rabel B, Bisset S, Cabaj W. Globule leukocytes in the lumen of the small intestine and the resistance status of sheep infected with parasitic nematodes. *J Parasitol.* (1993) 79:940–5. doi: 10.2307/3283734

54. Balic A, Bowles VM, Meeusen EN. The immunobiology of gastrointestinal nematode infections in ruminants. *Adv Parasitol.* (2000) 45:181–241. doi: 10.1016/S0065-308X(00)45005-0

55. Delves PJ, Martin SJ, Burton DR, Roitt IM. *Roitt's Essential Immunology 13th edn*. Wiley-Blackwell (2014).

56. Piedrafita D, Estuningsih E, Pleasance J, Prowse R, Raadsma HW, Meeusen EN, et al. Peritoneal lavage cells of Indonesian thin-tail sheep mediate antibody-dependent superoxide radical cytotoxicity in vitro against newly excysted juvenile *Fasciola gigantica* but not juvenile *Fasciola hepatica*. *Infect Immun.* (2007) 75:1954–63. doi: 10.1128/IAI.01034-06

57. Bossaert K, Farnir F, Leclipteux T, Protz M, Lonneux JF, Losson B. Humoral immune response in calves to single-dose, trickle and challenge infections with *Fasciola hepatica*. *Vet Parasitol.* (2000) 87:103–23. doi: 10.1016/S0304-4017(99)00177-6

58. Osman MM, Rashwan E, Farag HF. Phagocytic activity of neutrophils in human fasciolosis before and after treatment. *J Egypt Soc Parasitol.* (1995) 25:321–7.

59. Martínez-Moreno A, Jiménez-Luque V, Cámara S, Martínez-Moreno FJ, Acosta I, Hernández S. Oxidative responses during bacterial phagocytosis of polymorphonuclear leucocytes in primarily and secondarily *Fasciola hepatica* infected goats. *Int J Parasitol.* (2000) 30:1013–7. doi: 10.1016/S0020-7519(00)00082-5

60. Chauvin A, Moreau E, Boulard C. Responses of *Fasciola hepatica* infected sheep to various infection levels. *Vet Res.* (2001) 32:87–92. doi: 10.1051/vetres:2001113

61. Zhang WY, Moreau E, Hope JC, Howard CJ, Huang WY, Chauvin A. *Fasciola hepatica* and *Fasciola gigantica*: comparison of cellular response to experimental infection in sheep. *Exp Parasitol.* (2005) 111:154–9. doi: 10.1016/j.exppara.2005.06.005

62. Zafra R, Buffoni L, Martínez-Moreno A, Pérez-Ecija A, Martinez-Moreno FJ, Pérez J, et al. study of the liver of goats immunized with a synthetic peptide of the Sm14 antigen and challenged with *Fasciola hepatica*. *J Comp Pathol.* (2008) 139:169–76. doi: 10.1016/j.jcpa.2008.06.004

63. Wedrychowicz H, Kesik M, Kaliniak M, Kozak-Cieszczyk M, Jedlina-Panasiuk L, Jaros S, et al. Vaccine potential of inclusion bodies containing cysteine proteinase of *Fasciola hepatica* in calves and lambs experimentally challenged with metacercariae of the fluke. *Vet Parasitol.* (2007) 147:77–88. doi: 10.1016/j.vetpar.2007.03.023

64. Ruiz-Campillo MT, Molina Hernandez V, Escamilla A, Stevenson M, Perez J, Martinez-Moreno A, et al. Immune signatures of pathogenesis in the peritoneal compartment during early infection of sheep with *Fasciola hepatica*. *Sci Rep.* (2017) 7:2782. doi: 10.1038/s41598-017-03094-0

65. Escamilla A, Bautista MJ, Zafra R, Pacheco IL, Ruiz MT, Martínez-Cruz S, et al. *Fasciola hepatica* induces eosinophil apoptosis in the migratory and biliary stages of infection in sheep. *Vet Parasitol.* (2016) 216:84–8. doi: 10.1016/j.vetpar.2015.12.013

66. Meeusen E, Lee CS, Rickard MD, Brandon MR. Cellular responses during liver fluke infection in sheep and its evasion by the parasite. *Parasite Immunol.* (1995) 17:37–45. doi: 10.1111/j.1365-3024.1995.tb00964.x

67. Pleasance J, Raadsma HW, Estuningsih SE, Widjajanti S, Meeusen E, Piedrafita D. Innate and adaptive resistance of Indonesian thin tail sheep to liver fluke: a comparative analysis of *Fasciola gigantica* and *Fasciola hepatica* infection. *Vet Parasitol.* (2011) 178:264–72. doi: 10.1016/j.vetpar.2011.01.037

68. Piedrafita D, Parsons JC, Sandeman RM, Wood PR, Estuningsih SE, Partoutomo S, et al. Antibody-dependent cell-mediated cytotoxicity to newly excysted juvenile *Fasciola hepatica* in vitro is mediated by reactive nitrogen intermediates. *Parasite Immunol.* (2001) 23:473–82. doi: 10.1046/j.1365-3024.2001.00404.x

69. Golden O, Flynn RJ, Read C, Sekiya M, Donnelly SM, Stack C, et al. Protection of cattle against a natural infection of *Fasciola hepatica* by vaccination with recombinant cathepsin L1 (rFhCL1). *Vaccine.* (2010) 28:5551–7. doi: 10.1016/j.vaccine.2010.06.039

70. Sulaiman AA, Zolnierczyk K, Japa O, Owen JP, Maddison BC, Emes RD, et al. A trematode parasite derived growth factor binds and exerts influences on host immune functions via host cytokine receptor complexes. *PLoS Pathog.* (2016) 12:e1005991. doi: 10.1371/journal.ppat.1005991

71. Donnelly S, O'Neill SM, Sekiya M, Mulcahy G, Dalton JP. Thioredoxin peroxidase secreted by *Fasciola hepatica* induces the alternative activation of macrophages. *Infect Immun.* (2005) 73:166–73. doi: 10.1128/IAI.73.1.166-173.2005

72. Donnelly S, Stack CM, O'Neill SM, Sayed AA, Williams DL, Dalton JP. Helminth 2-Cys peroxiredoxin drives Th2 responses through a mechanism involving alternatively activated macrophages. *FASEB J.* (2008) 22:4022–32. doi: 10.1096/fj.08-106278

73. Ruiz-Campillo MT, Molina-Hernández V, Pérez J, Pacheco IL, Pérez R, Escamilla A, et al. Study of peritoneal macrophage immunophenotype in sheep experimentally infected with *Fasciola hepatica*. *Vet Parasitol.* (2018) 257:34–9. doi: 10.1016/j.vetpar.2018.05.019

74. Chung JY, Bae YA, Yun DH, Yang HJ, Kong Y. Experimental murine fascioliasis derives early immune suppression with increased levels of TGF-β and IL-4. *Korean J Parasitol.* (2012) 50:301–8. doi: 10.3347/kjp.2012.50.4.301

75. Clery D, Torgerson P, Mulcahy G. Immune responses of chronically infected adult cattle to *Fasciola hepatica*. *Vet Parasitol.* (1996) 62:71–82. doi: 10.1016/0304-4017(95)00858-6

76. Phiri IK, Phiri AM, Harrison LJ. Serum antibody isotype responses of Fasciola-infected sheep and cattle to excretory and secretory products of Fasciola species. *Vet Parasitol.* (2006) 141:234–42. doi: 10.1016/j.vetpar.2006.05.019

77. Mulcahy G, O'Connor F, McGonigle S, Dowd A, Clery DG, Andrews SJ, et al. Correlation of specific antibody titre and avidity with protection in cattle immunized against *Fasciola hepatica*. *Vaccine.* (1998) 16:932–9. doi: 10.1016/S0264-410X(97)00289-2

78. Mulcahy G, Dalton JP. Cathepsin L proteinases as vaccines against infection with *Fasciola hepatica* (liver fluke) in ruminants. *Res Vet Sci.* (2001) 70:83–6. doi: 10.1053/rvsc.2000.0425

79. O'Neill SM, Brady MT, Callanan JJ, Mulcahy G, Joyce P, Mills KH, et al. *Fasciola hepatica* infection downregulates Th1 responses in mice. *Parasite Immunol.* (2000) 22:147–55. doi: 10.1046/j.1365-3024.2000.00290.x

80. Pacheco IL, Abril N, Morales-Prieto N, Bautista MJ, Zafra R, Escamilla A, et al. Th1/Th2 balance in the liver and hepatic lymph nodes of vaccinated and unvaccinated sheep during acute stages of infection with *Fasciola hepatica*. *Vet Parasitol.* (2017) 238:61–5. doi: 10.1016/j.vetpar.2017.03.022

81. Ruiz-Campillo MT, Barrero-Torres DM, Abril N, Pérez J, Zafra R, Buffoni L, et al. *Fasciola hepatica* primoinfections and reinfections in sheep drive distinct Th1/Th2/Treg immune responses in liver and hepatic lymph node at early and late stages. *Vet Res.* (2023) 54:2. doi: 10.1186/s13567-022-01129-7

82. Meng Z, Zhai L, Guo Y, Zheng M, Li L, Wen C, et al. Secondary infection of *Fasciola gigantica* in buffaloes shows a similar pattern of serum cytokine secretion as in primary infection. *Front Vet Sci.* (2023) 10:1109947. doi: 10.3389/fvets.2023.1109947

83. Fu Y, Chryssafidis AL, Browne JA, O'Sullivan J, McGettigan PA, Mulcahy G. Transcriptomic study on ovine immune responses to *Fasciola hepatica* infection. *PLoS Negl Trop Dis.* (2016) 10:e0005015. doi: 10.1371/journal.pntd.0005015

84. Haçariz O, Sayers G, Baykal AT. A proteomic approach to investigate the distribution and abundance of surface and internal *Fasciola hepatica* proteins during the chronic stage of natural liver fluke infection in cattle. *J Proteome Res.* (2012) 11:3592–604. doi: 10.1021/pr300015p

85. Ravidà A, Aldridge AM, Driessen NN, Heus FA, Hokke CH, O'Neill SM. *Fasciola hepatica* surface coat glycoproteins contain mannosylated and phosphorylated N-glycans and exhibit immune modulatory properties independent of the mannose receptor. *PLoS Negl Trop Dis.* (2016) 10:e0004601. doi: 10.1371/journal.pntd.0004601

86. Sánchez-López CM, Trelis M, Jara L, Cantalapiedra F, Marcilla A, Bernal D. Diversity of extracellular vesicles from different developmental stages of *Fasciola hepatica*. *Int J Parasitol.* (2020) 50:663–9. doi: 10.1016/j.ijpara.2020.03.011

87. Murphy A, Cwiklinski K, Lalor R, O'Connell B, Robinson MW, Gerlach J, et al. *Fasciola hepatica* extracellular vesicles isolated from excretory-secretory products using a gravity flow method modulate dendritic cell phenotype and activity. *PLoS Negl Trop Dis.* (2020) 14:e0008626. doi: 10.1371/journal.pntd.0008626

88. Fontenla S, Langleib M, de la Torre-Escudero E, Domínguez MF, Robinson MW, Tort J. Role of *Fasciola hepatica* Small RNAs in the interaction with the mammalian host. *Front Cell Infect Microbiol.* (2022) 11:812141. doi: 10.3389/fcimb.2021.812141

89. Herron CM, O'Connor A, Robb E, McCammick E, Hill C, Marks NJ, et al. Developmental regulation and functional prediction of microRNAs in an expanded *Fasciola hepatica* miRNome. *Front Cell Infect Microbiol.* (2022) 12:811123. doi: 10.3389/fcimb.2022.811123

90. Ricafrente A, Cwiklinski K, Nguyen H, Dalton JP, Tran N, Donnelly S. Stage-specific miRNAs regulate gene expression associated with growth, development and parasite-host interaction during the intra-mammalian migration of the zoonotic helminth parasite *Fasciola hepatica*. *BMC Genomics.* (2022) 23:419. doi: 10.1186/s12864-022-08644-z

91. Fromm B, Ovchinnikov V, Høye E, Bernal D, Hackenberg M, Marcilla A. On the presence and immunoregulatory functions of extracellular microRNAs in the trematode *Fasciola hepatica*. *Parasite Immunol.* (2017) 39. doi: 10.1111/pim.12399

92. Cancela M, Acosta D, Rinaldi G, Silva E, Durán R, Roche L, et al. A distinctive repertoire of cathepsins is expressed by juvenile invasive *Fasciola hepatica*. *Biochimie.* (2008) 90:1461–75. doi: 10.1016/j.biochi.2008.04.020

93. Robinson MW, Dalton JP, Donnelly S. Helminth pathogen cathepsin proteases: it's a family affair. *Trends Biochem Sci.* (2008) 33:601–8. doi: 10.1016/j.tibs.2008.09.001

94. Xifeng W, Jiahua Z, Ningxing L, Guowu Z, Yunxia S, Xuepeng C, et al. The regulatory roles of *Fasciola hepatica* GSTO1 protein in inflammatory cytokine expression and apoptosis in murine macrophages. *Acta Trop.* (2023) 245:106977. doi: 10.1016/j.actatropica.2023.106977

95. Carmona C, Dowd AJ, Smith AM, Dalton JP. Cathepsin L proteinase secreted by *Fasciola hepatica* in vitro prevents antibody-mediated eosinophil attachment to newly excysted juveniles. *Mol Biochem Parasitol.* (1993) 62:9–17. doi: 10.1016/0166-6851(93)90172-T

96. Mebius MM, Op Heij JMJ, Tielens AGM, de Groot PG, Urbanus RT, van Hellemond JJ. Fibrinogen and fibrin are novel substrates for

Fasciola hepatica cathepsin L peptidases. *Mol Biochem Parasitol.* (2018) 221:10–3. doi: 10.1016/j.molbiopara.2018.02.001

97. Falcón CR, Masih D, Gatti G, Sanchez MC, Motrán CC, Cervi L. *Fasciola hepatica* Kunitz type molecule decreases dendritic cell activation and their ability to induce inflammatory responses. *PLoS ONE.* (2014) 9:e114505. doi: 10.1371/journal.pone.0114505

98. Ramos-Benítez MJ, Ruiz-Jiménez C, Aguayo V, Espino AM. Recombinant *Fasciola hepatica* fatty acid binding protein suppresses toll-like receptor stimulation in response to multiple bacterial ligands. *Sci Rep.* (2017) 7:5455. doi: 10.1038/s41598-017-05735-w

99. Ruiz-Jiménez C, Celias D, Valdés B, Ramos-Pérez WD, Cervi L, Espino AM. *Fasciola hepatica* fatty acid binding protein (Fh12) induces apoptosis and tolerogenic properties in murine bone marrow derived dendritic cells. *Exp Parasitol.* (2021) 231:108174. doi: 10.1016/j.exppara.2021.108174

100. Alvarado R, O'Brien B, Tanaka A, Dalton JP, Donnelly S. A parasitic helminth-derived peptide that targets the macrophage lysosome is a novel therapeutic option for autoimmune disease. *Immunobiology.* (2015) 220:262–9. doi: 10.1016/j.imbio.2014.11.008

101. Cancela M, Santos GB, Carmona C, Ferreira HB, Tort JF, Zaha A. *Fasciola hepatica* mucin-encoding gene: expression, variability and its potential relevance in host-parasite relationship. *Parasitology.* (2015) 142:1673–81. doi: 10.1017/S0031182015001134

102. Noya V, Brossard N, Rodríguez E, Dergan-Dylon LS, Carmona C, Rabinovich GA, et al. mucin-like peptide from *Fasciola hepatica* instructs dendritic cells with parasite specific Th1-polarizing activity. *Sci Rep.* (2017) 7:40615. doi: 10.1038/srep40615

103. De Marco Verissimo C, Jewhurst HL, Dobó J, Gál P, Dalton JP, Cwiklinski K. *Fasciola hepatica* is refractory to complement killing by preventing attachment of mannose binding lectin (MBL) and inhibiting MBL-associated serine proteases (MASPs) with serpins. *PLoS Pathog.* (2022) 18:e1010226. doi: 10.1371/journal.ppat.1010226

104. Zhang K, Liu Y, Zhang G, Wang X, Li Z, Shang Y, et al. Molecular characteristics and potent immunomodulatory activity of *Fasciola hepatica* cystatin. *Korean J Parasitol.* (2022) 60:117–26. doi: 10.3347/kjp.2022.60.2.117

105. Zawistowska-Deniziak A, Wasyl K, Norbury LJ, Wesołowska A, Bień J, Grodzik M, et al. Characterization and differential expression of cathepsin L3 alleles from *Fasciola hepatica*. *Mol Biochem Parasitol.* (2013) 190:27–37. doi: 10.1016/j.molbiopara.2013.06.001

106. McNulty SN, Tort JF, Rinaldi G, Fischer K, Rosa BA, Smircich P, et al. Genomes of *Fasciola hepatica* from the Americas reveal colonization with neorickettsia endobacteria related to the agents of potomac horse and human sennetsu fevers. *PLoS Genet.* (2017) 13:e1006537. doi: 10.1371/journal.pgen.1006537

107. Flynn RJ, Mulcahy G, Elsheikha HM. Coordinating innate and adaptive immunity in *Fasciola hepatica* infection: implications for control. *Vet Parasitol.* (2010) 169:235–40. doi: 10.1016/j.vetpar.2010.02.015

108. Tliba O, Sibille P, Boulard C, Chauvin A. Local hepatic immune response in rats during primary infection with *Fasciola hepatica*. *Parasite.* (2000) 7:9–18. doi: 10.1051/parasite/2000071009

109. Serradell MC, Guasconi L, Cervi L, Chiapello LS, Masih DT. Excretory-secretory products from *Fasciola hepatica* induce eosinophil apoptosis by a caspase-dependent mechanism. *Vet Immunol Immunopathol.* (2007) 117:197–208. doi: 10.1016/j.vetimm.2007.03.007

110. Guasconi L, Serradell MC, Masih DT. *Fasciola hepatica* products induce apoptosis of peritoneal macrophages. *Vet Immunol Immunopathol.* (2012) 148:359–63. doi: 10.1016/j.vetimm.2012.06.022

111. Fu Y, Browne JA, Killick K, Mulcahy G. Network analysis of the systemic response to *Fasciola hepatica* infection in sheep reveals changes in fibrosis, apoptosis, toll-like receptors 3/4, and B cell function. *Front Immunol.* (2017) 8:485. doi: 10.3389/fimmu.2017.00485

112. Garcia-Campos A, Correia CN, Naranjo-Lucena A, Garza-Cuartero L, Farries G, Browne JA, et al. *Fasciola hepatica* infection in cattle: analyzing responses of Peripheral Blood Mononuclear Cells (PBMC) using a transcriptomics approach. *Front Immunol.* (2019) 10:2081. doi: 10.3389/fimmu.2019.02081

113. Flynn RJ, Mulcahy G. The roles of IL-10 and TGF-beta in controlling IL-4 and IFN-gamma production during experimental *Fasciola hepatica* infection. *Int J Parasitol.* (2008) 38:1673–80. doi: 10.1016/j.ijpara.2008.05.008

114. Guasconi L, Serradell MC, Garro AP, Iacobelli L, Masih DT. C-type lectins on macrophages participate in the immunomodulatory response to *Fasciola hepatica* products. *Immunology.* (2011) 133:386–96. doi: 10.1111/j.1365-2567.2011.03449.x

115. Flynn RJ, Irwin JA, Olivier M, Sekiya M, Dalton JP, Mulcahy G. Alternative activation of ruminant macrophages by *Fasciola hepatica*. *Vet Immunol Immunopathol.* (2007) 120:31–40. doi: 10.1016/j.vetimm.2007.07.003

116. Garza-Cuartero L, O'Sullivan J, Blanco A, McNair J, Welsh M, Flynn RJ, et al. *Fasciola hepatica* infection reduces mycobacterium bovis burden and mycobacterial uptake and suppresses the pro-inflammatory response. *Parasite Immunol.* (2016) 38:387–402. doi: 10.1111/pim.12326

117. Kreider T, Anthony RM, Urban JF Jr, Gause WC. Alternatively activated macrophages in helminth infections. *Curr Opin Immunol.* (2007) 19:448–53. doi: 10.1016/j.coi.2007.07.002

118. Hamilton CM, Dowling DJ, Loscher CE, Morphew RM, Brophy PM, O'Neill SM. The *Fasciola hepatica* tegumental antigen suppresses dendritic cell maturation and function. *Infect Immun.* (2009) 77:2488–98. doi: 10.1128/IAI.00919-08

119. Falcón C, Carranza F, Martínez FF, Knubel CP, Masih DT, Motrán CC, et al. Excretory-secretory products (ESP) from *Fasciola hepatica* induce tolerogenic properties in myeloid dendritic cells. *Vet Immunol Immunopathol.* (2010) 137:36–46. doi: 10.1016/j.vetimm.2010.04.007

120. Falcón CR, Carranza FA, Aoki P, Motrán CC, Cervi L. Adoptive transfer of dendritic cells pulsed with *Fasciola hepatica* antigens and lipopolysaccharides confers protection against fasciolosis in mice. *J Infect Dis.* (2012) 205:506–14. doi: 10.1093/infdis/jir606

121. Vukman KV, Adams PN, O'Neill SM. *Fasciola hepatica* tegumental coat antigen suppresses MAPK signalling in dendritic cells and up-regulates the expression of SOCS3. *Parasite Immunol.* (2013) 35:234–8. doi: 10.1111/pim.12033

122. Mei XF, Shi W, Zhang YY, Zhu B, Wang YR, Hou LJ, et al. DNA methylation and hydroxymethylation profiles reveal possible role of highly methylated TLR signaling on *Fasciola gigantica* excretory/secretory products (FgESPs) modulation of buffalo dendritic cells. *Parasit Vectors.* (2019) 12:358. doi: 10.1186/s13071-019-3615-4

123. Walsh KP, Brady MT, Finlay CM, Boon L, Mills KH. Infection with a helminth parasite attenuates autoimmunity through TGF-beta-mediated suppression of Th17 and Th1 responses. *J Immunol.* (2009) 183:1577–86. doi: 10.4049/jimmunol.0803803

124. Rodríguez E, Kalay H, Noya V, Brossard N, Giacomini C, van Kooyk Y, et al. *Fasciola hepatica* glycoconjugates immuneregulate dendritic cells through the dendritic cell-specific intercellular adhesion molecule-3-grabbing non-integrin inducing T cell anergy. *Sci Rep.* (2017) 7:46748. doi: 10.1038/srep46748

125. Ruiz-Campillo MT, Molina-Hernández V, Bautista MJ, Pacheco IL, Zafra R, Buffoni L, et al. Characterization of dendritic cells and follicular dendritic cells in the hepatic lymph nodes and liver of sheep experimentally infected with *Fasciola hepatica*. *Vet Res.* (2020) 51:33. doi: 10.1186/s13567-020-00757-1

126. Pacheco IL, Abril N, Zafra R, Molina-Hernández V, Morales-Prieto N, Bautista MJ, et al. *Fasciola hepatica* induces Foxp3 T cell, proinflammatory and regulatory cytokine overexpression in liver from infected sheep during early stages of infection. *Vet Res.* (2018) 49:56. doi: 10.1186/s13567-018-0550-x

127. Taylor MD, Van Der Werf N, Maizels RM. T cells in helminth infection: the regulators and the regulated. *Trends Immunol.* (2012) 33:181–9. doi: 10.1016/j.it.2012.01.001

128. McNeilly TN, Rocchi M, Bartley Y, Brown JK, Frew D, Longhi C, et al. Suppression of ovine lymphocyte activation by teladorsagia circumcincta larval excretory–secretory products. *Vet Res.* (2013) 44:70. doi: 10.1186/1297-9716-44-70

129. Dalton JP, Robinson MW, Mulcahy G, O'Neill SM, Donnelly S. Immunomodulatory molecules of *Fasciola hepatica*: candidates for both vaccine and immunotherapeutic development. *Vet Parasitol.* (2013) 195:272–85. doi: 10.1016/j.vetpar.2013.04.008

130. Doy TG, Hughes DL. *Fasciola hepatica*: site of resistance to reinfection in cattle. *Exp Parasitol.* (1984) 57:274–8. doi: 10.1016/0014-4894(84)90101-2

131. Piedrafita D, Raadsma HW, Prowse R, Spithill TW. Immunology of the host-parasite relationship in fasciolosis (Fasciola hepatica and Fasciola gigantica). *Can J Zool.* (2004) 82:233–50. doi: 10.1139/z03-216

132. Chauvin A, Bouvet G, Boulard C. Humoral and cellular immune responses to Fasciola hepatica experimental primary and secondary infection in sheep. *Int J Parasitol.* (1995) 10:1227–41. doi: 10.1016/0020-7519(95)00039-5

133. Villa-Mancera A, Olivares-Pérez J, Olmedo-Juárez A, Reynoso-Palomar A. Phage display-based vaccine with cathepsin L and excretory-secretory products mimotopes of *Fasciola hepatica* induces protective cellular and humoral immune responses in sheep. *Vet Parasitol.* (2021) 289:109340. doi: 10.1016/j.vetpar.2020.109340

134. Villa-Mancera A, Reynoso-Palomar A, Utrera-Quintana F, Carreón-Luna L. Cathepsin L1 mimotopes with adjuvant Quil A induces a Th1/Th2 immune response and confers significant protection against *Fasciola hepatica* infection in goats. *Parasitol Res.* (2014) 113:243–50. doi: 10.1007/s00436-013-3650-6

135. Toet H, Piedrafita DM, Spithill TW. Liver fluke vaccines in ruminants: strategies, progress and future opportunities. *Int J Parasitol.* (2014) 44:915–27. doi: 10.1016/j.ijpara.2014.07.011

136. Dalton JP, McGonigle S, Rolph TP, Andrews SJ. Induction of protective immunity in cattle against infection with *Fasciola hepatica* by vaccination with cathepsin L proteinases and with hemoglobin. *Infect Immun.* (1996) 64:5066–74. doi: 10.1128/iai.64.12.5066-5074.1996

137. Morrison CA, Colin T, Sexton JL, Bowen F, Wicker J, Friedel T, et al. Protection of cattle against *Fasciola hepatica* infection by vaccination with glutathione S-transferase. *Vaccine.* (1996) 14:1603–12. doi: 10.1016/S0264-410X(96)00147-8

138. Orbegozo-Medina RA, Martínez-Sernández V, González-Warleta M, Castro-Hermida JA, Mezo M, Ubeira FM. Vaccination of sheep with Quil-A® adjuvant

expands the antibody repertoire to the Fasciola MF6p/FhHDM-1 antigen and administered together impair the growth and antigen release of flukes. *Vaccine.* (2018) 36:1949–57. doi: 10.1016/j.vaccine.2018.02.115

139. Villa-Mancera A, Méndez-Mendoza M. Protection and antibody isotype responses against *Fasciola hepatica* with specific antibody to pIII-displayed peptide mimotopes of cathepsin L1 in sheep. *Vet J.* (2012) 194:108–12. doi: 10.1016/j.tvjl.2012.03.003

140. Villa-Mancera A, Alcalá-Canto Y, Reynoso-Palomar A, Olmedo-Juárez A, Olivares-Pérez J. Vaccination with cathepsin L phage-exposed mimotopes, single or in combination, reduce size, fluke burden, egg production and viability in sheep experimentally infected with *Fasciola hepatica*. *Parasitol Int.* (2021) 83:102355. doi: 10.1016/j.parint.2021.102355

141. Villa-Mancera A, Alcalá-Canto Y, Olivares-Pérez J, Molina-Mendoza P, Hernández-Guzmán K, Utrera-Quintana F, et al. Vaccination with cathepsin L mimotopes of *Fasciola hepatica* in goats reduces worm burden, morphometric measurements, and reproductive structures. *Microb Pathog.* (2021) 155:104859. doi: 10.1016/j.micpath.2021.104859

142. Wesołowska A, Kozak Ljunggren M, Jedlina L, Basałaj K, Legocki A, Wedrychowicz H, et al. A preliminary study of a lettuce-based edible vaccine expressing the cysteine proteinase of *Fasciola hepatica* for fasciolosis control in livestock. *Front Immunol.* (2018) 9:2592. doi: 10.3389/fimmu.2018.02592

143. Maggioli G, Acosta D, Silveira F, Rossi S, Giacaman S, Basika T, et al. The recombinant gut-associated M17 leucine aminopeptidase in combination with different adjuvants confers a high level of protection against *Fasciola hepatica* infection in sheep. *Vaccine.* (2011) 29:9057–63. doi: 10.1016/j.vaccine.2011.09.020

144. Raina OK, Nagar G, Varghese A, Prajitha G, Alex A, Maharana BR, et al. Lack of protective efficacy in buffaloes vaccinated with *Fasciola gigantica* leucine aminopeptidase and peroxiredoxin recombinant proteins. *Acta Trop.* (2011) 118:217–22. doi: 10.1016/j.actatropica.2011.02.008

145. López-Abán J, Casanueva P, Nogal J, Arias M, Morrondo P, Diez-Baños P, et al. Progress in the development of *Fasciola hepatica* vaccine using recombinant fatty acid binding protein with the adjuvant adaptation system ADAD. *Vet Parasitol.* (2007) 145:287–96. doi: 10.1016/j.vetpar.2006.12.017

146. Nambi PA, Yadav SC, Raina OK, Sriveny D, Saini M. Vaccination of buffaloes with *Fasciola gigantica* recombinant fatty acid binding protein. *Parasitol Res.* (2005) 97:129–35. doi: 10.1007/s00436-005-1397-4

147. Kumar N, Anju V, Gaurav N, Chandra D, Samanta S, Gupta SC, et al. Vaccination of buffaloes with *Fasciola gigantica* recombinant glutathione S-transferase and fatty acid binding protein. *Parasitol Res.* (2012) 110:419–26. doi: 10.1007/s00436-011-2507-0

148. Buffoni L, Martínez-Moreno FJ, Zafra R, Mendes RE, Pérez-Écija A, Sekiya M, et al. Humoral immune response in goats immunised with cathepsin L1, peroxiredoxin and Sm14 antigen and experimentally challenged with *Fasciola hepatica*. *Vet Parasitol.* (2012) 185:315–21. doi: 10.1016/j.vetpar.2011.09.027

149. Maggioli G, Bottini G, Basika T, Alonzo P, Salinas G, Carmona C. Immunization with *Fasciola hepatica* thioredoxin glutathione reductase failed to confer protection against fasciolosis in cattle. *Vet Parasitol.* (2016) 224:13–9. doi: 10.1016/j.vetpar.2016.05.007

150. Wesołowska A, Basałaj K, Zawistowska-Deniziak A, Januszkiewicz K, Kozak Ljunggren M, Jedlina L, et al. The failure of a DNA prime/protein boost regime and CTLA-4 mediated targeting to improve the potency of a DNA vaccine encoding *Fasciola hepatica* phosphoglycerate kinase in sheep. *Vet Immunol Immunopathol.* (2019) 217:109941. doi: 10.1016/j.vetimm.2019.109941

151. Pérez-Caballero R, Siles-Lucas M, González-Miguel J, Martínez-Moreno FJ, Escamilla A, Pérez J, et al. Pathological, immunological and parasitological study of sheep vaccinated with the recombinant protein 14-3-3z and experimentally infected with *Fasciola hepatica*. *Vet Immunol Immunopathol.* (2018) 202:115–21. doi: 10.1016/j.vetimm.2018.07.006

152. Zerna G, Rathinasamy VA, Toet H, Anderson G, Dempster R, Spithill TW, et al. Evaluation of immunogenicity and efficacy of *Fasciola hepatica* tetraspanin 2 (TSP2) Fused to E. *coli* heat-labile enterotoxin B subunit LTB adjuvant following intranasal vaccination of cattle. *Vaccines.* (2021) 9:1213. doi: 10.3390/vaccines9111213

153. Garza-Cuartero L, Geurden T, Mahan SM, Hardham JM, Dalton JP, Mulcahy G. Antibody recognition of cathepsin L1-derived peptides in *Fasciola hepatica*-infected and/or vaccinated cattle and identification of protective linear B-cell epitopes. *Vaccine.* (2018) 36:958–68. doi: 10.1016/j.vaccine.2018.01.020

154. Norbury LJ, Basałaj K, Zawistowska-Deniziak A, Sielicka A, Wilkowski P, Wesołowska A, et al. Intranasal delivery of a formulation containing stage-specific recombinant proteins of *Fasciola hepatica* cathepsin L5 and cathepsin B2 triggers an anti-fecundity effect and an adjuvant-mediated reduction in fluke burden in sheep. *Vet Parasitol.* (2018) 258:14–23. doi: 10.1016/j.vetpar.2018.05.008

155. Ortega-Vargas S, Espitia C, Sahagún-Ruiz A, Parada C, Balderas-Loaeza A, Villa-Mancera A, et al. Moderate protection is induced by a chimeric protein composed of leucine aminopeptidase and cathepsin L1 against *Fasciola hepatica* challenge in sheep. *Vaccine.* (2019) 37:3234–40. doi: 10.1016/j.vaccine.2019.04.067

156. McCusker P, Toet H, Rathinasamy V, Young N, Beddoe T, Anderson G, et al. Molecular characterisation and vaccine efficacy of two novel developmentally regulated surface tegument proteins of *Fasciola hepatica*. *Vet Parasitol.* (2020) 286:109244. doi: 10.1016/j.vetpar.2020.109244

157. Zafra R, Buffoni L, Pérez-Caballero R, Molina-Hernández V, Ruiz-Campillo MT, Pérez J, et al. Efficacy of a multivalent vaccine against *Fasciola hepatica* infection in sheep. *Vet Res.* (2021) 52:13. doi: 10.1186/s13567-021-00895-0

158. Becerro-Recio D, Serrat J, López-García M, Molina-Hernández V, Pérez-Arévalo J, Martínez-Moreno Á, et al. Study of the migration of *Fasciola hepatica* juveniles across the intestinal barrier of the host by quantitative proteomics in an ex vivo model. *PLoS Negl Trop Dis.* (2022) 16:e0010766. doi: 10.1371/journal.pntd.0010766

frontiers | Frontiers in Veterinary Science

TYPE Review
PUBLISHED 19 March 2024
DOI 10.3389/fvets.2024.1330990

OPEN ACCESS

EDITED BY
Vassilis Papatsiros,
University of Thessaly, Greece

REVIEWED BY
Giuseppe Marruchella,
University of Teramo, Italy
Jean-Pierre Frossard,
Animal and Plant Health Agency (United Kingdom), United Kingdom

*CORRESPONDENCE
Inés Ruedas-Torres
✉ iruedas@uco.es
José María Sánchez-Carvajal
✉ v42sancj@uco.es

†These authors have contributed equally to this work and share first authorship

RECEIVED 31 October 2023
ACCEPTED 22 February 2024
PUBLISHED 19 March 2024

CITATION
Ruedas-Torres I, Sánchez-Carvajal JM, Salguero FJ, Pallarés FJ, Carrasco L, Mateu E, Gómez-Laguna J and Rodríguez-Gómez IM (2024) The scene of lung pathology during PRRSV-1 infection. *Front. Vet. Sci.* 11:1330990. doi: 10.3389/fvets.2024.1330990

The scene of lung pathology during PRRSV-1 infection

Inés Ruedas-Torres[1,2*†], José María Sánchez-Carvajal[2*†], Francisco Javier Salguero[1], Francisco José Pallarés[2], Librado Carrasco[2], Enric Mateu[3], Jaime Gómez-Laguna[2] and Irene Magdalena Rodríguez-Gómez[2]

[1]United Kingdom Health Security Agency (UKHSA Porton Down), Salisbury, United Kingdom, [2]Department of Anatomy and Comparative Pathology and Toxicology, Pathology and Immunology Group (UCO-PIG), UIC Zoonosis y Enfermedades Emergentes ENZOEM, International Agrifood Campus of Excellence (CeiA3), Faculty of Veterinary Medicine, University of Córdoba, Córdoba, Spain, [3]Department of Animal Health and Anatomy, Autonomous University of Barcelona, Barcelona, Spain

Porcine reproductive and respiratory syndrome (PRRS) is one of the most economically important infectious diseases for the pig industry worldwide. The disease was firstly reported in 1987 and became endemic in many countries. Since then, outbreaks caused by strains of high virulence have been reported several times in Asia, America and Europe. Interstitial pneumonia, microscopically characterised by thickened alveolar septa, is the hallmark lesion of PRRS. However, suppurative bronchopneumonia and proliferative and necrotising pneumonia are also observed, particularly when a virulent strain is involved. This raises the question of whether the infection by certain strains results in an overstimulation of the proinflammatory response and whether there is some degree of correlation between the strain involved and a particular pattern of lung injury. Thus, it is of interest to know how the inflammatory response is modulated in these cases due to the interplay between virus and host factors. This review provides an overview of the macroscopic, microscopic, and molecular pathology of PRRSV-1 strains in the lung, emphasising the differences between strains of different virulence.

KEYWORDS

PRRSV-1, pathology, lung, interstitial pneumonia, bronchopneumonia, inflammation, virulence

1 Introduction

More than 30 years after its first description (1, 2), porcine reproductive and respiratory syndrome (PRRS) continues to be one of the greatest threats to the swine industry worldwide (3–6). It has been recently estimated that the economic losses attributable to PRRS in Europe are € 74,181 per farm per year, corresponding to an average of € 255 per sow per year (5). For the American swine industry, the disease costs about $ 664 million annually according to the study performed by Holtkamp et al. (6). Despite many attempts of the scientific community to develop an effective vaccine in the past decades, current available vaccines are not fully protective and only induce partial protection against heterologous strains (7).

The aetiological agent of this disease are PRRS viruses (PRRSV-1 and PRRSV-2), positive-single stranded RNA viruses classified within the genus *Betaarterivirus* (8, 9). The first European and American strains isolated at the beginning of the 90s, Lelystad (LV) strain and VR-2332 strain, respectively (2, 10), which displayed only about 60% of nucleotide similarity,

led to the consideration of two different genotypes of the virus, named as European or genotype-1 (also known as PRRSV-1) and American or genotype-2 (also known as PRRSV-2) (11). Recently, the International Committee on Taxonomy of Viruses reclassified them as two different viral species, *Betaarterivirus suid-1* (PRRSV-1) and *Betaarterivirus suid-2* (PRRSV-2) (9). Four PRRSV-1 subtypes have been identified so far: the pan-European subtype-1, Eastern European subtypes-2 and 3, and subtype-4 with strains from Latvia and Belarus (12–15). PRRSV-2 is mostly prevalent in America and Asia with at least nine well-defined lineages (16). Following the isolation of Lena and SU1-bel strains, enhanced virulence of PRRSV-1 strains was rapidly associated to those included within subtype-3 (17, 18). However, other strains belonging to subtype-1, such as PR40, AUT15-33 and Rosalía, or subtype-2, such as BOR59 strain, showed also high virulence (19–23).

Clinical manifestations depend mostly on the virulence of the PRRSV-1 strain, although other factors, such as management practices, the immunological herd status, genetics of the pigs or co-infections are of importance. The main characteristics and differences in clinical signs, lesions, tropism, and immunological parameters between classic (moderately virulent) and highly virulent PRRSV strains have been recently reviewed (24). Moderately virulent PRRSV-1 strains are often involved in outbreaks of reproductive failure in sows and respiratory disease in growing pigs (2, 10). The manifestations of reproductive failure may vary from sporadic abortions to abortion storms, mainly in the third trimester of gestation, together with premature parturition, delivery of stillborn piglets, mummified piglets or weak-born piglets (2, 10, 18). In piglets of all ages, the virus targets the alveolar macrophages, producing some degree of interstitial pneumonia and impacting secondarily on the body weight gain (19, 25, 26). Experimental infections have shown that moderately virulent PRRSV-1-infected animals usually show lethargy, mild fever and mild to moderate respiratory signs, such as slight dyspnoea, but they usually fully recover after a few days (17–19, 21, 26, 27).

When a virulent PRRSV-1 strain is causing the infection, the clinical pattern changes substantially. High mortality (>20%), prolonged high fever (≥41°C) and severe respiratory disease are common findings of all infections with virulent PRRSV-1 strains (17, 19–21, 24, 25, 27–30). Cyanosis on the ears and tail, conjunctival hyperaemia, and diarrhoea are also clinical manifestations observed in pigs infected with virulent PRRSV-1 strains (19–21, 30). Moreover, clinical manifestations of virulent PRRSV-1 strains appear early after infection, even after 1 day, with a rapid disease onset (18, 19, 21, 27).

The emergence of these virulent PRRSV-1 strains during the last two decades in Europe, such as Lena and SU1-bel strains in Belarus (18), PR40 strain in Italy (19) or Rosalía in Spain (22, 23), has gained special concerns within the pig industry and the research community, due to the high morbidity and mortality rates as well as the severity of the lesions, mainly in the lung (18, 19). Additionally, particular attention has been given to the potential mutation rate and recombination among endemic and emerging strains which may lead to a scenario with the appearance of potentially devastating outbreaks, such as the one caused by Rosalía strain in Spain in 2020, which resulted from the recombination of different PRRSV-1 isolates (22, 23).

PRRSV possesses a restricted cell tropism for $CD163^+$ cells (31, 32). CD163 is mainly expressed on cells of the monocyte/macrophage lineage, especially the pulmonary alveolar macrophage (PAM), making the lung its main target organ (33). This review discusses in depth the pathology of PRRS in the lung, emphasising the different patterns of lung injury observed among PRRSV-1 strains and the possible interaction between the virus and host factors.

2 PRRSV-1 lung lesions

2.1 Macroscopic lung lesions after PRRSV-1 infection

2.1.1 Interstitial pneumonia as PRRSV-induced gross lung lesion

Moderately virulent PRRSV-1-infected grower pigs usually show mild lesions in the lung which frequently go unnoticed, but in the worst-case scenario, pigs develop mild to moderate interstitial pneumonia (2, 10, 29).

The key macroscopic finding in moderately virulent PRRSV-1-infected animals is interstitial pneumonia that macroscopically is characterised by a mottled tan to red and rubbery pulmonary parenchyma which fails to collapse after opening the thoracic cavity, mainly visible at the caudal lobe, (Figure 1A, arrowheads), which can be particularly severe in cases of virulent strains, such as Rosalía strain (Figure 1B, arrowheads) (2, 10, 17, 19, 25–28, 34, 35). The macroscopic scoring system developed by Halbur et al. (36) has been frequently used to evaluate the severity and distribution of pulmonary lesions in PRRS, which considers each lung lobe at the dorsal and ventral view within the entire lung parenchyma (17, 25–28, 34, 37). According to the study performed by Morgan et al. (17) in pigs infected with the prototypical PRRSV-1 strain LV, interstitial pneumonia is visible from day 7 post-infection (pi) onwards; however, no gross lesions are usually detected at 1 month pi in these infected animals (17, 28, 34, 38). Gradual increase of lung consistency on cranial and middle lobes with the progression of the disease over time has been reported, indicating foci of consolidation due to secondary bacterial infections (27, 37). Macroscopically, consolidated areas were swollen, firm and reddish, and clearly demarcated from the rest of the lung. At sectioning, mucopurulent exudate could be observed on airways sometimes, all of it indicative of suppurative bronchopneumonia (39).

2.1.2 Suppurative bronchopneumonia as accompanying lesion to interstitial pneumonia in virulent PRRSV-1-infected animals

In general, field PRRSV infections are frequently accompanied by secondary bacterial complications, conveying to suppurative bronchopneumonia. However, when a virulent PRRSV-1 strain infects the pig under experimental conditions, gross lung lesions are more marked, showing severe diffuse interstitial pneumonia which, different to moderately virulent PRRSV-1 strains, is more commonly accompanied by foci of consolidation from very early stages of infection, resulting from suppurative bronchopneumonia in cranioventral areas (Figure 1C, arrows and inset) (18–20, 25, 27, 28, 30, 34, 37). According to different experimental studies, in infections caused by virulent strains, suppurative bronchopneumonia is already present at very early time points (3 days pi, dpi) and usually culminates between the first and the second-week pi (wpi), exhibiting higher gross pathology scores than the lungs from moderately virulent PRRSV-1-infected animals according to the scoring system developed

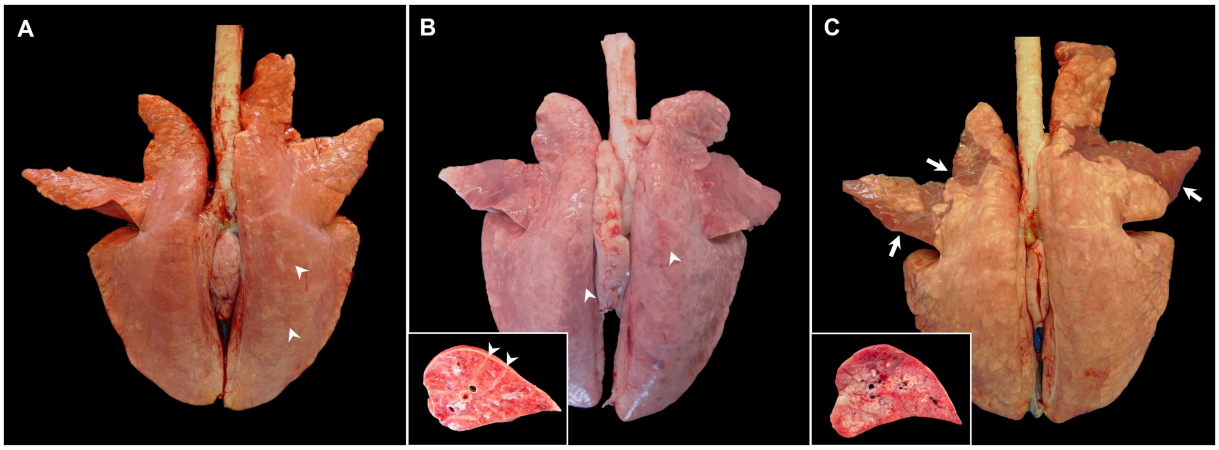

FIGURE 1
Gross pictures of lungs from pigs experimentally infected with PRRSV-1 strains of different virulence and euthanised at 8–10 dpi. **(A)** Lung of a pig infected with 3249 strain showing tan mottling areas (arrowheads), and not collapsing after removal from thoracic cavity. **(B)** Lung from a pig infected with the highly virulent Rosalía strain displaying a marked reddish mottle pattern and diffuse firmness, especially in the dorsal aspect of the lung (arrowheads). Inset shows higher magnification and section of one of the affected lobes. Arrowheads show interstitial oedema. **(C)** Lung from a Lena-infected pig exhibiting tan areas and rubbery texture but also patchy ventral areas of consolidation of the cranial and middle lung lobes (arrows). Inset shows higher magnification and section of the consolidation area of one of the affected lobes.

by Halbur et al. (17, 27, 34, 38). For example, in the study performed by Morgan et al. (17), lungs from animals infected with the virulent SU1-bel strain showed more than 20 score points of difference than those infected with LV strain at 7 dpi, due to secondary bronchopneumonia (17). Interestingly, gross lesions were not visible in the lungs of SU1-bel-infected piglets at 1-month pi (17) and were not observed either in the lung of Lena-infected piglets (38). On the contrary, Frydas et al. (37) showed a similar gross lesion percentage between the low-virulent PRRSV-1 07V063 strain and the 13V091 strain, considered as a virulent PRRSV-1 strain (subtype-1) (37). The discrepancies among these and other studies could be associated to the differences between each experimental set-up, including the dose and route of infection, the inoculum passage and volume, the age of the pigs and their genetic background. Lung weight relative to body weight is a potential indicator of lung inflammation and was used by Weesendorp et al. (40) to evidence differences between lungs from Lena- and LV-infected animals. Lungs from Lena-infected pigs showed higher relative lung weight in comparison with those from LV-infected pigs and uninfected control animals at 1 wpi (40). This relative lung weight decreased drastically at 46 dpi in the Lena-infected group (40), which could indicate a partial resolution of the induced pulmonary lesion.

Although bronchopneumonia is associated with the presence of pathogenic bacteria, their isolation has not been always demonstrated when present in PRRSV-infected animals. Severe lung consolidation was reported in animals infected with 07 V063 and 13 V091 strains, however, no specific bacterial pathogens were isolated (37). On the other hand, the participation of *Staphylococcus hyicus* was demonstrated by conventional bacterial culture in an outbreak that took place in Austria in 2015, caused by the virulent strain AUT15-33, in animals that showed suppurative bronchopneumonia as well as porcine circovirus type 2 (PCV2) coinfection (20). Other macroscopic lung lesions have been described in the lung of virulent PRRSV-1-infected animals. For instance, Karniychuk et al. (18) reported fibrinous pleuropneumonia in 7 out of 10 pigs infected with the virulent PRRSV-1 Lena strain. *Arcanobacterium pyogenes* (currently *Trueperella pyogenes*) and *Streptococcus suis* were isolated in 2 of these animals, whereas no viruses, including PCV2 or swine influenza virus (SIV) were detected (18). Pleurisy was also observed in 2 out of 8 Lena-infected piglets in the study published by Renson et al. (29). Gross lesions secondary to interstitial pneumonia and bronchopneumonia such as multifocal to coalescing areas of atelectasis, congestion, and interstitial and alveolar oedema have also been described in other virulent PRRSV-1 infections (19). The disturbance of the physical barriers and immune response by several viruses, such as PRRSV, PCV2 or SIV, and *Mycoplasma hyopneumoniae*, among others, which are primary agents of the porcine respiratory disease complex (PRDC), is plausible to play a role in the coinfection with secondary endemic bacteria (*Pasteurella multocida*, *Bordetella bronchiseptica*, *Gläesserella parasuis*, etc.) (41, 42) or the proliferation of lung commensal microorganisms. Thus, further studies should address a proper characterisation of the pathogenic bacteria involved in the pathogenesis of the bronchopneumonia that is frequently observed concomitantly in virulent PRRSV-1 infections under experimental and field conditions.

2.2 Microscopic lesions induced by PRRSV-1 strains

2.2.1 Histopathological features of PRRSV-induced interstitial pneumonia

Microscopically, interstitial pneumonia has been reported as the distinctive lesion during PRRS, characterised by multifocal hypertrophy and hyperplasia of type II pneumocytes and alveolar septa thickening with infiltration of mononuclear cells, mainly lymphocytes and macrophages (36, 39, 43). Macrophage alveolar exudation is usually present and hyperplastic pneumocytes may form a continuous layer of cuboidal epithelium lining the alveolus (39, 44). Typically, the bronchiolar epithelium from PRRSV-infected animals

is not affected, a finding that could point into the direction of other viral infections, such as SIV (39). Interstitial pneumonia induced by PCV2 shows a granulomatous pattern with syncytial cells, lymphocytes and polymorphonuclear cells infiltrating the alveolar septa (39, 44). Nonetheless, these findings are not always evident and a clear distinction between PCV2 and PRRSV infection may be hard to find. In PRRSV-1 uncomplicated cases, a mild to moderate multifocal to extensive interstitial pneumonia is usually observed (Figure 2A), which increases in severity alongside the virulence of the strain, and occasionally finding syncytia in those cases too (Figure 2B, inset) (17, 19, 21, 27, 38). Halbur et al. (36) described a scoring system to evaluate interstitial pneumonia which is widely used in porcine pathology studies and for both PRRSV species (27, 28, 34). Briefly, no microscopic lesion is scored as 0, mild interstitial pneumonia is scored as 1 (Figure 3A), moderate multifocal interstitial pneumonia is scored as 2 (Figure 3B), moderate diffuse interstitial pneumonia is scored as 3 (Figure 3C), and severe interstitial pneumonia is scored as 4 (Figure 3D) (36). A separate evaluation of each lung lobe, cranial, middle, and caudal is highly recommended to evaluate the distribution of the lesions as well as to avoid misinterpretation of lung lobes affected by bronchopneumonia. According to this scoring system, lungs from animals infected with virulent PRRSV-1 strains such as SU1-bel or Lena strains, displayed the most severe lesions in comparison with the low-virulent strains used in different experimental trials after 1 wpi (27, 28, 34).

2.2.2 Histopathological features of suppurative bronchopneumonia in virulent PRRSV-1 strains

Although, interstitial pneumonia is the hallmark of PRRSV infection, the presence and proliferation of specific commensal

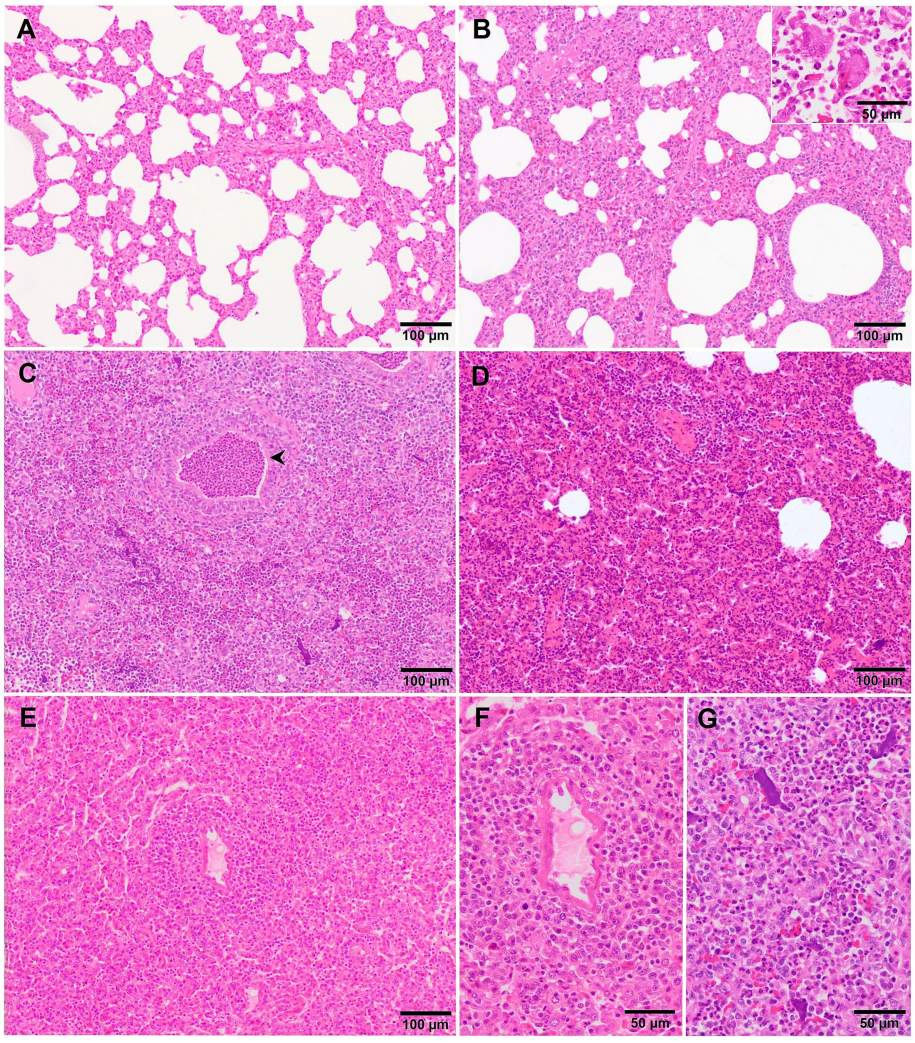

FIGURE 2
Microscopic pictures of the lung of representative pigs experimentally infected with PRRSV-1 strains of different virulence and euthanised at 8–10 dpi. **(A)** Mild thickening of the alveolar septa because of minimal infiltration of macrophages and lymphocytes in the lung tissue of a piglet infected with 3249 strain. **(B)** Moderate to severe thickening of the alveolar septa due to marked infiltration of mononuclear cells with the presence of a syncytia (inset) in the lung of a Lena-infected pig. **(C)** Lung tissue of a Lena-infected pig showing, together with thickening of the alveolar septa, degenerated neutrophils within the lumen of bronchioles (arrowhead) and alveoli as well as cellular debris and aggregates of free chromatin (see for details "**G**"). **(D)** Moderate thickening of alveolar septa with characteristic perivascular lymphocytic and histiocytic infiltrate together with areas of moderate atelectasis in the lung of SU1-bel-infected pig. **(E)** Similar lesions as reported in "**D**" with marked infiltration of macrophages in the alveolar septa and atelectasis in the lung of a pig infected with Rosalía strain. See "**F**" for detail of the periarteriolar infiltrate.

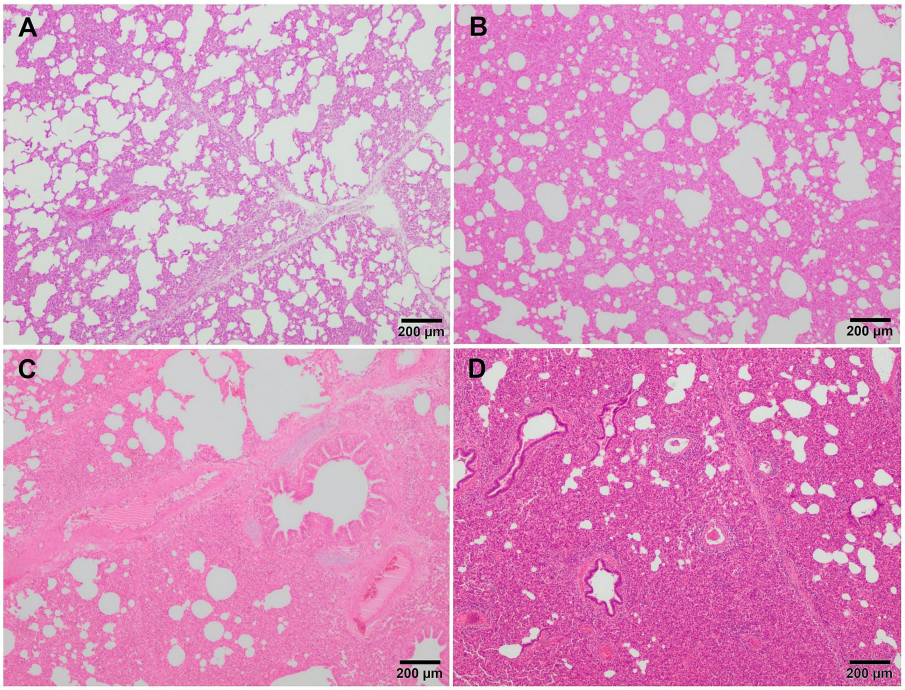

FIGURE 3
Microscopic pictures of representative score of interstitial pneumonia in PRRSV-1 infected pigs. **(A)** Score 1, mild interstitial pneumonia. Mild thickening of the alveolar septa because of minimal infiltration of macrophages and lymphocytes in the lung tissue of a piglet infected with 3249 strain. **(B)** Score 2, moderate interstitial pneumonia. Thickening of the alveolar walls due to moderate infiltration of macrophages and lymphocytes in the lung tissue of a piglet infected with the virulent Lena strain. **(C)** Score 3, moderate diffuse interstitial pneumonia. Infiltration of macrophages and scattered lymphocytes in the lung tissue of a piglet infected with the virulent Lena strain. **(D)** Score 4, severe diffuse interstitial pneumonia in the lung tissue of a piglet infected with the virulent Lena strain.

pathogens from the lung microbiome together with secondary bacterial infections cause suppurative bronchopneumonia, frequently found in virulent PRRSV-infected animals (Figure 2C) (20, 25, 27). Suppurative bronchopneumonia is characterised by abundant granulocytes, macrophages, and cellular debris within the lumen of bronchi, bronchioles, and alveoli (39). This made it necessary to create a scoring system to evaluate this lesion, if present (27). The score system estimates the severity and distribution of the suppurative bronchopneumonia as follows: 0, no microscopic lesions; 1, mild bronchopneumonia (Figure 4A); 2, moderate multifocal bronchopneumonia (Figure 4B); 3, moderate diffuse bronchopneumonia (Figure 4C); and 4, severe bronchopneumonia (Figure 4D). With this scoring system, lung sections from pigs infected with the virulent PRRSV-1 Lena strain showed a score of 1 or 2 at 6 dpi, whereas animals infected with the moderately virulent 3249 strain, reached these scores 1 week later (13 dpi) (27). This suppurative bronchopneumonia is usually accompanied by secondary atelectasis, oedema of the interlobular septa and dilation of lymphatic vessels (20, 27). The presence of fibrinous material in the pleura has been also described as a finding related to infection of the animals with the virulent PRRSV-1 Lena strain (Figure 5A) (18, 27).

Multifocal pyknosis and presence of cellular debris in the septal interstitium and within alveoli have been described in piglets infected with some virulent PRRSV-1 strains (25, 27, 28) in association with regulated cell death (28). The presence of clumps of free chromatin (Figures 2C,G) demonstrated using Feulgen staining (Feulgen^{+}) was frequently observed in Lena- and Rosalía-infected animals with the highest bronchopneumonia scores (27) (Figure 6A). Moreover, this amorphous material was identified as TUNEL^{-}, a technique to detect DNA fragmentation (Figure 6B) and cleaved-caspase-3^{-} (executioner caspase, main marker of apoptosis) (Figure 6C), suggesting that these clumps may be associated with neutrophil extracellular traps (NETs) triggered within foci of suppurative bronchopneumonia (45). NETs formation in the context of virulent PRRSV strains might play a role either preventing microorganisms spread or favouring bacterial growth (45).

2.2.3 Kinetics of microscopic changes in the lung of PRRSV-1 infected animals

Whereas in animals experimentally infected with moderately virulent PRRSV strains lesions are noticeable around the first wpi (27, 28, 34), in those infected with virulent PRRSV-1 strains microscopical lesions develop from 3 dpi onwards, reaching the maximum scores between the first and second wpi (27, 28, 34, 38). At 1-month after infection, interstitial pneumonia is only occasionally present and is of mild intensity (28, 34, 38). Balka et al. (25) observed a significant decrease in the presence of intra-alveolar cellular debris and in the number of intra-alveolar neutrophils throughout the course of the infection (from 10 to 21 dpi) with the virulent German 205817 strain together with an extensive type II pneumocyte proliferation, which was associated with the resolution of the lesion (25). In this sense, type II pneumocytes have been poorly characterised along PRRSV infection and might represent a target cell to understand the progression of the pathogenesis of this disease.

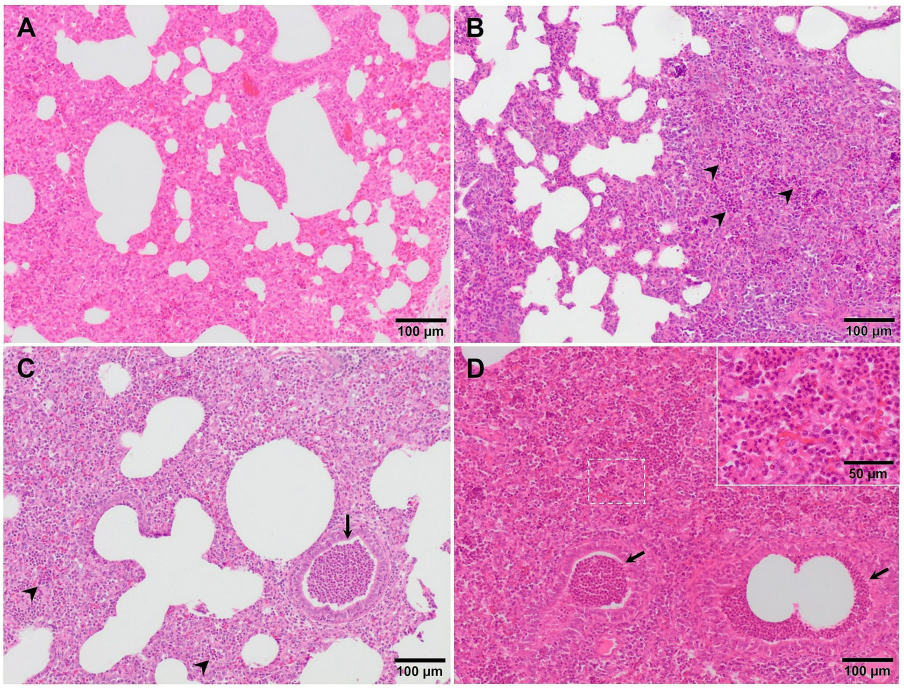

FIGURE 4
Microscopic pictures of representative score of suppurative bronchopneumonia in PRRSV-1 infected pigs. **(A)** Score 1, mild bronchopneumonia in the lung from 3249 infected animal. Granulocytes and macrophages are present in the alveolar septa. **(B)** Score 2, moderate multifocal bronchopneumonia in the lung from an animal infected with the virulent Lena strain. A high number of granulocytes (arrowheads) and macrophages, together with cell debris infiltrate the alveolar walls. **(C)** Score 3, moderate diffuse bronchopneumonia in the lung from an animal infected with Lena strain. Granulocytes (arrowheads), macrophages, and cellular debris within the lumen of bronchi, bronchioles (arrow), and alveoli. Inset show infiltration of macrophages and scattered lymphocytes and granulocytes. **(D)** Score 4, severe bronchopneumonia in the lung from an animal infected with Lena strain. Arrowheads and inset show infiltration of granulocytes within bronchioli and alveoli, respectively.

2.2.4 Other microscopic lung lesional patterns associated with PRRSV-1 infection

Depending on the intensity of the pathological process, additional prominent lesions may be observed, such as proliferative and necrotising pneumonia (PNP), extensive areas of haemorrhage, and varying degrees of vasculitis, characterised by a prominent perivascular mononuclear infiltrate (19, 34, 46, 47). PNP is a severe form of interstitial pneumonia, characterised by two main histological features: (i) lymphohistiocytic interstitial inflammation with hypertrophy and proliferation of type II pneumocytes and (ii) presence of clumps of necrotic inflammatory cells within the alveolar spaces (44, 46, 48, 49). In a recent experimental study, several piglets infected with Rosalía strain developed PNP lesions as soon as 10 dpi (Figures 5B,C) (50). However, besides PRRSV, other aetiological agents such as PCV2 or SIV are usually involved in this lesional pattern (44, 46, 48, 49).

Additionally, other lesional patterns have been described in experimental studies performed with virulent PRRSV-1 strains. For example, Stadejek et al. (21) described a "honeycomb" pattern mostly in animals infected with the virulent PRRSV-1 strain BOR59, isolated in Belarus in 2009. This lesion, observed in animals euthanised at 17- and 22-dpi consisted of areas of fibroblast proliferation and fibrosis of the lung parenchyma, which gave the lung an appearance of loss of its structure (21). Additionally, in these infected animals, a high number of eosinophils, which were sometimes degranulated, was mainly observed in areas of severe lung fibrosis and around blood vessels (21). Associated with these lesions, hyperplasia of lymphoid follicles was also described, being especially noticeable in those animals infected with the virulent PRRSV-1 BOR59 strain in comparison with the moderately virulent strains evaluated: 18794 and ILI6 (21). Similarly, Weesendorp et al. (38), described a higher peribronchiolar cell infiltrate score, mainly formed by macrophage and monocytes at 7 dpi in lungs from animals infected with virulent PRRSV-1 Lena strain compared to the two other moderately virulent strains used in their study. However, this lesion was not so patent in the study performed with the same strain by Rodríguez-Gómez et al. (27), which could be due to the differences on the experimental design between both studies, such as the infectious dose or the age of the animals. A perivascular pattern of inflammatory cells, mainly lymphohistiocytic, was observed in lungs of animals infected with other virulent PRRSV-1 strains such as Lena, SU1-bel and Rosalía (Figures 2D–F) from 3 dpi onwards, being specially marked and obvious in lungs from Rosalía-infected pigs. However, this finding has been also observed from 8 dpi onwards in moderately virulent strains, like 3249 strain (25, 34, 45, 50). Interestingly, and different to what has been previously described for virulent strains, tertiary lymphoid organs were frequently observed in the lungs of Rosalía-infected piglets at 35 dpi (Figure 5D) (50). These structures have been related to robust immune responses to local inflammation at sites of tissue injury (51), indicating an ongoing pulmonary process, far from what has been described for other virulent PRRSV-1 strains in which after 1 month pi, the resolution of the pneumonia was taking place (25, 40).

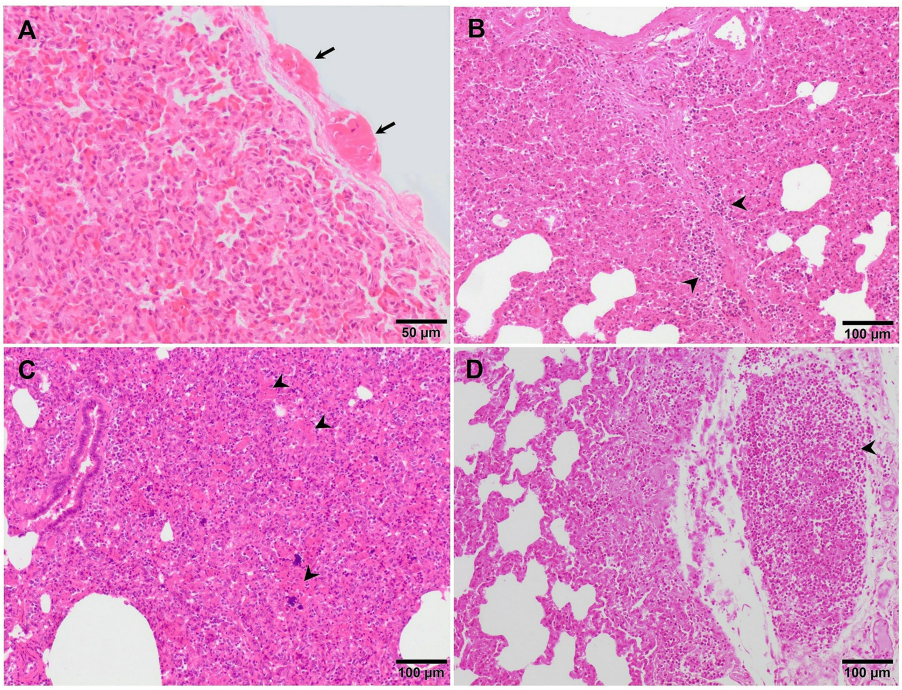

FIGURE 5
Microscopic pictures of the lung of representative pigs experimentally infected with the virulent Lena strain euthanised at 8 dpi **(A)** and with the highly virulent Rosalía strain and euthanised at 10 **(B,C)** and 35 dpi **(D)**. **(A)** Thickening of the pleura due to the presence of fibrin (fibrinous pleuritis). **(B)** Alveolar septa are thickened by macrophages and lymphocytes which also predominantly infiltrate the interlobular septa (arrowheads). **(C)** The lung is moderately atelectatic, with type II pneumocytes hyperplasia and alveoli filling in by necrotic cellular debris (arrowheads), including basophilic clumps of chromatin, compatible with proliferative and necrotising areas of pneumonia. **(D)** Subpleural well-demarcated accumulation of lymphocytes consistent with a tertiary lymphoid organ.

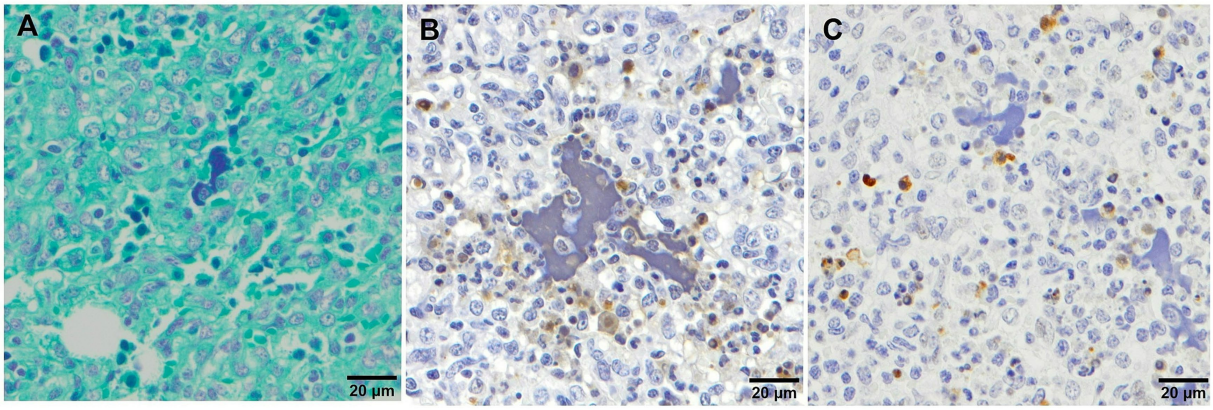

FIGURE 6
Microscopic pictures of clumps of free chromatin demonstrated using Feulgen staining **(A)**, TUNEL **(B)** and cleaved-caspase-3 **(C)** immunohistochemical staining in the lung tissue from virulent Lena infected animals with severe bronchopneumonia. **(A)** Feulgen^{+} staining which demonstrates the presence of clumps of free chromatin. **(B)** TUNEL and **(C)** cleaved-caspase-3 stainings showing the negativity of the clumps of free chromatin.

3 Pathogenic mechanisms of pulmonary lesion in PRRS

3.1 Role of macrophages

The lung mononuclear phagocytic system comprises PAMs, interstitial lung macrophages, and, in several species including pigs, pulmonary intravascular macrophages (PIMs) (52). Whereas the primary function of PAMs is to establish a first line of phagocytic defence against microbial infections, septal macrophages (interstitial macrophages and PIMs) are more specialised in the release of proinflammatory cytokines that contribute to regulate pulmonary homeostasis (26, 53–55). PAMs are the primary target cells of PRRSV, although PIMs and interstitial macrophages are also

susceptible to the infection (26, 33, 56). In this sense, immunolabelling of PRRSV-N-protein is mainly observed in PAMs and to a lesser extent in PIMs and interstitial macrophages (Figure 7A), with clusters of PRRSV-N-protein$^+$ macrophages surrounded by apoptotic bodies within areas of bronchopneumonia in piglets infected with virulent strains (Figure 7B). PAMs express high levels of the CD163 scavenger receptor (56, 57), which plays a crucial role in PRRSV internalisation and disassembly by interacting with GP2 and GP4 viral proteins (32, 58, 59). Replication of PRRSV in PAMs, PIMs and interstitial macrophages leads to an impairment in their fundamental functions including: (a) phagocytosis, which is influenced by the interaction between the virus and CD169 receptor, (b) antigen presentation, and (c) production of proinflammatory cytokines (54, 60–64).

Furthermore, during infection, there is also early cell death of infected PAMs, as well as necrosis and apoptosis of other macrophages and lymphocytes in the lung and lymphoid organs (45, 65–68). These changes contribute to induce an imbalance in the pulmonary immune homeostasis of PRRSV-1-infected piglets, making them more susceptible to a wide range of respiratory pathogens, both viral and bacterial (69), leading to increased severity of clinical signs and pulmonary lesions in co-infected piglets (61).

In this sense, a significant depletion in the frequency of pulmonary CD163$^+$ cells has been reported in PAMs and lung tissue sections of piglets infected with virulent strains such as Lena or SU1-bel around 7–10 dpi (27, 29, 45, 70, 71). CD163$^+$ macrophages play a crucial role in tackling bacterial infections due to the sensing function of this molecule (72). Therefore, a reduction in the population of pulmonary CD163$^+$ cells could potentially compromise lung phagocytic function, complicating cell debris clearance (29). This scenario could potentially create a favourable environment for co-infection with secondary commensal microorganisms, contributing to the development of suppurative bronchopneumonia. This phenomenon, resulting from the direct cytopathic effect of the virus on its target cells and the induction of regulated cell death in both infected and non-infected cells, has been extensively observed in the lungs and lymphoid organs of piglets infected with virulent PRRSV-1 strains (17, 45, 67).

On the other hand, a replenishment of CD163$^+$ cells in the lung of SU1-bel infected pigs at 1 month after infection or at 2 wpi from Lena-infected piglets have been observed. This recovery of CD163$^+$ PAMs has been reported parallel to an increase of arginase1$^+$ (Arg1) macrophages (45), a common feature of M2-macrophages (73), suggesting a role in tissue repair, accelerating the resolution of inflammation (57, 74), which will be in accordance to what was observed during macroscopic lung examination in other studies (25, 40).

Considering *in vitro* studies using monocyte-derived macrophages (MDMs) and supported by the high functional plasticity of pulmonary macrophages and their ability to adapt to different microenvironments (75, 76), it is plausible to hypothesise that during PRRSV-1 infection, pulmonary macrophages undergo distinct activation phases. In the initial phase, macrophages undergo classic activation, also known as M1 polarisation, which is characterised by robust antimicrobial activity (77–79). After PRRSV-1 replication and PAMs cell death, there is an influx of monocytes and macrophages that replenish lung resident macrophages. These recruited cells would undergo a transition to an alternative activation phase, referred to as M2 polarisation as a consequence of the proinflammatory microenvironment induced by virulent PRRSV-1 strains in the lung. Although M2 macrophages are more susceptible to PRRSV infection (74, 80), these macrophages also exhibit anti-inflammatory properties and play a role in tissue repair and inflammation resolution (77–79).

3.2 Mechanisms involved in the regulation of lung inflammation

3.2.1 Type I interferon, an interplay among IFN antiviral response and PRRSV replication

Type I interferons (IFNs), which include IFN-α, IFN-β, IFN-ε, IFN-ω, IFN-k, IFN-δ and IFN-τ, are essential for orchestrating effective antiviral innate and adaptive immune responses, restricting viral replication and viral spread (81, 82). Although PRRSV is highly susceptible to IFN-α both *in vitro* (62, 83, 84) and *in vivo* (85), it induces a weak or negligible production of type I IFN in PAMs and monocyte-derived dendritic cells (MoDCs) *in vitro*. However, systemic IFN-α has been detected following infection with various PRRSV isolates (26, 30, 85–89).

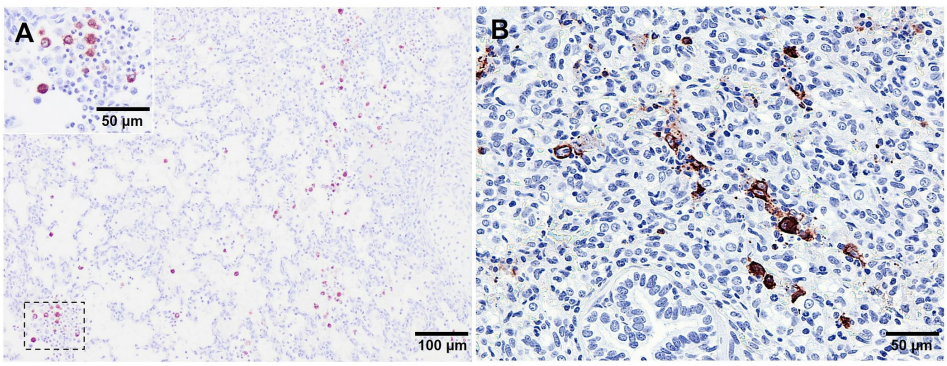

FIGURE 7
Microscopic pictures of PRRSV-N-protein immunohistochemical staining in lung tissue from virulent Lena infected animals euthanised at 8 dpi. **(A)** PRRSV-N-protein$^+$ alveolar macrophages in a field of representative interstitial pneumonia. Inset shows higher magnification of PRRSV-N-protein$^+$ alveolar macrophages. **(B)** Clusters of PRRSV-N-protein$^+$ macrophages surrounded by apoptotic bodies.

This finding suggests that specific cell types are engaged in sensing the infection, and the variation in IFN-α production could be attributed to strain-specific differences in IFN-α induction (30, 74). Notably, the virulent Lena strain, and probably other strains not studied in depth, increase in IFN-α mRNA in blood parallel to the viral load (30). A screening of IFN-stimulated genes (ISGs), a powerful instrument that interferes with viral replication, displayed an upregulation of these genes in bronchoalveolar lavage (BAL) cells from both virulent Lena- and moderately virulent 3249-infected piglets at 3 and 6 dpi (35). Interferon regulatory factors have been also found to be overexpressed in PAMs infected *in vitro* with Lena and LV strains (90). These findings add complexity to the immunopathogenesis of PRRSV infections, as IFN-α should serve as a trigger signal to the immune system and initiate the induction of adaptive immune responses, a process known to be inefficient during PRRSV infection in pigs (74, 91).

3.2.2 Mechanisms of the proinflammatory response at lung level and its mirroring at systemic level

The acute inflammatory response plays a crucial role in the host's innate immune response. In piglets experimentally infected with moderately virulent PRRSV-1 strains, there is a local increase in the expression of IL-1α/β, IL-6, and TNF-α, which correlates with the development of interstitial pneumonia (Figure 8). Unlike other swine viruses, such as African swine fever virus (ASFV), SIV or PRCV, which induce a robust systemic inflammatory response, the serum levels of proinflammatory cytokines in PRRSV infection are limited (26, 53, 92, 93). Furthermore, the levels of these cytokines may vary depending on the PRRSV strain (94, 95). A recent *in vitro* model has reported that PRRSV-2 established similar infection landscapes in PIMs and PAMs but induced more acute and severe inflammatory responses and associated endothelial barrier damage in PIMs than PAMs. Additionally, the TNF-α and IL-1β induced by PRRSV infection disrupted the integrity of the endothelial barrier by dysregulating the tight junction proteins ocludin, claudin-1 and claudin-8, which might improve the permeability of pulmonary capillaries to further enhance the exchange of inflammatory substances and cells, ultimately promoting the development of interstitial pneumonia (96). These findings might be extrapolated to PRRSV-1 and suggest that while the lung tissue exhibits an inflammatory response

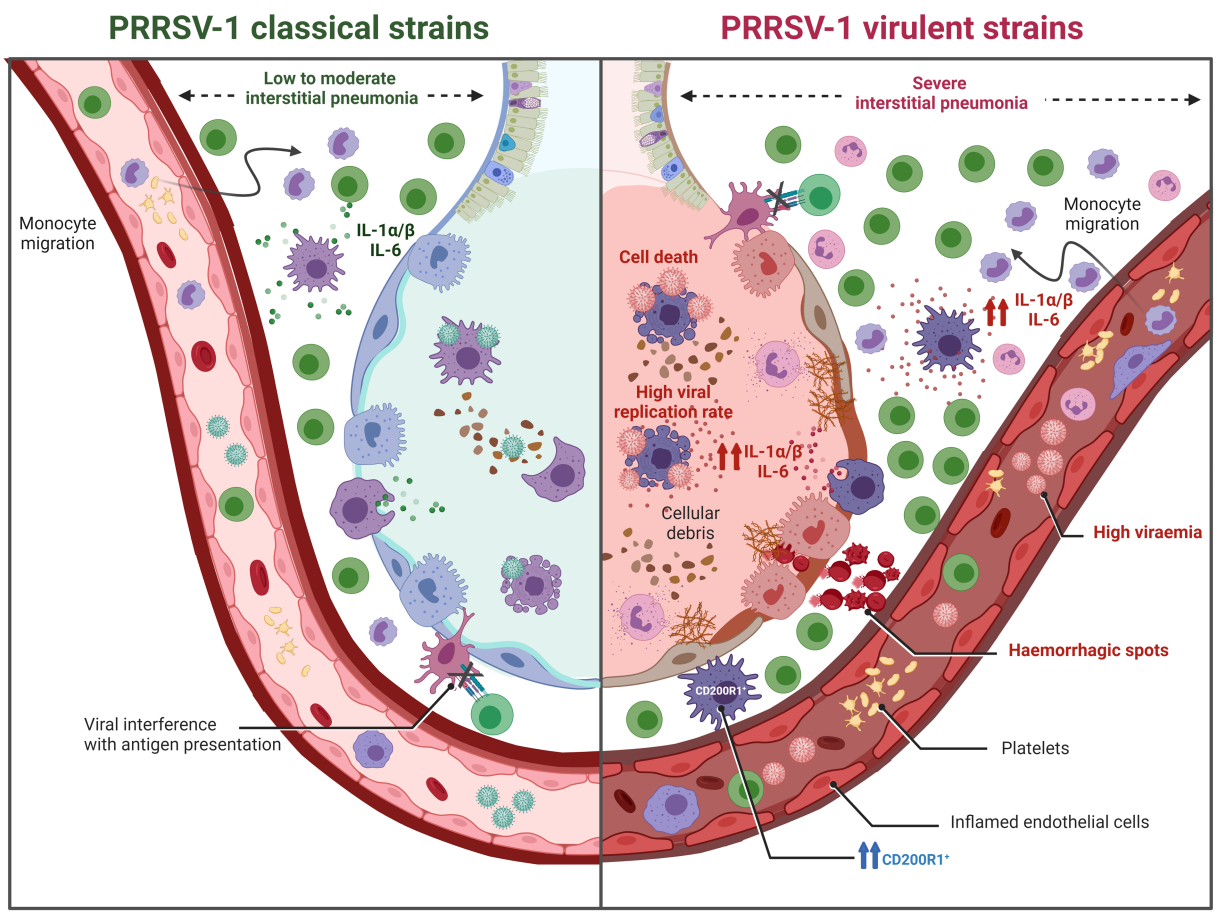

FIGURE 8
Graphic representation of pulmonary lesions induced by PRRSV-1 strains of different virulence (created with BioRender.com). PRRSV-1 classical strains (moderately virulent) typically induce a low to moderate interstitial pneumonia. In contrast, virulent PRRSV-1 strains exhibit heightened viral replication, leading to a significant reduction in pulmonary alveolar macrophages (PAMs) accompanied by early cell death of infected PAMs. Additionally, these strains trigger necrosis and apoptosis in other macrophages and lymphocytes, resulting not only in severe interstitial pneumonia but also, in some instances, in bronchitis, bronchiolitis, and bronchopneumonia. These alterations contribute to an imbalance in pulmonary immune homeostasis, making the host more susceptible to a wide spectrum of respiratory pathogens. The immunopathogenesis of these lesions is partly attributed to a stronger inflammatory response mediated by IL-1α/β when compared to low to moderately virulent strains.

primarily mediated by PIMs and interstitial macrophages, there is a lack of a systemic response. This phenomenon has been associated with a PRRSV strategy to evade the host's immune response and promote viral persistence (61, 97).

Nevertheless, virulent PRRSV-1 strains are able to induce a strong activation of the immune system eliciting a robust systemic inflammatory response (Figure 8). This response is characterised by elevated levels of proinflammatory cytokines such as IL-1α/β, IL-6, TNF-α, or IFN-γ in the bloodstream, leading to high body temperature (ranging from 40.5°C to 42°C) and more severe and acute respiratory clinical signs and lesions. Virulent PRRSV-1 strains have demonstrated enhanced viral replication, resulting in a significant reduction of PAMs and an intensified inflammatory response, leading not only to severe interstitial pneumonia but also in some cases to bronchitis, bronchiolitis, and bronchopneumonia. The pathogenesis of these lesions is partly attributed to the inflammatory response mediated by IL-1α/β. It has been reported that virulent strains, such as Lena or SU1-bel, induced a higher expression of these proinflammatory cytokines compared to moderately virulent strains like LV or Belgium A (34, 38). Moreover, it is important to highlight the synergistic effect of co-infections between PRRSV-1 and bacteria, which triggers a cascade of proinflammatory cytokines that significantly intensify lung damage (98). Notably, not only virulent PRRSV-1 can upregulate the production of IL-1α/β but also some bacteria, such as *Glaesserella parasuis* or *Mycoplasma hyopneumoniae* (99, 100). This interaction between pathogens leads to more severe respiratory complications and exacerbate the overall disease outcome, particularly under field (natural) conditions where multiple pathogens may be present simultaneously.

Several mechanisms have been proposed to contribute to the increased severity of clinical signs and pulmonary lesions in PRRSV-1/bacteria co-infected animals. Firstly, the upregulation of CD14, the main receptor of the LBP (lipopolysaccharide-binding protein) complex. For instance, PRRSV-1 virulent strains, such as Lena, and Rosalía, along with other moderately virulent PRRSV-1 strains, induce the infiltration of $CD14^+$ monocytes in the lungs, as well as PIMs and interstitial macrophages, which infiltrate extensive areas of the interstitium (71, 98, 99). While the influx of $CD14^+$ immature macrophages and monocytes may represent an attempt to replenish the loss of $CD163^+$ macrophages and restore the normal lung function, the increase in $CD14^+$ cells also implies a higher availability of the LPS (lipopolysaccharide)-LBP complex receptor. This increased availability would predispose the lung to a higher production of proinflammatory cytokines upon exposure to bacterial LPS (98, 100–102).

The influence of the respiratory microbiota on the immune response to PRRSV-1 would be another mechanism involved in the increased severity of clinical signs and pulmonary lesions. Among the secondary bacteria isolated from PRRSV-1-infected pigs are low-virulent strains of *Actinobacillus pleuropneumoniae*, *Actinobacillus suis*, *Glaesserella parasuis*, *Pasteurella multocida*, and *Streptococcus suis*. These isolates are commonly associated with suppurative bronchopneumonia. The damage caused by PRRSV in the lung may create an imbalance in the respiratory microbiota, facilitating the growth and proliferation of these secondary bacterial infections, and leading to the development of more complex pneumonia processes, particularly in the case of virulent strains (69, 103, 104).

3.2.3 Modulation and balance of the inflammatory response at lung level

Anti-inflammatory cytokines play an important role in immune homeostasis. Indeed, after a cascade of proinflammatory reactions and apoptosis in the lung, the host should be able to trigger the release of anti-inflammatory and/or regulatory mediators to limit the extent of the lung injury. During the acute phase of PRRSV-1 infection, an increase in $CD200R1^+$ intravascular and interstitial macrophages and $FoxP3^+$ cells have been associated with the severity of lung lesion, particularly within or surrounding foci of bronchopneumonia in piglets infected with the virulent Lena or 3249 PRRSV-1 strains (71). CD200R1 is known for its role in reducing the expression of proinflammatory cytokines in various inflammatory diseases (105). On the other side, FoxP3 is a marker of regulatory T cells (Tregs), which may act as inhibitor of the cell-mediated immune response in pigs upon PRRSV infection (106–109). Therefore, the upregulation of $CD200R1^+$ and $FoxP3^+$ cells represent potential mechanisms involved in the constraint and recovery of lung injury during acute PRRSV-1 infection together with the migration and replenishment of M2 macrophages to the lung.

Furthermore, recently, it has been published that PRRSV-1 may induce an imbalance between costimulatory and coinhibitory immune checkpoints at lung level during the acute phase of infection (110). Thus, it was reported that a modest increase in costimulatory molecules was accompanied by an earlier and more robust upregulation of coinhibitory molecules, particularly in the lungs of those infected with the virulent Lena strain (110). The concurrent expression of these coinhibitory immune checkpoints, as evidenced by the strong correlations observed among them, implies a synergistic action of these molecules, likely aimed at modulating the heightened inflammatory response and mitigating associated lung tissue damage.

The production of IL-10 would be another described mechanism involved in the resolution of inflammation during PRRSV infection. IL-10, a potent anti-inflammatory cytokine, can be induced by certain strains of PRRSV, including the more virulent ones. IL-10 not only controls tissue damage caused by the inflammatory response but also Th1 immune response. IL-10 induction can counteract the effects of IFN-γ and potentially stimulate the proliferation of Tregs. Some studies indicate that PRRSV infection leads to an increase in IL-10 levels, while others have not reported changes in the expression of this cytokine (107, 111–113). The lack of consensus among studies can be attributed to the fact that not all PRRSV strains induce IL-10 release (94, 95, 109, 112, 113).

4 Conclusion

This review delves into the macroscopic, microscopic, and molecular pathology induced by PRRSV-1 strains of different virulence in the lung, relating the different lesion and the molecular patterns. Although the hallmark lesion of interstitial pneumonia is always present in PRRSV infections, its temporal development, severity, and the possible occurrence of PNP and concurrent bronchopneumonia, are influenced by the virulence of the strain and the host-virus interactions. In addition, the way in which the survival and functionality of macrophage population is affected by the infection, and the mechanisms of activation and control of the inflammation occur, play a critical role in the manifestation of the disease. Differences in experimental settings and the emergence of new virulent strains make it difficult to draw a definitive picture of the

immunopathogenesis of this disease, calling for the development of comparative experiments with the inclusion of reference strains.

Author contributions

IR-T: Writing – review & editing, Writing – original draft. JS-C: Writing – review & editing, Writing – original draft. FS: Writing – review & editing, Writing – original draft, Conceptualization. FP: Writing – review & editing. LC: Writing – review & editing. EM: Writing – review & editing. JG-L: Writing – review & editing, Writing – original draft, Conceptualization. IMR-G: Writing – review & editing, Writing – original draft, Conceptualization.

Funding

The author(s) declare that financial support was received for the research, authorship, and/or publication of this article. IR-T and JS-C were supported by a Margarita Salas contract of the Spanish Ministry of Universities. This work was supported by the Spanish Ministry of Economy and Competitiveness (PID2019-109718GB-I00) and by the Junta de Andalucia (ProyExcel_00997).

Conflict of interest

The authors declare that the research was conducted in the absence of any commercial or financial relationships that could be construed as a potential conflict of interest.

The author(s) declared that they were an editorial board member of Frontiers, at the time of submission. This had no impact on the peer review process and the final decision.

Publisher's note

References

1. Keffaber KK. Reproductive failure of unknown etiology. *Am Assoc Swine Pract News*. (1989) 1:1–10.

2. Wensvoort G, Terpstra C, Pol JM, ter Laak EA, Bloemraad M, de Kluyver EP, et al. Mystery swine disease in the Netherlands: the isolation of Lelystad virus. *Vet Q*. (1991) 13:121–30. doi: 10.1080/01652176.1991.9694296

3. Corzo CA, Mondaca E, Wayne S, Torremorell M, Dee S, Davies P, et al. Control and elimination of porcine reproductive and respiratory syndrome virus. *Virus Res*. (2010) 154:185–92. doi: 10.1016/j.virusres.2010.08.016

4. Neumann EJ, Kliebenstein JB, Johnson CD, Mabry JW, Bush EJ, Seitzinger AH, et al. Assessment of the economic impact of porcine reproductive and respiratory syndrome on swine production in the United States. *J Am Vet Med Assoc*. (2005) 227:385–92. doi: 10.2460/javma.2005.227.385

5. Renken C, Nathues C, Swam H, Fiebig K, Weiss C, Eddicks M, et al. Application of an economic calculator to determine the cost of porcine reproductive and respiratory syndrome at farm-level in 21 pig herds in Germany. *Porc Health Manag*. (2021) 7:3. doi: 10.1186/s40813-020-00183-x

6. Holtkamp DJ, Kliebenstein JB, Neumann EJ, Zimmerman JJ, Rotto HF, Yoder TK, et al. Assessment of the economic impact of porcine reproductive and respiratory syndrome virus on United States pork producers. *J Swine Health Prod*. (2013) 21:72–84.

7. Nan Y, Wu C, Gu G, Sun W, Zhang Y-J, Zhou E-M. Improved vaccine against PRRSV: current progress and future perspective. *Front Microbiol*. (2017) 8:1635. doi: 10.3389/fmicb.2017.01635

8. Meulenberg JJ. PRRSV, the virus. *Vet Res*. (2000) 31:11–21. doi: 10.1051/vetres:2000103

9. Brinton MA, Gulyaeva AA, Balasuriya UBR, Dunowska M, Faaberg KS, Goldberg T, et al. ICTV virus taxonomy profile: Arteriviridae 2021. *J Gen Virol*. (2021) 102:001632. doi: 10.1099/jgv.0.001632

10. Collins JE, Benfield DA, Christianson WT, Harris L, Hennings JC, Shaw DP, et al. Isolation of swine infertility and respiratory syndrome virus (isolate ATCC VR-2332) in North America and experimental reproduction of the disease in gnotobiotic pigs. *J Vet Diagn Invest*. (1992) 4:117–26. doi: 10.1177/104063879200400201

11. Murtaugh MP, Elam MR, Kakach LT. Comparison of the structural protein coding sequences of the VR-2332 and Lelystad virus strains of the PRRS virus. *Arch Virol*. (1995) 140:1451–60. doi: 10.1007/BF01322671

12. Stadejek T, Oleksiewicz MB, Potapchuk D, Podgórska K. Porcine reproductive and respiratory syndrome virus strains of exceptional diversity in eastern Europe support the definition of new genetic subtypes. *J Gen Virol*. (2006) 87:1835–41. doi: 10.1099/vir.0.81782-0

13. Stadejek T, Oleksiewicz MB, Scherbakov AV, Timina AM, Krabbe JS, Chabros K, et al. Definition of subtypes in the European genotype of porcine reproductive and respiratory syndrome virus: nucleocapsid characteristics and geographical distribution in Europe. *Arch Virol*. (2008) 153:1479–88. doi: 10.1007/s00705-008-0146-2

14. Stadejek T, Stankevicius A, Murtaugh MP, Oleksiewicz MB. Molecular evolution of PRRSV in Europe: current state of play. *Vet Microbiol*. (2013) 165:21–8. doi: 10.1016/j.vetmic.2013.02.029

15. Balka G, Podgórska K, Brar MS, Bálint Á, Cadar D, Celer V, et al. Genetic diversity of PRRSV 1 in Central Eastern Europe in 1994–2014: origin and evolution of the virus in the region. *Sci Rep*. (2018) 8:7811. doi: 10.1038/s41598-018-26036-w

16. Shi M, Lam TT-Y, Hon C-C, Murtaugh MP, Davies PR, Hui RK-H, et al. Phylogeny-based evolutionary, demographical, and geographical dissection of North American type 2 porcine reproductive and respiratory syndrome viruses. *J Virol*. (2010) 84:8700–11. doi: 10.1128/JVI.02551-09

17. Morgan SB, Graham SP, Salguero FJ, Sánchez Cordón PJ, Mokhtar H, Rebel JMJ, et al. Increased pathogenicity of European porcine reproductive and respiratory syndrome virus is associated with enhanced adaptive responses and viral clearance. *Vet Microbiol*. (2013) 163:13–22. doi: 10.1016/j.vetmic.2012.11.024

18. Karniychuk UU, Geldhof M, Vanhee M, Van Doorsselaere J, Saveleva TA, Nauwynck HJ. Pathogenesis and antigenic characterization of a new East European subtype 3 porcine reproductive and respiratory syndrome virus isolate. *BMC Vet Res*. (2010) 6:30. doi: 10.1186/1746-6148-6-30

19. Canelli E, Catella A, Borghetti P, Ferrari L, Ogno G, De Angelis E, et al. Phenotypic characterization of a highly pathogenic Italian porcine reproductive and respiratory syndrome virus (PRRSV) type 1 subtype 1 isolate in experimentally infected pigs. *Vet Microbiol*. (2017) 210:124–33. doi: 10.1016/j.vetmic.2017.09.002

20. Sinn LJ, Klingler E, Lamp B, Brunthaler R, Weissenböck H, Rümenapf T, et al. Emergence of a virulent porcine reproductive and respiratory syndrome virus (PRRSV) 1 strain in Lower Austria. *Porc Health Manag*. (2016) 2:28. doi: 10.1186/s40813-016-0044-z

21. Stadejek T, Larsen LE, Podgórska K, Bøtner A, Botti S, Dolka I, et al. Pathogenicity of three genetically diverse strains of PRRSV type 1 in specific pathogen free pigs. *Vet Microbiol*. (2017) 209:13–9. doi: 10.1016/j.vetmic.2017.05.011

22. Martín-Valls GE, Cortey M, Allepuz A, Illas F, Tello M, Mateu E. Description of a new clade within subtype 1 of *Betaarterivirus suid 1* causing severe outbreaks in Spain. *Microbiol Resour Announc*. (2022) 11:e00304–22. doi: 10.1128/mra.00304-22

23. Martín-Valls GE, Cortey M, Allepuz A, Illas F, Tello M, Mateu E. Introduction of a PRRSV-1 strain of increased virulence in a pig production structure in Spain: virus evolution and impact on production. *Porc Health Manag*. (2023) 9:1. doi: 10.1186/s40813-022-00298-3

24. Ruedas-Torres I, Rodríguez-Gómez IM, Sánchez-Carvajal JM, Larenas-Muñoz F, Pallarés FJ, Carrasco L, et al. The jigsaw of PRRSV virulence. *Vet Microbiol*. (2021) 260:109168. doi: 10.1016/j.vetmic.2021.109168

25. Balka G, Ladinig A, Ritzmann M, Saalmüller A, Gerner W, Käser T, et al. Immunohistochemical characterization of type II pneumocyte proliferation after challenge with type I porcine reproductive and respiratory syndrome virus. *J Comp Pathol*. (2013) 149:322–30. doi: 10.1016/j.jcpa.2012.12.006

26. Gómez-Laguna J, Salguero FJ, Barranco I, Pallarés FJ, Rodríguez-Gómez IM, Bernabé A, et al. Cytokine expression by macrophages in the lung of pigs infected with the porcine reproductive and respiratory syndrome virus. *J Comp Pathol*. (2010) 142:51–60. doi: 10.1016/j.jcpa.2009.07.004

27. Rodríguez-Gómez IM, Sánchez-Carvajal JM, Pallarés FJ, Mateu E, Carrasco L, Gómez-Laguna J. Virulent Lena strain induced an earlier and stronger downregulation of CD163 in bronchoalveolar lavage cells. *Vet Microbiol*. (2019) 235:101–9. doi: 10.1016/j.vetmic.2019.06.011

28. Morgan SB, Frossard JP, Pallares FJ, Gough J, Stadejek T, Graham SP, et al. Pathology and virus distribution in the lung and lymphoid tissues of pigs experimentally inoculated with three distinct type 1 PRRS virus isolates of varying pathogenicity. *Transbound Emerg Dis*. (2016) 63:285–95. doi: 10.1111/tbed.12272

29. Renson P, Rose N, le Dimna M, Mahé S, Keranflec'h A, Paboeuf F, et al. Dynamic changes in bronchoalveolar macrophages and cytokines during infection of pigs with a highly or low pathogenic genotype 1 PRRSV strain. *Vet Res*. (2017) 48:15. doi: 10.1186/s13567-017-0420-y

30. Weesendorp E, Morgan S, Stockhofe-Zurwieden N, Graaf DJP-D, Graham SP, Rebel JMJ. Comparative analysis of immune responses following experimental infection of pigs with European porcine reproductive and respiratory syndrome virus strains of differing virulence. *Vet Microbiol*. (2013) 163:1–12. doi: 10.1016/j.vetmic.2012.09.013

31. Calvert JG, Slade DE, Shields SL, Jolie R, Mannan RM, Ankenbauer RG, et al. CD163 expression confers susceptibility to porcine reproductive and respiratory syndrome viruses. *J Virol*. (2007) 81:7371–9. doi: 10.1128/JVI.00513-07

32. Whitworth KM, Rowland RRR, Ewen CL, Trible BR, Kerrigan MA, Cino-Ozuna AG, et al. Gene-edited pigs are protected from porcine reproductive and respiratory syndrome virus. *Nat Biotechnol*. (2016) 34:20–2. doi: 10.1038/nbt.3434

33. Duan X, Nauwynck HJ, Pensaert MB. Virus quantification and identification of cellular targets in the lungs and lymphoid tissues of pigs at different time intervals after inoculation with porcine reproductive and respiratory syndrome virus (PRRSV). *Vet Microbiol*. (1997) 56:9–19. doi: 10.1016/S0378-1135(96)01347-8

34. Amarilla SP, Gómez-Laguna J, Carrasco L, Rodríguez-Gómez IM, Caridad y Ocerín JM, Morgan SB, et al. A comparative study of the local cytokine response in the lungs of pigs experimentally infected with different PRRSV-1 strains: upregulation of IL-1α in highly pathogenic strain induced lesions. *Vet Immunol Immunopathol*. (2015) 164:137–47. doi: 10.1016/j.vetimm.2015.02.003

35. Sánchez-Carvajal JM, Rodríguez-Gómez IM, Ruedas-Torres I, Zaldívar-López S, Larenas-Muñoz F, Bautista-Moreno R, et al. Time series transcriptomic analysis of bronchoalveolar lavage cells from piglets infected with virulent or low-virulent porcine reproductive and respiratory syndrome virus 1. *J Virol*. (2022) 96:e0114021. doi: 10.1128/JVI.01140-21

36. Halbur PG, Paul PS, Meng X-J, Lum MA, Andrews JJ, Rathje JA. Comparative pathogenicity of nine US porcine reproductive and respiratory syndrome virus (PRRSV) isolates in a five-week-old cesarean-derived, colostrum-deprived pig model. *J Vet Diagn Invest*. (1996) 8:11–20. doi: 10.1177/104063879600800103

37. Frydas IS, Trus I, Kvisgaard LK, Bonckaert C, Reddy VR, Li Y, et al. Different clinical, virological, serological and tissue tropism outcomes of two new and one old Belgian type 1 subtype 1 porcine reproductive and respiratory virus (PRRSV) isolates. *Vet Res*. (2015) 46:37. doi: 10.1186/s13567-015-0166-3

38. Weesendorp E, Rebel JMJ, Popma-De Graaf DJ, Fijten HPD, Stockhofe-Zurwieden N. Lung pathogenicity of European genotype 3 strain porcine reproductive and respiratory syndrome virus (PRRSV) differs from that of subtype 1 strains. *Vet Microbiol*. (2014) 174:127–38. doi: 10.1016/j.vetmic.2014.09.010

39. Caswell JL, Williams KJ. Respiratory system In: M Grant, editor. *Pathology of domestic animals*. St. Louis, MO: Elsevier (2016). 465.

40. Weesendorp E, Stockhofe-Zurwieden N, Nauwynck HJ, Popma-De Graaf DJ, Rebel JMJ. Characterization of immune responses following homologous reinfection of pigs with European subtype 1 and 3 porcine reproductive and respiratory syndrome virus strains that differ in virulence. *Vet Microbiol*. (2016) 182:64–74. doi: 10.1016/j.vetmic.2015.10.033

41. Assavacheep P, Thanawongnuwech R. Porcine respiratory disease complex: dynamics of polymicrobial infections and management strategies after the introduction of the African swine fever. *Front Vet Sci*. (2022) 9:1048861. doi: 10.3389/fvets.2022.1048861

42. Zhao D, Yang B, Yuan X, Shen C, Zhang D, Shi X, et al. Advanced research in porcine reproductive and respiratory syndrome virus co-infection with other pathogens in swine. *Front Vet Sci*. (2021) 8:699561. doi: 10.3389/fvets.2021.699561

43. Janke BH. Diagnosis of viral respiratory in swine. *J Swine Health Prod*. (1995) 3:116–20.

44. Sarli G, D'Annunzio G, Gobbo F, Benazzi C, Ostanello F. The role of pathology in the diagnosis of swine respiratory disease. *Vet Sci*. (2021) 8:256. doi: 10.3390/vetsci8110256

45. Sánchez-Carvajal JM, Ruedas-Torres I, Carrasco L, Pallarés FJ, Mateu E, Rodríguez-Gómez IM, et al. Activation of regulated cell death in the lung of piglets infected with virulent PRRSV-1 Lena strain occurs earlier and mediated by cleaved caspase-8. *Vet Res*. (2021) 52:12. doi: 10.1186/s13567-020-00882-x

46. Grau-Roma L, Segalés J. Detection of porcine reproductive and respiratory syndrome virus, porcine circovirus type 2, swine influenza virus and Aujeszky's disease virus in cases of porcine proliferative and necrotizing pneumonia (PNP) in Spain. *Vet Microbiol*. (2007) 119:144–51. doi: 10.1016/j.vetmic.2006.09.009

47. Han J, Zhou L, Ge X, Guo X, Yang H. Pathogenesis and control of the Chinese highly pathogenic porcine reproductive and respiratory syndrome virus. *Vet Microbiol*. (2017) 209:30–47. doi: 10.1016/j.vetmic.2017.02.020

48. Drolet R, Larochelle R, Morin M, Delisle B, Magar R. Detection rates of porcine reproductive and respiratory syndrome virus, porcine circovirus type 2, and swine influenza virus in porcine proliferative and necrotizing pneumonia. *Vet Pathol*. (2003) 40:143–8. doi: 10.1354/vp.40-2-143

49. Magar R, Larochelle R, Carman S, Thomson G. Porcine reproductive and respiratory syndrome virus identification in proliferative and necrotizing pneumonia cases from Ontario. *Can Vet J*. (1994) 35:523–4.

50. Sánchez-Carvajal JM, Gómez-Laguna J, Fristikova K, Álvarez-Delgado C, Ruedas-Torres I, Larenas Muñoz F, et al. (2020). Caracterización de una nueva cepa virulenta del PRRSV-1 circulante en España desde. Proceedings of XXXIV Meeting of the Spanish Society of Veterinary Anatomy Pathology. Available at: https://www.uchceu.es/actividades_culturales/2023/jornadas/documentos/Libro%20abstracts.pdf?p=3

51. Bery AI, Shepherd HM, Li W, Krupnick AS, Gelman AE, Kreisel D. Role of tertiary lymphoid organs in the regulation of immune responses in the periphery. *Cell Mol Life Sci*. (2022) 79:359. doi: 10.1007/s00018-022-04388-x

52. Longworth KE. The comparative biology of pulmonary intravascular macrophages. *Front Biosci*. (1997) 2:d232–41. doi: 10.2741/a186

53. Carrasco L, Núñez A, Salguero FJ, Díaz San Segundo F, Sánchez-Cordón P, Gómez-Villamandos JC, et al. African swine fever: expression of interleukin-1 alpha and tumour necrosis factor-alpha by pulmonary intravascular macrophages. *J Comp Pathol*. (2002) 126:194–201. doi: 10.1053/jcpa.2001.0543

54. De Baere MI, Van Gorp H, Delputte PL, Nauwynck HJ. Interaction of the European genotype porcine reproductive and respiratory syndrome virus (PRRSV) with sialoadhesin (CD169/Siglec-1) inhibits alveolar macrophage phagocytosis. *Vet Res*. (2012) 43:47. doi: 10.1186/1297-9716-43-47

55. Sierra MA, Carrasco L, Gómez-Villamandos JC, Martin de las Mulas J, Méndez A, Jover A. Pulmonary intravascular macrophages in lungs of pigs inoculated with African swine fever virus of differing virulence. *J Comp Pathol*. (1990) 102:323–34. doi: 10.1016/s0021-9975(08)80021-7

56. Sánchez C, Doménech N, Vázquez J, Alonso F, Ezquerra A, Domínguez J. The porcine 2A10 antigen is homologous to human CD163 and related to macrophage differentiation. *J Immunol*. (1999) 162:5230–7. doi: 10.4049/jimmunol.162.9.5230

57. Van Gorp H, Delputte PL, Nauwynck HJ. Scavenger receptor CD163, a Jack-of-all-trades and potential target for cell-directed therapy. *Mol Immunol*. (2010) 47:1650–60. doi: 10.1016/j.molimm.2010.02.008

58. Burkard C, Lillico SG, Reid E, Jackson B, Mileham AJ, Ait-Ali T, et al. Precision engineering for PRRSV resistance in pigs: macrophages from genome edited pigs lacking CD163 SRCR5 domain are fully resistant to both PRRSV genotypes while maintaining biological function. *PLoS Pathog*. (2017) 13:e1006206. doi: 10.1371/journal.ppat.1006206

59. Das PB, Dinh PX, Ansari IH, de Lima M, Osorio FA, Pattnaik AK. The minor envelope glycoproteins GP2a and GP4 of porcine reproductive and respiratory syndrome virus interact with the receptor CD163. *J Virol*. (2010) 84:1731–40. doi: 10.1128/JVI.01774-09

60. Darwich L, Díaz I, Mateu E. Certainties, doubts and hypotheses in porcine reproductive and respiratory syndrome virus immunobiology. *Virus Res*. (2010) 154:123–32. doi: 10.1016/j.virusres.2010.07.017

61. Gómez-Laguna J, Salguero FJ, Pallarés FJ, Carrasco L. Immunopathogenesis of porcine reproductive and respiratory syndrome in the respiratory tract of pigs. *Vet J*. (2013) 195:148–55. doi: 10.1016/j.tvjl.2012.11.012

62. Sang Y, Rowland RRR, Blecha F. Interaction between innate immunity and porcine reproductive and respiratory syndrome virus. *Anim Health Res Rev*. (2011) 12:149–67. doi: 10.1017/S1466252311000144

63. Thanawongnuwech R, Halbur PG, Thacker EL. The role of pulmonary intravascular macrophages in porcine reproductive and respiratory syndrome virus infection. *Anim Health Res Rev*. (2000) 1:95–102. doi: 10.1017/S1466252300000086

64. Thanawongnuwech R, Young TF, Thacker BJ, Thacker EL. Differential production of proinflammatory cytokines: *in vitro* PRRSV and *Mycoplasma hyopneumoniae* co-infection model. *Vet Immunol Immunopathol*. (2001) 79:115–27. doi: 10.1016/s0165-2427(01)00243-4

65. Amarilla SP, Gómez-Laguna J, Carrasco L, Rodríguez-Gómez IM, Caridad y Ocerín JM, Graham SP, et al. Thymic depletion of lymphocytes is associated with the virulence of PRRSV-1 strains. *Vet Microbiol*. (2016) 188:47–58. doi: 10.1016/j.vetmic.2016.04.005

66. Rodríguez-Gómez IM, Barranco I, Amarilla SP, García-Nicolás O, Salguero FJ, Carrasco L, et al. Activation of extrinsic- and Daxx-mediated pathways in lymphoid tissue of PRRSV-infected pigs. *Vet Microbiol*. (2014) 172:186–94. doi: 10.1016/j.vetmic.2014.05.025

67. Ruedas-Torres I, Rodríguez-Gómez IM, Sánchez-Carvajal JM, Pallares FJ, Barranco I, Carrasco L, et al. Activation of the extrinsic apoptotic pathway in the thymus of piglets infected with PRRSV-1 strains of different virulence. *Vet Microbiol*. (2020) 243:108639. doi: 10.1016/j.vetmic.2020.108639

68. Gómez-Laguna J, Salguero FJ, Fernández de Marco M, Barranco I, Rodríguez-Gómez IM, Quezada M, et al. Type 2 porcine reproductive and respiratory syndrome virus infection mediated apoptosis in B- and T-cell areas in lymphoid organs of experimentally infected pigs. *Transbound Emerg Dis*. (2013) 60:273–8. doi: 10.1111/j.1865-1682.2012.01338.x

69. Saade G, Deblanc C, Bougon J, Marois-Créhan C, Fablet C, Auray G, et al. Coinfections and their molecular consequences in the porcine respiratory tract. *Vet Res*. (2020) 51:80. doi: 10.1186/s13567-020-00807-8

70. Sánchez-Carvajal JM, Rodríguez-Gómez IM, Carrasco L, Barranco I, Álvarez B, Domínguez J, et al. Kinetics of the expression of CD163 and CD107a in the lung and tonsil of pigs after infection with PRRSV-1 strains of different virulence. *Vet Res Commun*. (2019) 43:187–95. doi: 10.1007/s11259-019-09755-x

71. Sánchez-Carvajal JM, Rodríguez-Gómez IM, Ruedas-Torres I, Larenas-Muñoz F, Díaz I, Revilla C, et al. Activation of pro- and anti-inflammatory responses in lung tissue injury during the acute phase of PRRSV-1 infection with the virulent strain Lena. *Vet Microbiol*. (2020) 246:108744. doi: 10.1016/j.vetmic.2020.108744

72. Fabriek BO, van Bruggen R, Deng DM, Ligtenberg AJM, Nazmi K, Schornagel K, et al. The macrophage scavenger receptor CD163 functions as an innate immune sensor for bacteria. *Blood*. (2009) 113:887–92. doi: 10.1182/blood-2008-07-167064

73. Sautter CA, Auray G, Python S, Liniger M, Summerfield A. Phenotypic and functional modulations of porcine macrophages by interferons and interleukin-4. *Dev Comp Immunol*. (2018) 84:181–92. doi: 10.1016/j.dci.2018.01.018

74. García-Nicolás O, Baumann A, Vielle NJ, Gómez-Laguna J, Quereda JJ, Pallarés FJ, et al. Virulence and genotype-associated infectivity of interferon-treated macrophages by porcine reproductive and respiratory syndrome viruses. *Virus Res*. (2014) 179:204–11. doi: 10.1016/j.virusres.2013.08.009

75. Guth AM, Janssen WJ, Bosio CM, Crouch EC, Henson PM, Dow SW. Lung environment determines unique phenotype of alveolar macrophages. *Am J Physiol Lung Cell Mol Physiol*. (2009) 296:L936–46. doi: 10.1152/ajplung.90625.2008

76. Hussell T, Bell TJ. Alveolar macrophages: plasticity in a tissue-specific context. *Nat Rev Immunol*. (2014) 14:81–93. doi: 10.1038/nri3600

77. Gordon S, Martinez FO. Alternative activation of macrophages: mechanism and functions. *Immunity*. (2010) 32:593–604. doi: 10.1016/j.immuni.2010.05.007

78. Mosser DM. The many faces of macrophage activation. *J Leukoc Biol*. (2003) 73:209–12. doi: 10.1189/jlb.0602325

79. Mosser DM, Edwards JP. Exploring the full spectrum of macrophage activation. *Nat Rev Immunol*. (2008) 8:958–69. doi: 10.1038/nri2448

80. Wang L, Hu S, Liu Q, Li Y, Xu L, Zhang Z, et al. Porcine alveolar macrophage polarization is involved in inhibition of porcine reproductive and respiratory syndrome virus (PRRSV) replication. *J Vet Med Sci*. (2017) 79:1906–15. doi: 10.1292/jvms.17-0258

81. Perry AK, Chen G, Zheng D, Tang H, Cheng G. The host type I interferon response to viral and bacterial infections. *Cell Res*. (2005) 15:407–22. doi: 10.1038/sj.cr.7290309

82. Sadler AJ, Williams BRG. Interferon-inducible antiviral effectors. *Nat Rev Immunol*. (2008) 8:559–68. doi: 10.1038/nri2314

83. Loving CL, Brockmeier SL, Sacco RE. Differential type I interferon activation and susceptibility of dendritic cell populations to porcine arterivirus. *Immunology*. (2007) 120:217–29. doi: 10.1111/j.1365-2567.2006.02493.x

84. Luo R, Fang L, Jin H, Jiang Y, Wang D, Chen H, et al. Antiviral activity of type I and type III interferons against porcine reproductive and respiratory syndrome virus (PRRSV). *Antivir Res*. (2011) 91:99–101. doi: 10.1016/j.antiviral.2011.04.017

85. Brockmeier SL, Loving CL, Nelson EA, Miller LC, Nicholson TL, Register KB, et al. The presence of alpha interferon at the time of infection alters the innate and adaptive immune responses to porcine reproductive and respiratory syndrome virus. *Clin Vaccine Immunol*. (2012) 19:508–14. doi: 10.1128/CVI.05490-11

86. Albina E, Piriou L, Hutet E, Cariolet R, L'Hospitalier R. Immune responses in pigs infected with porcine reproductive and respiratory syndrome virus (PRRSV). *Vet Immunol Immunopathol*. (1998) 61:49–66. doi: 10.1016/S0165-2427(97)00134-7

87. Gómez-Laguna J, Salguero FJ, De Marco MF, Pallarés FJ, Bernabé A, Carrasco L. Changes in lymphocyte subsets and cytokines during European porcine reproductive and respiratory syndrome: increased expression of IL-12 and IL-10 and proliferation of $CD4^{-}CD8^{high}$. *Viral Immunol*. (2009) 22:261–71. doi: 10.1089/vim.2009.0003

88. Liu X, Bai J, Wang H, Fan B, Li Y, Jiang P. Effect of amino acids residues 323–433 and 628–747 in Nsp2 of representative porcine reproductive and respiratory syndrome virus strains on inflammatory response *in vitro*. *Virus Res*. (2015) 208:13–21. doi: 10.1016/j.virusres.2015.05.016

89. Dwivedi V, Manickam C, Binjawadagi B, Linhares D, Murtaugh MP, Renukaradhya GJ. Evaluation of immune responses to porcine reproductive and respiratory syndrome virus in pigs during early stage of infection under farm conditions. *Virol J*. (2012) 9:45. doi: 10.1186/1743-422X-9-45

90. Badaoui B, Rutigliano T, Anselmo A, Vanhee M, Nauwynck H, Giuffra E, et al. RNA-sequence analysis of primary alveolar macrophages after *in vitro* infection with porcine reproductive and respiratory syndrome virus strains of differing virulence. *PLoS One*. (2014) 9:e91918. doi: 10.1371/journal.pone.0091918

91. Baumann A, Mateu E, Murtaugh MP, Summerfield A. Impact of genotype 1 and 2 of porcine reproductive and respiratory syndrome viruses on interferon-α responses by plasmacytoid dendritic cells. *Vet Res*. (2013) 44:33. doi: 10.1186/1297-9716-44-33

92. Khatri M, Dwivedi V, Krakowka S, Manickam C, Ali A, Wang L, et al. Swine influenza H1N1 virus induces acute inflammatory immune responses in pig lungs: a potential animal model for human H1N1 influenza virus. *J Virol*. (2010) 84:11210–8. doi: 10.1128/JVI.01211-10

93. Van Reeth K, Labarque G, Nauwynck H, Pensaert M. Differential production of proinflammatory cytokines in the pig lung during different respiratory virus infections: correlations with pathogenicity. *Res Vet Sci*. (1999) 67:47–52. doi: 10.1053/rvsc.1998.0277

94. Darwich L, Gimeno M, Sibila M, Diaz I, de la Torre E, Dotti S, et al. Genetic and immunobiological diversities of porcine reproductive and respiratory syndrome genotype I strains. *Vet Microbiol*. (2011) 150:49–62. doi: 10.1016/j.vetmic.2011.01.008

95. Gimeno M, Darwich L, Diaz I, de la Torre E, Pujols J, Martín M, et al. Cytokine profiles and phenotype regulation of antigen presenting cells by genotype-I porcine reproductive and respiratory syndrome virus isolates. *Vet Res*. (2011) 42:9. doi: 10.1186/1297-9716-42-9

96. Sun W, Wu W, Jiang N, Ge X, Zhang Y, Han J, et al. Highly pathogenic PRRSV-infected alveolar macrophages impair the function of pulmonary microvascular endothelial cells. *Viruses*. (2022) 14:452. doi: 10.3390/v14030452

97. Lunney JK, Fang Y, Ladinig A, Chen N, Li Y, Rowland B, et al. Porcine reproductive and respiratory syndrome virus (PRRSV): pathogenesis and interaction with the immune system. *Annu Rev Anim Biosci*. (2016) 4:129–54. doi: 10.1146/annurev-animal-022114-111025

98. Van Gucht S, Labarque G, Van Reeth K. The combination of PRRS virus and bacterial endotoxin as a model for multifactorial respiratory disease in pigs. *Vet Immunol Immunopathol*. (2004) 102:165–78. doi: 10.1016/j.vetimm.2004.09.006

99. Kavanová L, Prodělalová J, Nedbalcová K, Matiašovic J, Volf J, Faldyna M, et al. Immune response of porcine alveolar macrophages to a concurrent infection with porcine reproductive and respiratory syndrome virus and *Haemophilus parasuis in vitro*. *Vet Microbiol*. (2015) 180:28–35. doi: 10.1016/j.vetmic.2015.08.026

100. Thanawongnuwech R, Thacker B, Halbur P, Thacker EL. Increased production of proinflammatory cytokines following infection with porcine reproductive and respiratory syndrome virus and *Mycoplasma hyopneumoniae*. *Clin Diagn Lab Immunol*. (2004) 11:901–8. doi: 10.1128/CDLI.11.5.901-908.2004

101. Qiao S, Jiang Z, Tian X, Wang R, Xing G, Wan B, et al. Porcine FcγRIIb mediates enhancement of porcine reproductive and respiratory syndrome virus (PRRSV) infection. *PLoS One*. (2011) 6:e28721. doi: 10.1371/journal.pone.0028721

102. Van Gucht S, Van Reeth K, Nauwynck H, Pensaert M. Porcine reproductive and respiratory syndrome virus infection increases CD14 expression and lipopolysaccharide-binding protein in the lungs of pigs. *Viral Immunol*. (2005) 18:116–26. doi: 10.1089/vim.2005.18.116

103. Brockmeier SL, Loving CL, Palmer MV, Spear A, Nicholson TL, Faaberg KS, et al. Comparison of Asian porcine high fever disease isolates of porcine reproductive and respiratory syndrome virus to United States isolates for their ability to cause disease and secondary bacterial infection in swine. *Vet Microbiol*. (2017) 203:6–17. doi: 10.1016/j.vetmic.2017.02.003

104. Karst SM. The influence of commensal bacteria on infection with enteric viruses. *Nat Rev Microbiol*. (2016) 14:197–204. doi: 10.1038/nrmicro.2015.25

105. Vaine CA, Soberman RJ. The CD200-CD200R1 inhibitory signaling pathway: immune regulation and host-pathogen interactions. *Adv Immunol*. (2014) 121:191–211. doi: 10.1016/B978-0-12-800100-4.00005-2

106. Ferrarini G, Borghetti P, De Angelis E, Ferrari L, Canelli E, Catella A, et al. Immunoregulatory signal FoxP3, cytokine gene expression and IFN-γ cell responsiveness upon porcine reproductive and respiratory syndrome virus (PRRSV) natural infection. *Res Vet Sci*. (2015) 103:96–102. doi: 10.1016/j.rvsc.2015.09.018

107. Nedumpun T, Sirisereewan C, Thanmuan C, Techapongtada P, Puntarotairung R, Naraprasertkul S, et al. Induction of porcine reproductive and respiratory syndrome virus (PRRSV)-specific regulatory T lymphocytes (Treg) in the lungs and tracheobronchial lymph nodes of PRRSV-infected pigs. *Vet Microbiol*. (2018) 216:13–9. doi: 10.1016/j.vetmic.2018.01.014

108. Silva-Campa E, Flores-Mendoza L, Reséndiz M, Pinelli-Saavedra A, Mata-Haro V, Mwangi W, et al. Induction of T helper 3 regulatory cells by dendritic cells infected with porcine reproductive and respiratory syndrome virus. *Virology*. (2009) 387:373–9. doi: 10.1016/j.virol.2009.02.033

109. Silva-Campa E, Cordoba L, Fraile L, Flores-Mendoza L, Montoya M, Hernández J. European genotype of porcine reproductive and respiratory syndrome (PRRSV) infects monocyte-derived dendritic cells but does not induce Treg cells. *Virology*. (2010) 396:264–71. doi: 10.1016/j.virol.2009.10.024

110. Ruedas-Torres I, Sánchez-Carvajal JM, Carrasco L, Pallarés FJ, Larenas-Muñoz F, Rodríguez-Gómez IM, et al. PRRSV-1 induced lung lesion is associated with an imbalance between costimulatory and coinhibitory immune checkpoints. *Front Microbiol*. (2022) 13:1007523. doi: 10.3389/fmicb.2022.1007523

111. Ruedas-Torres I, Gómez-Laguna J, Sánchez-Carvajal JM, Larenas-Muñoz F, Barranco I, Pallarés FJ, et al. Activation of T-bet, FOXP3, and EOMES in target organs from piglets infected with the virulent PRRSV-1 Lena strain. *Front Immunol*. (2021) 12:773146. doi: 10.3389/fimmu.2021.773146

112. Wongyanin P, Buranapraditkun S, Chokeshai-Usaha K, Thanawonguwech R, Suradhat S. Induction of inducible $CD4^{+}$ $CD25^{+}$ $Foxp3^{+}$ regulatory T lymphocytes by porcine reproductive and respiratory syndrome virus (PRRSV). *Vet Immunol Immunopathol*. (2010) 133:170–82. doi: 10.1016/j.vetimm.2009.07.012

113. Wongyanin P, Buranapraditkul S, Yoo D, Thanawongnuwech R, Roth JA, Suradhat S. Role of porcine reproductive and respiratory syndrome virus nucleocapsid protein in induction of interleukin-10 and regulatory T-lymphocytes (Treg). *J Gen Virol*. (2012) 93:1236–46. doi: 10.1099/vir.0.040287-0

Glossary

PRRS	Porcine reproductive and respiratory syndrome
PRRSV	Porcine reproductive and respiratory syndrome virus
LV	Lelystad strain
PAM	Pulmonary alveolar macrophage
pi	Post-infection
dpi	Days post-infection
wpi	Weeks post-infection
PIM	Pulmonary intravascular macrophage
PCV2	Porcine circovirus type 2
SIV	Swine influenza virus
PRDC	Porcine respiratory disease complex
NETs	Neutrophil extracellular traps
PNP	Proliferative and necrotising pneumonia
PIM	Pulmonary intravascular macrophages
PRCV	Porcine respiratory coronavirus
MDMs	Monocyte-derived macrophages
IFNs	Type I interferons
MoDCs	Monocyte-derived dendritic cells
pDCs	Plasmacytoid dendritic cells
ISGs	IFN-stimulated genes
BAL	bronchoalveolar lavage
ASFV	African swine fever virus
LBP	Lipopolysaccharide-binding protein
LPS	Lipopolysaccharide
Tregs	Regulatory T cells

frontiers | Frontiers in Veterinary Science

TYPE Mini Review
PUBLISHED 24 April 2024
DOI 10.3389/fvets.2023.1266499

OPEN ACCESS

EDITED BY
Francisco José Pallarés,
University of Cordoba, Spain

REVIEWED BY
Francisco Rivera-Benítez,
Instituto Nacional de Investigaciones Forestales, Agrícolas y Pecuarias (INIFAP), Mexico

*CORRESPONDENCE
Diego Ferreira da Silva
✉ ferreira.diego@usp.br

RECEIVED 25 July 2023
ACCEPTED 13 December 2023
PUBLISHED 24 April 2024

CITATION
Silva RRd, Silva DFd, Silva VHd and Castro AMMGd (2024) Porcine circovirus 3: a new challenge to explore.
Front. Vet. Sci. 10:1266499.
doi: 10.3389/fvets.2023.1266499

Porcine circovirus 3: a new challenge to explore

Rosecleer Rodrigues da Silva[1], Diego Ferreira da Silva[2,3]*, Victor Hugo da Silva[3] and Alessandra M. M. G. de Castro[3]

[1]Department of Undergraduate Studies in Veterinary Medicine, Faculdade Anclivepa, São Paulo, Brazil, [2]Postgraduate Program in Adult Health Nursing (PROESA), Escola de Enfermagem da Universidade de São Paulo (EEUSP), São Paulo, Brazil, [3]Graduate Program in Environmental and Experimental Pathology, Universidade Paulista (UNIP), São Paulo, Brazil

The intensification of production processes, resulting from the rise in pork production, contributes to environmental changes and increased interaction between humans, animals, and wildlife. This favorable scenario promotes the spread of potent viral species, such as PCV3, increasing the potential for the emergence of new pathogenic agents and variants. These changes in the epidemiology and manifestation of PCV3 highlight the need for enhanced understanding and control. The current literature presents challenges in the classification of PCV3, with different groups proposing diverse criteria. Establishing common terminology is crucial to facilitate comparisons between studies. While consensus among experts is valuable, new approaches must be transparent and comparable to existing literature, ensuring reproducible results and proper interpretation, and positively impacting public health. This study aims to review the literature on PCV3 infection, exploring its key aspects and highlighting unanswered questions.

KEYWORDS

emerging, porcine circovirus, swine, PCR, hosts

Introduction

Brazil, the fourth-largest global pork producer, has witnessed a remarkable increase in production over the past four decades, rising from 1.15 million tons in 1980 to 4.95 million tons in 2022 (1). Projections indicate a further increase to 5.1 million tons by 2023, according to the Brazilian Swine Breeders Association (ABCS) and the Brazilian Animal Protein Association (ABPA) (2, 3). This expanding context is crucial for comprehending the emergence of Porcine Circovirus 3 (PCV3) as a new challenge.

The increase in pork production has a direct impact on the intensification of production processes. Coupled with the rise in the human population, urbanization, environmental alterations, and interaction with wildlife, this trend creates a favorable environment for the spread and perpetuation of potent viral species. Consequently, this scenario increases the potential of new pathogen emergence and/or variants, leading to shifts in epidemiology and disease manifestation (4–6).

Since 1980, various significant viruses were reported in pigs' productions systems across multiple countries, including certain species of porcine circovirus (PCV). PCVs belong to the *Circovirus* genus of the *Circoviridae* family and currently encompass four species: *Porcine circovirus* 1 (PCV1), *Porcine circovirus* 2 (PCV2), *Porcine circovirus* 3 (PCV3), and *Porcine circovirus* 4 (PCV4). Among these, PCV2 is the primary emerging virus documented so far (7–9).

Porcine circovirus 3 (PCV3), the focus of this study, was first identified in 2015 in sows and mummified fetuses from a pig farm in North Carolina. Since then, PCV3 has been reported in various countries (10–16). It is one of the most extensively studied PCVs, second only to PCV2, as evidenced by the high number ($n = 624$) of publications on PUBMED[1] using the term "Porcine circovirus 3" since 2016. PCV3 presents significant challenges in its classification due to the notable genetic variability and the diverse proposals for taxonomic criteria in the literature. Therefore, it is imperative to conduct in-depth research to establish common terminology and solid classification criteria, ensuring reproducible results and promoting essential advances in the understanding and management of viral diseases, with substantial impacts on animal health and potential public health ramifications (17).

Characterization and viral diversity

PCV3, which is a member of the *Circovirus* genus within the *Circoviridae* family, has an icosahedral morphology with approximately 17 nm in diameter and is non-enveloped. Its genome is composed of a circular single-stranded DNA. Over time, PCV3 detection in swine herds has been increasing worldwide since its initial discovery. In addition, although the PCV3's mutation rate is lower than that of PCV2, several studies have identified the classification of PCV3 into two separate subtypes (PCV3a and PCV3b) or three genotypes (PCV3a, PCV3b, and PCV3c). The PCV3 genome consists of single circular DNA strand consisting of 2000 nucleotides (nt), with two primary genes oriented in opposite directions (ambisense expression). The genome is comprised of 50% GC and features three main Open Reading Frames (ORF) (10, 11, 18).

Like the others PCVs, the genomic arrangement of PCV3 includes two main genes, ORF1 and ORF2, which are positioned in opposite directions. ORF2 codes for the viral capsid proteins, known as the cap gene, while ORF1 codes for the replicase, or rep gene. Additionally, there is a hairpin structure (*stem-loop*) in the 5' 235 nt intergenic region between ORF1 and ORF2 that contains a conserved sequence (TAGTATTAC). This conserved sequence serves as the origin of replication (ori) during the rolling circle replication process. A schematic representation of the PCVs genome is presented in (Figure 1) (10, 11, 21, 22).

The ORF1 gene is located on the positive strand (sense) of the circovirus genome and is known to be the most conserved region. In PCV3, ORF1 also encodes a single replicase protein consisting of 296-297 amino acids (aa). Additionally, the gene features three Rolling Circle Replication (RCR) motifs (FTINN, HLQG, and YCKK) and an initiation codon (GTC) located at the 5' end of the rep gene (9, 11). Analysis of circovirus RCR motifs has revealed that PCV3, goose circovirus (GoCV), and pigeon circovirus (PiCV) share a degree of similarity. However, there is one mutation that has been identified in the FTLNN motif, which is present as FTINN in PCV3 (11). Although three other motifs (WWDGY, DDFGWVP, and DRYP) have been identified in PCV3, their functions remain unknown (11). Similarly, as in PCV4, the ORF1 in PCV3 encodes a replicase protein with 296 amino acids (23). ORF1 codes for the Rep and Rep' proteins in PCV1 and PCV2. In PCV1, the Rep and Rep' proteins consist of 312 and 168 amino acids, respectively. In PCV2, the Rep protein consists of 314 amino acids, while the Rep' protein consists of 297 amino acids (24). Therefore, the comparison between the ORF1 of PCV3 and PCV4 reveals crucial nuances in viral research. While PCV3 features a replicase of 296-297 amino acids with three RCR motifs, PCV4 shares a configuration of 296 amino acids, resembling PCV3 (25). However, thorough investigation of RCR motifs in PCV4 is currently underway. This analysis is pivotal in unraveling the evolutionary and functional adaptations of these circoviruses, providing valuable insights for swine disease control strategies. Therefore, future research utilizing advanced techniques is essential to elucidate the complexities of ORF1 in PCV4 and its implications for swine health.

Located on the negative strand (antisense) of the viral DNA, ORF2 encodes only one structural protein known as Cap, which is considered the most variable and immunogenic. The Cap protein comprises 230-233 amino acids in PCV1, 233-236 amino acids in PCV2, 214 amino acids in PCV3, and 228 amino acids in PCV4. Phylogenetic analyses have shown that PCV1 and PCV2 have a 67% similarity in the Cap protein, whereas the similarity reduces to 24% between PCV1 and PCV3, and of 26 to 37% between PCV2 and PCV3 (10, 11, 26).

ORF3 displays a different sense among PCVs, as it is located on the sense strand in PCV3 and on the antisense strand in PCV1 and PCV2. In both PCV1 and PCV2, this region encodes a non-structural protein capable of inducing apoptosis, with 206 aa and 104 aa, respectively. ORF3 in PCV3 codes for a 231 aa protein, but the function and initiation codon remain unknown (10, 11). According to Ye et al. (27), the amino acid sequence of PCV3 shows homology to PCV1 and PCV2 at only 31 and 48%, respectively. No information is available on ORF3 in PCV4.

According to phylogenetic studies, the origin of PCV3 is distinct from other PCVs, and it shares a common ancestor with circoviruses found in bats. A comparative analysis of the genomics indicated that the most conserved area among PCV3, PCV2, and bat circovirus is confined to ORF1, which is responsible for encoding the rep protein. Conversely, no significant alignment was detected in ORF2, which encodes the cap protein. Despite presenting conserved segments with other circoviruses, the PCV3 ORF1 is genetically distant and has accumulated several mutations over time, indicating that the divergence between virus species occurred approximately 50 years ago (28).

It must be highlighted that PCV3 can be divided into two (PCV3a and PCV3b) (13) or three (PCV3a, PCV3b, and PCV3c) (9, 14) genotypes based on the mutation of two amino acids (A24V and R27K) found in the cap protein (11, 29). Several studies have also pointed toward the subdivision of PCV3a (13, 29–31). According to Li et al. (13), PCV3a can be divided into two stable subclades (PCV3a-1 and PCV3a-2) and an intermediate clade (PCV3a-3), which supports the subdivision proposed by Zheng et al. (29). However, a more recent study by Chen et al. (30) described, also, the division of PCV3b into two subclades (PCV3b-1 and PCV3b-2), in addition to the subclades of PCV3a (PCV3a-1, PCV3a-2, PCV3-a-3) (32). conducted a PCV3 mapping based on a viral coding gene that resulted in three genotypes and several subtypes (genotype 1, genotype 2 with subtypes a and b, genotype 3 with subtypes a–h). These findings highlight the genetic diversity of PCV3 and its tendency to increase

1 https://pubmed.ncbi.nlm.nih.gov/

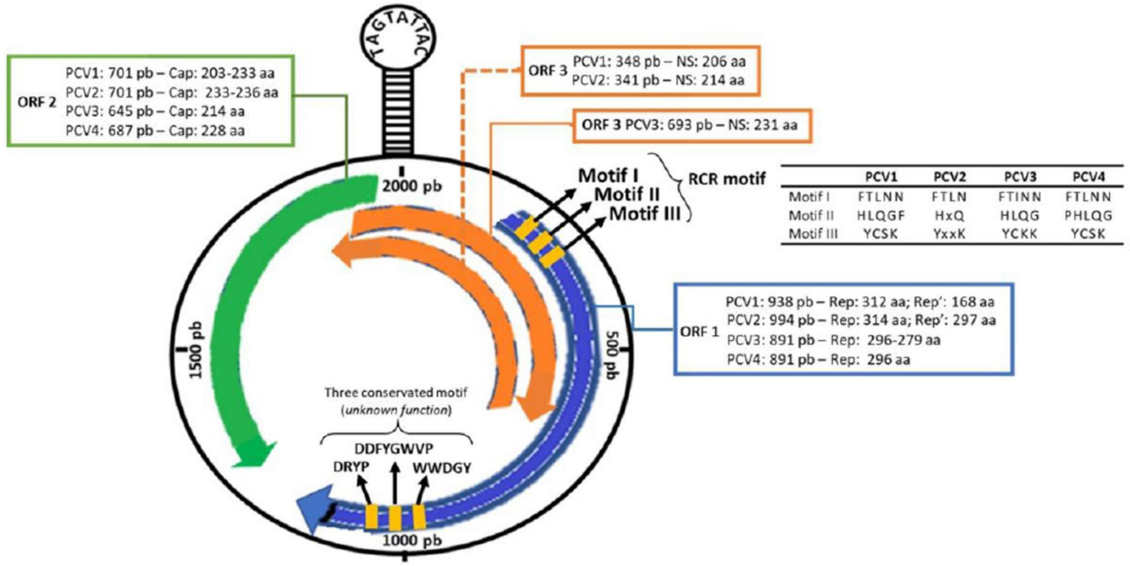

FIGURE 1
Schematic representation of the PCV3 genome. Information for comparing the open reading regions (ORF1, ORF2, ORF3) and their encoded proteins (rep, rep' and cap) among the four porcine circovirus species (PCV1, PCV2, PCV3 and PCV4) [Updated with information from Chen et al. (19), Klaumann et al. (20), and Ouyang et al. (14)].

within the global swine population, while also underscoring the challenge in establishing the pathogenesis caused by PCV3 infection (13, 33). The nomenclatures utilized thus far for PCV3 are succinctly outlined in Table 1.

Like the extensively studied PCV2, which has undergone various subclassifications (clades, genogroups and genotypes) since its discovery, PCV3 follows a comparable pattern of classification. In summary, validated criteria for defining a PCV3 genotype include a maximum genetic distance of 3% at the complete genome and 6% at ORF2 levels, as well as a bootstrap support or posterior probability on the phylogenetic tree greater than 90% (10).

Other studies (13, 15, 34) classified PCV3 into three distinct genotypes, i.e., PCV3a, 3b, and 3c. However, when aligning sequences from these genotypes, a remarkable genetic similarity to previously classified as PCV3a emerged. The maximum genetic distance observed among reported ORF2 sequences was 0.0388 (3.8%), below the recommended threshold for defining a new genotype. Hence, following established criteria, all these sequences would be categorized within the PCV3a classification. Currently, efforts have been made to standardize the classification of the PCV3 virus at the subspecies level. A standard classification will be essential for effective disease control, offering substantial benefits to animal and public health initiatives.

Epidemiology

PCV3, which was initially identified in the United States in 2016. However, through retrospective studies, it has been detected in clinical samples from the years 60, suggesting that virus was circulating on pigs earlier their first report (39, 40). PCV3 has been identified in pig herds in several countries across the globe, including Asia (China, Korea, Japan, and Thailand), Europe (Denmark, Spain, Hungary, Ireland, Italy, Portugal, the United Kingdom, Russia, and Sweden), South America (Argentina, Brazil, Chile, and Colombia), and North America (Canada and Mexico). This widespread distribution of the virus highlights its global presence (11, 18, 41–47).

Several countries have conducted studies to determine the prevalence of viral infections using the polymerase chain reaction (PCR) technique. In Brazil, a study analyzed tissue samples from swine herds in nine states (Mato Grosso, Mato Grosso do Sul, Goiás, Minas Gerais, São Paulo, Espírito Santo, Santa Catarina, Rio Grande do Sul, and Paraná), and found that 47.8% of the samples were positive for PCV3 (35).

A study conducted in Thailand analyzed tissue and serum samples from 26 farms between 2006 and 2017 and found a 36.7% positive rate for PCV3 (48). In other countries such as Ireland, the United States, Poland, Denmark, and Sweden, positive rates ranged from 16.61 to 56.41% (11, 27, 48–50). Spain showed rates of 11.47 and 14.89% (20, 49).

According to studies by Franzo et al. (49), Italy recorded PCV3 positive rates of 39.56 and 50%, respectively. In China, there have been several studies conducted on the circulation of PCV3, with the virus being detected in more than 24 Chinese provinces, including the identification of its genotypes (PCV3a-1, PCV3a-2, PCV3a-3, PCV3b-1, and PCV3b-2) (30). Positive rates in China have shown significant fluctuations (ranging from 10 to 60%), with some farms even recording a 100% rate (13, 51–57). Anahory et al. (58) analyzed 172 archived DNA samples consisting of spleen, tonsils, liver, and ganglia collected from 91 pigs in nine of the ten provinces of Mozambique between 2011 and 2019. Their analysis provided the first evidence of PCV3 presence in Africa, with a total of 7 (7.5%) positive animals (Figure 2).

The origin of PCV3 is distinct from other PCVs, and it is believed to have evolved from the bat circovirus before adapting to pigs and other animals, allowing for cross-species transmission (10, 59). In

TABLE 1 Taxonomic classification and distinctive features of PCV3 subgroups in samples collected Internationally 2023. (Source: Author).

Identification	Country	Year	Authors
PCV3a, PCV3b and PCV3c	China	2015 and 2017	Qi et al. (15)
		2021	Cui et al. (25)
PCV3a and PCV3b	Brazil	2006- 2007	Saraiva et al. (35)
PCV3 a1, a2, b1 and b2.	Colombia	2018	Vargas-Bermudez et al. (36)
PCV3a-1, a-2, a-3, b-1 and 3b-2	China	1996 and 2019	Chen et al. (30)
PCV3a	USA	2019	Franzo et al. (37)
PCV3-1, 3-2a and 2b, 3-3a to 3h.	Korea	2017-2018	Chung et al. (38)

addition to domestic pigs, PCV3 has been found in other mammals, both wild and domestic, including dogs, cattle, mice, chamois (*Rupicara rupicara*), deer (*Cervus elaphus* and *Capreolus capreolus*), and wild boar (*Sus scrofa*), as well as arthropods such as ticks (49, 60–62). In Italy, PCV3 has been detected in chamois, deer, mouflons (*Ovis musimon*), and wild boars (49).

Samples from dogs, cattle, and mice in China have also tested positive for PCV3, in addition to pigs (62, 63). In Spain, PCV3 has been detected in deer (*Cervus elaphus* and *Dama dama*) and mouflons (*Ovis aries*) (64). PCV3 has also been found in invertebrates, including ticks (*Ixodus ricinus*) in Italy and mosquitoes (*Aedes vexans*, *Anopheles sinensis*, *Culex tritaeniorhynchus*, and *Culex pipiens pallens*) in China (65, 66). Records of PCV3 presence in wild boars are reported in Brazil (67). A study conducted by Franzo et al. (49) in the Colli Euganei Regional Park of northern Italy collected 187 serum samples from wild boars and showed a high prevalence of PCV3, around 30%. Although almost all the animals were in good health, this study highlights the potential role of wild boars as a reservoir for PCV3, endangering pig farming (49). Due to the significant mutation rate of PCV3 and its discovery in various animal species, there is a concern about the likelihood of human infection. In a recent case, PCV3 was found in a herd of triple-modified pigs, which were raised for xenotransplantation. A PCV3-positve heart was transplanted into a baboon recipient and the virus was detected in all organs of the baboon recipient. The higher viral load, observed in animals with longer transplant survival times, suggested active virus replication (68) (Figure 3).

PCV3 infection can affect both, healthy and sick pig (15, 35, 52) found a strong correlation between PCV3 infection and respiratory and digestive diseases, with 26.6% of pigs with respiratory diseases and 10.4% with digestive diseases testing positive for the virus (54) also showed that PCV3 rates were significantly higher in pigs with severe respiratory disease (63.75%) or diarrhea (17.14%) compared to those with mild respiratory disease (13.14%), no diarrhea (2.86%), or no symptoms (1.85%). Furthermore, healthy sows (21.9%) and pigs from slaughterhouses (19.14%) also tested positive for PCV3 (52, 57). In Brazil, the positive rates of PCV3 were higher in healthy pigs (29.8%) compared to diseased pigs (17.9%) (35). The virus can infect pigs of all ages, including animals aged 1 day to 24 weeks, gilts, and multiparous sows (45). Therefore, the available evidence suggests that PCV3 infection is not related to the health status, sex, or age of the animal, but rather to the presence of environmental and animal condition that favor viral infection (14).

The PCV3 DNA has been detected in various tissues and fluids, including the brain, kidney, heart, spleen, serum, oral and nasal fluids, feces, colostrum, and semen of both healthy and sick animals (Table 2). Additionally, PCV3-specific antigens have been identified in the skin, lung, heart, kidney, lymph nodes, spleen, liver, and small intestine of infected piglets, both symptomatic and asymptomatic (73, 74), PCV3 DNA was detected in serum samples from healthy boars imported from the United States and Western European countries, indicating the potential for global transmission (73, 75). Vertical transmission is also a concern since the virus is widely distributed in various tissues (14).

PCV3 has been linked to reproductive issues and has a high potential for vertical transmission. A study by Zheng et al. (29) analyzed 222 tissue samples from stillborn fetuses in China and found that most samples tested negative for PCV2, but viral metagenomic sequencing revealed the presence of PCV3 in 59.5% (132/222) samples. Another study aimed to investigate PCV3's association with reproductive issues in healthy sows. They analyzed serum samples from 85 sows with a history of reproductive disorders and 105 healthy sows, with a significantly higher PCV3 positive rate found in sows with reproductive failure (45.9%) than in healthy ones (21.9%) (57). In Brazil, a study conducted by Dal Santo et al. (67) found that 270 out of 276 mummified fetuses tested positive for PCV3. Similarly, in Argentina, mummified and stillborn fetuses resulting from reproductive failures showed 100% positivity for PCV3 (44).

Retrospective studies have revealed that PCV3 has been circulating in Poland since 2014, in Ireland since 2002, in Spain and China since the 1990s (20, 39), and in Brazil since 1967 (40). These findings suggest that the virus has been present in pig populations for decades prior to its initial reporting, regardless of whether it is linked to clinical symptoms.

Some studies have shown the still unknown impact of PCV3 on public health (14, 20). PCV1 and PCV2 DNA have already been found in vaccines intended for human use, probably originating from reagents of porcine origin in their manufacture, in addition to detection in samples from children who received live vaccine against rotavirus (76). It is known that PCV2 can infect human cells, both normal and cancerous, therefore, as it is a virus of the same genus, it may be that PCV3 can infect humans, a fact that still needs to be further studied. Recently, a herd of triple genetically modified pigs generated for xenotransplantation observed a sudden introduction of PCV3. These pigs served as donors for orthotopic heart transplants in baboons, with four cases involving PCV3-positive hearts resulting in transmission of the virus to the recipients. PCV3 was detected in all organs of the baboons, and a higher viral load was found in animals with a longer survival time, indicating replication of the virus. This marks the first reported instance of PCV3 trans-species transmission to baboons through heart transplantation from a PCV3-positive pig donor (68).

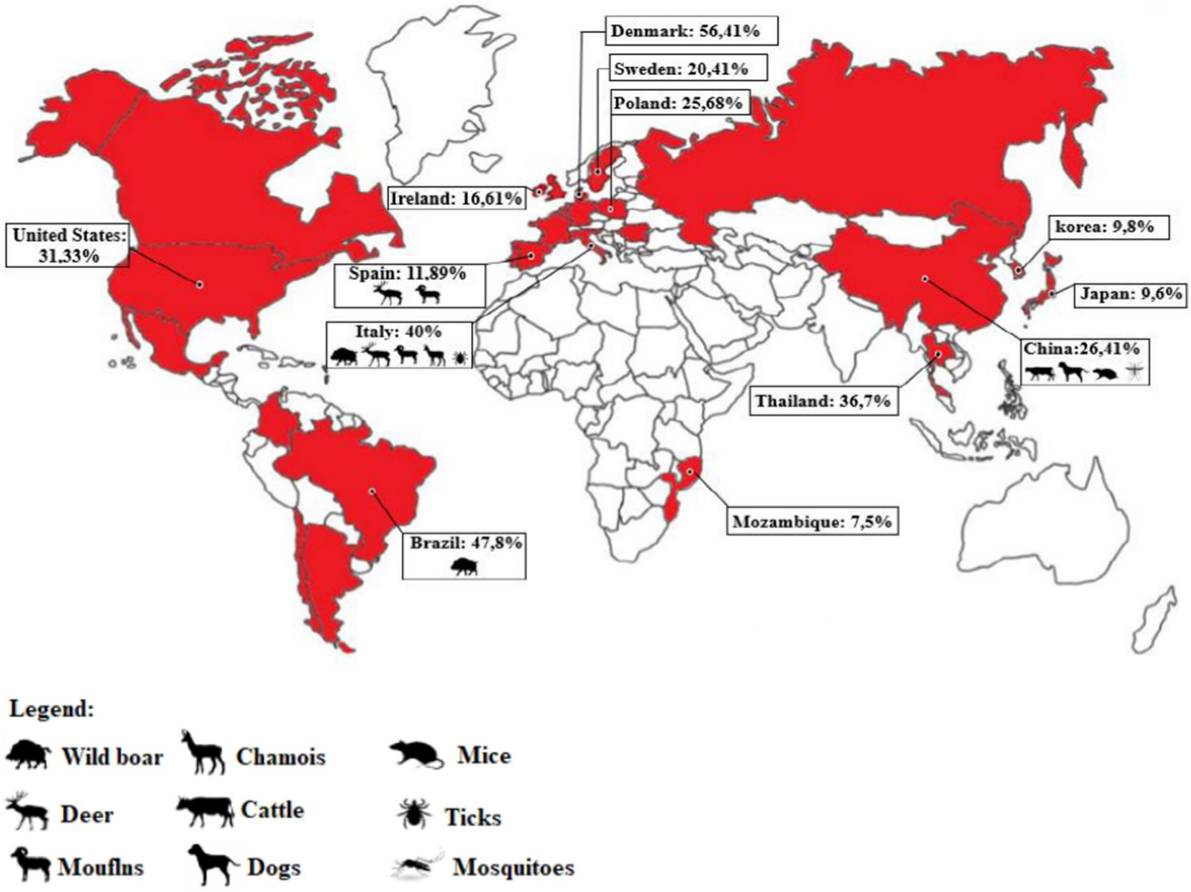

FIGURE 2
Map representation indicating the countries where PCV3 infection has been detected (highlighted in red). The percentage of positive samples in pigs and other animals' species is also displayed for each country, based on the available literature. In cases where multiple studies were conducted in a country (such as China, Spain, and Italy), the percentage was calculated based on the total number of samples tested across all studies, to obtain an average for the country (Source: author).

In a study conducted in a specific region of China, Porcine Circovirus 3 (PCV3), an emerging virus associated with swine dermatitis and nephropathy syndrome in swine, was thoroughly investigated for its prevalence and genotypic distribution. A total of 1,291 samples were collected from 211 pig farms in 15 provinces and municipalities in the region in question. Of these samples, 312 were positive for PCV3 using PCR, and a subsample consisting of 164 of these positive samples was subjected to sequencing and analysis (34). The results revealed that the overwhelming majority (61.8%) of the sequenced isolates belonged to the PCV3c genotype. Notably, the PCV3c genotype also emerged as predominant in Hubei, Hunan, Hebei provinces and Chongqing city. Furthermore, the analysis identified three sites under positive selection, located within the predicted epitope peptide, suggesting that porcine immunity may be influencing this highly positive selection. These findings are of significant relevance for understanding the spread of PCV3 in the studied region, as well as for continued research and development of control strategies (34).

A study carried out in the provinces of Sichuan and Gansu, China, with the purpose of evaluating the frequency of detection of Porcine Circovirus 3 (PCV3) in Tibetan pigs in three different provinces surrounding the Qinghai-Tibet plateau, it was observed that the prevalence of virus was significantly higher in samples from pigs with diarrhea compared to samples from healthy animals. Phylogenetic analysis of Cap proteins revealed the presence of three distinct clades among the 20 PCV3 strains, comprising PCV3a (40.00%), PCV3b (25%), and PCV3c (35.00%). These results highlight the prevalence of PCV3 in Tibetan pigs in high-altitude regions in China, highlighting the higher prevalence rates of PCV3a and PCV3b subtypes in samples from pigs with diarrhea. Such observations emphasize the need to consider PCV3 genotypes in research related to its pathogenicity, highlighting the importance of surveillance and control of this virus at a regional and global level (15).

Another study carried out in Vietnam investigated the genetic diversity of PCV3 in 249 pig samples from eight provinces. About 11.65% of the samples contained PCV3. Genetic analyzes revealed that 23 samples were of the PCV3b subtype and six belonged to subtypes c and a (a-1 and a-2). The sequences were highly similar (96.90-100% in genome and 96.19-100% in amino acids), and fifteen amino acid substitutions were found in the capsid proteins of Vietnamese PCV3 strains, contributing to the understanding of regional genetic diversity (77).

Some studies have shown curiosity about the still unknown impact of PCV3 on public health (13, 15, 34) PCV1 and PCV2 DNA

TABLE 2 Clinical sign observed in field studies in animals with different disorders linked to PCV3.

Clinical signs	Tested samples	Country	References
Respiratory disorders			
Mild and severe respiratory diseases.	Pulmonary homogenate/oral	USA	Phan et al. (10)
Moderate and diffuse lymph histiocytic interstitial dyspnea/ pneumonia	Lung tissues	China	Palinski et al. (11)
Acute bronchitis	Tissues/Serums	China	Qi et al. (15)
Gastrointestinal disorders			
Diarrhea	Fecal specimens	China	Zhai et al. (54)
Diarrhea/vomiting	Intestinal tissues and lung tissues	China	Qi et al. (10)
Digestive disorders/catarrhal enteritis and catarrhal colitis	serum	Spain	Saporiti, et al. (69)
Reproductive disorders			
Reproductive failure	Serum/ Semen	China	Zou et al. (57)
Mortality of sows (aborted mummified fetuses)	Tissue pool from aborted fetus and stillborn piglet	Brazil/ Italy	Dal Santo et al. (67) Faccini et al. (64)
Sows giving birth to stillborn piglets	Tissues from mummified fetuses	USA	Arruda et al. (70)
Neurological disorders			
Congenital tremors	Brain tissue	China	Chen et al. (19)
Congenital tremors, neurological signs in piglets after birth	Brain tissue	United Kingdom	Williamson et al. (71)
Tremors, newborn piglets born weakly/myocarditis, encephalitis, gliosis, and lymphocytic perivascular cuff	Brain tissue	USA	Arruda et al. (70)
Other disorders			
Myocarditis/periarteritis	Different tissues	USA	Phan et al. (10)
Porcine Dermatitis and Nephropathy Syndrome	Tissues from kidneys and spleen	USA	Palinski et al. (11)
Acute deaths/myocarditis	Kidneys and spleen	Russia	Yuzhakov et al. (72)
Arteritis/systemic inflammation	Kidneys and spleen	Russia	Yuzhakov et al. (72)

have already been found in vaccines intended for human use, probably originating from reagents of porcine origin in their manufacture, in addition to detection in samples from children who received live vaccine against rotavirus (DOI: 10.4161/hv.26731) (80). It is known that PCV2 can infect human cells, both normal and cancerous, therefore, as it is a virus of the same genus, it may be that PCV3 can infect humans, a fact that still needs to be further studied.

Clinical signs and pathology

PCV3 has been described and continues to be detected in pigs that exhibit a range of clinical signs including respiratory and digestive disorders, neurological alterations, cardiac and multisystemic inflammation, and reproductive disorders, as well as conditions like PDNS (10, 11, 46).

However, the mere presence of PCV3 genome in a diseased animal does not necessarily imply that the virus is the causative agent of the clinical signs or lesions observed. Most of the studies carried out so far lack a proper negative control to compare viral infection and disease (46). Furthermore, the detection of PCV3 through PCR in tissue, blood, and serum samples is frequently reported, but without any correlation with the animal's lesions. In other words, few studies have yet demonstrated the virus's presence in the lesions (20, 46, 78).

Arruda et al. (70) conducted a study on pigs from various farms in the United States at different production stages to detect the presence of PCV3 in lesions using histopathology and *in situ* hybridization (ISH) techniques. The results of the study suggested that PCV3 could be a potential cause of multisystemic inflammation and reproductive failure in pigs during the perinatal, growth, and termination phases. Several other studies have also detected PCV3 in lesions using ISH (10, 36, 46, 70–86).

There have been limited experimental investigations conducted on PCV3. In a study by Jiang et al. (74), 4 and 8-week-old SPF piglets were inoculated with PCV3. In the context of this experimental study involving PCV3 infection, the inoculum was obtained from clinical samples from pigs diagnosed with the infection. Tissues such as lungs, spleen and lymph nodes were collected post-mortem from infected pigs. The genetic material containing PCV3 was then extracted from these tissues using homogenization and processing techniques, followed by a purification step. The purified genetic material was amplified in cell culture or by the PCR technique to obtain an adequate quantity of the virus. This resulting inoculum, containing PCV3, was used for experimental infection in pigs, allowing the investigation of clinical, pathogenic and immunological aspects associated with PCV3 infection. All piglets that received PCV3 at 4 weeks old, exhibited symptoms such as fever, anorexia, coughing, sneezing, diarrhea, lethargy, rubefaction on the skin and ears, multifocal papules, shivering, and/or hyperspasmia. Among this group, two piglets displayed severe clinical signs, cardiac pathologies, multisystemic

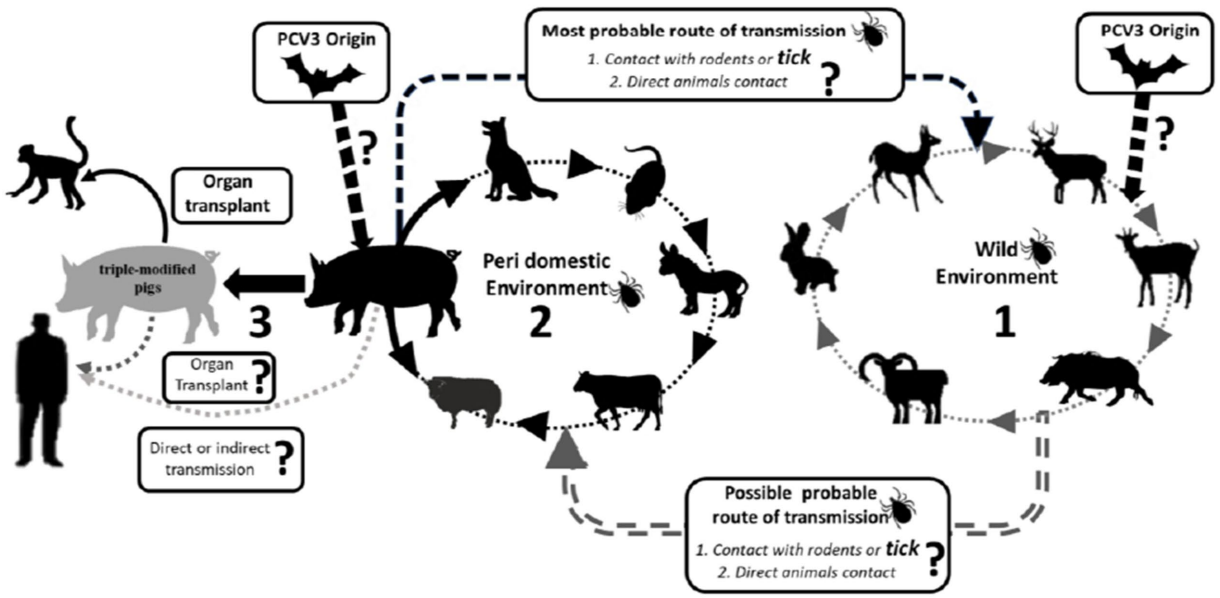

FIGURE 3
Schematic representation of potential occurrence PCV3 transmission route across different species is a potential occurrence based on the available literature. Continuous arrows indicate confirmed transmission. Dashed from commercial herds to triple-modified pigs' herds for organ transplant.

inflammation, and died during the experiment. In 8-week-old piglets administered with PCV3, typical clinical signs of PDNS were observed, although all the piglets survived for the entire duration of the study (28 days). Immunohistochemical staining detected PCV3-positive cells in various tissues and organs (including the lung, heart, kidney, lymph nodes, spleen, liver, and small intestines) of PCV3-inoculated piglets. The peak of viremia (approximately 7.72×10^8 PCV3 copies/mL) in the 4-week-old PCV3-inoculated piglets was detected at 21 days post-inoculation (dpi). Similarly, the highest level of PCV3 (7.92×10^7 copies/mL) in the 8-week-old PCV3-inoculated piglets was also detected at 21 dpi. Mora-Diaz et al. (87) inoculated colostrum-deprived (CD/CD) pigs that were 6 weeks old. PCV3 was isolated from multiple tissues, including the lung, kidney, heart, and brain of perinatal pigs with encephalitis and/or myocarditis, and stillborn and mummified fetuses. Although all animals that were infected with the PCV3 isolate remained clinically healthy throughout the study, histological evaluation revealed lesions of ongoing multisystemic inflammation, lymphoplasmacytic myocarditis, and periarteritis in 4 out of 8 pigs. PCV3 replication was confirmed by *in situ* hybridization (ISH). The study also demonstrated lymphoplasmacytic interstitial nephritis and periarteritis in kidney tissue, and lymphoplasmacytic periarteritis and arteritis of the intestinal serosa of PCV3-inoculated pigs. PCV3 replication was also confirmed within inflammatory cells, the tubular renal epithelium, endothelial cells, and the tunica media of arteries. Viremia was first detected at 7 days post-inoculation (dpi) and was detected in all animals by 28 dpi.

Coinfections

Due to its global spread, there have been reports of co-infections involving PCV3. Given that PCV2 and PCV3 are from the same genus and considering that co-infections of PCV2 with other pathogens have been shown to worsen the disease both in field and experimental settings, it is possible that PCV3 infection may also facilitate co-infections with other disease-causing agents in pigs (14, 20, 46, 19).

Previous studies have shown that *Porcine circovirus* 3 (PCV3) can co-infect with various other pathogens such as Porcine Reproductive and Respiratory Syndrome Virus (PRRS), Porcine Epidemic Diarrhea Virus (PEDV), *Torque teno sus virus* (TTSuV; comprise TTSuV1a and TTSuVκ2a), *Porcine parvovirus* (PPV), Virus of Classical Swine Fever (CSFV), Atypical porcine pestivirus (APPV), Porcine pseudorabies virus (PRV), *Streptococcus* spp., *Mycoplasma hyopneumoniae*, and *Leptospira* spp. The co-infection prevalence rates of these pathogens with PCV3 range from 5% (PRV) to 100% (*Mycoplasma hyopneumoniae*) (15, 26, 29, 30, 34, 45, 36, 53, 61, 66, 81, 86, 88–90).

Other studies have reported triple co-infections involving PCV3, PCV2, and PRRSV; PCV3, PCV1, and PCV2; and PCV3, TTSuV1, and TTSuV2, with prevalence rates of 1.9, 3.6, and 50%, respectively (31, 56, 91). Moreover, the recent discovery of PCV3 in Mozambique, Africa revealed co-infection with the African Swine Fever Virus (ASFV), where 6 out of 7 positive PCV3 samples also tested positive for ASFV (6.5% of total samples) (58) (Figure 4).

Although co-infections are not well understood, PCV3 is widely prevalent in healthy animals and previous experimental studies have shown that the virus can cause lesions and clinical symptoms, with the age of infection being a significant factor. However, the impact of co-infections remains uncertain. Nevertheless, as observed with PCV2, co-infections may lead to severe clinical symptoms observed in field studies.

Continuing to explore alternative animal models beyond pigs, (60) realized a study employing infectious clones of PCV3 to induce infection in Kunming mice. They successfully demonstrated the pathogenic potential of the acquired infectious clones of PCV3, establishing Kunming

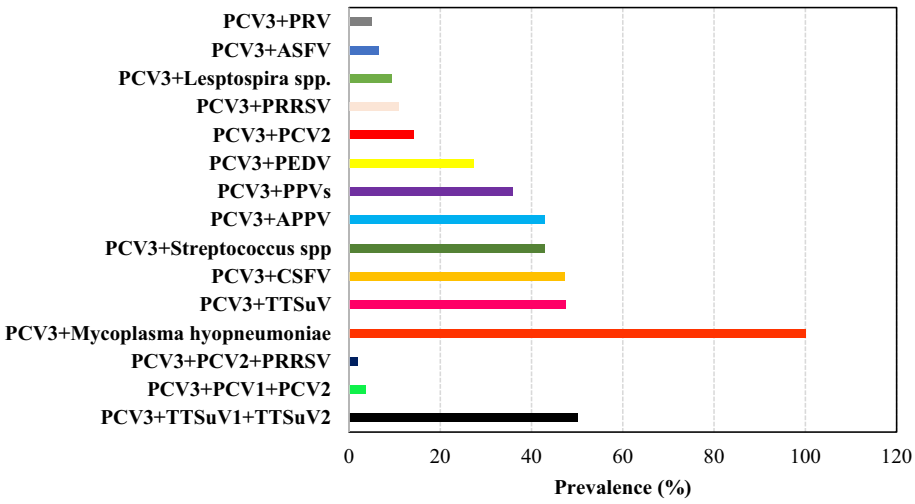

FIGURE 4
Overall prevalence (%) of pathogens involved in co-infections with PCV3 based on consulted literature.

mice as an animal model. Findings from RT-PCR, Western blotting, and ISH highlighted the ability of PCV3 to infect both the myocardium and alveoli of Kunming mice.

The alterations within the pulmonary and cardiac tissues revealed a proliferation of alveolar epithelial cells in the local lung region, resulting in congestion at the periphery of the lobules. Notably, strong positive reactions for PCV3 were evident in the lung. Within the heart, intense positive reactions for PCV3 were detected in necrotic tissues and vascular content, (74) emphasized the significance of their findings by detecting PCV3 in laboratory mice. This underscores the necessity for testing all animal species used in experimental infections, highlighting the importance of thorough screening protocols.

Diagnosis

The most used detection methods so far are: *in situ* hybridization (ISH), quantitative polymerase chain reaction (PCRq) and enzyme-linked immunosorbent assay (ELISA) (29, 46, 92–95) (Table 3).

PCRq analysis has been widely used to analyze the tissues collected from field cases. In Hungary, viral DNA was detected in fetal and neonatal thymus (89%; 49/55), lymph nodes (60%; 33/55), placenta (50.9%, 28/55), spleen (21.8%, 12/55), kidneys (7.2%, 4/55), and liver (5.4%, 3/55), indicating a high prevalence of PCV3 in reproductive failure cases (42). The highest viral loads were reported in fetal or neonatal heart tissues, ranging from 10^9 to 10^{12} genomic copies/gram, followed by fetal kidneys and lungs, with loads ranging from 10^9 to 10^{11} genomic copies/gram (91, 96). High viral loads of PCV3 have also been observed in brain tissues of cases with congenital tremors (96). Viral DNA of PCV3 was detected in semen, serum, feces, colostrum, and oral fluid, with viral loads ranging from $10^{2.5}$ to $10^{7.2}$ copies/mL (12, 26, 97–99).

Different laboratory techniques are available for the detection of PCV3 antigen and/or nucleic acid. For instance, *in situ* hybridization (ISH) has been used to identify the virus in the intestine, heart, and lung (26, 70, 81), while immunohistochemistry (IHC) has been used to detect the virus in the lungs, lymph nodes, kidneys, liver, and heart (74).

Unfortunately, information about PCV3 remains limited and few studies have successfully elucidated the cause of the disease associated with this new virus. This shortage of data may hinder diagnosis, as the overall picture of the infection has not been fully established (20, 46).

To make an accurate diagnosis, it is crucial to analyze clinical signs or evidence of decreased productivity, the evolution of events that may interfere with the onset of the problem, and the detection of the pathogen associated with the lesions present in the animals at the onset of the disease. This latter factor is particularly important for certain infectious agents, such as PCVs.

Detection of the PCV3 virus in pigs involves the collection of several samples, the most common being blood, serum, tissues such as liver and lymph nodes, as well as saliva and feces samples. To research this virus, laboratory techniques such as polymerase chain reaction (PCR), real-time PCR (qPCR), real-time reverse transcriptase PCR (RT-qPCR) and *in situ* hybridization techniques are widely used. Furthermore, histopathological and immunohistochemical analysis of tissues also play a fundamental role in the identification and characterization of PCV3 in pigs, contributing to the understanding of the epidemiology and pathogenesis of this viral infection in pig farms.

Conclusion

Na linha 1043 excluir o parágrafo e acrescentar este: As final considerations, PCV3's extensive genetic diversity is evident through the multitude of genotypes identified thus far. It has been documented across nearly all continents, except for Oceania and Antarctica. Its detection in various animal species shows its one health implications and the potential for zoonotic transmission. Worthy of significant consideration. While linked with diverse clinical manifestations, PCV3's most notable impact remains on reproductive disorders. Recognizing the significance of asymptomatic carriers-whether swine or non-swine-is crucial, as they serve as potential reservoirs for the virus. Field studies shows co-infections with other microorganisms, yet the role of these co-agents in initiating or exacerbating clinical signs, whether mild or severe, lacks conclusive association. Various sample types can be utilized for PCV3 detection, with molecular tests like PCR and qPCR being the most used to detect the virus. However, non-molecular tests play an important role in establishing the

TABLE 3 Laboratory methods for PCV3 detection in field studies from various samples in different countries.

Method	Country	Sample	No. of samples	Positive samples	References
PCR	Poland	Serum	1,050	268 (25.5%)	Stadejek et al. (50)
	Northern Ireland	Tissue and feces	240	48 (20%)	Collins et al. (48)
	England	Tissue	80	4 (5%)	Collins et al. (48)
	Italy*	Tissue/tissue serum and nasal swabs	16/99	2 (12.5%)/37 (37.4%)	Faccini et al. (64) Franzo et al. (47)
	Denmark	Tissue and serum	78	44 (56.4%)	Franzo et al. (47)
	Spain**	Serum/Serum/Tissue	94/ 654/300	14 (14.9%)/75 (11.5%)/74 (24.6%)	Franzo et al. (47)/ Klaumann et al. (97) /Ruiz et al. (78)
	Sweden	Tissue	49	10 (20.4%)	Ye et al. (27)
	United Kingdon	Serum	126	8 (6.3%)	Feng et al. (50)
	France	Serum	139	9 (6.5%)	Feng et al. (50)
	Hungary*	Tissue/Serum and oral fluid	330/2.128	129 (43%)/558 (30.8%)/	Deim et al. (42)/Igriczi et al. (79)
	Japan	Tissue	73	7 (9.6%)	Hayashi et al. (80)
	Korea	Tissue	690	57 (9.8%)	Kim et al. (81)
	China**	Tissue/Tissue/Tissue and blood	105/616/535	35 (33.3%)/75 (12.2%)/216 (40.4%)	Ha et al. (66) /Qi et al. (15)/Zou et al. (23)
	Thailand	Serum and tissue	79	29 (36.7%)	Sukmak et al. (82)
	United States**	Serum/Tissue and serum	36/336/2,177	22 (61.1%)/37 (11.1%)/577 (27%)	Arruda et al. (70)/Feng et al. (47)/ Yang et al. (83)
	Brazil**	Tissue/tissue and FFPE/ Tissue	67/35/ 143/276	32 (47.8%)/ 14 (40%); 12 (8.4%)/270 (97%)	Saraiva et al.(35) /Rodrigues et al. (39) Dal Santo et al. (84)
	Colombia	Serum and tissue	8	2 (25%)	Vargas-Bermúdez et al. (36)
	Chile	Tissue	50	35 (70%)	Rubilar et al. (43)
	Argentina	Tissue	203	18 (8.9%)	Serena et al. (41)
	Mozambique	Tissue	91	7 (7.5%)	Anahory et al. (55)
ISH	United States	Serum/Tissue and serum	5	5 (100%)	Arruda et al. (70)
	Brazil	Tissue	11	6 (54.5%)	Molossi1 et al. (85)
ELISA	China*	Serum	190	64 (33.8%)	Zhang et al. (67)
	China	Serum	2568	1101 (42.7%)	Ge et al. (16)
	China	Serum	1,688	840 (49.8%)	Deng et al. (92)

*= data comprise two studies; **= data comprise three studies; FFPE = formalin-fixed paraffin-embedded; /= used to separate information from different studies.

association between the agent and lesions alongside tests demonstrating viral replication (such as RT-qPCR and RNA-ISH). Finally, since its discovery, PCV3 has proven to be a significant and challenging emerging agent in global swine production. Like PCV2, it displays a high capacity for mutation, potentially exacerbating clinical signs when combined with other agent and due its extensive distribution.

Author contributions

DS: Methodology, Writing – review & editing. RS: Data curation, Investigation, Writing – original draft, Writing – review & editing. VS: Data curation, Investigation, Writing – review & editing. AC: Funding acquisition, Project administration, Software, Supervision, Validation, Writing – original draft, Writing – review & editing.

Funding

The author(s) declare that no financial support was received for the research, authorship, and/or publication of this article.

Conflict of interest

The authors declare that the research was conducted in the absence of any commercial or financial relationships that could be construed as a potential conflict of interest.

Publisher's note

References

1. CNA (Confederation of Agriculture and Livestock of Brazil). *Cenário Econômico da Suinocultura. Confederação da Agricultura e Pecuária do Brasil (CNA)*.

2. Ferreira AHCBDDMGMLPRRS. Produção de Suínos: Teoria e Prática. *Associação Brasileira dos Criadores de Suínos – ABCS*. (2014) 1:01–908.

3. Ferreira AH. CBDDMGMLPRRS. Produção de Suínos: Teoria e Prática. *Associação Brasileira dos Criadores de Suínos (ABCS)*.

4. Conway DJ, Roper C. Micro-evolution and emergence of pathogens. *Int J Parasitol*. (2000) 30:1423–30. doi: 10.1016/S0020-7519(00)00126-0

5. Correa-Fiz F, Franzo G, Llorens A, Segalés J, Kekarainen T. Porcine circovirus 2 (PCV-2) genetic variability under natural infection scenario reveals a complex network of viral quasispecies. *Sci Rep*. (2018) 8:15469. doi: 10.1038/s41598-018-33849-2

6. Fournié G, Kearsley-Fleet L, Otte J, Pfeiffer DU. Spatiotemporal trends in the discovery of new swine infectious agents. *Vet Res*. (2015) 46:114. doi: 10.1186/s13567-015-0226-8

7. Opriessnig T, Meng X-J, Halbur PG. Porcine circovirus type 2–associated disease: update on current terminology, clinical manifestations, pathogenesis, diagnosis, and intervention strategies. *J Vet Diagn Investig*. (2007) 19:591–615. doi: 10.1177/104063870701900601

8. Opriessnig T, Karuppannan AK, Castro AM, Xiao CT. Porcine circoviruses: current status, knowledge gaps and challenges. *Virus Res*. (2020) 286:198044. doi: 10.1016/j.virusres.2020.198044

9. Yao J, Qin Y, Zeng Y, Ouyang K, Chen Y, Huang W, et al. Genetic analysis of porcine circovirus type 2 (PCV2) strains between 2002 and 2016 reveals PCV2 mutant predominating in porcine population in Guangxi, China. *BMC Vet Res*. (2019) 15:118. doi: 10.1186/s12917-019-1859-z

10. Phan TG, Giannitti F, Rossow S, Marthaler D, Knutson TP, Li L, et al. Detection of a novel circovirus PCV3 in pigs with cardiac and multi-systemic inflammation. *Virol J*. (2016) 13:184. doi: 10.1186/s12985-016-0642-z

11. Palinski R, Piñeyro P, Shang P, Yuan F, Guo R, Fang Y, et al. A novel porcine circovirus distantly related to known circoviruses is associated with porcine dermatitis and nephropathy syndrome and reproductive failure. *J Virol*. (2017) 91:e01879-16. doi: 10.1128/JVI.01879-16

12. Eddicks M, Müller M, Fux R, Ritzmann M, Stadler J. Detection of porcine circovirus type 3 DNA in serum and semen samples of boars from a German boar stud. *Vet J*. (2022) 279:105784. doi: 10.1016/j.tvjl.2021.105784

13. Li G, He W, Zhu H, Bi Y, Wang R, Xing G, et al. Origin, genetic diversity, and evolutionary dynamics of novel porcine circovirus 3. *Adv Sci*. (2018) 5:1800275. doi: 10.1002/advs.201800275

14. Ouyang T, Niu G, Liu X, Zhang X, Zhang Y, Ren L. Recent progress on porcine circovirus type 3. *Infect Genet Evol*. (2019) 73:227–33. doi: 10.1016/j.meegid.2019.05.009

15. Qi S, Su M, Guo D, Li C, Wei S, Feng L, et al. Molecular detection and phylogenetic analysis of porcine circovirus type 3 in 21 provinces of China during 2015–2017. *Transbound Emerg Dis*. (2019) 66:1004–15. doi: 10.1111/tbed.13125

16. Ge M, Ren J, Xie YL, Zhao D, Fan FC, Song XQ, et al. Prevalence and genetic analysis of porcine circovirus 3 in China from 2019 to 2020. *Front Vet Sci*. (2021) 8:773912. doi: 10.3389/fvets.2021.773912

17. Franzo G, Segalés J. Porcine circovirus 3 (PCV-3) variability: is it in the virus or in the classification criteria? *Virol J*. (2023) 20:26. doi: 10.1186/s12985-023-01984-6

18. Tochetto C, Lima DA, Varela APM, Loiko MR, Paim WP, Scheffer CM, et al. Full-genome sequence of porcine circovirus type 3 recovered from serum of sows with stillbirths in Brazil. *Transbound Emerg Dis*. (2018) 65:5–9. doi: 10.1111/tbed.12735

19. Chen S, Zhang L, Li X, Niu G, Ren L. Recent Progress on epidemiology and pathobiology of porcine circovirus 3. *Viruses*. (2021) 13:1944. doi: 10.3390/v13101944

20. Klaumann F, Correa-Fiz F, Franzo G, Sibila M, Núñez JI, Segalés J. Current knowledge on porcine circovirus 3 (PCV-3): a novel virus with a yet unknown impact on the swine industry. *Front Vet Sci*. (2018) 5:315. doi: 10.3389/fvets.2018.00315

21. Cheung AK. A stem–loop structure, sequence non-specific, at the origin of DNA replication of porcine circovirus is essential for termination but not for initiation of rolling-circle DNA replication. *Virology*. (2007) 363:229–35. doi: 10.1016/j.virol.2007.01.017

22. Mankertz A, Çaliskan R, Hattermann K, Hillenbrand B, Kurzendoerfer P, Mueller B, et al. Molecular biology of Porcine circovirus: analyses of gene expression and viral replication. *Vet Microbiol*. (2004) 98:81–8. doi: 10.1016/j.vetmic.2003.10.014

23. Zou J, Liu H, Chen J, Zhang J, Li X, Long Y, et al. Development of a TaqMan-probe-based multiplex real-time PCR for the simultaneous detection of porcine circovirus 2, 3, and 4 in East China from 2020 to 2022. *Vet Sci*. (2022) 10:29. doi: 10.3390/vetsci10010029

24. Hamel AL, Lin LL, Nayar GPS. Nucleotide sequence of porcine circovirus associated with postweaning multisystemic wasting syndrome in pigs. *J Virol*. (1998) 72:5262–7. doi: 10.1128/JVI.72.6.5262-5267.1998

25. Cui Y, Hou L, Pan Y. Reconstruction of the Evolutionary Origin, Phylodynamics, and Phylogeography of the Porcine Circovirus Type 3. *Front Microbiol; 13. Epub ahead of print*. (2022). doi: 10.3389/fmicb.2022.898212

26. Kedkovid R, Woonwong Y, Arunorat J, Sirisereewan C, Sangpratum N, Kesdangsakonwut S, et al. Porcine circovirus type 3 (PCV3) shedding in sow colostrum. *Vet Microbiol*. (2018) 220:12–7. doi: 10.1016/j.vetmic.2018.04.032

27. Ye X, Berg M, Fossum C, Wallgren P, Blomström AL. Detection and genetic characterisation of porcine circovirus 3 from pigs in Sweden. *Virus Genes*. (2018) 54:466–9. doi: 10.1007/s11262-018-1553-4

28. Saraiva GL, Vidigal PMP, Fietto JLR, Bressan GC, Silva Júnior A, de Almeida MR. Evolutionary analysis of porcine circovirus 3 (PCV3) indicates an ancient origin for its current strains and a worldwide dispersion. *Virus Genes*. (2018) 54:376–84. doi: 10.1007/s11262-018-1545-4

29. Zheng S, Wu X, Zhang L, Xin C, Liu Y, Shi J, et al. The occurrence of porcine circovirus 3 without clinical infection signs in Shandong Province. *Transbound Emerg Dis*. (2017) 64:1337–41. doi: 10.1111/tbed.12667

30. Chen Y, Xu Q, Chen H, Luo X, Wu Q, Tan C, et al. Evolution and genetic diversity of porcine circovirus 3 in China. *Viruses*. (2019) 11:786. doi: 10.3390/v11090786

31. Chen N, Huang Y, Ye M, Li S, Xiao Y, Cui B, et al. Co-infection status of classical swine fever virus (CSFV), porcine reproductive and respiratory syndrome virus (PRRSV) and porcine circoviruses (PCV2 and PCV3) in eight regions of China from 2016 to 2018. *Infect Genet Evol*. (2019) 68:127–35. doi: 10.1016/j.meegid.2018.12.011

32. Chung H, Nguyen VG, Park Y, Park BK. Genotyping of PCV3 based on reassembled viral gene sequences. *Vet Med Sci*. (2021) 7:474–82. doi: 10.1002/vms3.374

33. Kroeger M, Temeeyasen G, Piñeyro PE. Five years of porcine circovirus 3: what have we learned about the clinical disease, immune pathogenesis, and diagnosis. *Virus Res*. (2022) 314:198764. doi: 10.1016/j.virusres.2022.198764

34. Ku X, Chen F, Li P, Wang Y, Yu X, Fan S, et al. Identification and genetic characterization of porcine circovirus type 3 in China. *Transbound Emerg Dis*. (2017) 64:703–8. doi: 10.1111/tbed.12638

35. Saraiva G, Vidigal P, Assao V, Fajardo M, Loreto A, Fietto J, et al. Retrospective detection and genetic characterization of porcine circovirus 3 (PCV3) strains identified between 2006 and 2007 in Brazil. *Viruses*. (2019) 11:201. doi: 10.3390/v11030201

36. Vargas-Bermudez DS, Campos FS, Bonil L, Mogollon D, Jaime J. First detection of porcine circovirus type 3 in Colombia and the complete genome sequence demonstrates the circulation of PCV3a1 and PCV3a2. *Vet Med Sci*. (2019) 5:182–8. doi: 10.1002/vms3.155

37. Franzo G, Delwart E, Fux R. Genotyping Porcine Circovirus 3 (PCV-3) Nowadays: Does It 517 Make Sense?. *Viruses*. (2020) 12:265.

38. Chung H, Nguyen VG, Park Y. Genotyping of PCV3 based on reassembled viral gene 504 sequences. *Vet Med Sci*. (2021) 7, 474–482.

39. Sun J, Wei L, Lu Z, Mi S, Bao F, Guo H, et al. Retrospective study of porcine circovirus 3 infection in China. *Transbound Emerg Dis*. (2018) 65:607–13. doi: 10.1111/tbed.12853

40. Rodrigues ILF, Cruz ACM, Souza AE, Knackfuss FB, Costa CHC, Silveira RL, et al. Retrospective study of porcine circovirus 3 (PCV3) in swine tissue from Brazil (1967–2018). *Braz J Microbiol*. (2020) 51:1391–7. doi: 10.1007/s42770-020-00281-6

41. EUROPEAN SYMPOSIUM OF PORCINE HEALTH MANAGEMENT, 10th, 2018, Barcelona. Proceedings. Proceedings. Barcelona: [n.p.]. (2018). Available at: https://www.ecphm.org/sites/www.ecvdi.org/files/medias/documents/ECPHM/ESPHM%202018%20-%20Proceedings.pdf (Accessed March 12, 2024).

42. Deim Z, Dencső L, Erdélyi I, Valappil SK, Varga C, Pósa A, et al. Porcine circovirus type 3 detection in a Hungarian pig farm experiencing reproductive failures. *Vet Rec*. (2019) 185:84–4. doi: 10.1136/vr.104784

43. Rubilar PS, Tognarelli J, Fernández J, Valdes C, Broitman F, Mandakovic D, et al. Swine viral detection by adapted Next-Generation Sequencing (NGS) for RNA and DNA

species reveals first detection of porcine circovirus type 3 (PCV3) in Chile. *bioRxiv*. (2020)

44. Serena MS, Cappuccio JA, Barrales H, Metz GE, Aspitia CG, Lozada I, et al. First detection and genetic characterization of porcine circovirus type 3 (PCV3) in Argentina and its association with reproductive failure. *Transbound Emerg Dis*. (2021) 68:1761–6. doi: 10.1111/tbed.13893

45. Sukmak M, Thanantong N, Poolperm P, Boonsoongnern A, Ratanavanichrojn N, Jirawattanapong P, et al. The retrospective identification and molecular epidemiology of porcine circovirus type 3 (PCV) in swine in Thailand from 2006 to 2017. *Transbound Emerg Dis*. (2019) 66:611–6. doi: 10.1111/tbed.13057

46. Saporiti V, Franzo G, Sibila M, Segalés J. Porcine circovirus 3 (PCV-3) as a causal agent of disease in swine and a proposal of PCV-3 associated disease case definition. *Transbound Emerg Dis*. (2021) 68:2936–48. doi: 10.1111/tbed.14204

47. Franzo G, Legnardi M, Hjulsager CK, Klaumann F, Larsen LE, Segales J, et al. Full-genome sequencing of porcine circovirus 3 field strains from Denmark, Italy and Spain demonstrates a high within-Europe genetic heterogeneity. *Transbound Emerg Dis*. (2018) 65:602–6. doi: 10.1111/tbed.12836

48. Collins PJ, McKillen J, Allan G. Porcine circovirus type 3 in the UK. *Vet Rec*. (2017) 181:599–9. doi: 10.1136/vr.j5505

49. Franzo G, Tucciarone CM, Drigo M, Cecchinato M, Martini M, Mondin A, et al. First report of wild boar susceptibility to porcine circovirus type 3: high prevalence in the Colli Euganei Regional Park (Italy) in the absence of clinical signs. *Transbound Emerg Dis*. (2018) 65:957–62. doi: 10.1111/tbed.12905

50. Stadejek T, Woźniak A, Miłek D, Biernacka K. First detection of porcine circovirus type 3 on commercial pig farms in Poland. *Transbound Emerg Dis*. (2017) 64:1350–3. doi: 10.1111/tbed.12672

51. Fu X, Fang B, Ma J, Liu Y, Bu D, Zhou P, et al. Insights into the epidemic characteristics and evolutionary history of the novel porcine circovirus type 3 in southern China. *Transbound Emerg Dis*. (2018) 65:e296–303. doi: 10.1111/tbed.12752

52. Wen S, Sun W, Li Z, Zhuang X, Zhao G, Xie C, et al. The detection of porcine circovirus 3 in Guangxi, China. *Transbound Emerg Dis*. (2018) 65:27–31. doi: 10.1111/tbed.12754

53. Xu P-L, Zhang Y, Zhao Y, Zheng HH, Han HY, Zhang HX, et al. Detection and phylogenetic analysis of porcine circovirus type 3 in Central China. *Transbound Emerg Dis*. (2018) 65:1163–9. doi: 10.1111/tbed.12920

54. Zhai S-L, Zhou X, Zhang H, Hause BM, Lin T, Liu R, et al. Comparative epidemiology of porcine circovirus type 3 in pigs with different clinical presentations. *Virol J*. (2017) 14:222. doi: 10.1186/s12985-017-0892-4

55. Zhao D, Wang X, Gao Q, Huan C, Wang W, Gao S, et al. Retrospective survey and phylogenetic analysis of porcine circovirus type 3 in Jiangsu province, China, 2008 to 2017. *Arch Virol*. (2018) 163:2531–8. doi: 10.1007/s00705-018-3870-2

56. Zheng S, Shi J, Wu X, Peng Z, Xin C, Zhang L, et al. Presence of torque Teno sus virus 1 and 2 in porcine circovirus 3-positive pigs. *Transbound Emerg Dis*. (2018) 65:327–30. doi: 10.1111/tbed.12792

57. Zou Y, Zhang N, Zhang J, Zhang S, Jiang Y, Wang D, et al. Molecular detection and sequence analysis of porcine circovirus type 3 in sow sera from farms with prolonged histories of reproductive problems in Hunan, China. *Arch Virol*. (2018) 163:2841–7. doi: 10.1007/s00705-018-3914-7

58. Anahory IV, Franzo G, Settypalli TBK, Mapaco LP, Achá SJ, Molini U, et al. Identification of porcine circovirus-3 in Mozambique. *Vet Res Commun*. (2022) 46:593–6. doi: 10.1007/s11259-021-09858-4

59. Davies PR. One world, one health: the threat of emerging swine diseases. A north American perspective. *Transbound Emerg Dis*. (2012) 59:18–26. doi: 10.1111/j.1865-1682.2012.01312.x

60. Jiang H, Wang D, Wang J, Zhu S, She R, Ren X, et al. Induction of porcine dermatitis and nephropathy syndrome in piglets by infection with porcine circovirus type 3. *J Virol*. (2019) 93, 1–16w. doi: 10.1128/JVI.02045-18

61. Wang J, Zhang Y, Wang J, Liu L, Pang X, Yuan W. Development of a TaqMan-based real-time PCR assay for the specific detection of porcine circovirus 3. *J Virol Methods*. (2017) 248:177–80. doi: 10.1016/j.jviromet.2017.07.007

62. Zhang J, Liu Z, Zou Y, Zhang N, Wang D, Tu D, et al. First molecular detection of porcine circovirus type 3 in dogs in China. *Virus Genes*. (2018) 54:140–4. doi: 10.1007/s11262-017-1509-0

63. Czyżewska-Dors E, Núñez JI, Saporiti V, Huerta E, Riutord C, Cabezón O, et al. Detection of porcine circovirus 3 in wildlife species in Spain. *Pathogens*. (2020) 9:341. doi: 10.3390/pathogens9050341

64. Faccini S, Barbieri I, Gilioli A. Detection and genetic characterization of Porcine circovirus type 3 in Italy. *Transbound Emerg Dis*. (2017) 64:1661–1664.

65. Franzo G, Grassi L, Tucciarone CM, Drigo M, Martini M, Pasotto D, et al. A wild circulation: high presence of *porcine circovirus* 3 in different mammalian wild hosts and ticks. *Transbound Emerg Dis*. (2019):tbed.13180. doi: 10.1111/tbed.13180

66. Ha Z, Li J-F, Xie C-Z, Li CH, Zhou HN, Zhang Y, et al. First detection and genomic characterization of porcine circovirus 3 in mosquitoes from pig farms in China. *Vet Microbiol*. (2020) 240:108522. doi: 10.1016/j.vetmic.2019.108522

67. Dal Santo AC, Gressler LT, Costa SZR, Centenaro JR, Dazzi IM, Martins M. Porcine circovirus 2 and 3 in wild boars in southern Brazil. *Ciência Rural*. (2022) 52, 1–01. doi: 10.1590/0103-8478cr20210209

68. Krüger L, Längin M, Reichart B, Fiebig U, Kristiansen Y, Prinz C, et al. Transmission of porcine circovirus 3 (PCV3) by xenotransplantation of pig hearts into baboons. *Viruses*. (2019) 11:650. doi: 10.3390/v11070650

69. Saporiti V, Martorell S, Cruz TF, Klaumann F, Correa-Fiz F, Balasch M, et al. Frequency of detection and phylogenetic analysis of porcine circovirus 3 (PCV-3) in healthy Primiparous and multiparous sows and their mummified fetuses and stillborn. *Pathogens*. (2020) 9:533. doi: 10.3390/pathogens9070533

70. Arruda B, Piñeyro P, Derscheid R, Hause B, Byers E, Dion K, et al. PCV3-associated disease in the United States swine herd. *Emerg Microbes Infect*. (2019) 8:684–98. doi: 10.1080/22221751.2019.1613176

71. Williamson S. Natimortos, artrogripose e doença nervosa pré- desmame: evidências de envolvimento do circovírus suíno 3 (PCV-3). Nos Anais do 12o Simpósio Europeu de Gestão da Saúde Suína..

72. Yuzhakov AG, Raev SA, Alekseev KP. First detection and full genome sequence of porcine circovirus type 3 in Russia. *Virus Genes*. (2018) 54, 608–611.

73. Feng C, Wang C, Zhang Y, du F, Zhang Z, Xiao F, et al. Establishment of a sensitive TaqMan-based real-time <scp>PCR</scp> assay for porcine circovirus type 3 and its application in retrospective quarantine of imported boars to China. *Vet Med Sci*. (2019) 5:168–75. doi: 10.1002/vms3.141

74. Jiang S, Zhou N, Li Y, An J, Chang T. Detection and sequencing of porcine circovirus 3 in commercially sourced laboratory mice. *Vet Med Sci*. (2019) 5:176–81. doi: 10.1002/vms3.144

75. Zhang S, Wang D, Jiang Y, Li Z, Zou Y, Li M, et al. Development and application of a baculovirus-expressed capsid protein-based indirect ELISA for detection of porcine circovirus 3 IgG antibodies. *BMC Vet Res*. (2019) 15:79. doi: 10.1186/s12917-019-1810-3

76. Esona MD, Mijatovic-Rustempasic S, Yen C, Parashar UD, Gentsch JR, Bowen MD, et al. Detection of PCV-2 DNA in stool samples from infants vaccinated with RotaTeq ®. *Hum Vaccin Immunother*. (2014) 10:25–32. doi: 10.4161/hv.26731

77. Dinh PX, Nguyen HN, Lai DC, Nguyen TT, Nguyen NM, do DT. Genetic diversity in the capsid protein gene of porcine circovirus type 3 in Vietnam from 2018 to 2019. *Arch Virol*. (2023) 168:30. doi: 10.1007/s00705-022-05661-x

78. Ruiz A, Saporiti V, Huerta E, Balasch M, Segalés J, Sibila M. Exploratory study of the frequency of detection and tissue distribution of porcine circovirus 3 (PCV-3) in pig fetuses at different gestational ages. *Pathogens*. (2022) 11:118. doi: 10.3390/pathogens11020118

79. Igriczi, B, Dénes, L, Biksi, I, Albert, E, Révész, T, and Balka, G. High Prevalence of Porcine Circovirus 3 in Hungarian Pig Herds: Results of a Systematic Sampling Protocol. *Viruses*. (2022). 14:1219. doi: 10.3390/v14061219

80. Hayashi, S, Ohshima, Y, Furuya, Y. First detection of porcine circovirus type 3 in Japan. *Journal of Veterinary Medical Science* (2018) 80:1468–1472.

81. Kim S-C, Nazki S, Kwon S, Juhng JH, Mun KH, Jeon DY, et al. The prevalence and genetic characteristics of porcine circovirus type 2 and 3 in Korea. *BMC Vet Res*. (2018) 14:294. doi: 10.1186/s12917-018-1614-x

82. Sukmak, M, Thanantong, N, Poolperm, P, Boonsoongnern, A, Ratanavanichrojn, N, Jirawattanapong, P, et al The retrospective identification and molecular epidemiology of porcine circovirus type 3 (PCV3) in swine in Thailand from 2006 to 2017. *Transbound Emerg Dis.* (2019). 66, 611–616.

83. Yang, Z, Marthaler, DG, and Rovira, A. Frequency of porcine circovirus 3 detection and histologic lesions in clinical samples from swine in the United States. *J Vet Diagn Invest.* (2022) 34, 602–611. doi: 10.1177/10406387221099538

84. Dal Santo, AC, Cezario, KC, Bennemann, PE, Machado, SA, and Martins, M. Full-genome sequences of porcine circovirus 3 (PCV3) and high prevalence in mummified fetuses from commercial farms in Brazil. *Microb Pathog.* (2020) 141:104027. doi: 10.1016/j.micpath.2020.104027

85. Molossi, FA, de Cecco, BC, de Almeida, BA. PCV3-associated reproductive failure in pig herds in Brazil. *Trop Anim Health Prod* (2022) 54:293.

86. Kim S-H, Park J-Y, Jung J-Y, Kim HY, Park YR, Lee KK, et al. Detection and genetic characterization of porcine circovirus 3 from aborted fetuses and pigs with respiratory disease in Korea. *J Vet Sci*. (2018) 19:721–4. doi: 10.4142/jvs.2018.19.5.721

87. Mora-Díaz, J, Piñeyro, P, Shen, H, Schwartz, K, Vannucci, F, Li, G, et al. Isolation of PCV3 from Perinatal and Reproductive Cases of PCV3-Associated Disease and In Vivo Characterization of PCV3 Replication in CD/CD Growing Pigs. *Viruses.* (2020) 12:219. doi: 10.3390/v12020219

88. Han H-Y, Zheng H-H, Zhao Y, Tian RB, Xu PL, Hou HL, et al. Development of a SYBR green I-based duplex real-time fluorescence quantitative PCR assay for the simultaneous detection of porcine epidemic diarrhea virus and porcine circovirus 3. *Mol Cell Probes*. (2019) 44:44–50. doi: 10.1016/j.mcp.2019.02.002

89. Woźniak A, Miłek D, Bąska P, Stadejek T. Does porcine circovirus type 3 (PCV3) interfere with porcine circovirus type 2 (PCV2) vaccine efficacy? *Transbound Emerg Dis*. (2019) 66:tbed.13221–1461. doi: 10.1111/tbed.13221

90. Xia D, Huang L, Xie Y, Zhang X, Wei Y, Liu D, et al. The prevalence and genetic diversity of porcine circovirus types 2 and 3 in Northeast China from 2015 to 2018. *Arch Virol*. (2019) 164:2435–49. doi: 10.1007/s00705-019-04336-4

91. Prinz C, Stillfried M, Neubert LK, Denner J. Detection of PCV3 in German wild boars. *Virol J*. (2019) 16:25. doi: 10.1186/s12985-019-1133-9

92. Deng J, Li X, Zheng D, Wang Y, Chen L, Song H, et al. Establishment and application of an indirect ELISA for porcine circovirus 3. *Arch Virol*. (2018) 163:479–82. doi: 10.1007/s00705-017-3607-7

93. Park Y-R, Kim H-R, Kim S-H, Lee KK, Lyoo YS, Yeo SG, et al. Loop-mediated isothermal amplification assay for the rapid and visual detection of novel porcine circovirus 3. *J Virol Methods*. (2018) 253:26–30. doi: 10.1016/j.jviromet.2017.12.006

94. Alomar J, Saporiti V, Pérez M, Gonçalvez D, Sibila M, Segalés J. Multisystemic lymphoplasmacytic inflammation associated with PCV-3 in wasting pigs. *Transbound Emerg Dis*. (2021) 68:2969–74. doi: 10.1111/tbed.14260

95. Wang W, Sun W, Cao L, Zheng M, Zhu Y, Li W, et al. An epidemiological investigation of porcine circovirus 3 infection in cattle in Shandong province, China. *Vet Res*. (2019) 15:60. doi: 10.1186/s12917-019-1793-0

96. Chen GH, Mai KJ, Zhou L, Wu RT, Tang XY, Wu JL, et al. Detection and genome sequencing of porcine circovirus 3 in neonatal pigs with congenital tremors in South China. *Transbound Emerg Dis*. (2017) 64:1650–4. doi: 10.1111/tbed.12702

97. Klaumann F, Franzo G, Sohrmann M, Correa-Fiz F, Drigo M, Núñez JI, et al. Retrospective detection of *porcine circovirus 3* (PCV-3) in pig serum samples from Spain. *Transbound Emerg Dis*. (2018) 65:1290–6. doi: 10.1111/tbed.12876

98. Plut J, Jamnikar-Ciglenecki U, Golinar-Oven I, Knific T, Stukelj M. A molecular survey and phylogenetic analysis of porcine circovirus type 3 using oral fluid, faeces and serum. *BMC Vet Res*. (2020) 16:281. doi: 10.1186/s12917-020-02489-y

99. Woźniak A, Miłek D, Stadejek T. Wide range of the prevalence and viral loads of porcine circovirus type 3 (PCV3) in different clinical materials from 21 polish pig farms. *Pathogens*. (2020) 9:411. doi: 10.3390/pathogens9050411

Frontiers in Veterinary Science

Transforms how we investigate and improve animal health

The third most-cited veterinary science journal, bridging animal and human health with a comparative approach to medical challenges. It explores innovative biotechnology and therapy for improved health outcomes.

Discover the latest Research Topics

See more →

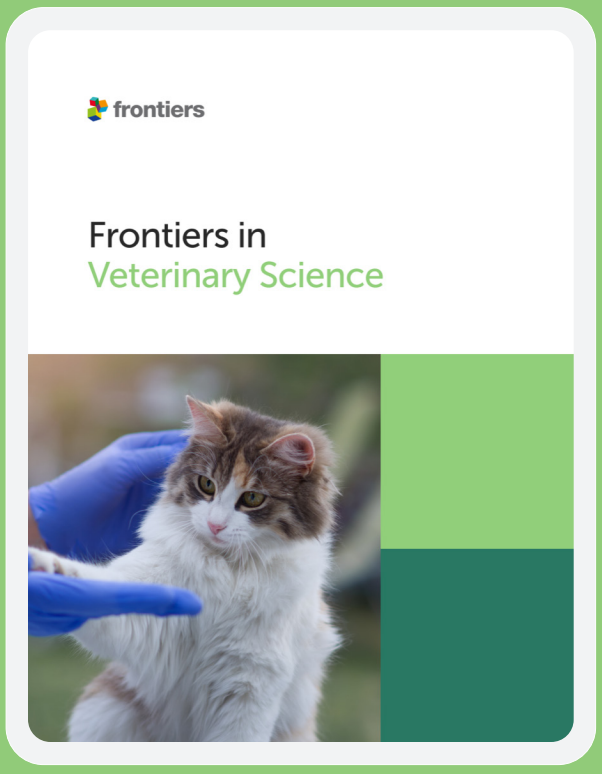

Frontiers

Avenue du Tribunal-Fédéral 34
1005 Lausanne, Switzerland
frontiersin.org

Contact us

+41 (0)21 510 17 00
frontiersin.org/about/contact